Natural Fiber-Plastic Composites for Construction Applications

by

Ehsan Shafiee Monfared

A thesis

presented to the University of Waterloo

in fulfillment of the

thesis requirement for the degree of

Master of Applied Science

In

Chemical Engineering

Waterloo, Ontario, Canada, 2016

Author's Declaration

I hereby declare that I am the sole author of this thesis. This is a true copy of the thesis, including any required final revisions, as accepted by my examiners.

I understand that my thesis may be made electronically available to the public.

Abstract

Natural fiber-plastic composites containing natural fibers as dispersed phase (filler) and polypropylene as matrix are an important and emerging type of compounds used in construction, automotive, consumer products, etc. To evaluate and understand the properties of NFPCs in construction industry, it is important to check the mechanical properties of laboratory prepared NFPCs with various fibers, polypropylene grades and additives. To achieve this goal, the fibers are needed to be ground and be thoroughly analyzed for fiber sizes distributions and aspect ratios distributions to identify the size and shape of fibers to correlate such information with mechanical properties of the NFPC. In this dissertation, it was found that oat hull fibers were smaller than bagasse fibers on average and had lower aspect ratios compared to bagasse fibers.

Using Minitab software, two-level factorial experimental design was employed in three design of experiments (DOEs) to check the effect of fiber type, fiber content, coupling agent content, impact modifier type and impact modifier content on mechanical and impact properties of NFPC. Samples as per DOE runs were conditioned, compounded with twin screw co-rotating extruder, injection molded and tested. The results indicated that bagasse interacts much better compared to oat hull with coupling agent. As well, styrene copolymerized with ethylene/propylene rubber appeared to be more effective in increasing impact properties. Coupling agent appeared to very effective increasing tensile properties although had mild deteriorating effect on impact properties. It was found that compared to unfilled polypropylene, bagasse as a natural filler was very effective on Flexural properties, however, bagasse decreased the tensile properties when compared to unfilled polypropylene. SEM microscopy was used to observe mechanism of impact and appeared to support numerical tests results of Izod Impact Energy responses. Statistical methods generally validated the results and best normal residual plot fit was for Izod Impact results which was almost linear. The worst fit however, belonged to mean failure Energy results. Statistical validity of results was also considered in detail using normal residual plots and were reported in detail for each DOE. Generally, the results were validated with some exceptions.

It is important to evaluate and understand the effect of UV weathering on properties of commercially available NFPC products. To achieve this goal, a Design of experiment was designed to run tests for effect of weathering and physical impact location on multi-axial impact properties of an NFPC product. Commercial products were cut to size and impacted by multi-axial impact tester

and work versus displacement graphs were generated. Effect of UV weathering and impact location was studied on Multi-Axial impact responses of NFPC commercial roofing product and results indicated UV weathering deteriorated total energy, energy to maximum load and maximum load of roofing product. The location of impact either in middle or side or with/without back reinforcement, was not found to be effective on multi-axial impact properties The statistical method used was mildly validated using normal residual plots.

Acknowledgements

I would like to hereby express my most sincere gratitude to my supervisor, Professor Leonardo Simon for his guidance, advices and more importantly for encouragements throughout my graduate research study.

I would also like to thank my thesis review committee Dr Ali Elkamel and Dr Michael Pope for accepting to be readers of my thesis and for their advices and recommendations.

I would also like to thank my colleagues in Chemical Engineering graduate department, Dr Muhammad Arif, Andrew Finkle, Ryan Park, Dr. Ravindra Reddy and Dr Diogenes Vedoy for friendly assistances throughout my research study. I would also like to thank Mr Chong Meng for technical assistances and Mr. Saad Ahmed and Mr. Young Kim and other co-op students for assistances in running tests. I would like to thank Dr. Arash Joushaghani of University of Toronto for his assistances.

I also would like to thank NSERC and Ford Motor Company for providing financial support for this project and Braskem and SPB Solutions for supporting this project with donation of materials. I also want to thank Mr Keith Ward and Mr Marius Chitu of Magna Exteriors and Interiors for Dynatup tests and would like to thank Debel Neopan Corporation of Iran for providing access to particleboard factory and samples of Bagasse fibers and also would like to thank Pars Carpet Corporation of Iran for donating polypropylene samples for laboratory tests.

Finally, I would like to thank late Mr. Jim Nash of Enviroshake Inc. Too pity he cannot see me graduate.

Dedication

I would like to dedicate this thesis to my beloved wife Sogol, my parents, Ahmad and Faegheh and my siblings Amirhossein, Hanieh and Hassan Shafiee Monfared.

Table of Contents

List of Figures

List of Tables

List of Abbreviations

"	:	inches
μ	:	Microns
α	:	Level of Significance
ANOVA	:	Analysis of Variance
AO	:	Anti-Oxidant
ASTM	:	American Society for Testing and Materials
Back-rein	:	Back Reinforcement
BG	:	Bagasse
BRSK	:	Braskem Polypropylene Homopolymer
°C	:	Degrees Celsius
C	:	Carbon
C. Agent	:	Coupling Agent
CA	:	Coupling Agent
cm	:	Centimeters
CPC	:	Cellulose-Plastic Composite
D-LFT	:	Direct Long Fiber Reinforced Thermoplastic
D_{max}	:	Multi-Axial Impact Deflection at Maximum Load
DOE	:	Design of Experiment
DSC:	:	Digital Scanning Calorimetry
Et	:	Ethylene Group
F	:	Force
F_{max}	:	Multi-Axial Impact Maximum Load
g	:	grams
h	:	Hours
HALS	:	Hindered amine light stabilizers
HDPE	:	High Density Polyethylene
HO	:	Hydroxide or Hydroxyl group
IMA	:	Impact Modifier A (see SEBS)
IMB	:	Impact Modifier B (see SEPS)
J	:	Joules
K	:	Kelvin
kg	:	Kilograms
KN	:	Kilo Newton
kV	:	Kilo Volts
lb	:	pounds
LFT	:	long fibre reinforced thermoplastics
LOC	:	Location of Impact
m	:	Meters
MAPP	:	Polypropylene Grafted Maleic Anhydride
MFI	:	Melt Flow Indexing
mg	:	Milligrams

mid	:	Middle
min	:	minutes
ml	:	Milliliters
mm	:	millimeters
Mpa	:	Mega Pascals
N	:	Newtons
NFPC	:	Natural Fiber - Plastic Composite
nm	:	Nanometer
O	:	Oxygen
OH	:	Oat Hull
P	:	Phosphorous
PE	:	Polyethylene
PLYNR	:	Polynar Polypropylene Homopolymer
PP:	:	Polypropylene
PPMA	:	Polypropylene Grafted Maleic Anhydride
PSI	:	Pounds per Square Inches
P-value	:	Smallest Level of Significance for rejecting null hypothesis
PVC	:	Poly Vinyl Chloride
R*	:	Free Radical
R.	:	Free Radical
RO.	:	Alkoxide
ROH	:	Alcohol
ROO.	:	Peroxyl
ROOH	:	Hydroperoxide
ROOH	:	Alkyl-Peroxide
rpm	:	Rounds per Minute
S	:	Seconds
SEBS	:	Styrene Copolymerized with Ethylene/Butylene Copolymer
SEM	:	Scanning Electron Microscopy
SEPS	:	Styrene Copolymerized with Ethylene/Propylene Copolymer
t	:	Time
Tg	:	Glass Transition Temperature
TGA	:	Thermogravimetric analysis
T_m	:	Melting Temperature
UV	:	Ultra Violet
W	:	Watts
WPC	:	Wood-Plastic Composite
x	:	Displacement

1 Introduction

1.1 Objectives and Motivation

Natural fiber-plastic composites have gained great interest in recent years. Environmental regulations and the fact that fossil fuel resources of the world are approaching exhaustion, has been a motivation for researchers and scientists to find alternative materials to replace petroleum-based plastics used in consumer products, construction materials, logistics, automotive parts, etc.

Natural fibers are considered green alternatives to glass fibers that are currently used to reinforce petroleum-based plastics. The advantages of natural fibers over man-made fibers such as glass fibers are low cost, low density, competitive specific mechanical properties, carbon dioxide sequestration, sustainability, recyclability, and biodegradability (Mohanty, Misra, & Drzal, 2005). These are some motivations for replacing synthetic fibers with natural fibers for reinforcing plastics.

Combining petroleum based polymers and natural fibers have been of great interest in recent years for engineers and scientists. As Figure 1-1 illustrates, exponential interest has been observed in "Natural Fiber Plastic Composites" in past 7 years.

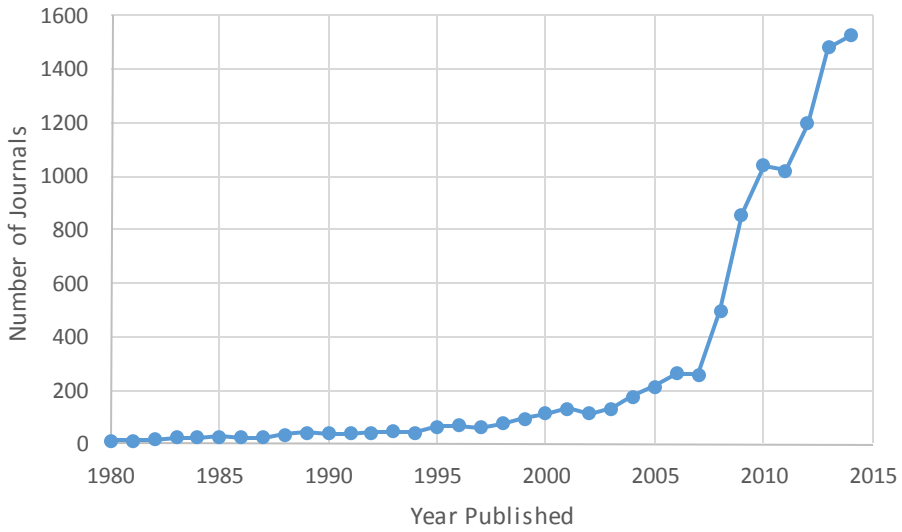

Figure 1-1: Number of Journals with keyword: "Natural Fiber Plastic Composite" on Scholar's portal of total 9823 published from 1980 to 2014

Some gaps of knowledge, that will be discussed in more details throughout section 2, were observed in the literature that motivated the author further, to perform this study. In brief, no study has been performed to compare effect of oat hull and bagasse on NFPC materials properties. As well, no study with both SEPS and SEBS materials as impact modifiers extruded with bagasse or oat hull has been performed. Furthermore, in majority of related literature papers and dissertations, a full DOE approach was not used to be able to verify test results using numerically measured confidence levels. In this dissertation, it is intended to provide a comparison of two types of fibers (bagasse and oat hull) in polypropylene based natural fiber plastic composites through comparing their mechanical properties. This comparison is done and validated using a purely statistical approach of fully factorial design of experiment.

The goal of this comparison is to better understand the role of adding bagasse, oat hull and additives to polypropylene as a means to produce economically reasonable product and meet target mechanical properties of the NFPC material in construction applications.

As well, in this dissertation, weathering of a final commercial building product and its relation to mechanical properties of the product is fully analyzed and validated using fully factorial design of experiment to be able to simulate effect of sunlight on mechanical properties of roofing material of a house.

1.2 Scope

This thesis evaluates two fiber types, one type of coupling agent, two types of impact modifiers and two grades of polypropylene. Composites were extruded, injection molded and tested for mechanical properties. Additionally, roofing shakes exposed to UV radiation were mechanically tested and evaluated. Statistical approach based on fully replicated factorial design of experiment was used throughout the above two groups of studies.

This thesis is composed of five key chapters. Chapter one consists of an introduction to the study and motivations of author for this study. In chapter two, a review of literature about materials, processing and characterization methods is presented. Chapter three describes materials preparation and equipment usage methods. Chapter four presents the results obtained from tests and discusses these results in detail. Finally, chapter five presents conclusions drawn based on chapter four results and discussions, and proposes some recommendations for future studies.

2 Literature Review

2.1 Definition: Natural Fiber Plastic Composite

According to ASTM standard (ASTM D7031-11, 2011) wood plastic composite is defined as a composite made primarily from plastics and wood or cellulose based materials. Another term for such composites is called Biocomposite and is defined as composite materials made from natural fiber and petroleum-derived non-biodegradable polymers.(Mohanty et al., 2005) As Natural Fibers and wood both include cellulose, it is reasonable to define cellulose plastic composite (CPC) a composite made primarily from plastics and cellulose based materials. As the main cellulose based material in this dissertation is Natural fiber, therefore Natural Fiber Plastic Composite (NFPC), Wood Plastic Composite (WPC), Cellulose Plastic Composite (CPC) and Biocomposite are used interchangeably and refer to same class of materials.

Natural Fiber Plastic Composites (NFPCs) are categorized into two sections, first fiber-thermoplastic composites and 2nd fiber-thermosetting composites. (C. Clemons, 2002) Application of thermosetting fiber plastic composites dates back to 1906 where it was used in Roll Royce Shifting knob. However, the interest is currently mainly on Natural Fiber Thermoplastic composites.

2.2 NFPC Markets and Challenges

According to Jacob, the decking and railing market in North America, the automotive market in Europe and the consumer market in Japan drive the demand of NFPC. (Jacob, 2006). In contrast to that, Haider and Eder report that the most application of NFPC in Europe, North America and Asia is decking (Haider & Eder, 2010) which is part of the construction sector.

In a more recent market report, the NFPC demand for building and construction sector was reported to have highest share in year 2014. The total size of the NFPC market worldwide is projected to reach $4,601.7 million in year 2019 with North America being largest consumer followed by Asia.(*Global wood plastic composite (polyethylene, polyvinylchloride, propylene, and others) market - trends & forecasts (2014 - 2019)*2014) It may be reasonable to conclude that majority of NFPC market in the world is heading towards the construction sector in next few years.

It is reported in the literature that the early uses for NFPC materials was applications such as automotive door panels, parcel shelves and roof panels, however, it has been reported as well that in year 2004, two thirds of worldwide NFPC market was in construction applications such as decking, railing, fencing, windows etc. (Pritchard, 2004) Figure 2-1 confirms the great and high portion of application of NFPCs in construction sector in North America.

Faruk et al. believe that flexibility during processing, highly specific stiffness, and low cost (on a volumetric basis) make natural fibers attractive to manufacturers of NFPC. (Faruk, Bledzki, Fink, & Sain, 2012) Faruk et al. as well concede that the greatest challenge in working with natural fiber reinforced plastic composites is their large variation in properties and characteristics. (Faruk et al., 2012)

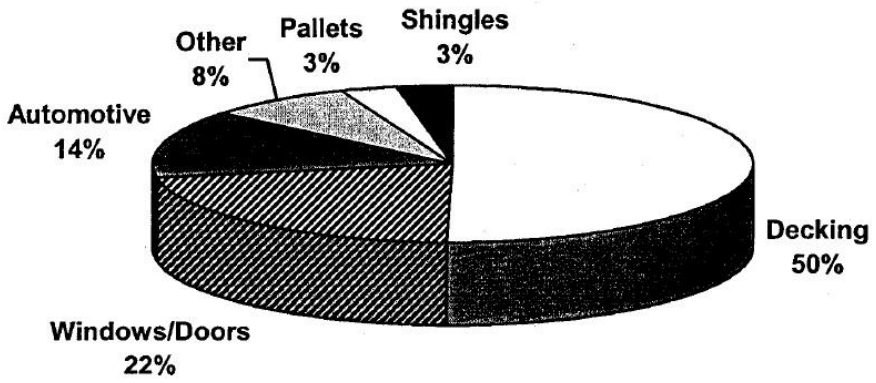

Figure 2-1: North American NFPC Market Shares (C. M. Clemons, 2000)

2.3 NFPC in Construction applications

Market reports confirm a strong presence of NFPC in construction sector of North America estimated to be $1200 million for year 2006 as presented in Table 2-1.

Table 2-1: NFPC Decking and Railing Market Size in North America (Klyosov, 2007)

	2004	2005	2006(projection)
Product		Dollar value(million)	
NFPC decking	670	766	929
NFPC railing	150	190	271
NFPC decking and railing	820	956	1,200

In a separate report for US market only, Stewart reports that Decking makes up 40% of the overall

US demand, moulding and trim 29%, fencing 10% and other outdoor products about 11%. (Stewart, 2010) It may be inferred that approximately 90% of the US NFPC market share belongs to construction applications and remaining 10% belongs to other NFPC applications.

NFPC has been used as roof shingles by a company called Teel-Global Resource Technologies using Polyethylene and recycled natural fibers and polyethylene. (C. Clemons, 2002)

Stewart suggests that NFPC roof shingles in Figure 2-2 are lighter and more durable, with a much less expensive installed cost. (Stewart, 2010)

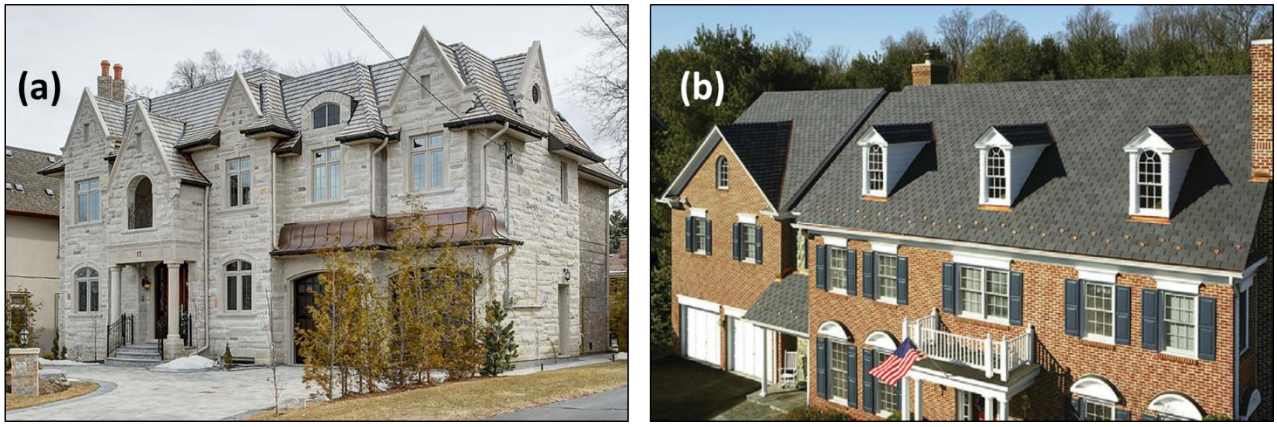

Figure 2-2: (a) A typical luxury house in Toronto with cedar roofing shakes. (b) A house in USA with NFPC Roofing shingles from CertainTeed ***((b):Stewart, 2010)***

2.4 NFPC Composition

Any NFPC material consists of three main parts. The matrix, the filler (fibers) and the additives. The matrix is the main structure in which other materials are connected to it to form the material. Fillers are materials either natural or unnatural that position themselves within the matrix and the additives that can be sub categorized into coupling agents, impact modifiers, and stabilizers.

Klyosov reports that in year 2005 90% of the matrix of NFPC used in North America was estimated to be polyethylene and the remaining 10% was estimated to be either polypropylene or poly vinyl chloride. (Klyosov, 2007) It is important to consider various properties of above three matrices commonly used in NFPC industry. Table 2-2 qualitatively summarizes some advantages of popular NFPC matrices over each other.

Table 2-2: NFPC Thermoplastic Matrix comparison ***(Klyosov, 2007)***

NFPC Matrix:			is preferred to	NFPC Matrix:			Due to
PE	PP	PVC		PE	PP	PVC	
●					●	●	Lower T_m (reduced filler degradation)
●					●	●	Easy to nail and screw
●					●	●	High resistance to oxidation
	●			●		●	Lighter (Lower Density)
	●			●		●	Higher Stiffness
	●			●		●	Improved creep resistance
	●			●		●	Higher flexural strength
		●		●	●		Higher Flame resistance

Based on Table 2-2, it appears that polyethylene offers a variety of advantages for outdoor construction application such as resistance to oxidation and easiness to install, however, polypropylene offers more mechanical benefits such as higher stiffness and higher flexural strength.

As mentioned above, polyethylene has been the dominant NFPC matrix thermoplastic in the past recent years, however, polypropylene, while having mechanical advantages, only has 5% of the NFPC matrix market in NFPC construction materials of North America. IHS Chemical estimates that average price for year 2015 per metric ton of high density polyethylene to be 1457 USD and for polypropylene homopolymer to be 1357 USD. Therefore, polypropylene being economically more advantageous. To gain further insight into the role of polypropylene in NFPC industry, this thermoplastic was chosen to be the composite's matrix material for this study.

2.4.1 Polypropylene as the Matrix

Polypropylene is a thermoplastic polyolefin manufactured through polymerization of propylene in presence of catalyst. With global demand of approximately 55 million MT in year 2013 (Market study: Polypropylene (3rd edition).) Polypropylene is one of main raw materials of the plastics industries. Various processes to manufacture this product are fluidized bed, bulk loop, stirred slurry tank, stirred gas phase bed and others. The gas phase process Spheripol® and Spherizone®, owned by LyondellBasell Industries N.V. are major licensed technologies used in polypropylene manufacturing companies. Figure 2-3 illustrates distribution of various technologies used worldwide.

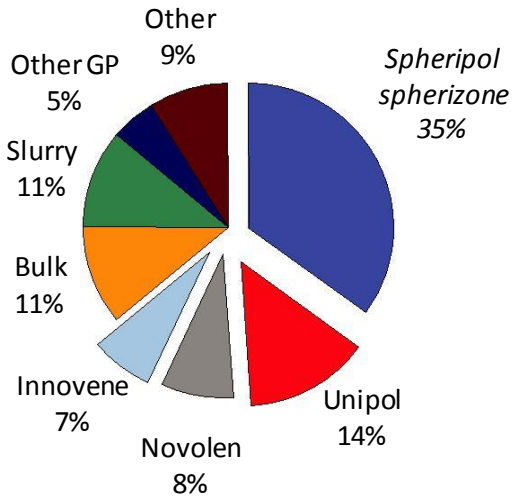

Figure 2-3: Polypropylene Manufacturing Technology Licenses worldwide (Mei et al., 2009)

Polypropylene general formula is presented in Figure 2-4. This macromolecule is the simplest appearance of polypropylene and it is referred to as polypropylene homopolymer, however, polypropylene macromolecules are not as simple as shown in this figure.

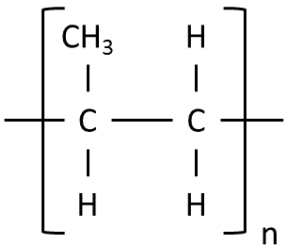

Figure 2-4: Repeating unit of Polypropylene

The spatial position of the hanging methyl group around the polymer chain is effective on the crystallinity of the polypropylene macromolecule and therefore effective on the properties of the final product. Based on position of the hanging methyl groups in the space around the backbone, three stereochemical configurations of polypropylene homopolymer macromolecules are identified. When the methyl groups are all on one side of the polymer chain backbone, the polymer chain is referred to be isotactic. If the methyl groups are on alternate sides of the chain, they are referred to as syndiotactic. When the methyl groups are randomly arranged around the carbon backbone of polymer chains, the polypropylene homopolymer is referred to as atactic. Figure 2-5 shows various spatial arrangements of polypropylene homopolymer.

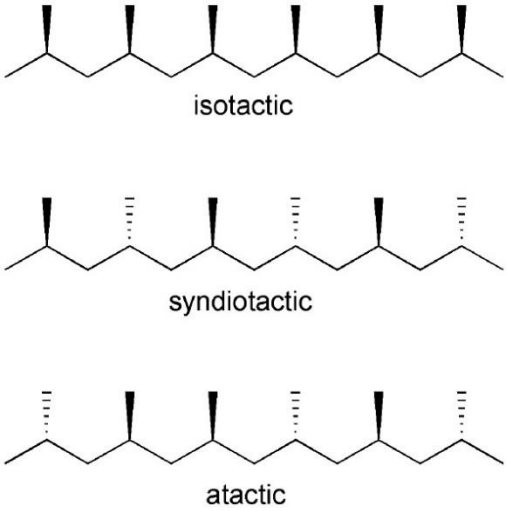

Figure 2-5: Stereochemical arrangements of polypropylene stereo isomers (Hagen, Boersma, & van Koten, 2002)

Tacticity therefore, refers to percent of methyl groups symmetrically arranged around the polymer chain, with 100% tacticity for all of the methyl groups being arranged on one side of the backbone (same definition applies for syndiotactic arrangement but on alternate positions) and 0% tacticity for fully random arrangement of methyl groups around the chain. High-tacticity polypropylene has appropriate mechanical, physical and thermal properties, although atactic polypropylene is soft and sticky mainly used in caulking and sealant applications. (Karian, 2003) Tacticity of polypropylene strongly influences the crystallinity of polypropylene. Defects in tacticity of the chain causes the chains not to pack well during crystallization and therefore decrease the crystallinity percentage and increase the amorphous regions. (Moore, 1996)

The glass transition of polypropylene homopolymer at about 0°C causes the material to act brittle below this temperature which is undesirable. For some applications, the homopolymer is too rigid and has poor transparency which is undesirable. (Moore, 1996) Ethylene co-monomers may be added to polypropylene during polymerization reaction to appear within carbon backbone of polypropylene macromolecules to improve the undesirable properties. If the ethylene added to the polypropylene backbone is at 1-8% levels, resulting material is called random copolymer. The ethylene content decreases the total crystallinity of the polymer leading to a decrease of stiffness and melting point with this polypropylene grade. Some applications of random copolymer are in optical and sealability applications. A random copolymer at 45%-65% ethylene content commixed with polypropylene homopolymer results in a heterophasic copolymer which is referred to as impact copolymer with applications where enhanced impact resistance is needed at freezer temperatures

and below. (Karian, 2003) Figure 2-6 illustrates inputs and three major outputs of a typical polypropylene manufacturing factory.

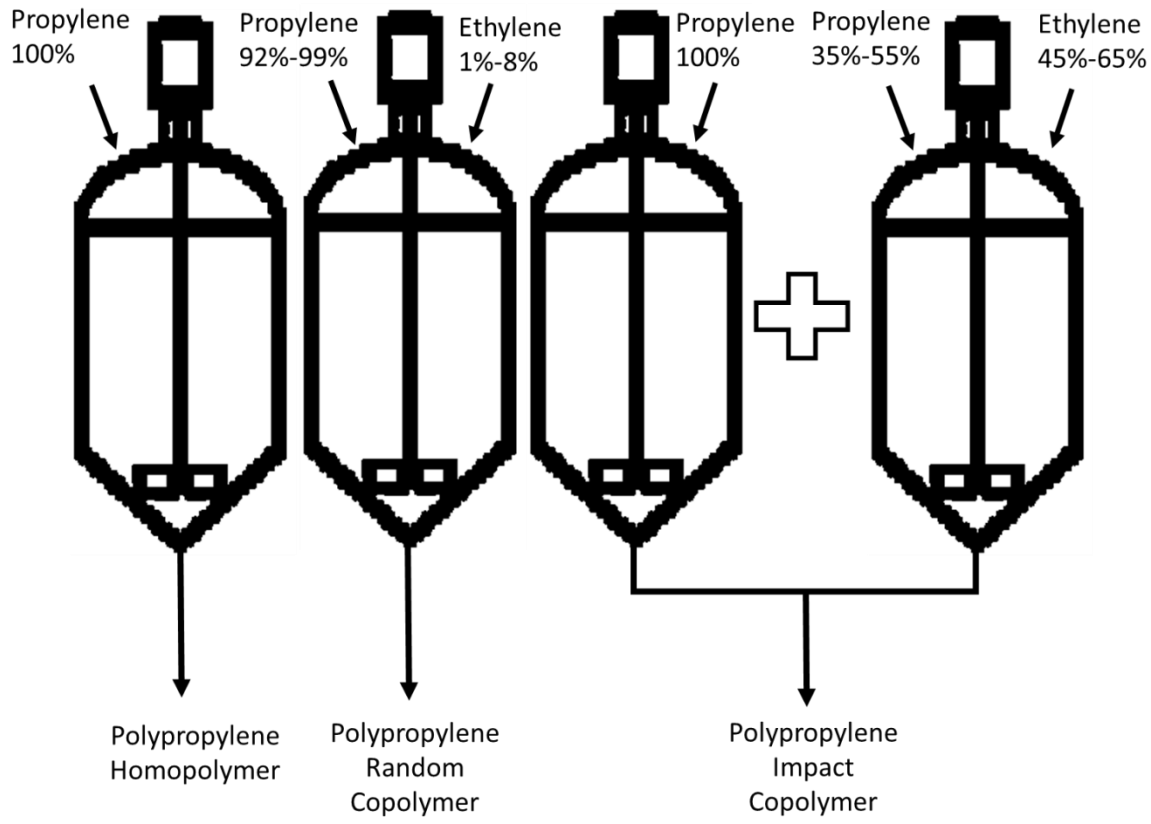

Figure 2-6: Polypropylene Homopolymer, Random Copolymer and Impact copolymer production schematics

2.4.2 Natural Fibers as Fillers

Faruk et al. suggests that natural fibers are attractive fillers for composites industry due to flexibility in processing, low cost and highly specific stiffness. (Faruk et al., 2012)

Table 2-3 shows six general types of fibers based on the botanical type of natural fibers. (Pickering, 2008) Other fiber classifications have been done in the literature. Bogoeva et. al. classify natural fibers based on performance of the fiber within the polymer matrix into three categories: (1) wood flour particulate, which improves the tensile and flexural modulus of the composites. (2) Fibers of higher aspect ratio that improve the composites modulus and strength with suitable additives and (3) long natural fibers with highest efficiency amongst the lignocellulosic reinforcements. (Bogoeva-Gaceva et al., 2007)

Table 2-3: six general types of natural fibers (Pickering, 2008)

Bast	Leaf	Seed					Core	Grass/ reeds	Other
		Fibers	Pod	Husk	Fruit	Hulls			
Hemp	Pineapple	Cotton					Kenaf	Wheat	Wood
Ramie	Sisal		Kapok				Jute	Oat	Roots
Flax	Agava		Loofah				Hemp	Barley	Galmpi
Kenaf	Henequen		Milk weed				Flax	Rice	
Jute	Curaua			Coir				Bamboo	
Mesta	Banana				Oil palm			Bagasse	
Urena	Abaca					Rice		Corn	
Roselle	Palm					Oat		Rape	
	Cabuja					Wheat		Rye	
	Albardine					Rye		Esparto	
	Raphia							Sabai	
	Curauá							Canary grass	

Worldwide inventory of natural fibers is reported in Table 2-4.

Table 2-4: Worldwide inventory of natural fibers (Pickering, 2008)

Fiber source	World (dry tonnes)
Wood	1 750 000 000
Straw (wheat, rice, oat, barley, rye, flax, grass)	1 145 000 000
Stalks (corn, sorghum, cotton)	970 000 000
Sugar cane bagasse	75 000 000
Reeds	30 000 000
Bamboo	30 000 000
Cotton staple	15 000 000
Core (jute, kenaf, hemp)	8 000 000
Papyrus	5 000 000
Bast (jute, kenaf, hemp)	2 900 000
Cotton linters	1 000 000
Esparto grass	500 000
Leaf (sisal, abaca, henequen)	480 000
Sabai grass	200 000
Total	**4 033 080 000**

Literature suggests that major fibers currently being used in natural fiber plastic composites are hemp, kenaf, flax, and sisal. (Mohanty et al., 2005) Faruk et. al. report and review thirteen kinds of

natural fibers commonly used in natural fiber plastic composite industry: flax, hemp, jute, kenaf, sisal, abaca, pineapple leaf fiber, ramie, coir, bamboo, rice husk, palm fiber and bagasse. (Faruk et al., 2012) Based on Table 2-4, bagasse alone appears to be an inert fiber with a comparatively huge supply worldwide. On the other hand, oat hull is hardly referred to in the literature for application in natural fiber plastic composites. Bagasse and oat hull will be further examined and studied as natural fiber filler of this study.

2.4.2.1 Bagasse

Bagasse, illustrated in Figure 2-7, is a fibrous residue that remains after crushing the stalks of sugar cane and contains short fibers and consists of cellulose, hemicellulose and lignin as three main constituents.

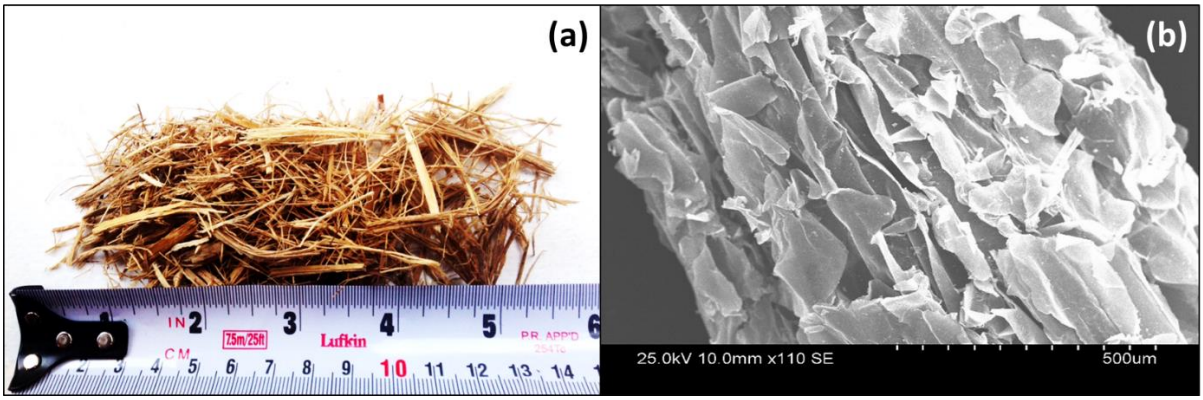

Figure 2-7: (a) Bagasse Fibers in inches scale (b) Bagasse fiber in microns scale

Therefore, bagasse is referred to in the literature as a lignocellulosic fiber. Nilza et al. reports that 27 wt% of bagasse fibers to be Si^{4+} ions and other ions such as Al^{3+}, Ca^{2+}, Mg^{2+} and Na^{+} present in a fraction of Si^{4+} wt%. As mentioned in Table 2-4, worldwide yearly production of dry bagasse is approximately 75M tonnes which is very substantial, however, it is regretful to mention that according to Verma et. at. approximately 85% of bagasse produced worldwide is burnt (Verma, Gope, Maheshwari, & Sharma, 2012)

Table 2-5: Dimensions and chemical composition of some natural fibers(Mohanty et al., 2005)

Type of Fiber	Cellulose (%)	Lignin (%)	Fiber Dimension (mm)	
			Mean length	Mean width
Cotton	85–90	0.7–1.6	25.0	0.02
Seed flax	43–47	21–23	30.0	0.02
Hemp	57–77	9–13	20.0	0.022
Abaca	56–63	7–9	6.0	0.024
Coniferous wood	40–45	26–34	4.1	0.025
Sisal	47–62	7–9	3.3	0.02
Bamboo	26–43	21–31	2.7	0.014
Kenaf	44–57	15–19	2.6	0.02
Jute	45–63	21–26	2.5	0.02
Esparto	33–38	17–19	1.9	0.013
Papyrus	38–44	16–19	1.8	0.012
Sugar cane bagasse	32–37	18–26	1.7	0.02
Cereal straw	31–45	16–19	1.5	0.023
Corn straw	32–35	16–27	1.5	0.018
Wheat straw	33–39	16–23	1.4	0.015
Rice straw	28–36	12–16	1.4	0.008
Deciduous wood	38–49	23–30	1.2	0.03
Coir	35–62	30–45	0.7	0.02

Table 2-5 shows chemical composition and dimensions of some of natural fibers. Length of bagasse fibers appear to be in the shorter region of the table with 30% cellulose content and 20% lignin content. Sasaki et. al report the chemical composition of bagasse to be cellulose 35.0%, hemicellulose 35.8%, lignin 16.1% and water content 3.5%.(Sasaki, Adschiri, & Arai, 2003) On the other hand Nilza et al. report that Bagasse lignin content to be 13%, Cellulose 30% and hemicellulose 57% (Jústiz-Smith, Virgo, & Buchanan, 2008) As well, Sun et al. report that about 40 to 50% of bagasse is cellulose, (a crystalline structure, 25 to 35% is hemicelluloses, an amorphous polymer and the rest mostly lignin.(Sun, Sun, Zhao, & Sun, 2004)

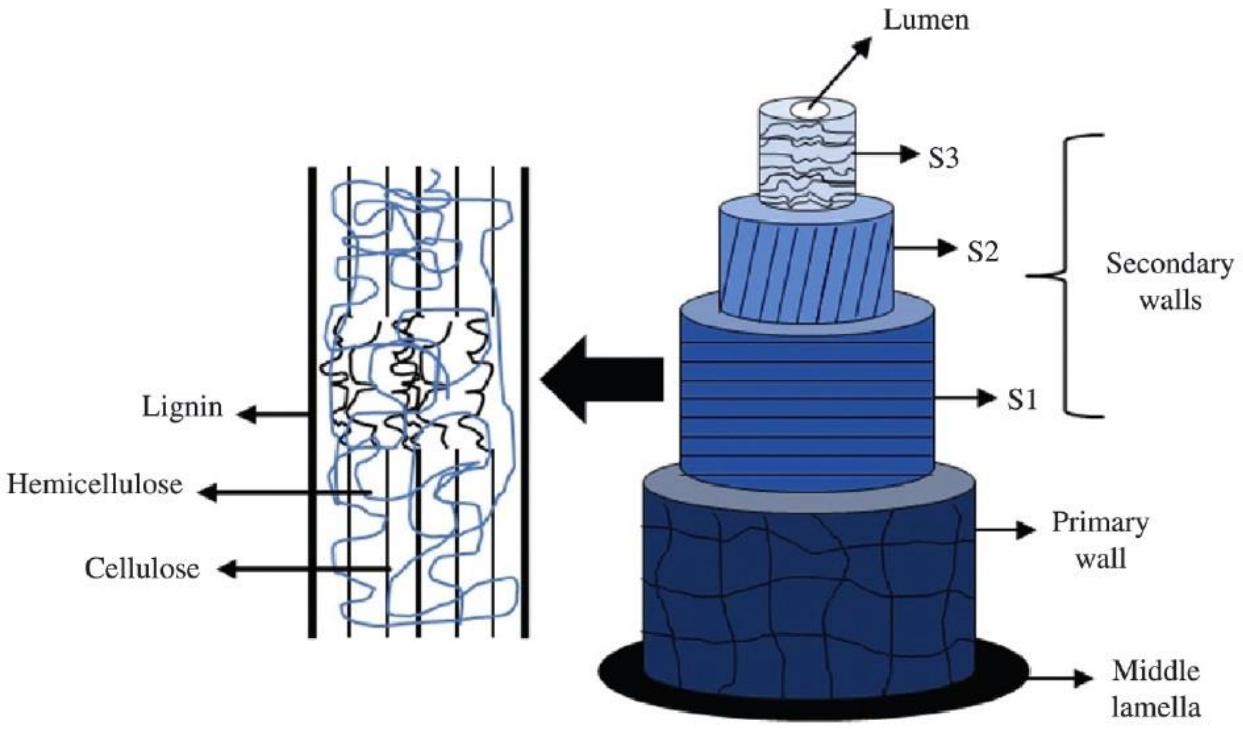

Figure 2-8: Schematic representation of plant fiber structure: primary wall, middle lamella, lumen, S1 - external secondary wall, S2 - middle secondary wall and S3 -internal secondary wall **(Pereira et al., 2015)**

Figure 2-8 shows a typical structure of a vegetal fiber such as bagasse with cellulose as the crystalline part and hemicellulose as the amorphous region.

Pereira et al. report bagasse chemical composition to be 69.4 wt% cellulose, 21 wt% hemicellulose, 4.4 wt% lignin and the rest ashes. The crystallinity index is reported to be 45.2% (Pereira et al., 2015)

Nilza et al. propose that since cellulose is a natural polymer and its structure serves as a carbon reservoir, it has a higher Young's modulus compared to thermoplastic materials and therefore contributes a higher increment of stiffness to the natural fiber plastic composite, as well, high lignin content allows the fibre to be resistant to rotting under wet and dry conditions to have a better tensile strength. (Jústiz-Smith et al., 2008)

Luz et al. in a study in year 2008 compare various compounds of chemically conditioned and unmodified bagasse fibers and saw dust polypropylene composites without any coupling agent or additive through mechanical tests and conclude a poor interfacial bond between bagasse fibers and matrix and observed general increase in rigidity of such composites resulting in higher flexural

modulus. (Luz, Gonçalves, & Del'Arco, 2007) In contrast to Luz et al.'s study, Ramaraj studied acid and base washed bagasse fibers of 5-20 wt-% in polypropylene matrix with no coupling agent or additive and reported 10% to 30% increase in mechanical properties such as flexural, izod impact and charpy impact compared to pure polypropylene, however, he reported huge decrease in elongation at break of the composites compared to pure polypropylene. (Ramaraj, 2007)

In a different study, Shibata et al. compared bagasse polypropylene composites with Kenaf and polypropylene, again, with no coupling agent or additive added, and claimed a clear inverse correlation existing between Young's modulus of composites and density of fibers. (Shibata, Cao, & Fukumoto, 2006)

In a more recent study, Samariha et al. studied polypropylene bagasse composites with presence of MAPP coupling agent and concluded MAPP coupling agent to be effective on impact properties at high bagasse contents of 45 wt-%. (Samariha et al., 2013)

2.4.2.2 Oat hull

Oat hull is a seed type natural fiber as listed in Table 2-3. Oat hull fiber anatomy is illustrated in Figure 2-9.

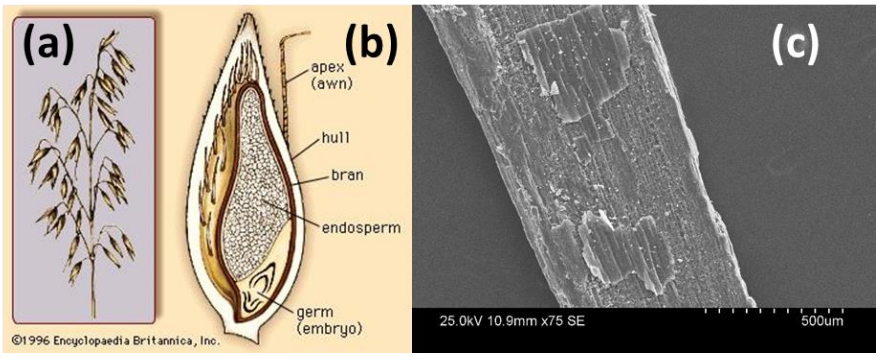

Figure 2-9: (a) oat oanicle, (b) oat grain cross section(Oats. Encyclopædia britannica.) *(c) SEM Image of Oat Hull*

It has been reported in literature that the chemical composition of oat hull is cellulose (70%), hemicellulose (25%), and lignin (max 5%) (Gras notice 000342: Oat hull fiber.2010)

Araujo et al. report that for oat hull polypropylene composites of oat hull content over 20%, mechanical strength of the composite decreases significantly due to discontinuities in polymer matrix in absence of coupling agent. (Margoto, Moris, Vírginia A da S., & Paiva, Jane M F de., 2015)

Rowel et al. compounded twelve types of natural fibers including polypropylene filled with 50% oat hull and coupling agent and compared results with 50% talc filled polypropylene and concluded approximately equal tensile strength, tensile modulus, flexural strength and flexural modulus for oat hull filled polypropylene compared to talc filled polypropylene. They also concluded deteriorated notched Izod impact energy for oat hull filled polypropylene compared to talc filled polypropylene. (Rowell, Sanadi, Caulfield, & Jacobson, 1997)

2.4.3 Coupling Agents

Faruk et al. emphasize that the adhesion of natural fiber to polymer matrix is the main issue as it dictates the properties of the composite (Faruk et al., 2012)

Two main purposes have been mentioned in the literature for using coupling agents in the composite blend. First is to distribute the filler in matrix as uniformly as possible and second to bridge the interface between the polymer matrix and the fiber. (Klyosov, 2007)

The dispersed phase of the blend contains fibers, where cellulose is the main structure in a fiber, and the mechanical properties of the natural fiber depends on its geometry. Cellulose possesses a crystalline structure and contains hydroxyl groups that can form hydrogen bonds both within the cellulose molecule and outside of the cellulose molecule and therefore cellulose is hydrophilic. The degree of crystallinity of cellulose is 10 to 100 times higher than hemicellulose, and hemicellulose is a branched polymer, whereas cellulose is a strictly linear polymer. (A. K. Bledzki & Gassan, 1999) A schematic of cellulose polymer is presented in Figure 2-10.

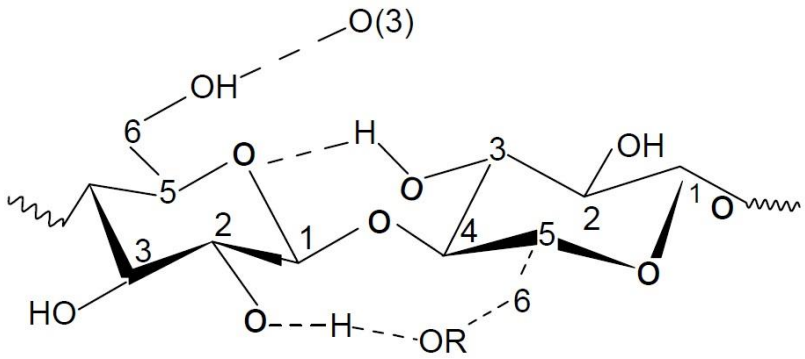

Figure 2-10: Cellulose molecule with intermolecular and intramolecular hydrogen bonds **(Mohanty et al., 2005)**

The matrix contains polymers such as polypropylene which is a non-polar substance and hydrophobic. Therefore, a poor adhesion exists between the two parts of the blend. Coupling agent is introduced to marry these two opposing phases to each other, to be able to blend well and increase mechanical properties of the composite. Therefore, a proper coupling agent such as polypropylene grafted maleic anhydride has two domains, one that forms entanglements or segmental crystallization with polypropylene matrix and the other domain strongly interacts with the filler via covalent bond, hydrogen bonds or ionic interactions. Figure 2-11 shows polypropylene grafted maleic anhydride. If the surface of fibers is conditioned with materials such as alkaline aqueous solutions, the surface area of cellulose would increase and therefore more bonds may form between coupling agent and cellulose.

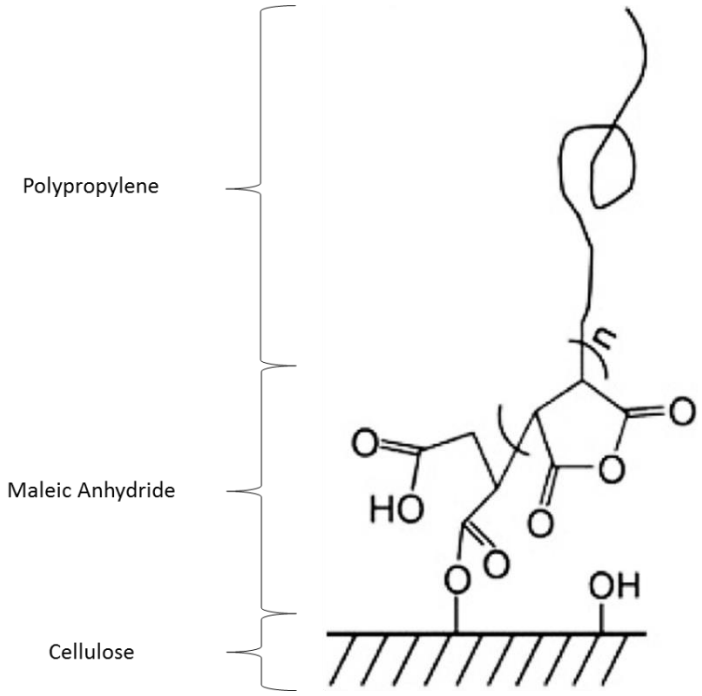

Figure 2-11: A chain of grafted polypropylene maleic anhydride bonded to cellulose surface (Qiu, Endo, & Hirotsu, 2006)

Extensive studies have been performed to study the effect of grafted polypropylene maleic anhydride coupling agent on mechanical properties of natural fiber plastics composites. As an example, Bledzki and Faruk studied effect of grafted polypropylene maleic anhydride coupling agent at 5% level on various types of wood samples and concluded to be very effective on tensile and flexural strengths and moderate positive effect on impact energies and substantial reduction in hygroscopicity of samples. (A. Bledzki & Faruk, 2003)

2.4.4 Impact Modifiers

Poor impact resistance of polypropylene matrix especially at low temperatures and high load conditions is the main deficiency of this commodity and therefore, to increase impact properties of polypropylene composites, elastomers are introduced into the blend. (Tjong, Xu, Li, & Mai, 2002)

Thermoplastic elastomers are one type of such impact modifiers with high processability but limited elasticity. TPEs have two domains, rigid and flexible phase, and are produced by copolymerization of rigid and flexible sequences in same molecule and then are blended in a thermoplastic matrix as illustrated in Figure 2-12.

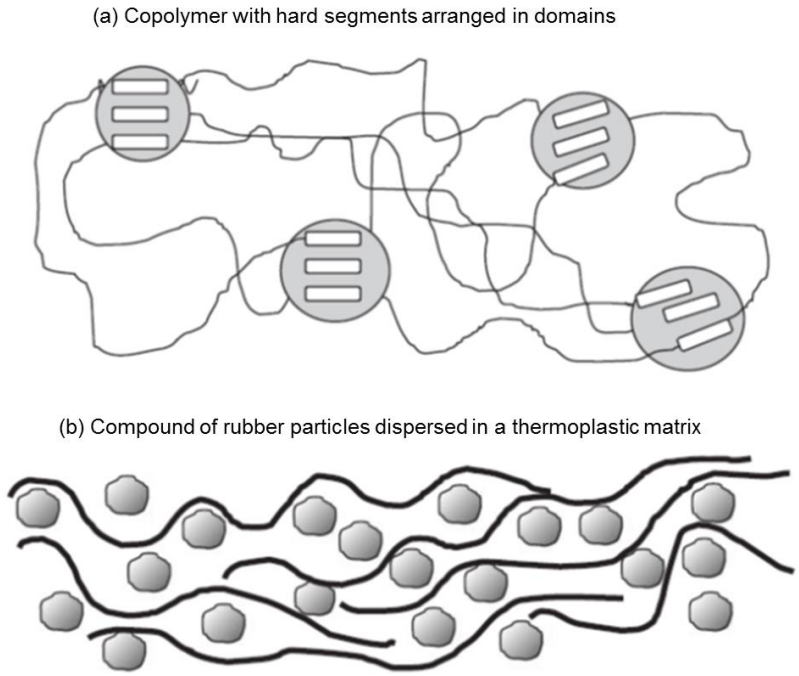

Figure 2-12: Thermoplastic Elastomers **(Biron, 2012)**

If the rigid phase of the TPE is chosen to be styrene, then the copolymerization of styrene with ethylene/butylene copolymer commixed with polystyrene will result in SEBS, and if styrene is copolymerized with ethylene/propylene co-monomers and commixed with polystyrene, SEPS is produced. SEBS and SEPS structures are illustrated in Figure 2-13 and Figure 2-14 respectively.

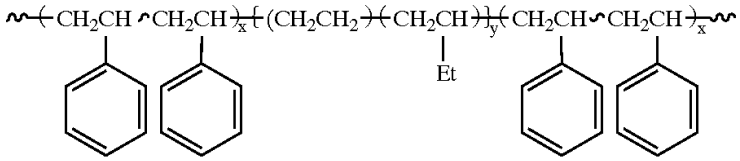

Figure 2-13: SEBS (IMA) chemical structure **(Vachon, 2002)**

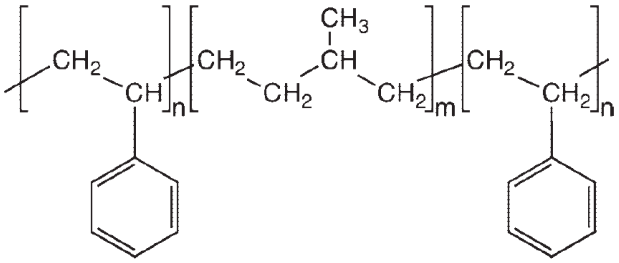

Figure 2-14: SEPS (IMB) chemical structure **(Shimizu & Saito, 2009)**

The rubber domains have low Tg and therefore are rubbery at room temp, however, styrene blocks have high Tg and therefore are rigid at room temperature. At elevated temperatures, the styrene blocks are destroyed and can be easily fabricated and act as thermoplastics and therefore are easily processed, but at low temperatures, they act as elastomers.

Tjong et al. studied effect of SEBS on polypropylene-glass fiber composites and report that highest tensile strength is achieved through blending SEBS and MAPP with polypropylene, although strong bond between glass fiber dispersed phase and polypropylene matrix can impair the fracture resistance of composites containing polypropylene, SEBS elastomer and polypropylene grafted maleic anhydride. (Tjong et al., 2002) In a more recent study, Sharma and Maiti studied NFPC composites of teak floor and PP/SEBS grafted maleic anhydride and reported that although introduction of teak floor in the blend increased the tensile modulus and strength of the composite due to good phase interactions, introduction of teak floor in the blend decreased its elongation at break and impact properties due to increased points of stress concentrations around wood fiber particles. (Sharma & Maiti, 2015)

Matsuda and Hara studied effect of volume fraction of styrene dispersed phase on toughness of SEBS, SEPS and SEP blends with isotactic polypropylene. They concluded that the efficiency of toughness improvements was affected both by the strength of the elastomer as well as the volume fraction of the styrene dispersed phase which depended on the compatibility to polypropylene matrix. (Matsuda, Hara, Mano, Okamoto, & Ishikawa, 2005) No study has yet been done using both SEPS and SEBS in a blend of natural fiber polypropylene composite.

2.4.5 Antioxidants

The micro-branched structure of polypropylene as presented in Figure 2-5, where hydrogens in tertiary carbons are present, makes formation of peroxides through thermo-oxidation and photo-oxidation easier compared to polyethylene. (Klyosov, 2007)

Polypropylene exposure to heat and shear causes polymer chain scission and getting exposed to oxygen causes self-propagated oxidation of the natural fiber-polypropylene composite. Due to branched structure of polypropylene, chain cleavage dominates the free radical degradation of the composite. Antioxidants interfere with propagation of free radical reactions through scavenging free radicals (Primary Antioxidants) or reacting with secondary hydroperoxides (Secondary Antioxidants).

Figure 2-15 illustrates a general degradation mechanism for polymers and interference of antioxidants in the process.

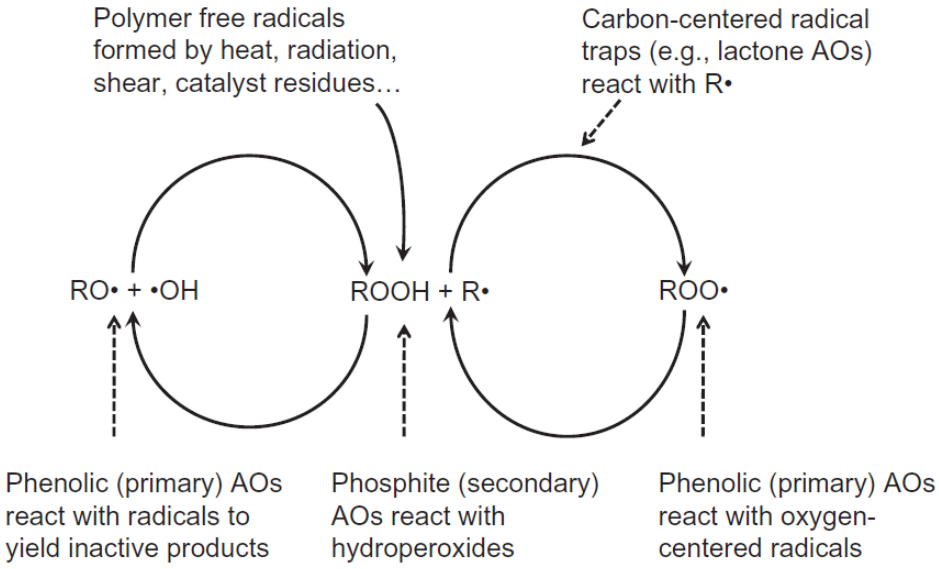

Figure 2-15: Self-propagating auto-oxidation of polymers. Dotted lines indicate points of Antioxidant interference for deactivating unwanted reactions (Tolinski, 2015)

Hindered phenolic antioxidants such as Irganox 1010, are one of the major primary antioxidants or radical scavengers, where hydroxide group is sterically hindered by adjacent hydro carbon units attached to phenolic ring which enables donating hydrogen to kill free radicals. The antioxidant converts to an inactive phenoxy radical and initiating new radicals are prevented.

Synergically, secondary antioxidants such as phosphite-based Irgafos 168, kill propagation reactions and convert ROOH to ROH which is an alcohol. The anti-oxidant converts to stabilize phosphates.

It has been reported in literature that secondary antioxidants can lower the amount of more expensive primary antioxidant. Phenolic and phosphite-based antioxidants help retain melt flow and color stability through repeated processing, better than each antioxidant individually. (Tolinski, 2015)

Voigt et al. suggest that best synergism is achieved when primary phenolic and secondary phosphite antioxidant ratio is set between 1:1 and 1:4 depending on process and substrate conditions. (Voigt & Todesco, 2002) Figure 2-16 illustrates a suggested mechanism for (a) radical scavenging and (b) propagation stabilization reactions.

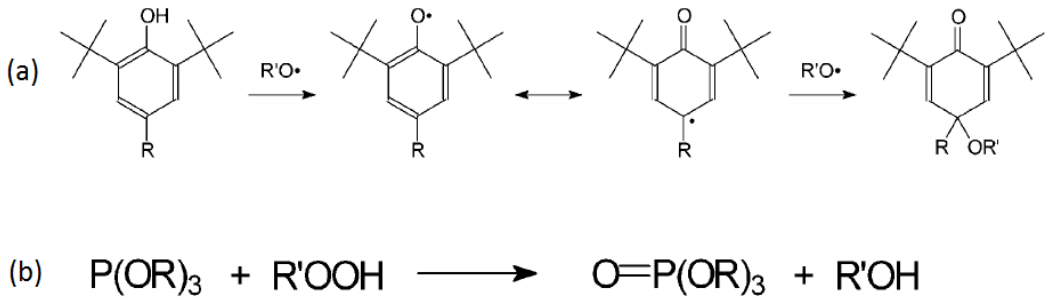

Figure 2-16:(a) Stablization mechanism for phenolic (primary) antioxidant, (b) Stabilization Mechanism for Phosphorous based (secondary) Antioxidant (Voigt & Todesco, 2002)

2.5 UV degradation

Ultraviolet (UV) degradation of polymers, which takes precedence over heat-induced degradation of polymer, is especially important when natural fiber plastic composite is exposed to sun light for extended times (i.e. in housing industry). Degradation is initiated by breaking double bonds and forming free radicals on UV-absorbing species or so called chromophorms such as pigments, catalyst residues, etc. mixed in the polymer. As the polypropylene or polyethylene molecules are saturated, UV radiation would not be absorbed by the polymer molecules.

Once the radicals are formed through UV degradation to chromophorms, the rest of the degradation cycle is similar to Autoxidation process portion of Figure 2-15. It has been reported in literature that required UV wave length for polyethylene degradation is 300 - 310 nm and 340 nm, however for polypropylene is 290 - 300 nm and 330 - 370 nm. Two major groups of additives to prevent UV degradation are (a) UVAs or UV absorbents like benzophenones, benzotriazoles, carbon black, pigments, TiO_2, etc., which physically shield polymer and absorb UV radiation while converting into heat and/or non-harmful materials, and (b) HALS or hindered amine light stabilizers which are radical scavengers, killing free radicals and stop propagation of free radicals. (Tolinski, 2015)

As an example of mechanism of UV absorption, Figure 2-17 shows mechanism of absorption of UV energy and dissipation of heat of a benzophenone-type UV absorber.

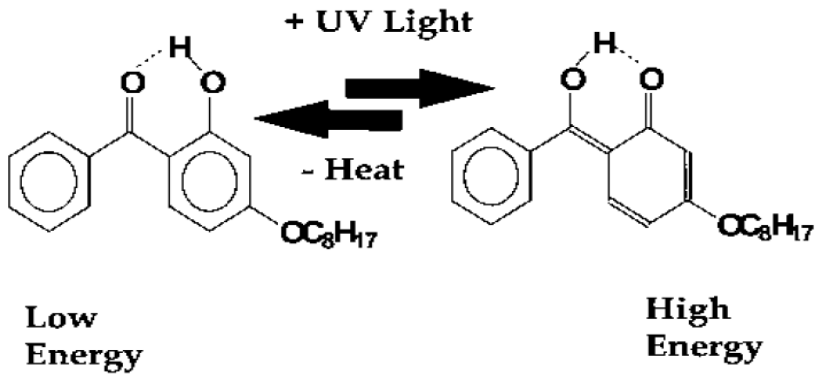

Figure 2-17: Mechanism of UV stabilization using a non-consuming Benzophenone-type UV absorber (Lowilite 22)(Karian, 2003)

Experts have studied effect of UV degradation on natural fiber polypropylene composites. Abu-Sharkh and Hamid studied effect of artificial and natural weathering conditions on date palm polypropylene composites with and without MAPP compatibilizers and UV stabilizing additives and concluded higher stability for natural fiber polypropylene composite compared to pure polypropylene; although; they also concluded that MAPP destabilizes the composite against weathering conditions.(Abu-Sharkh & Hamid, 2004) In a different study with HDPE based NFPC, Muasher and Sain studied effect of hindered amine light stabilizers and ultraviolet absorbers on stabilization of composite construction materials for a period of 2000 hours. Their study proposed some mechanisms of degradation including a mechanism for lignin degradation and concluded high molecular weight diester HALS to be most effective against discoloration and fading in long term. (Muasher & Sain, 2006) Treating fibers with MAPP, Joseph et al. studied effect of artificial UV radiation of 12 weeks on polypropylene sisal composites and concluded that tensile strength of MAPP treated composites degraded more than tensile strength of untreated samples. (Joseph, Rabello, Mattoso, Joseph, & Thomas, 2002)

2.6 NFPC processing methods

Processing technologies for natural fiber thermoplastic composites include extrusion, injection molding, compression molding, LFT-D-method, and thermoforming. (Faruk et al., 2012)

2.6.1 Extrusion

Extrusion is a process were hot molten pressurized natural fiber plastic composite is passed by a screw through a barrel were ultimately NFPC is converted either into a continuous sheet or pellet or

granules. There are various unit operations in an extruder design. Feeding, heating (through shear heating within materials or through external electrical heaters), mixing (dispersive or distributive), devolatilization (moisture and volatiles removal) and pumping (overcoming flow resistance) Figure 2-18 presents some of these operations and post extrusion processes.

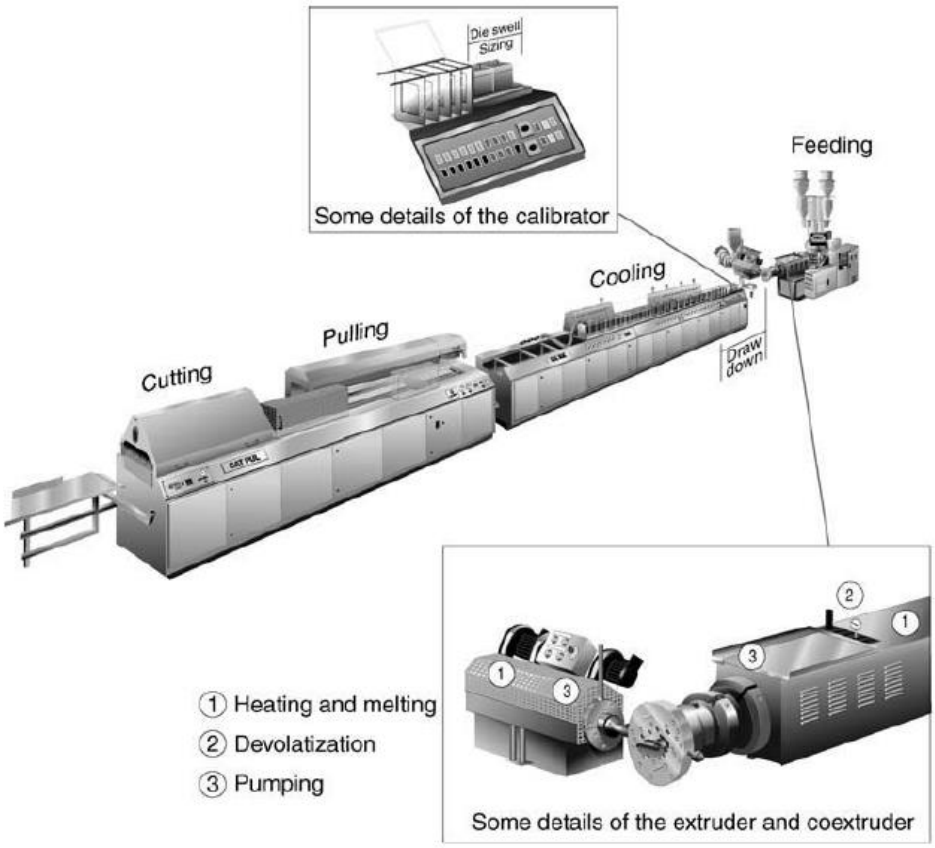

Figure 2-18: Schematic of unit operations of an extruder (Mohanty et al., 2005)

Experts suggest twin screw, co-rotating, self-wiping intermeshing extrusion is most suitable extrusion method to achieve best final attributes in natural fiber polymer composite mainly due to robust and intimate dispersive and distributive mixings. (Mohanty et al., 2005) Conical twin screws with counter rotation schematic are presented in Figure 2-19.

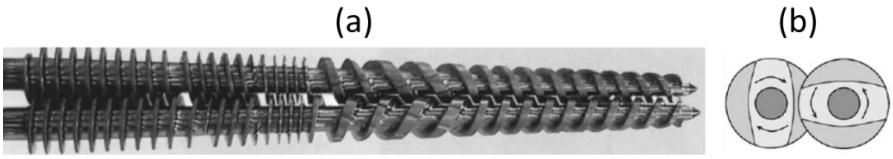

Figure 2-19: (a) Conical corotating twin screw extruder screws. (b) corotating configuration of twin screws(Giles Jr, Mount III, & Wagner Jr, 2004)

Filling of lumens of fibers during compounding is a function of residence time, difference in matrix and composite viscosity (affected by temperature), degree of moisture removal, die design and die pressure buildup. A descriptive diagram is presented in Figure 2-20.

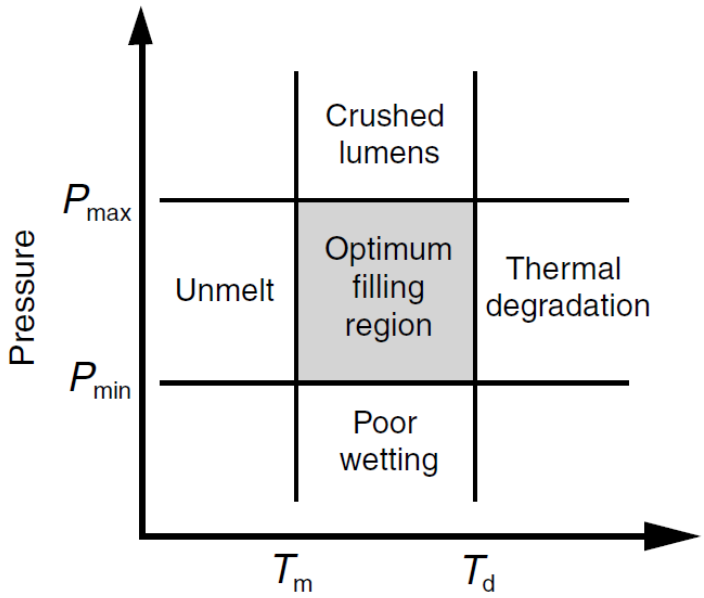

Figure 2-20: Criteria window for filling lumens of fibers **(Mohanty et al., 2005)**

Regarding the molten material flowing in the extruder barrel, moisture control and fibers aspect ratios are critical. Trapping of moisture in barrel causes unwanted reactions in the extruder and formation of acid that causes wear to the barrel. It is important to maintain aspect ratio of fibers to maintain fiber reinforcement efficiency in the composite. An important drawback in NFPC processing through extrusion is low heat conductivity of profiles. This affects line speed and profile design and ultimately the cost of the NFPC composite extruded product.

2.6.2 Injection molding

Injection molding is one of the major polymer processing methods accounting for approximately one third of all polymer processing methods. Some benefits of this method includes excellent dimensional tolerance, short cycles and little post processing needed.

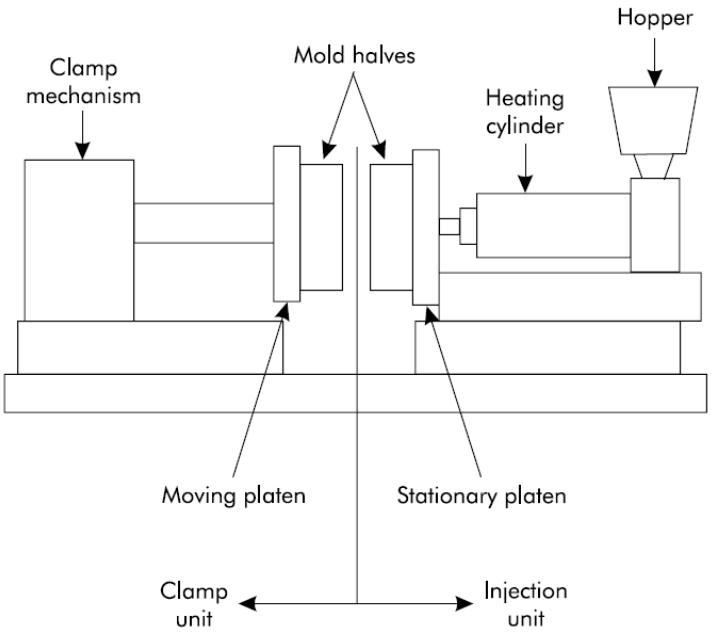

Figure 2-21: The injection molding process (Bryce, 1999)

It has been reported that most fiber attrition in injection molding processes occur in the transition section of screw. (Mohanty et al., 2005) Bledzki and Faruk report that NFPC samples of same composition show higher tensile strength, flexural modulus and impact resistance when injection molded compared to compression molded. (A. K. Bledzki & Faruk, 2004) A processing window for injection molding is presented in Figure 2-22. Figure 2-22: Processing window for injection molding of natural fiber plastics composites (Mohanty et al., 2005)

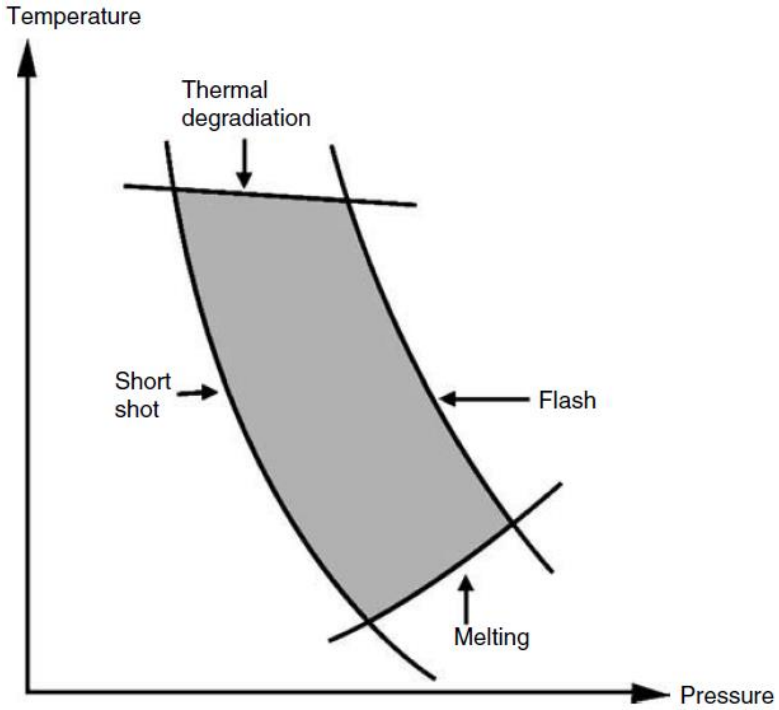

Figure 2-22: Processing window for injection molding of natural fiber plastics composites (Mohanty et al., 2005)

2.6.3 Compression Molding

Compression molding is a method for manufacturing large, light, strong and thin natural fiber plastic composites where low fiber attrition occurs compared to injection molding. Figure 2-23 shows a schematic of compression molding process. Bledzki and Faruk propose that compression molding processing method is appropriate for thermoplastic composites where different layers of composite material are retained after molding. As well they conclude that NFPC samples of same composition show increased charpy impact compared to same injection molded samples. (A. K. Bledzki & Faruk, 2004)

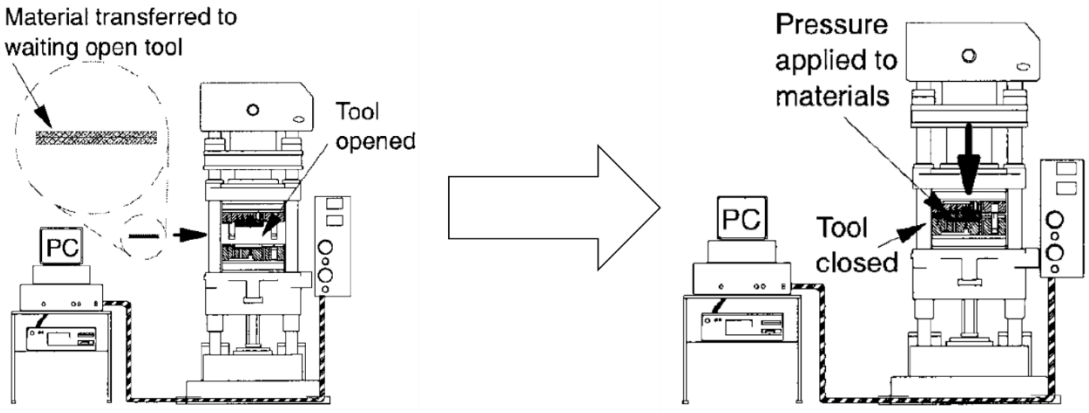

Figure 2-23: Schematic of a hot flow compression molding machine (Wakeman, Cain, Rudd, Brooks, & Long, 1999)

2.7 Characterization of Natural Fiber - Plastic Composites

2.7.1 Impact Properties

2.7.1.1 Notched Izod Impact

Notched Izod impact is a method to find if the notched piece will crack in a ductile or brittle behaviour and how much energy does it absorb to break. ASTM D256 fully describes this test. The test is based on the energy needed to be absorbed to break a piece were the cracking is already initiated by a small notch. Izod is the name of the pendulum that moves and hits the piece as shown in Figure 2-24.

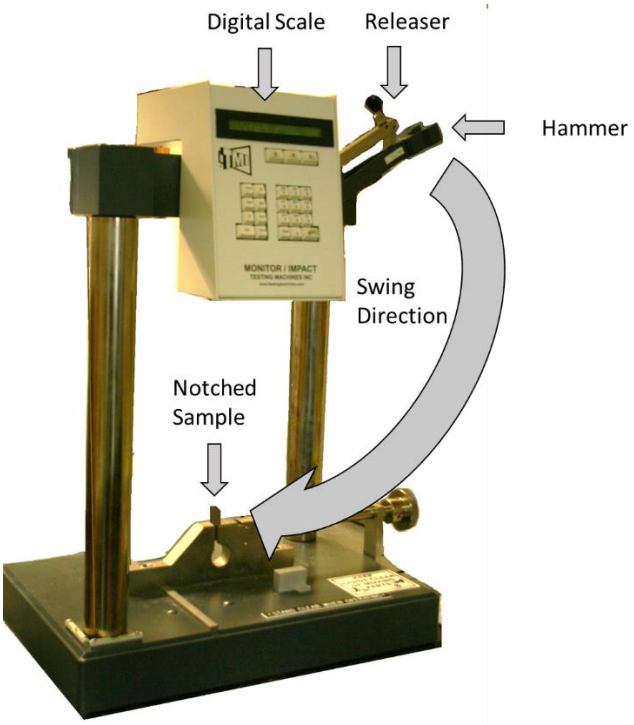

Figure 2-24: Izod Impact test apparatus

This test reports sum of energies to fracture, propagate fracture and throw away (in brittle failures) or bend (in ductile) failures and other negligible energies absorbed during impact. Rowell et al. reports notched Izod impact energy of 13 types of natural fibers (including wood fibers) polypropylene composites as well as talc-polypropylene composites and concludes natural fibers polypropylene composites (averaging 22.1 J/M) be favored to wood polypropylene composite in notched Izod impact energy, however, talc filled polypropylene can have Izod impact energy of up to 75 (J/M).

2.7.1.2 Falling Weight Impact (Gardner Impact)

This test, based on ASTM D5420, determines the energy required to shatter more than 50% of the mass of a test piece through adjusting the height of a falling weight on a hemispherical tup impactor. Using up-and-down (or Bruceton Staircase) method, the minimum height and therefore minimum energy required to shatter the sample is calculated. Figure 2-25 illustrates the Gardner impact test apparatus.

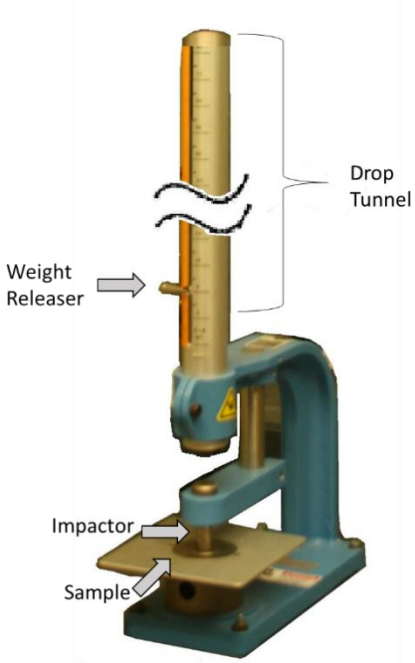

Figure 2-25: Falling Weight Impact Testing Apparatus

Park reports significant decrease of Gardner impact energy for increasing fiber concentration in wheat straw polypropylene composites. (Park, 2013) Lopez-Banuelos et al. as well report similar results for Polyethylene-agave fiber composites. (López-Bañuelos et al., 2012)

2.7.1.3 Multiaxial Impact (Dynatup)

In this test method, as per ASTM D3763, a hemispherical tup connected to a weight is released to hit the clamped flat sample. A load cell and a displacement sensor are connected to plunger tup, both connected to a microprocessor to measure increments of load versus displacement and time. When the plunger is released, and once the tup hits the sample, the sample either shatters (brittle) or is penetrated in a ductile manner. Either way, the history of multi-axial deformation of composite such as impact load, impact energy, tup velocity and displacement are recorded in an incremental procedure. Figure 2-26 illustrates the Dynatup impact apparatus.

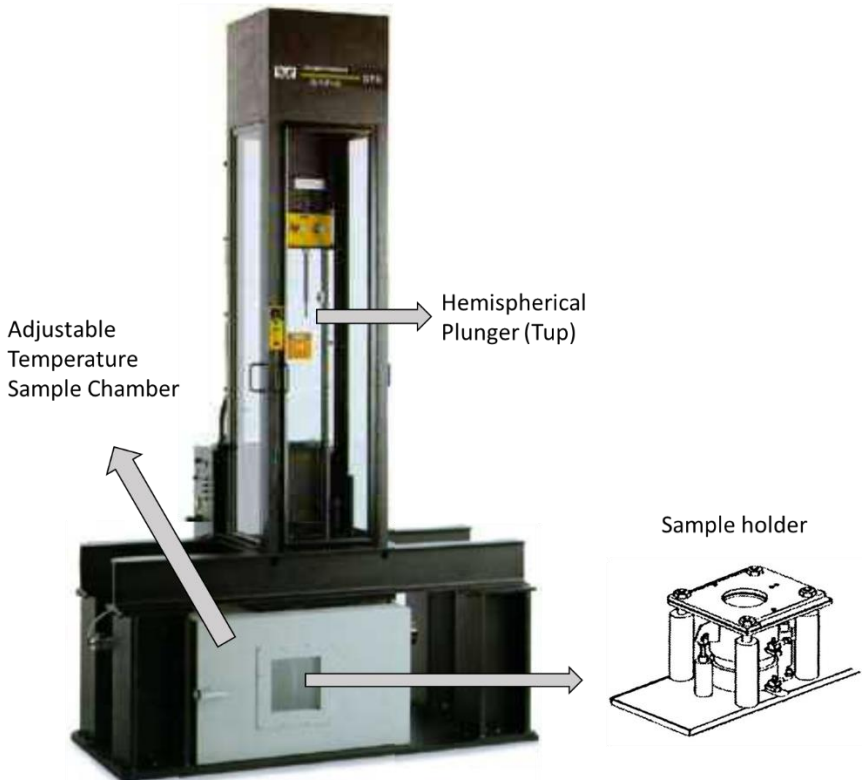

Figure 2-26: Dynatup Multiaxial Impact tester apparatus (sample holder image (Razi & Raman, 2000)*)*

Razi and Raman use this impact test to check effect of fiber size on impact properties of NFPC and report higher maximum load, energy to maximum load and total energy absorbed for long fiber NFPCs compared to medium and small size fiber NFPCs. (Razi & Raman, 2000)

2.7.2 Flexural Properties

Flexural testing based on three-point bending system, described in ASTM D790 and illustrated in Figure 2-27, essentially, measures the ability of a sample of natural fiber plastic composite to bend in the mid-point due to incremental force applied and measured by a load cell until failure. ASTM D790 describes this test method in details. The maximum bending stress before failure is called Flexural Strength. The ratio of bending force per unit area divided by strain which a unit less number indicating deformation of material, gives the flexural modulus of the material. Therefore, in a flexural stress strain curve, flexural modulus would be the slope of the curve in early stages of bending process.

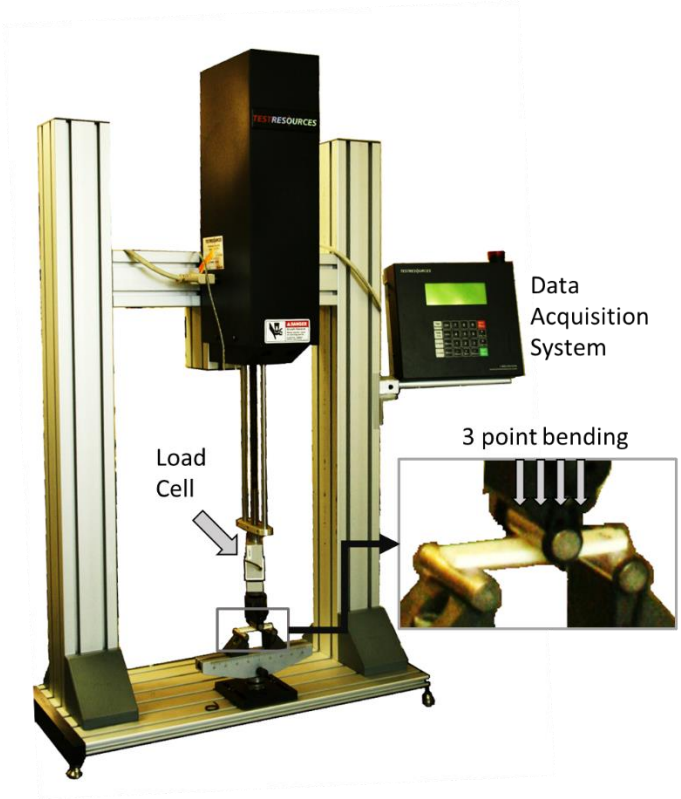

Figure 2-27: Flexural Test Apparatus

It has been reported in the literature that tensile modulus for natural fiber polypropylene composites is generally higher in value compared to flexural modulus for same materials tested. This can be explained further that in the flexural test, the result is greatly influenced by the top and bottom surface properties of the specimen, although, for tensile testing, the result reflects average property through the thickness of specimen. (Wambua, Ivens, & Verpoest, 2003)

2.7.3 Tensile Properties

Micro tensile test, contrary to flexural test, measures the reaction of natural fiber composite to tensile stress applied from two ends of a small sample illustrated in Figure 2-28. The force applied to sample from one end is measured by a load cell in an incremental manner and is transferred to a data acquisition system. ASTM D1708 describes the standard method to perform this test.

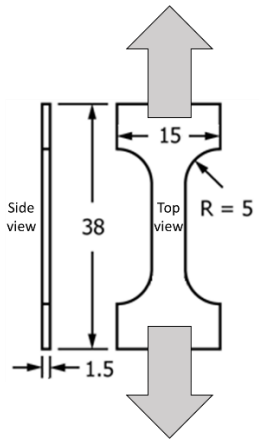

Figure 2-28: Forces applied to micro tensile test sample

A visco-elastic deformation occurs once the yield strength is reached. At yield, the deformation is permanent for thermoplastic-fiber composites and further application of force will cause material to fail. Similar to flexural tests, a stress strain curve illustrates history of the deformation in an incremental manner. Tensile strength is calculated by dividing maximum force detected by load cell divided by the average cross sectional area and is often reported in Pascals. The elongation (%) at break is calculated by dividing extension length by original gauge length.

2.7.4 Scanning Electron Microscopy

This imaging method uses an electron gun to bombard the sample with electrons in vacuum. Once electron beam hits the samples surface, it will scatter around and various detectors detect the scattered beam and create images. Some drawbacks associated with this method when used with polymers are: (a) low contrast between two polymers due to similarity of atomic numbers of those atoms in polymers, (b) some polymers may melt or be destroyed when electron beam hits the sample surface and (c) nonconductive nature of polymers causes charge and thermal heat up of sample.(Amelinckx, van Dyck, van Landuyt, & van Tendeloo, 2008) Polymers are needed to be coated with a conductive material like gold or graphite to create more accurate images.

Herrera-Franco and Valadez-Gonzalez use SEM to look at henequen fiber plastic composite fracture surfaces and use SEM to distinguish between matrix failure and interfacial failure of impact tests. (Herrera-Franco & Valadez-Gonzalez, 2005) Karnani et al. use SEM to compare wettability and matrix-fiber adhesion of kenaf fiber plastic composite and visually compare compatibilized and uncompatibilized plastic fiber composites. (Karnani, Krishnan, & Narayan, 1997)

2.7.5 UV Exposed Weathering

This test is intended to simulate cycles of effect of weathering conditions such as the UV portion of sunlight, heat and moisture, on natural fiber plastic composite. It does not simulate effect of atmospheric pollution, biological attack, saltwater, etc. Figure 2-29 illustrates the UV weathering instrument.

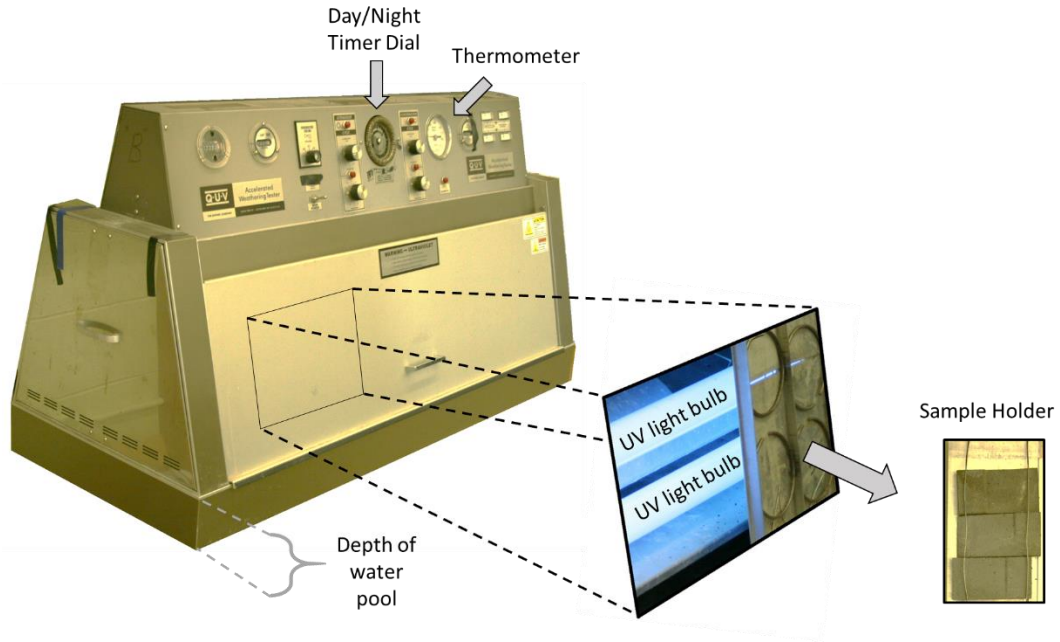

Figure 2-29: Weatherometer for UV weatheing test apparatus

Samples are exposed to UV lamp and an spectrum of light of wavelength between 295 nm to 365nm (Lamp: UVA-340) is created as illustrated in Figure 2-30. A heated water bath of around 50°C produces moisture inside the chamber to simulate moisture and heat of weather conditions.

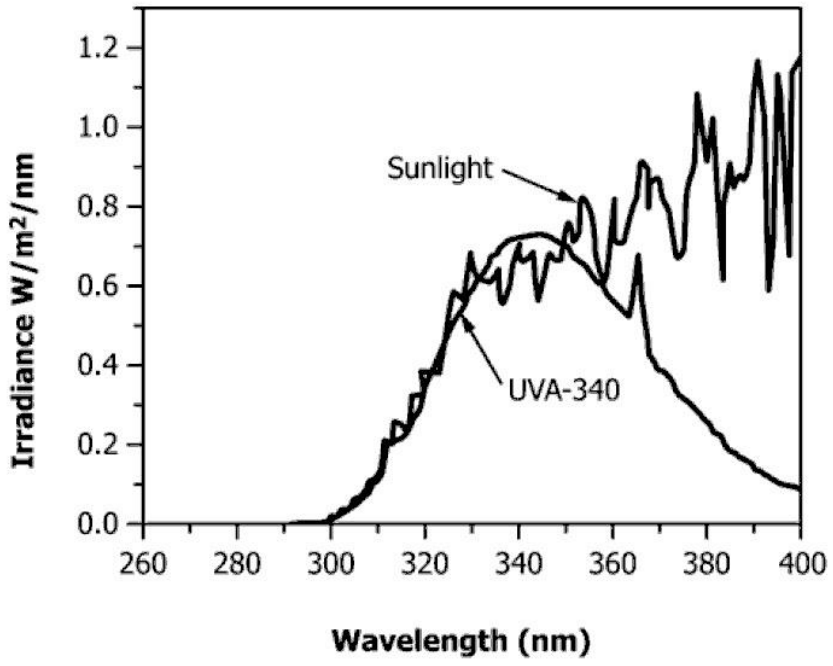

Figure 2-30: UVA-340 wavelength compared to direct sunlight wavelength (ASTM G154-12a, 2012)

2.7.6 Statistical Methods

Statistical approach is a key factor in reporting and analyzing results and drawing valid conclusions. As factors such as matrix material type and percentage, coupling agent type, coupling agent content percentage, elastomer type and content and finally fiber type and content can be designed in two levels of high and low, a fully replicated factorial design of experiments for testing various properties of NFPC materials is reasonably handy in design of experiments.

Montgomery suggests that the factorial design of experiment is more appropriate to study joint effect of factors on a response (MONTGOMERY, 2001), however, for more than 3 factors, the number of runs in the full factorial design of experiment is prohibitive. As an example, number of runs for 4 factor 3 level full factorial design of experiment is 81 runs which considering 5 replications per run will exceed 400 runs which too many runs and not reasonable. Therefore, it is reasonable to keep number of factors at two levels of high and low. In this dissertation, it is mainly aimed to perform cause-and-effect study and therefore 2 level replicated factorial design was chosen to be used.

3 Materials and Methods

3.1 Materials, Equipment and Software

Table 3-1 presents all equipment used in this dissertation along with function of each equipment in the research process.

Table 3-1: Equipment List

Equipment		
Function	Model Name	Manufacturer
Accelerated Weathering Test	QUV	The Q-Panel Company, US
Analytical Balance	AB304-S	Mettler-Toledo International Inc., US
Cut Composite Samples to size	20" Throat	T-JAW MACHINERY WORKS CO., LTD., Taiwan
Falling weight Impact Test	IM-IG-1142	Paul N. Gardner Company, Inc., US
Fiber Milling with 1mm sieve	Laboratory Mill Model 4	Arthur H. Thomas Company, US
Grinding	M 20 Universal mill	IKA-Werke GmbH & Co. KG, Germany
Injection Molding	RR/TSMA	Ray-Ran Test Equipment LTD, UK
Izod Impact Test	43-02-01	Testing Machines, Inc. US
Mechanical tests Samples Drying	5890A GC	Hewlett Packard Company, US
Melt Flow Indexing	D4001DE	Dynisco Instruments LLC, US
Multi-axial (Dynatup) Impact Test	Dynatup 9250HV High Speed Impact Tester	Instron Industrial Products, US
Optical Microscopy	Stereo Microscope MZ6, equipped with transmitted-light base TL BFD and digital camera	Leica Microsystems GmbH, Germany
Sample coating/preparation for SEM	FESEM gold coating unit Desk II with Argon	Denton Vacuum, LLC, US
Scanning Electron Microscopy	Leo 1550 Gemini	Carl Zeiss AG, Germany
Sieving Fibers	U.S standard testing sieves	VWR International Company, US
Specimen Notch Cutter	XQZ-1	Chengde Jinjian Testing Instrument Co., LTD., China
Tensile/Flexural Test	120 Family Dual Column Electromechanical Universal Test Machine	Test Resources Inc., US
Twin screw Mini Compounding	HAAKE MiniLab II	Thermo Fisher Scientific, US (Formerly Thermo Electron Co.)

Table 3-2 lists all of the materials and software used in this study. Datasheets of various polymers, coupling agents and additives are in the appendix (Figure 7-28 to Figure 7-34).

Table 3-2: Materials and Software List

Materials		
Function/Name	Grade	Vendor
Polymer Matrix/Polypropylene	Isotactic Homopolymer P-FI-160	Polynar Corporation, Tabriz, Iran
Polymer Matrix/Polypropylene	Isotactic Homopolymer D180M	Braskem America, Philadelphia, US
Coupling Agent/Fusabond	MD353P	Dupont Company, Canada
Impact Modifier/Kraton	G1650 (Called A in this thesis)	Polyone Corporation, Canada
Impact Modifier/Kraton	G1701 (Called B in this thesis)	Polyone Corporation, Canada
Antioxidant/Irgafos	168	BASF Corp, US (Formerly Ciba Inc)
Antioxidant/Irganox	1010	BASF Corp, US (Formerly Ciba Inc)
Fiber/Bagasse	Depithed	Debel Neopan Co, Ahwaz, Iran
Fiber/Oat Hull	Ekstend 100 OH 0-1	SPB Solutions, Peterborough, Canada
Roofing Shakes/Enviroshake	Enviroshake	Enviroshake Inc., Chatham, Canada
Software		
Purpose	Software Name	Company
Document processing	Office 365	Microsoft Corporation, US
Fiber image processing	ImageJ 1.38x	Wayne Rasband, National Institutes of Health, US
Fiber Image taking	Leica Applications Suite	Leica Microsystems GmbH, Germany
Statistical Analysis	Minitab 17.2.1	Minitab, Inc., US

3.2 Methods

3.2.1 Statistical methods

3.2.1.1 DOE for materials type and content effect on NFPC mechanical properties

To evaluate effect of raw materials listed in Table 3-2 and their contents on mechanical properties of composites, three replicated full factorial DOEs (5 replicates per run) using four factors each at two levels were constructed.

DOE (I) focuses on evaluation of effect of two fiber types on pp-fiber composite. However, DOE (II) and (III) focus on effect of two pp grades on pp-bagasse composite. DOE(I) was designed to find effect of fiber type and additives type and content on properties of Braskem pp - fiber composites, however, other two DOEs were designed to determine effect of pp grades and additives type and content on properties of bagasse-pp composites as in Figure 3-1, Figure 3-2 and Figure 3-3.

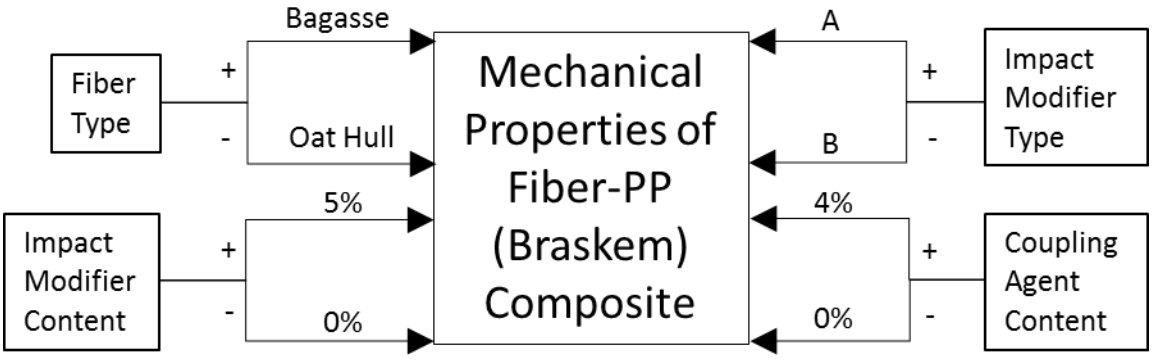

Figure 3-1: DOE (I) Effect of Fiber Type, Impact Modifier type and content and coupling agent content on Mechanical Properties of Fiber -PP (Braskem) Composite

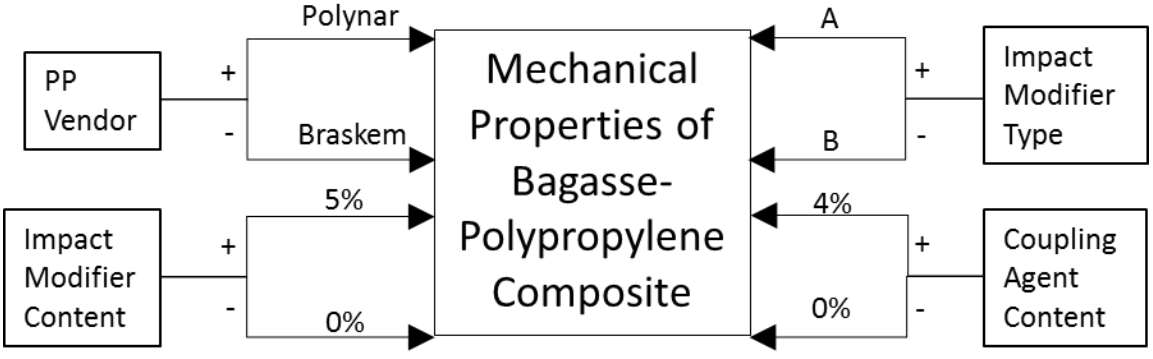

Figure 3-2: DOE (II) Effect of PP grade, Impact Modifier Type and content and Coupling agent content on mechanical properties of Bagasse-Polypropylene Composite

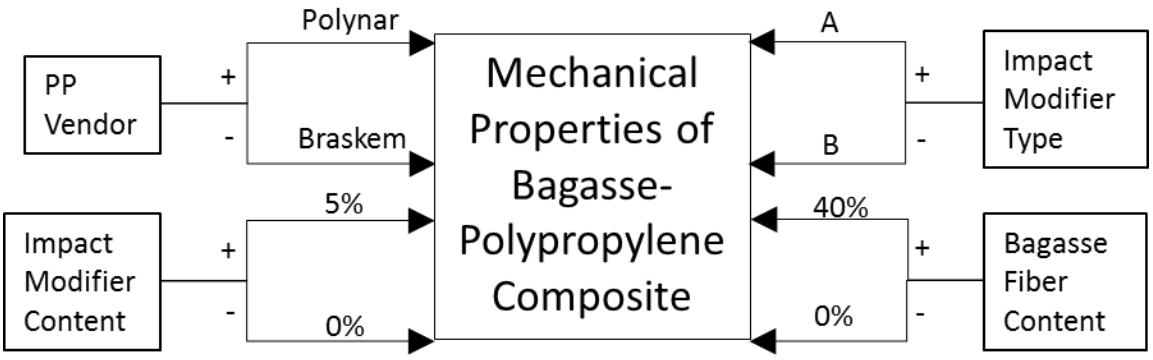

Figure 3-3: DOE (III): Effect of PP grade, impact modifier Type and Content and Bagasse fiber content on Mechanical Properties of Bagasse-Polypropylene Composite

Using Minitab Statistical software version 17.2.1, 2^4=16 runs were designed per DOE including all possible compounding scenarios. Theoretically, the number of runs for three, 4 factor, 2 level full factorial design of experiment is calculated to be 3 x 2^4 = 48, however, the number of runs is 32 due to existence of 16 common runs for the three DOEs. Following are the 32 runs which is the basis of DOE (I), (II) and (III).

Table 3-3: Experimental runs for DOEs (I), (II) and (III)

Run #	Fiber Type	Fiber %	Polypropylene Homopolymer		Kraton Impact Modifier		Antioxidant	Coupling Agent
			Braskem	Polynar	1650 (A)	1701 (B)		PPMA
1	none	0	99.5	0	0	0	0.5	0
2	none	0	94.5	0	5	0	0.5	0
3	none	0	94.5	0	0	5	0.5	0
4	none	0	94.5	0	2.5	2.5	0.5	0
5	Bagasse	40	50.5	0	5	0	0.5	4
6	Bagasse	40	50.5	0	0	5	0.5	4
7	Bagasse	40	50.5	0	2.5	2.5	0.5	4
8	Bagasse	40	55.5	0	0	0	0.5	4
9	Bagasse	40	54.5	0	5	0	0.5	0
10	Bagasse	40	54.5	0	0	5	0.5	0
11	Bagasse	40	54.5	0	2.5	2.5	0.5	0
12	Bagasse	40	59.5	0	0	0	0.5	0
13	Oat Hull	40	50.5	0	5	0	0.5	4
14	Oat Hull	40	50.5	0	0	5	0.5	4
15	Oat Hull	40	50.5	0	2.5	2.5	0.5	4
16	Oat Hull	40	55.5	0	0	0	0.5	4
17	Oat Hull	40	54.5	0	5	0	0.5	0
18	Oat Hull	40	54.5	0	0	5	0.5	0
19	Oat Hull	40	54.5	0	2.5	2.5	0.5	0
20	Oat Hull	40	59.5	0	0	0	0.5	0
21	none	0	0	99.5	0	0	0.5	0
22	none	0	0	94.5	5	0	0.5	0
23	none	0	0	94.5	0	5	0.5	0
24	none	0	0	94.5	2.5	2.5	0.5	0
25	Bagasse	40	0	50.5	5	0	0.5	4
26	Bagasse	40	0	50.5	0	5	0.5	4
27	Bagasse	40	0	50.5	2.5	2.5	0.5	4
28	Bagasse	40	0	55.5	0	0	0.5	4
29	Bagasse	40	0	54.5	5	0	0.5	0
30	Bagasse	40	0	54.5	0	5	0.5	0
31	Bagasse	40	0	54.5	2.5	2.5	0.5	0
32	Bagasse	40	0	59.5	0	0	0.5	0

3.2.1.2 DOE (IV) for UV weathering & impact location effects on multi-axial impact properties of NFPC roofing shakes

Due to limitations for obtaining fit samples for regular mechanical properties tests such as tensile, flexural, Izod and Gardner Impact properties of composites on roofing shakes, random samples of wood plastic composite shakes (Enviroshake roofing shake in Table 3-2 were obtained from actual production line at Enviroshake Inc. To test the effect of UV exposure, impact location and back reinforcement on multi-axial Impact (Dynatup) properties, a DOE with three factor, two level, replicated factorial experiment with 5 replicates per run was carried out. A schematic of the DOE for UV weathering and impact location effect is illustrated in Figure 3-4.

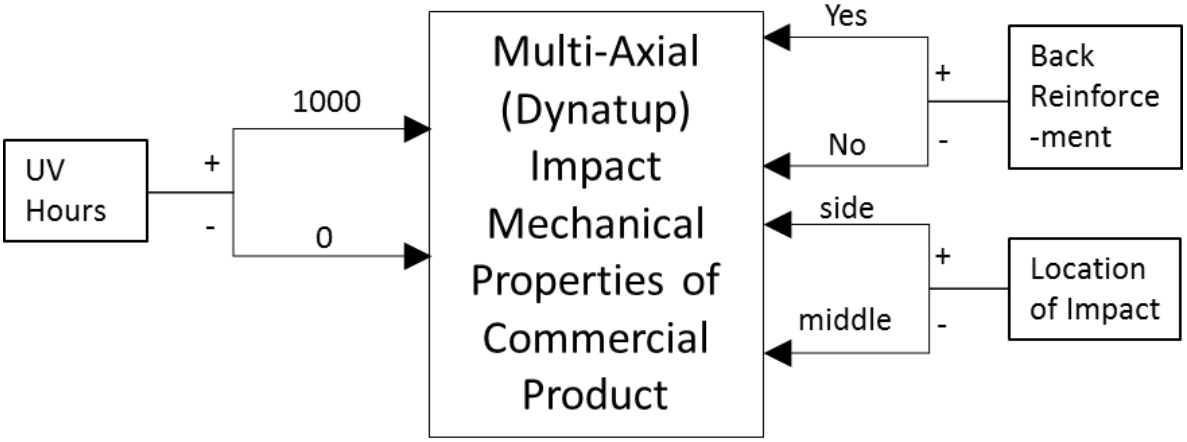

Figure 3-4: DOE (IV) for UV effect and impact locations effect on Dynatup impact properties of commercial product

Using Minitab Statistical software version 17.2.1, $2^3 = 8$ runs were designed including all possible factor combinations at two levels tabulated in Table 3-4.

Table 3-4: DOE (IV) runs list for UV weatherability and location of impact of Enviroshake

Run#	UV Exposure	Location of	Back Reinforcement
1	0 h	middle	No
2	0 h	middle	Yes
3	0 h	side	No
4	0 h	side	Yes
5	1000 h	middle	No
6	1000 h	middle	Yes
7	1000 h	side	No
8	1000 h	side	Yes

3.2.2 Fibers Preparation

Depithed bagasse fibers were obtained from Debel Neopan Co (A particle board manufacturer from Bagasse in Khuzestan, Iran). Oat hull fibers grade Ekstend 100 OH 0-1 were obtained from SPB Solutions Inc. (A food and agricultural by-products recovery and collection company in Canada). Materials were milled and passed through 1mm sieve using Laboratory Mill Model 4 of Arthur H Thomas Company as illustrated in Figure 3-5.

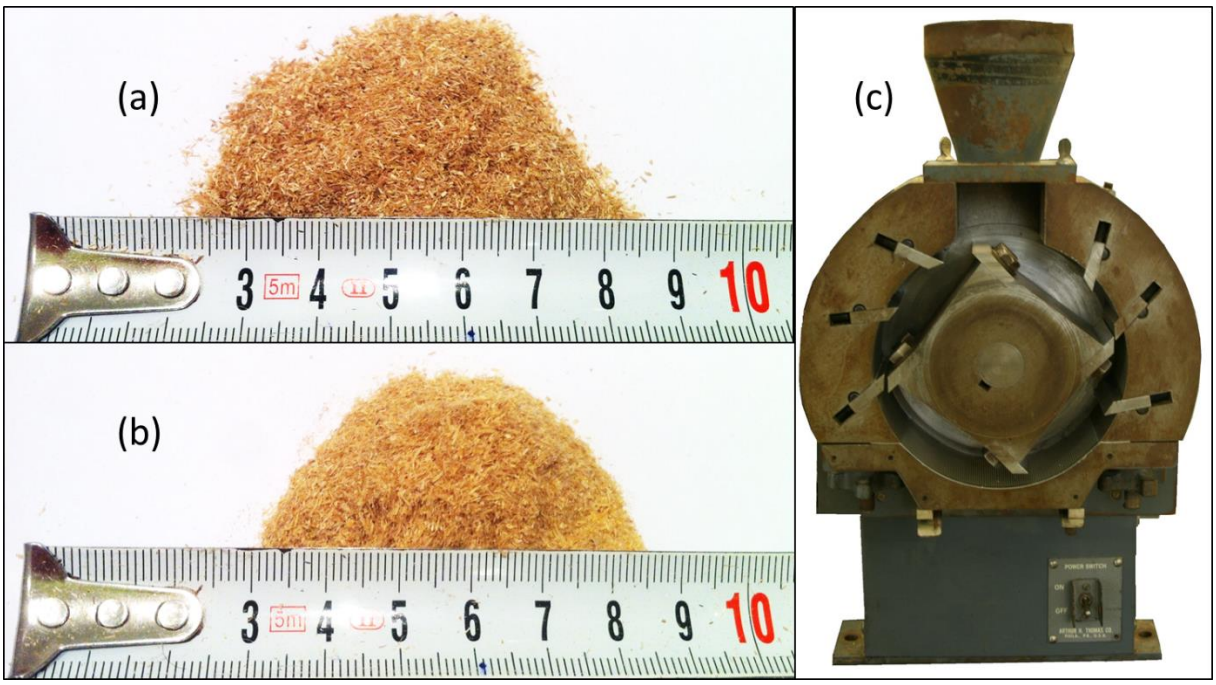

Figure 3-5: (a) Depithed Bagasse after milling and 1mm sieve (b) Oat Hull after milling and 1mm sieve (c) Arthur H Thomas Company Mill Model 4 with 1mm sieve

3.2.3 Fibers Imaging

A handful of each fiber prepared as per Section 3.2.2 was then sieved using the VWR standard sieve system with sieve opening sizes of 2.00mm, 1.00mm, 710µ, 500µ, 250µ, 150µ, 75µ, 45µ and 25µ. Fibers gathered in each sieve were placed under Leica optical microscope and using tweezers, fibers were individually and fully separated for each batch. An image of each batch was then recorded using Leica Application Suite software. Recorded images were exported to and analyzed by ImageJ (An Image Processing Software). Using ImageJ, pictures were converted to black and white (binary) images and a corresponding ellipse with a major axis and a minor axis was fitted to each fiber image. Then the ellipses, each represented by individual major and minor axes were sorted. All batches corresponding to bagasse fibers were integrated together and all batches corresponding to oat hull

fibers were integrated together as well. For each fiber, major and minor axes length of ellipses and aspect ratio (Major axis length divided by minor axis length) were tabulated for further analysis

Using ImageJ, particles were counted and major and minor axes were fit to the particles. ImageJ software assumes particles are 2 dimensional rather than 3-dimensional in reality.

Figure 3-6: Sample bagasse fibers prepared for imaging

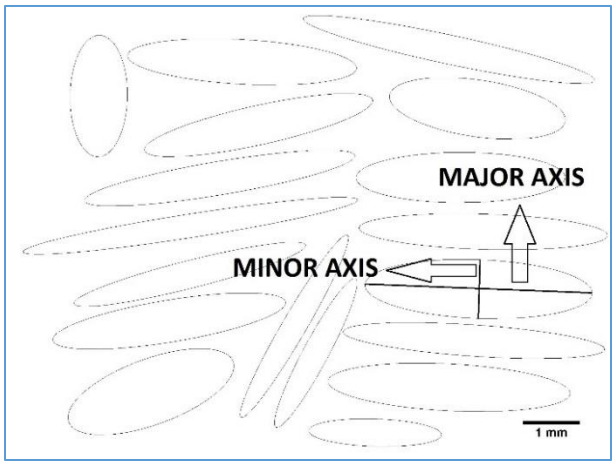

Figure 3-7: Sample bagasse fibers, ellipses fit to fiber particles

Figure 3-6 & Figure 3-7 show processed images.

Particle size distribution for bagasse and oat hull fibers were calculated using ImageJ as picture processor and Minitab histogram as a statistics tool.

3.2.4 Extrusion

Both polypropylene grades in Table 3-3 were ground using M20 IKA-Werke grinder. Each type of fiber prepared as per 3.2.2, and ground polypropylene, along with rest of formulation additives were weighed based on corresponding run number of Table 3-3, using Mettler-Toledo Analytical Balance and all recipe ingredients for each run was shaken and mixed homogeneously. The mixture was then fed into Haake MiniLab II twin screw extruder (compounder). The resulting material is illustrated in Figure 3-8.

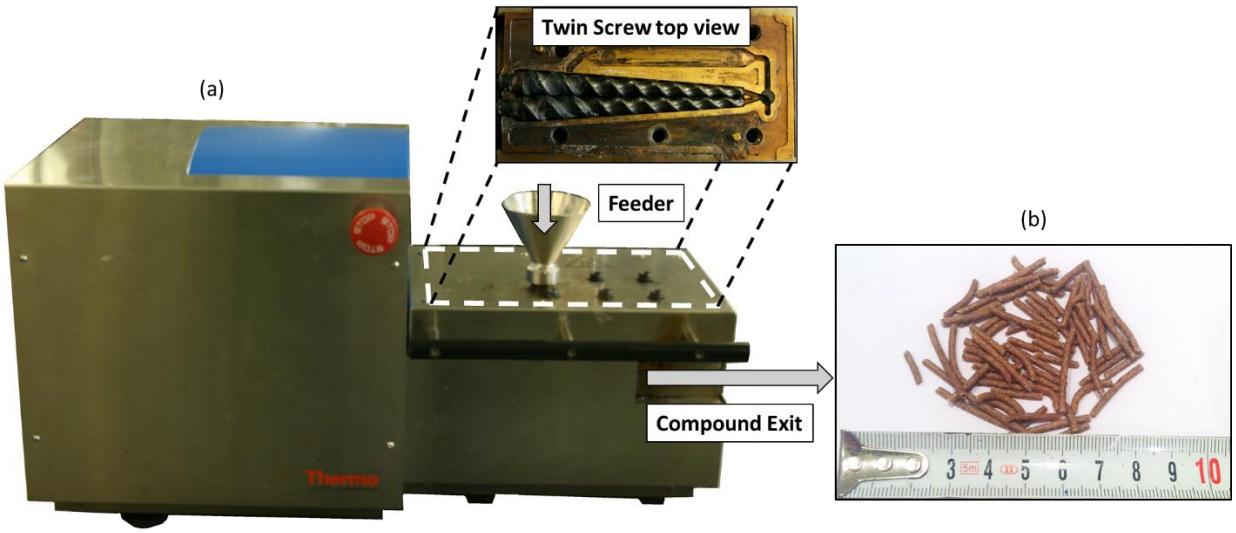

Figure 3-8: (a) Twin Screw Extruder (b) Extruded Compound

3.2.5 Injection Molding

Compounds obtained through the process described in section 3.2.4, were injection molded using Ray-Ran injection molding machine model RR/TSMA. Barrel temperature was set to 190°C and tool temperature was set to 50 °C. A handful of compounds in Figure 3-8 (b) were inserted in the barrel and kept until the material is heated enough to flow a small amount of melted compound out of the barrel exit orifice. The excess melted compound was cut and the piston was activated to start the injection of plasticized compound into the mold. The injection period lasted 15 seconds per sample at 100psi pressure and samples with shapes presented in Figure 3-9 were prepared.

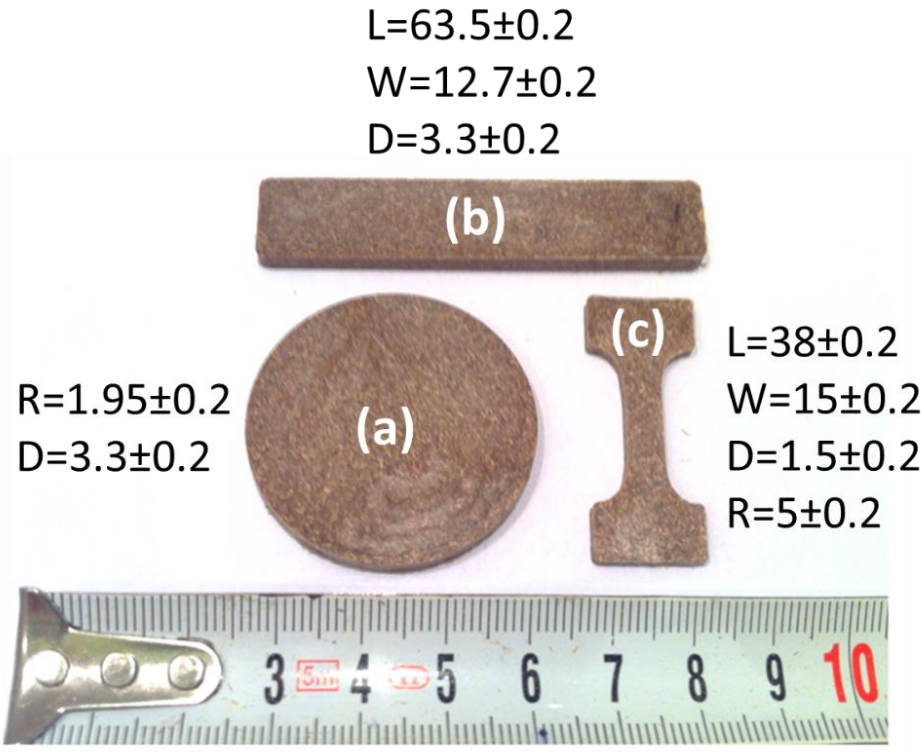

Figure 3-9: Injection Molded specimen images and dimensions (in mm) for (a) Gardner Impact (b) Flexural and Izod Impact (c) Micro Tensile

To erase thermal history on molded samples, they were annealed at 150°C for 10 minutes in an HP oven model number 5890A and then were cooled down at 10°C per minute to room temperature.

3.2.6 Characterization

3.2.6.1 Izod Impact Strength

Samples obtained in Figure 3-9 (b) were notched with depth of 2.54mm using Chengde Jinjian Notch Cutter model XQZ-1. Five samples per run from Table 3-3 were prepared and placed one at a time in Testing Machines Inc. Izod impact tester model 43-02-01 vice (Figure 2-24) and were impacted as per ASTM D256-10 (ASTM D256-10, 2010) Method A with 5ft-lb pendulum type

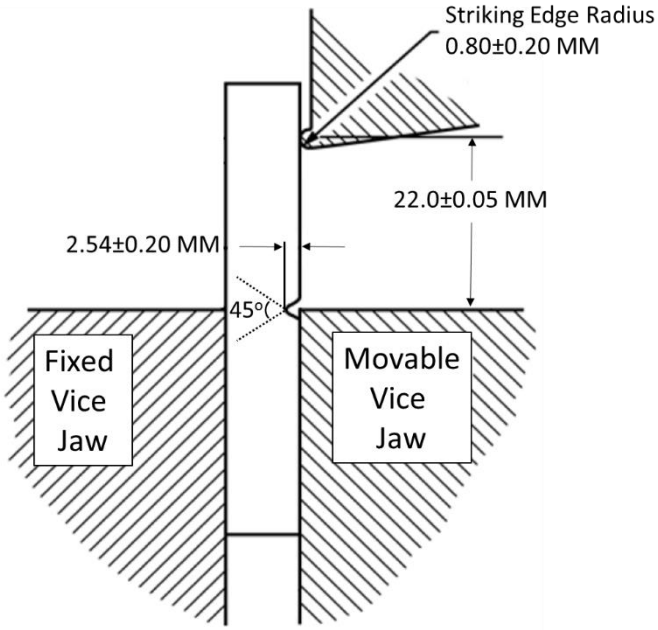

Figure 3-10: Notched Izod Impact sample a moment prior to Impact
(ASTM D256-10, 2010)

hammer and results including averages and standard deviations of each run were reported in Joules per Meter.

3.2.6.2 Mean Failure Energy

In this test, 20 samples per run from Table 3-3, prepared as illustrated in Figure 3-9 (a), were loaded one at a time in the sample holder of Paul N. Gardner Co. falling weight impact tester model IM-IG-1142 illustrated in Figure 2-25. Weight of the falling object in the tunnel was 2 lb. Using the Bruceton Staircase Procedure, as described in ASTM D5420-10 (ASTM D5420-10, 2010), 1st sample was placed in the sample holder location and weight was dropped from middle of the tower. If more than 50% of sample failed, the weight was lowered by half an inch and similar procedure was repeated for 2nd sample, although, if more than 50% of 1st sample did not fail, weight was elevated

by half an inch higher level. This procedure was repeated 20 times and each time thickness, height of impactor weight and failure/non-failure status of sample were recorded as illustrated in Table 3-5.

Table 3-5: Run # 6 Bruceton Staircase procedure matrix for falling weight impact (Gardner Impact) where O=more than 50% failure and X=lower than 50% failure

Sample #	1	2	3	4	5	6	7	8	9	10	11	12	13	14	15	16	17	18	19	20
height (in)																				
6.5																				
6																				x
5.5																			o	
5		x				x												o		
4.5	o		x		o		x		x						x		o			
4				o				o		x				o		o				
3.5											x		o							
3												o								
2.5																				
2																				
1.5																				
1																				
0.5																				
0																				

Mean failure height was calculated using Table 3-5 and following equation as per ASTM D5420-10 (ASTM D5420-10, 2010) :

$$h = h_o + d_h\left(\frac{A}{N} - 0.5\right)$$

Where:

$h =$ Mean Failure Height (inches)

$h_o =$ Lowest Height an event occurred (inches)

$d_h =$ Height increment (inch)

$A = \sum_{i=0}^{k} in_i$ Where:

$i = 0.1.2 \ldots . k$ (Counting index starts at h_o)

$n_i =$ Number of failures at h_i

$N =$ Number of Failures

Mean failure energy was calculated using mean failure height and following equation as per ASTM D5420-10 (ASTM D5420-10, 2010):

$$MFE = h \times m \times f$$

Where:

$MFE =$ Mean Failure Energy (J)

$h =$ Mean Failure height (inch)

$m =$ Mass of impacting mass (lbm) = 2 lbm

$f =$ 0.11298; Conversion factor from lbf.inch to Joules

3.2.6.3 Flexural Modulus

In this test, 5 samples (illustrated in Figure 3-9 (b)) of each run from Table 3-3, were loaded, one at a time, on three point sample vice of TestResources Inc. 120 Family, Dual Column Electromechanical Universal apparatus illustrated in Figure 2-27 for Flexural test based on ASTM D790-10 (ASTM D790-10, 2010) at a rate of 1.3 mm/min. Rate of crosshead motion, Flexural Stress, Flexural strain and Modulus of elasticity were calculated in following equations:

- $R = \frac{ZL^2}{6d}$ (Crosshead Motion Rate)
- $\sigma_f = \frac{3PL}{2bd^2}$ (Flexural Stress)
- $\varepsilon_f = \frac{6Dd}{L^2}$ (Flexural Strain)
- $E_B = \frac{\sigma_f}{\varepsilon_f}$ (Modulus of Elasticity)

Where:

L = support span (mm)

d = sample depth (mm)

Z = outer surface strain rate (mm/mm/min)

P = Load at a given point (N)

b = sample width (mm)

D = maximum deflection (mm)

3.2.6.4 Tensile Strength

Based on ASTM D1708-13 (ASTM D1708-13, 2013), using same equipment as in 3.2.6.3 but with a different vice and grip. 5 Samples per runs of Table 3-3 illustrated in Figure 3-9 (c) were loaded and tested. Samples were pulled from both ends until fractured at 1.3 mm/min and tensile strength and % elongation at break were reported.

$$\text{Tensile Strength} = \frac{Maximum\ Force}{Unit\ Coross-sectional\ area}$$

$$\%\ \text{Elongation at Break} = \frac{Final\ gage\ length - Initial\ gage\ length}{Initial\ gage\ length} \times 100\%$$

3.2.6.5 Scanning Electron Microscopy

Fractured surface of samples of Izod impact test described in section 3.2.6.1 were gold coated with 10nm thickness using Denton FESEM gold coating unit Desk II with Argon and SEM images were obtained at 25KV in vacuum using Leo 1550 Gemini Scanning Electron Microscope. Images were qualitatively evaluated for fiber-matrix adhesion, effect of impact on fibers adhesion to matrix and homogeneity and dispersion of fibers in polymer matrix.

3.2.6.6 UV Exposure Weathering

In this test, 3 samples per run for runs # 5, 6, 7 and 8 of Table 3-4, totaling 12 pieces, prepared as per 3.2.6.7, were placed into sample holders and mounted inside The Q-Panel Company QUV Weatherometer facing UVA-340 fluorescent light bulbs to be tested according to ASTM standard test (ASTM G154-12a, 2012). The water reservoir under QUV Weatherometer was filled up with water and connected to water supply to be automatically topped up once evaporation occurs. The heater temperature was set to 50°C and the day/night dial of Weatherometer was set to 23 hours of UV exposure followed by 1 hour of condensation per day. During condensation, UV light was turned off automatically although the heater still worked and kept the temperature of water reservoir at the proximity of 50°C. Samples were exposed to UV and moisture conditions a total of 1000 hours (44 days) with a total of 44 hours (about 2 days) of condensation. Samples were then collected and tested for Multi-Axial (Dynatup) Impact properties described in section 3.2.6.7.

3.2.6.7 Multi-Axial (Dynatup) Properties

5 samples per each of the runs listed in Table 3-4 of Enviroshake® roofing shakes from Table 3-2 were cut in 65mm x 50mm plaques using T-Jaw Machinery 20" Throat cutting machine. Samples

were cut based on "after UV weathering impact testing" location of impact (side or middle) and with/without back reinforcement as illustrated in Figure 3-11.

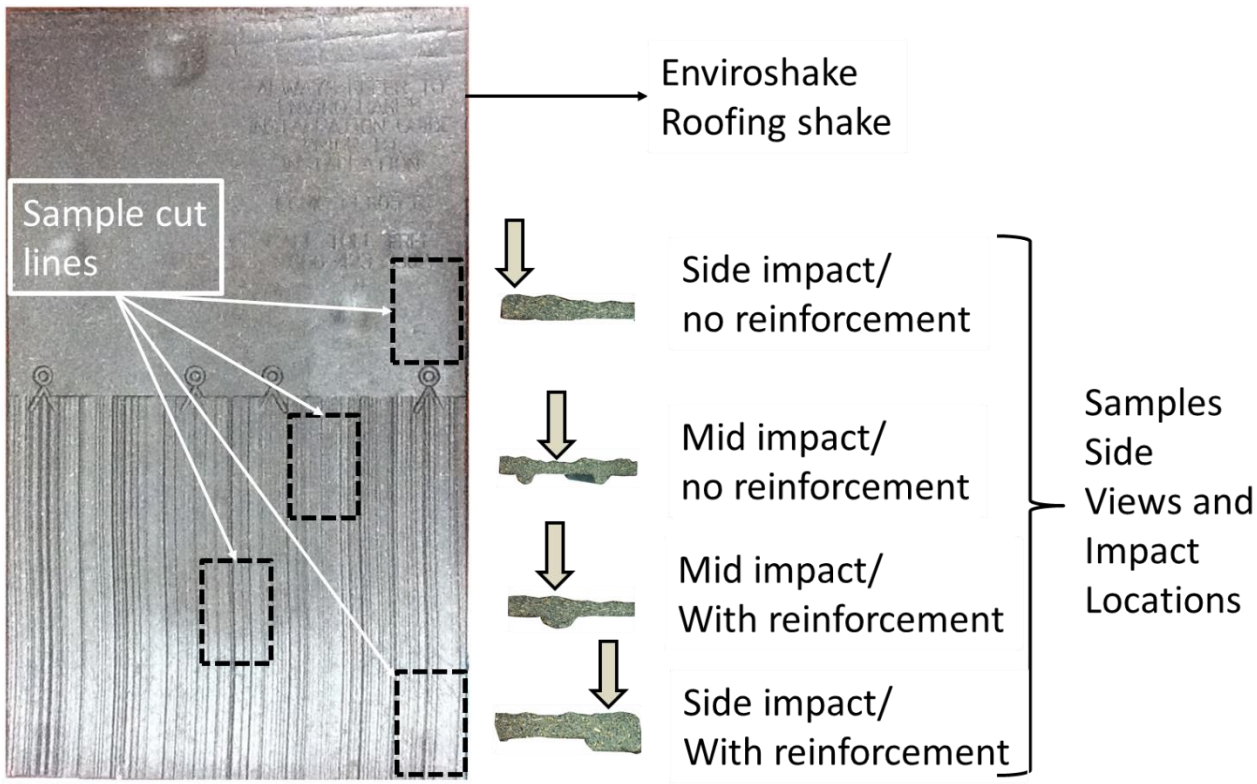

Figure 3-11: Dynatup samples and locations of impacts

Thickness of each sample was recorded and samples were loaded one at a time in Instron Multi-axial (Dynatup) Impact Tester Model 9250HV as per ASTM D31763-15 (ASTM D3763-15, 2015). The sample holder clamp hole diameter was 76.0 mm, however, loaded samples were at least 11mm smaller than clamp hole which was an inevitable constraint for this test. Location of impacts are illustrated in Figure 3-11. Sample holder consisting of two metal sheets screwed together held the sample from any possible slipping during impact. The hemispherical plunger (tup) with diameter of 12.7±0.13mm impacted samples at speed of 2.2 m/s or 132 m/min and a load (KN) vs. Displacement (mm) was created for each sample. Using load vs. displacement graphs, following values were reported:

- F_{max} Maximum Load (KN) = Maximum load recorded by the load cell
- D_{max} = Deflection at Maximum Load (mm) = The point where peak load occurs
- Energy to Maximum Load (J) =Area under the force-displacement curve from 0 displacement up to displacement at maximum load)

  $= \int_0^{D_{max}} F.dx$

  Where:

  D_{max} = Deflection at Maximum Load (mm)

  x = Displacement (mm)

  F=Force as a function of Displacement (KN)
- Total Energy (J) = Area under the force-displacement curve from 0 displacement up to maximum displacement

  $= \int_0^{D_{total}} F.dx$

  Where:

  D_{total} = Maximum Deflection point (mm)

  x = Displacement (mm)

  F=Force as a function of Displacement (KN)

4 Results and Discussion

4.1 Particle size analysis

Based on the process described in section 3.2.3, optical images of bagasse and oat hull fibers as illustrated in Figure 4-1 and Figure 4-2 were taken, measured and counted.

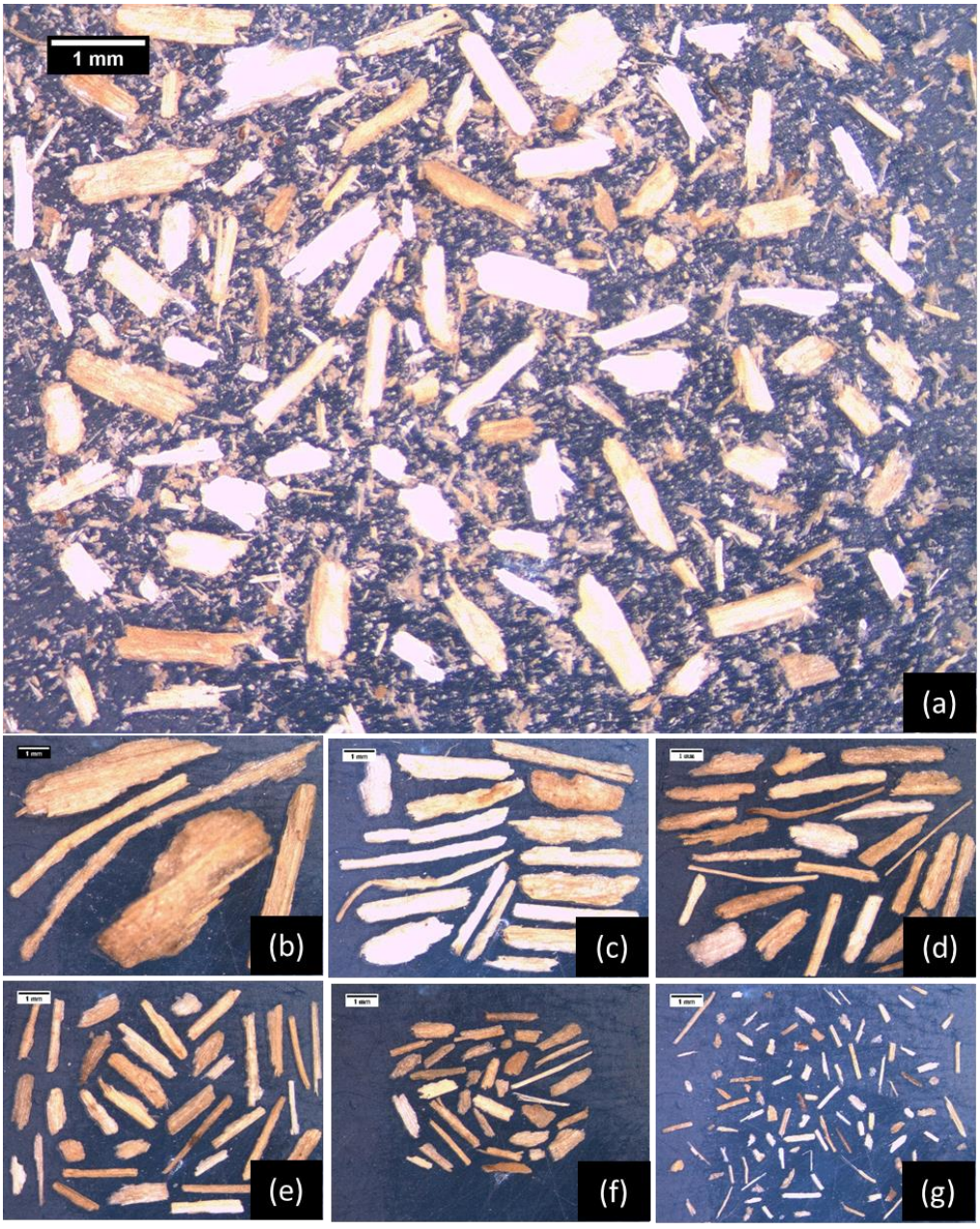

Figure 4-1: (a) Bagasse fibers before screening (b) 2mm sieve (c) 1mm sieve (d) 710micron sieve (e) 500micron sieve (f) 250micron sieve (g) 150 micron sieve

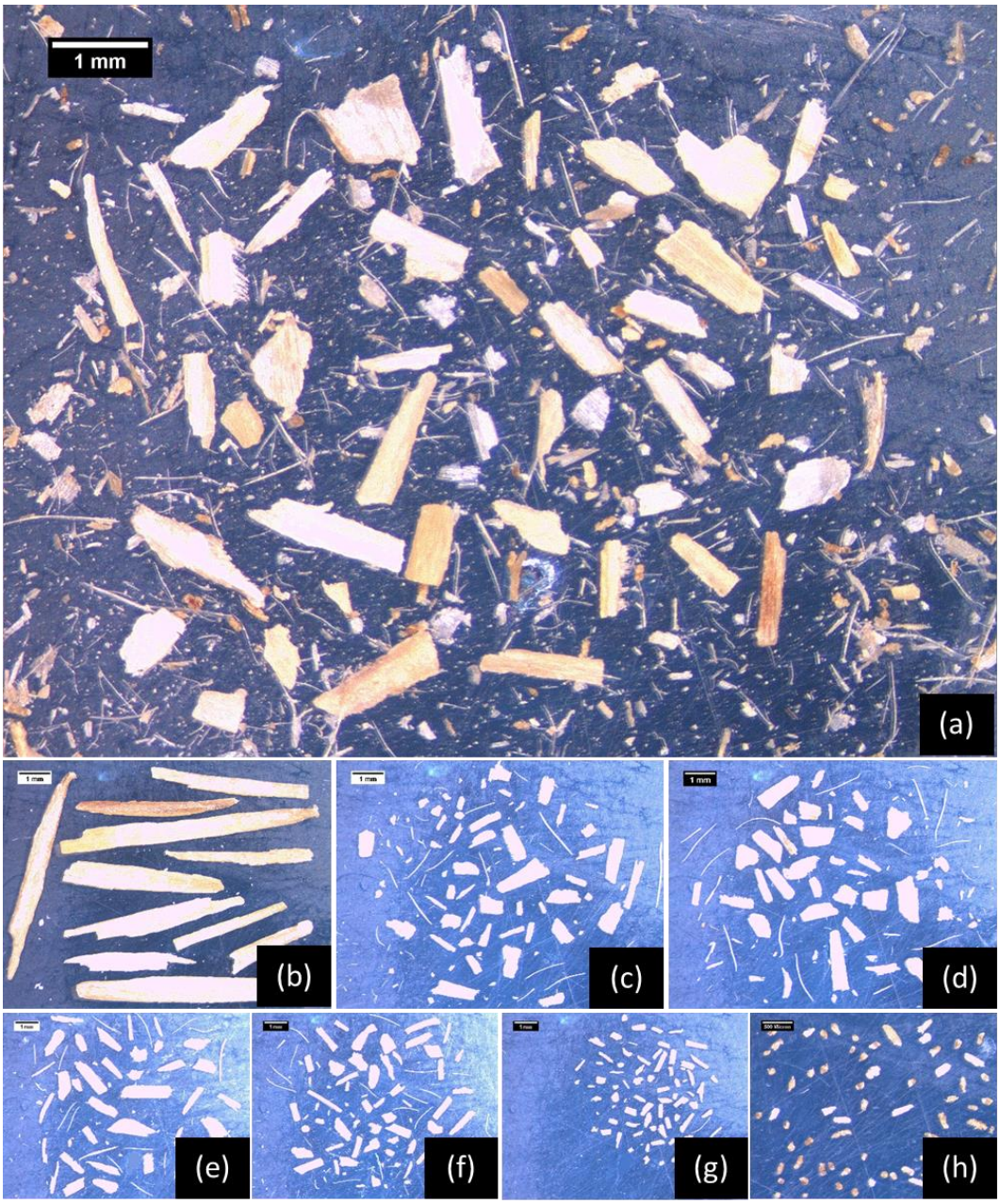

Figure 4-2: (a) Oat Hull fibers before screening (b) 2mm sieve (c) 1mm sieve (d) 710micron sieve (e) 500micron sieve (f) 250micron sieve (g) 150 micron sieve (h) 75micron sieve

A plot of all fibers length vs. aspect ratios is shown in Figure 4-3. Based on this plot, both fibers appear to have a high frequency in fine lengths (i.e. lower than 1mm) and aspect ratio of around 10. At lower fiber lengths (lower than 1mm), oat hull fibers tend to have higher aspect ratios compared to bagasse fibers, however, bagasse fibers tend to have lower aspect ratios at higher fiber lengths.

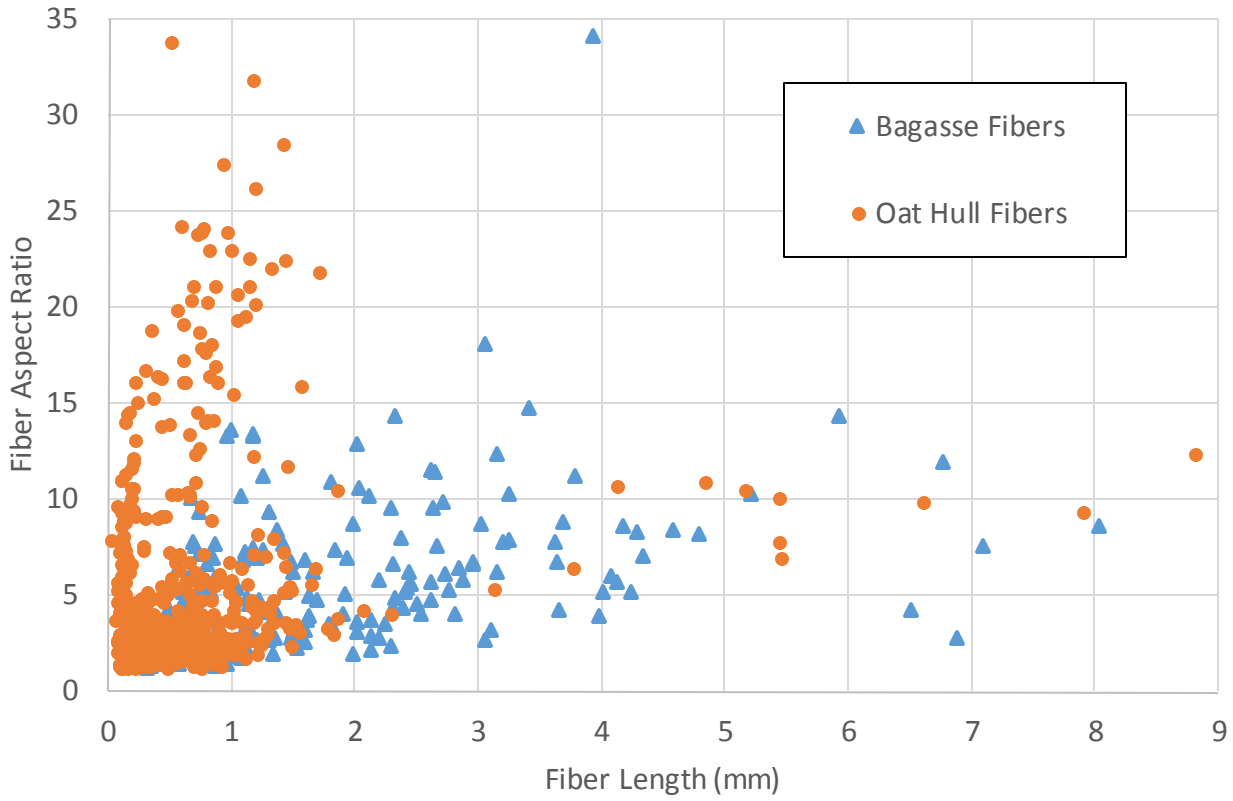

Figure 4-3: Oat Hull and Bagasse Fibers length (mm) vs. aspect ratio

Histogram of bagasse and oat hull fibers size-based frequency bar charts, are superimposed and plotted in Figure 4-4. Based on Figure 4-4, it appears that a comparatively high percentage of oat hull fibers lengths fall in the lower than 0.5mm region of the histogram. For the bagasse fibers, as the length of fibers increase, the frequency gradually decreases with exception of 0.5mm to 1.0mm region where an increase in frequency is observed.

Table 4-1 shows the numerically various percentages of fiber lengths in each specific bin. Fine (0.5mm or smaller) oat hull fibers are majority in the oat hull fibers batch. It is interesting to observe that approximately 40% of both fibers sizes fall in the 0.5mm to 1.5mm fiber sizes. For larger than 1.5mm fibers sizes, bagasse fibers frequency is about 40% while for Oat Hull this frequency is only approximately 4%. This indicates that although both bagasse fibers and oat hull fibers were crushed with same crusher as described in section 3.2.2, oat hull has been weaker against the blades of the mill. This can be explained probably by the lower amount of lignin in the structure of oat hull compared to bagasse as pointed out in the literature review.

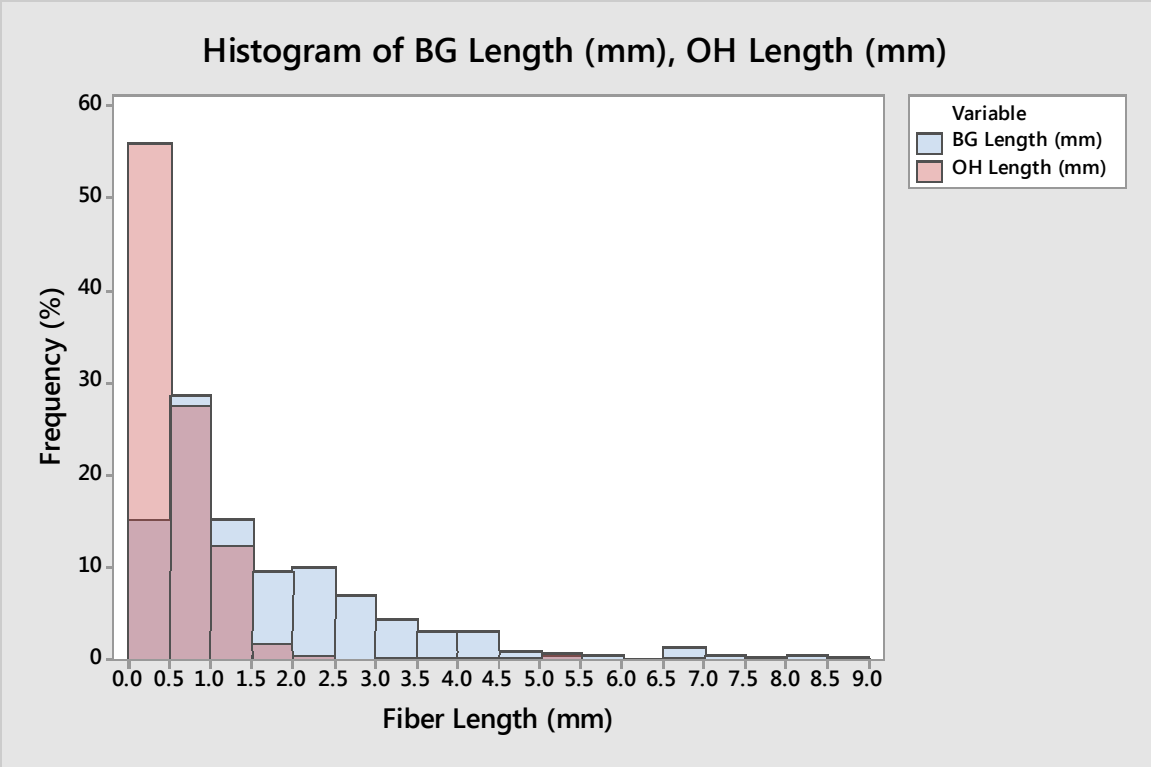

Figure 4-4: Frequency (%) Histogram of Fibers Length (mm)

Table 4-1: Frequency of Length (mm) of Bagasse and Oat Hull Fibers

Length	Frequency (%)	
(mm)	Bagasse	Oat Hull
0.0-0.5	15.0%	56.0%
0.5-1.0	29.0%	28.0%
1.0-1.5	15.0%	12.0%
1.5-2.0	10.0%	2.0%
2.0-5.0	28.0%	1.0%
5.0-9.0	3.0%	1.0%

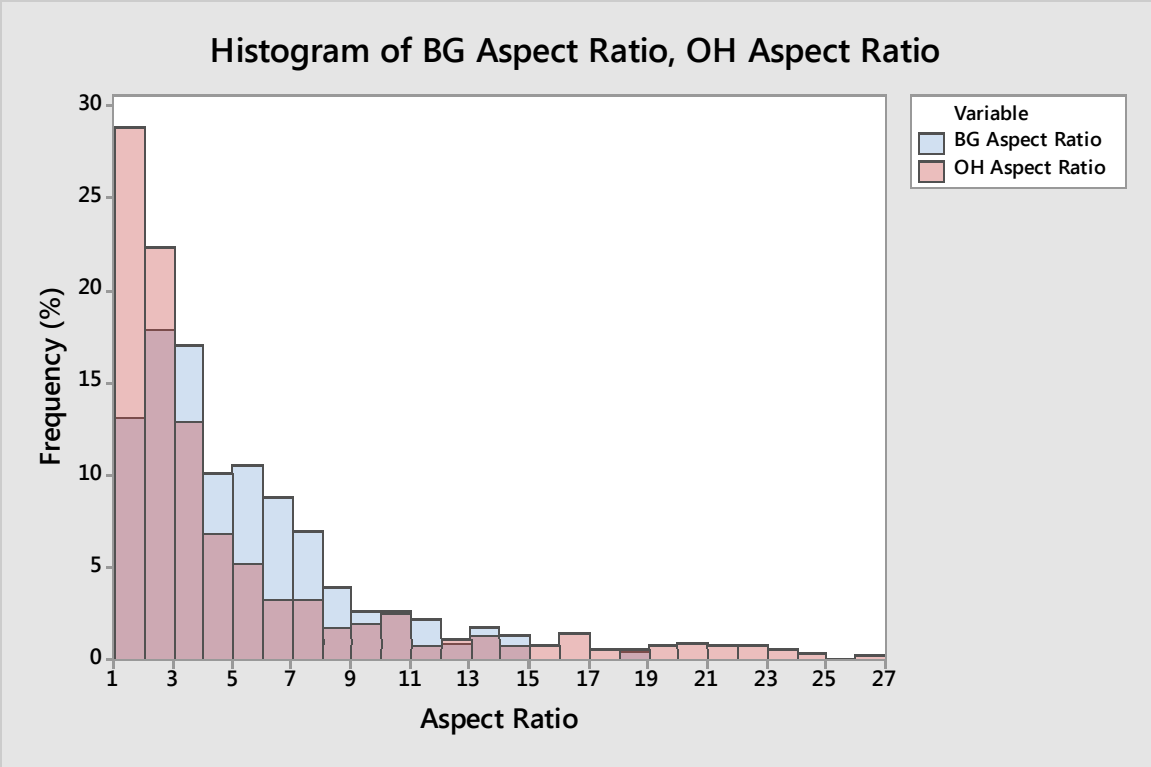

Figure 4-5: Frequency (%) Histogram of Fibers Aspect Ratio

Table 4-2: Frequency (%) of Aspect Ratio (mm/mm) of Bagasse and Oat Hull Fibers

Aspect Ratio	Frequency (%)	
(mm/mm)	Bagasse	Oat Hull
1.0-3.0	31.0%	51.3%
3.0-5.0	27.0%	19.8%
5.0-7.0	19.2%	8.5%
7.0-9.0	10.9%	5.0%
9.0-11.0	5.2%	4.6%
11.0-13.0	3.3%	1.6%
13.0-15.0	3.0%	2.0%
15.0-27.0	0.4%	7.2%

Based on the histogram in Figure 4-5, it appears that majority of oat hull fibers have lower aspect ratios compared to majority of bagasse fibers. Approximately half of oat hull fibers aspect ratios are between 1 to 3 (mm/mm) while for bagasse, only a third of aspect ratios are between 1 to 3 (mm/mm) . Majority of bagasse fibers have aspect ratios between 3 to 9 (mm/mm). This indicates that majority of oat hull fibers are visually fatter compared to bagasse fibers. Approximately 12% of both fibers aspect ratios are higher than 9 (mm/mm) up to 27 (mm/mm).

As the histograms for length and aspect ratio distributions of particles of oat hull and bagasse appear to be skewed to right, the distribution identification tool of Minitab was used to identify which of the 2-Parameter Exponential, Loglogistic, Weibull or Lognormal distributions best fit the histograms of particle size and aspect ratio distributions. It was found that Lognormal distribution best fits the fibers length distributions. It was also found that the 2-parameter exponential distribution best fits the fibers aspect ratio histogram of distributions.

Therefore, the lognormal distribution was fitted to all of the particle size distributions (length of fibers) and 2-parameter exponential distribution was fitted to aspect ratio distributions histogram (Figure 4-6) and median (mm), mean (mm), maximum frequency (%) and maximum frequency bin (mm) were identified for fibers length and aspect ratio distributions respectively.

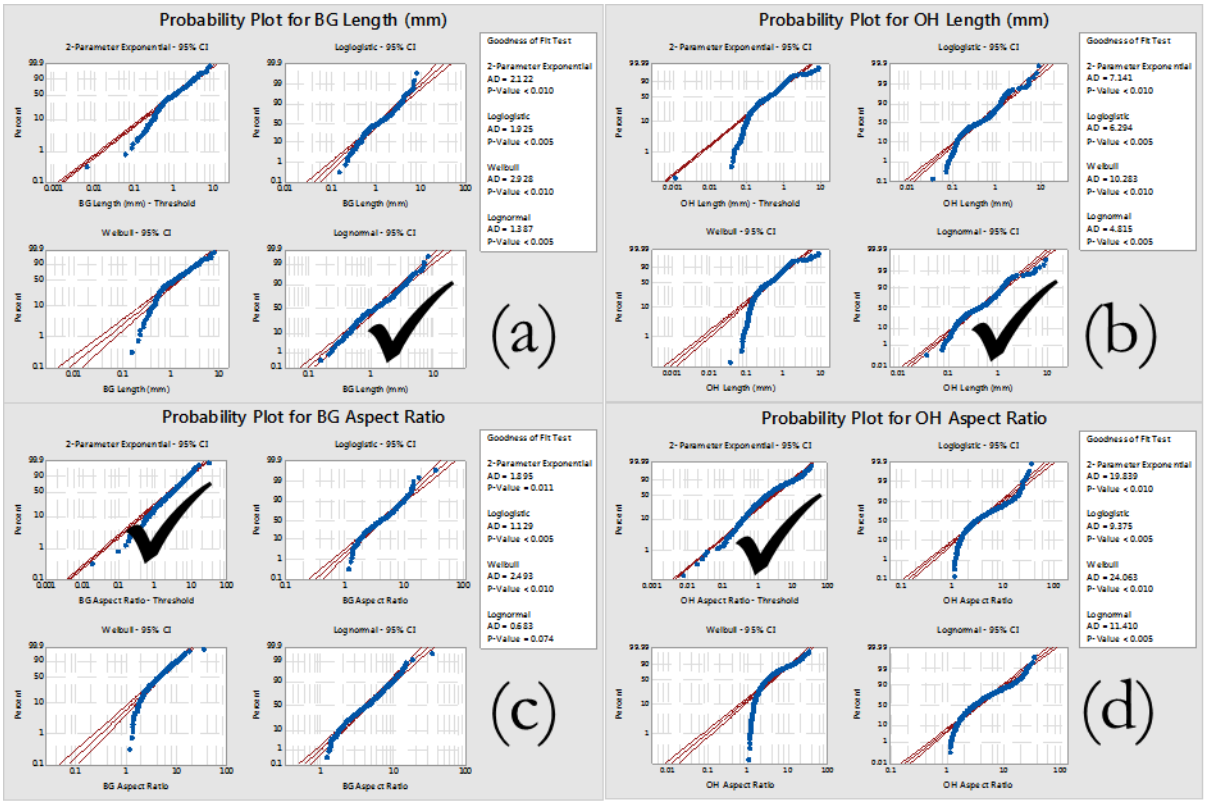

Figure 4-6: Selection of best fit for fiber distributions (a) Bagasse fiber lengths: LOGNORMAL distribution (b) Oat Hull fiber length: LOGNORMAL distribution (c) Bagasse Aspect Ratio: Exponential distribution (d) Oat Hull fiber Aspect Ratio Exponential distribution

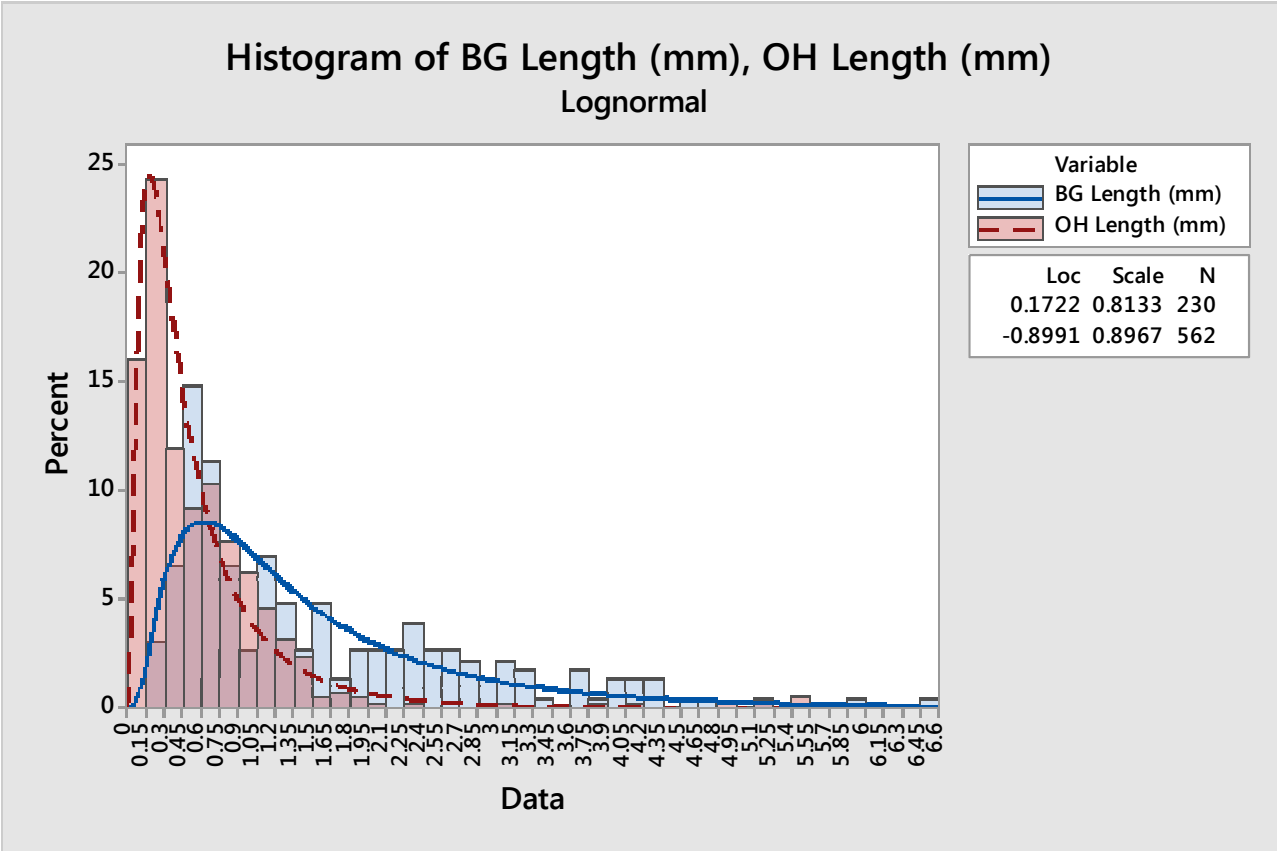

Figure 4-7: Histogram of Bagasse and Oat Hull fiber length distribution with fitted Lognormal distribution

Table 4-3: Histogram information of bagasse and oat hull fiber length distribution

Fiber Length (mm)	Bagasse	Oat Hull
Mean (mm)	1.64	0.63
Median (mm)	1.17	0.41
Maximum Frequency (%)	14.8%	24.4%
Max Frequency Bin (mm)	0.45-0.60	0.15-0.20

Based on Figure 4-7 and Table 4-3, bagasse appears to have longer fibers compared to oat hull. The mean length of bagasse fibers is approximately 160% higher than the mean length of oat hull fibers. As both histograms are skewed to right, it is helpful to compare the median of histograms. The median of bagasse length histogram is approximately 185% higher than the median of oat hull length distribution. The maximum frequency for bagasse fiber length is approximately 15% and occurs at 0.45 to 0.60 mm range of bagasse fiber lengths however, for oat hull fibers, maximum frequency is approximately 25% and occurs at 0.15 to 0.20 mm range of oat hull fiber lengths.

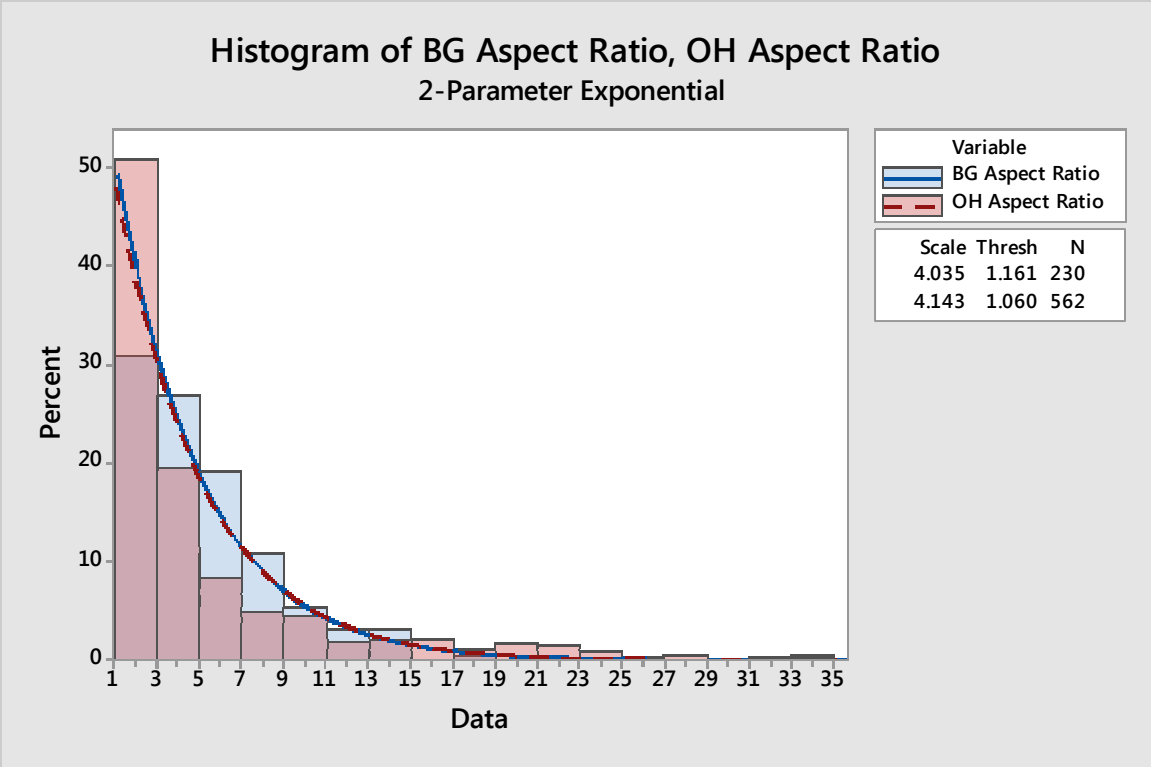

Figure 4-8: Histogram of Bagasse and Oat Hull aspect ratio distribution with fitted 2-parameter Exponential distribution

Table 4-4: Histogram information of bagasse and oat hull fiber aspect ratio distribution

Fiber Aspect Ratio	Bagasse	Oat Hull
Mean (no dimension)	5.20	5.20
Median (no dimension)	4.21	2.96
Maximum Frequency (%)	30.87	50.89
Max Frequency Bin (no dimension)	1-3	1-3

Based on Figure 4-8 and Table 4-4, both bagasse and oat hull fibers appear to have identical mean aspect ratios, however, as both histograms are skewed to right, it is helpful to compare the median of histograms. The median of bagasse fibers aspect ratio histogram is approximately 40% higher than the median of oat hull aspect ratio distribution. The maximum frequency for bagasse fiber aspect ratio is approximately 31% and occurs at 1-3 range of bagasse fiber aspect ratios, however, for oat hull fibers, maximum frequency is approximately 51% and it occurs at the same aspect ratio bin of 1-3. This indicates that overall, oat hull fibers, again, appear to be fatter compared to bagasse fibers. Approximately 50% of oat hull fibers have aspect ratios higher than 3, but on the other hand, approximately 70% of bagasse fibers have aspect ratios higher than 3.

4.2 Effect of Formulation on Mechanical Properties of Laboratory Prepared NFPC

Formulated and prepared Natural Fiber Polypropylene Composites were characterized for mechanical properties as described in sections 3.2.6.1to 3.2.6.4. A detailed table of formulations and replicated results averages and standard deviations are presented in Table 4-5. For reference, datasheet of a sample Trex WPC decking product is included in appendix in Figure 7-27

Plots of average flexural modulus at 1% vs average Izod impact strength for all runs and also plot of average tensile strength vs. mean failure energy for all runs are showed in Figure 4-9 & Figure 4-10.

Figure 4-9 illustrates that generally, the mean failure energy and tensile strength properties are evenly distributed in the range of 0.5 to 1.2 (J) for mean failure energy, and 20 to 50 (MPA) for tensile strength, with a few outliers. Figure 4-10, shows that flexural modulus generally ranges between 950-2950 (MPA) and Izod impact strength ranges between 20-45 (J/M). In contrast to Figure 4-9 however, this data is leaning toward upper right side of the graph which indicates that there is a tendency in all samples to have relatively high flexural modulus and high Izod impact energy properties, simultaneously.

As described in section 3.2.1.1, for DOE (I) the goal is to find effect of fiber type, impact modifier type and content percent, and coupling agent, on fiber –Braskem pp composite mechanical properties. In DOE (II) however, the goal is to find effect of pp grade, impact modifier type and content and coupling agent on bagasse-pp composite. Finally, for DOE (III), the goal is to find effect of pp grade, bagasse fiber and impact modifiers type and content on bagasse-pp composites.

Following sections will discuss and analyze each of the DOEs first for the statistical method used and second for the main effects and interactions.

Table 4-5: All experimental results for effect of formulation on NFPC

Run #	Fiber Type	Fiber content (%)	PP Supplier(%)		Impact Modifier (%)		Antioxidant (%)	Coupling Agent (%)	Izod Impact Strength (MPA)		Tensile Strength (MPA)		Flexural Modulus at 1% (MPA)		Mean failure energy(J)
			Braskem	Polynar	A	B		PP-MA	AVG	SD	AVG	SD	AVG	SD	AVG
1	none	0	99.5	0	0	0	0.5	0	19.6	1.5	40.1	1.3	1083.5	45.5	1.04
2	none	0	94.5	0	5	0	0.5	0	21.4	2.5	34.1	1.7	1005.7	40.8	0.85
3	none	0	94.5	0	0	5	0.5	0	21.8	1.9	34.2	5.2	982.5	42.1	1.14
4	none	0	94.5	0	2.5	2.5	0.5	0	24.2	3.3	34.0	1.4	1045.1	66.7	1.06
5	Bagasse	40	50.5	0	5	0	0.5	4	37.6	0.9	44.1	2.7	2521.5	51.4	0.97
6	Bagasse	40	50.5	0	0	5	0.5	4	41.2	1.6	44.0	2.9	2838.8	155.6	0.99
7	Bagasse	40	50.5	0	2.5	2.5	0.5	4	40.6	2.0	46.5	0.9	2713.9	105.1	1.15
8	Bagasse	40	55.5	0	0	0	0.5	4	28.5	0.8	46.9	0.8	2605.7	112.6	0.67
9	Bagasse	40	54.5	0	5	0	0.5	0	30.5	0.8	31.3	1.1	2511.8	28.0	0.82
10	Bagasse	40	54.5	0	0	5	0.5	0	38.4	2.3	26.2	1.9	2303.4	42.7	1.10
11	Bagasse	40	54.5	0	2.5	2.5	0.5	0	34.3	0.7	30.0	0.6	2293.9	113.1	0.90
12	Bagasse	40	59.5	0	0	0	0.5	0	30.7	1.2	30.6	1.4	2493.3	80.9	0.67
13	Oat Hull	40	50.5	0	5	0	0.5	4	29.1	1.9	35.9	1.5	1730.1	74.2	0.70
14	Oat Hull	40	50.5	0	0	5	0.5	4	29.8	1.3	36.6	0.7	1756.0	44.8	0.73
15	Oat Hull	40	50.5	0	2.5	2.5	0.5	4	29.2	1.5	34.6	0.8	1677.5	73.6	0.68
16	Oat Hull	40	32.208	0	0	0	0.5	4	23.3	0.9	35.8	3.5	2186.7	91.7	0.53
17	Oat Hull	40	54.5	0	5	0	0.5	0	33.6	1.7	26.6	0.9	1779.0	108.0	1.02
18	Oat Hull	40	54.5	0	0	5	0.5	0	35.7	2.0	26.9	0.5	1743.3	120.3	1.00
19	Oat Hull	40	54.5	0	2.5	2.5	0.5	0	36.8	1.2	25.8	0.3	1898.7	53.6	0.95
20	Oat Hull	40	59.5	0	0	0	0.5	0	27.0	0.8	29.2	0.9	2087.6	146.6	0.62
21	none	0	0	99.5	0	0	0.5	0	24.5	1.7	39.0	1.9	1246.0	61.8	1.35
22	none	0	0	94.5	5	0	0.5	0	26.2	3.4	33.0	0.7	1155.0	30.1	0.97
23	none	0	0	94.5	0	5	0.5	0	44.4	4.7	32.4	1.2	1182.6	37.5	1.15
24	none	0	0	94.5	2.5	2.5	0.5	0	41.1	3.2	31.8	0.8	1415.1	47.6	0.96
25	Bagasse	40	0	50.5	5	0	0.5	4	38.8	1.3	32.1	3.9	2538.9	93.8	0.75
26	Bagasse	40	0	50.5	0	5	0.5	4	40.2	0.9	28.3	5.6	2447.5	96.1	0.95
27	Bagasse	40	0	50.5	2.5	2.5	0.5	4	40.8	1.5	30.9	3.7	2628.1	83.3	0.92
28	Bagasse	40	0	55.5	0	0	0.5	4	29.5	1.6	30.6	4.3	2782.2	224.6	0.56
29	Bagasse	40	0	54.5	5	0	0.5	0	35.6	2.0	24.0	4.0	2276.0	59.1	0.79
30	Bagasse	40	0	54.5	0	5	0.5	0	34.1	0.6	13.9	10.5	2340.5	37.6	0.78
31	Bagasse	40	0	54.5	2.5	2.5	0.5	0	36.7	2.6	22.7	2.8	2350.8	36.1	0.80
32	Bagasse	40	0	59.5	0	0	0.5	0	30.1	4.2	22.0	3.9	2531.8	149.3	0.55

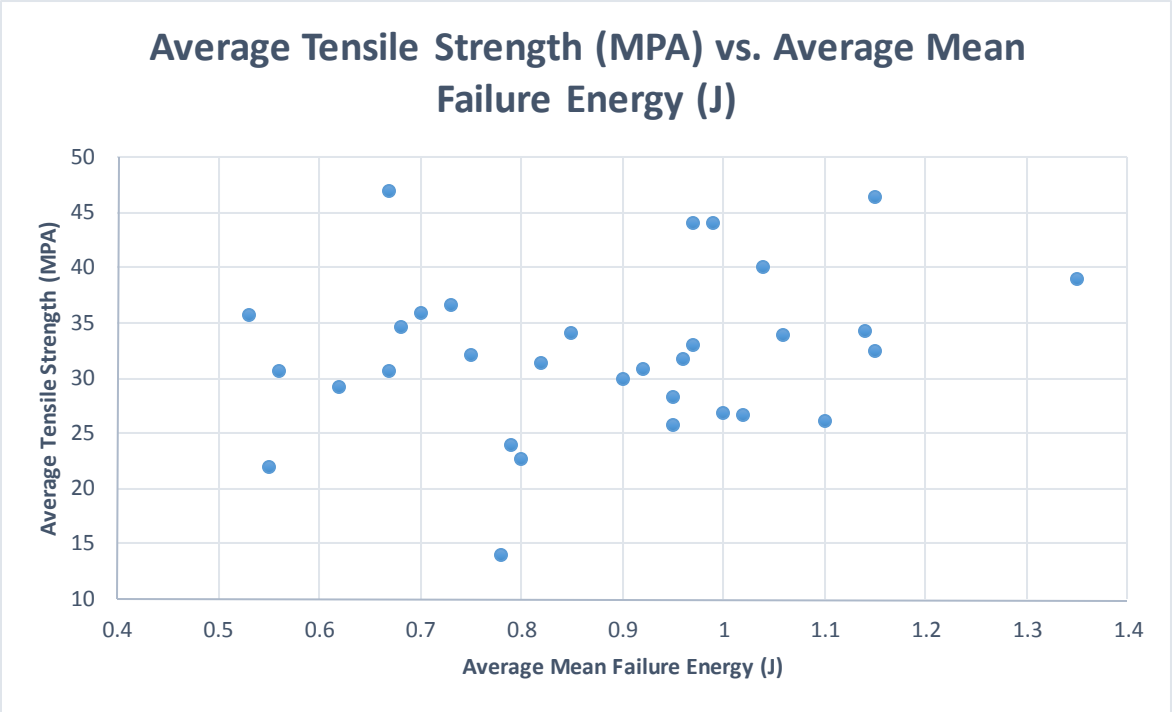

Figure 4-9: Average Tensile Strength vs. Average Mean Failure Energy for all runs

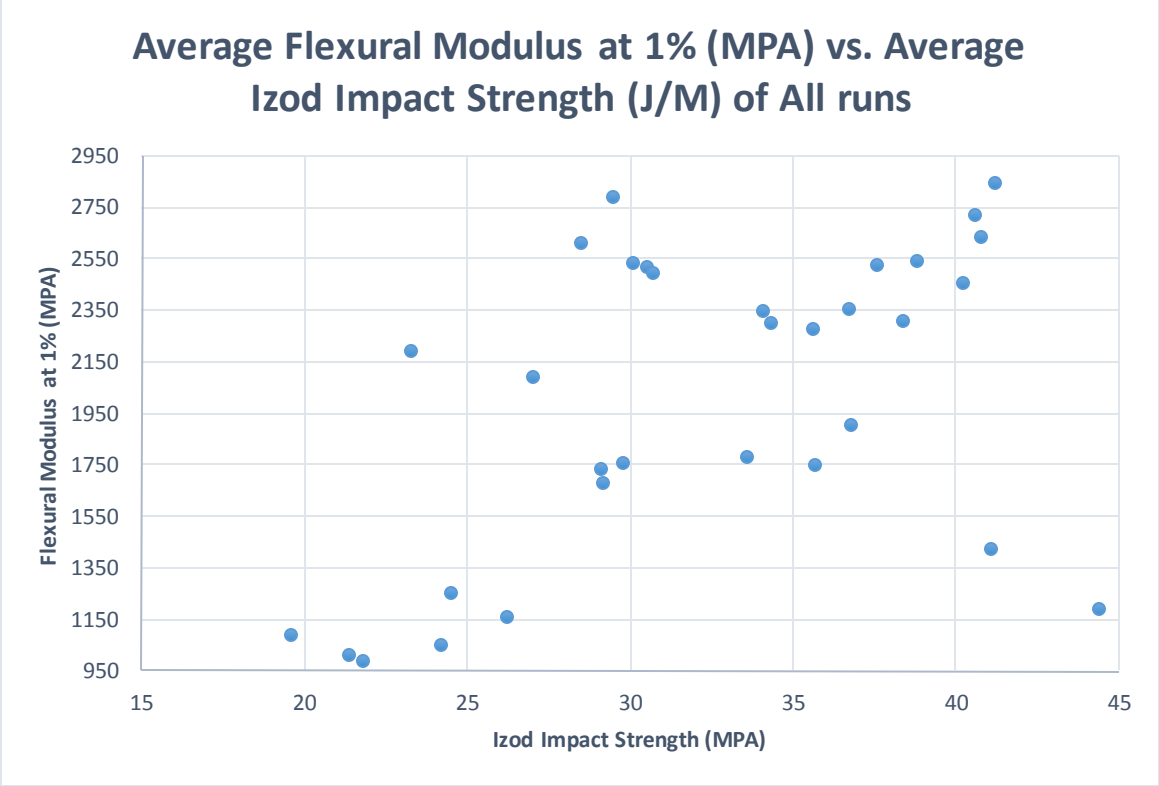

Figure 4-10: Average Flexural Modulus at 1% vs. Average Izod Impact Strength of all runs

4.2.1 Design of Experiment I (DOE I)

For DOE (I) presented in Table 4-6, results are presented in Table 4-5,where Braskem pp is kept constant as the composite matrix, and effect of fiber type (either oat hull or bagasse), impact modifier A (0% or 5%), impact modifier B (0% or 5%) and coupling agent (0% or 4%) was determined on 1- Izod impact strength, 2-Tensile strength and 3- Flexural modulus 4- Mean failure energy of compounded natural fiber – braskem polypropylene composite.`

Table 4-6: Design Matrix for DOE (I)

Run #	Fiber Type	Fiber %	PP	PP	Impact Modifier		Antioxidant	C. Agent
			Braskem	Polynar	A	B		PPMA
5	Bagasse	40	50.5	0	5	0	0.5	4
6	Bagasse	40	50.5	0	0	5	0.5	4
7	Bagasse	40	50.5	0	2.5	2.5	0.5	4
8	Bagasse	40	55.5	0	0	0	0.5	4
9	Bagasse	40	54.5	0	5	0	0.5	0
10	Bagasse	40	54.5	0	0	5	0.5	0
11	Bagasse	40	54.5	0	2.5	2.5	0.5	0
12	Bagasse	40	59.5	0	0	0	0.5	0
13	Oat Hull	40	50.5	0	5	0	0.5	4
14	Oat Hull	40	50.5	0	0	5	0.5	4
15	Oat Hull	40	50.5	0	2.5	2.5	0.5	4
16	Oat Hull	40	55.5	0	0	0	0.5	4
17	Oat Hull	40	54.5	0	5	0	0.5	0
18	Oat Hull	40	54.5	0	0	5	0.5	0
19	Oat Hull	40	54.5	0	2.5	2.5	0.5	0
20	Oat Hull	40	59.5	0	0	0	0.5	0

4.2.1.1 DOE (I) Statistical method Analysis

4.2.1.1.1 DOE (I): Statistical Method Analysis of IZOD IMPACT Response

We begin the analysis by developing an Anova table to identify significance of each main factor or interaction combination factors. Based on an alpha value of 5%, it is concluded that factors or interactions with a lower than 5% P value are significant. Table 7-1 illustrates the coded design matrix with responses and Table 7-2 illustrates Izod impact analysis of variance for DOE (I).

The Regression Equation based on above tables can be found in Equation 4-1. Significant main factors and interactions are included in the regression equation and insignificant main factors and interactions are omitted from the equation.

Equation 4-1: DOE (I) Regression equation of Izod Impact Responses

$$IZOD\ IMPACT\ STRENGTH\ (J/M)$$
$$= 32.987 + 2.368\,A + 1.197\,B + 2.936\,C - 0.515\,D$$
$$- 0.466\,A*B + 0.543\,A*C + 2.328\,A*D - 1.646\,B*C$$
$$+ 0.491\,B*D + 1.011\,A*B*D + 0.636\,A*C*D$$
$$- 0.398\,B*C*D$$

$$Where: A = 1\ for\ BAGASSE\ as\ fiber, A = -1\ for\ OAT\ HULL\ as\ fiber$$
$$B = 1\ for\ IMA = 5\%, B = -1\ for\ IMA = 0\%$$
$$C = 1\ for\ IMB = 5\%, C = -1\ for\ IMB = 0\%$$
$$D = 1\ for\ Coupling\ Agent = 4\%, D = -1\ for\ Coupling\ Agent = 0\%$$

Based on Anova table in Table 7-2 , a normal probability plot of effects is constructed as follows. The deviation of effects data point from the straight line shows that the data points are significant.

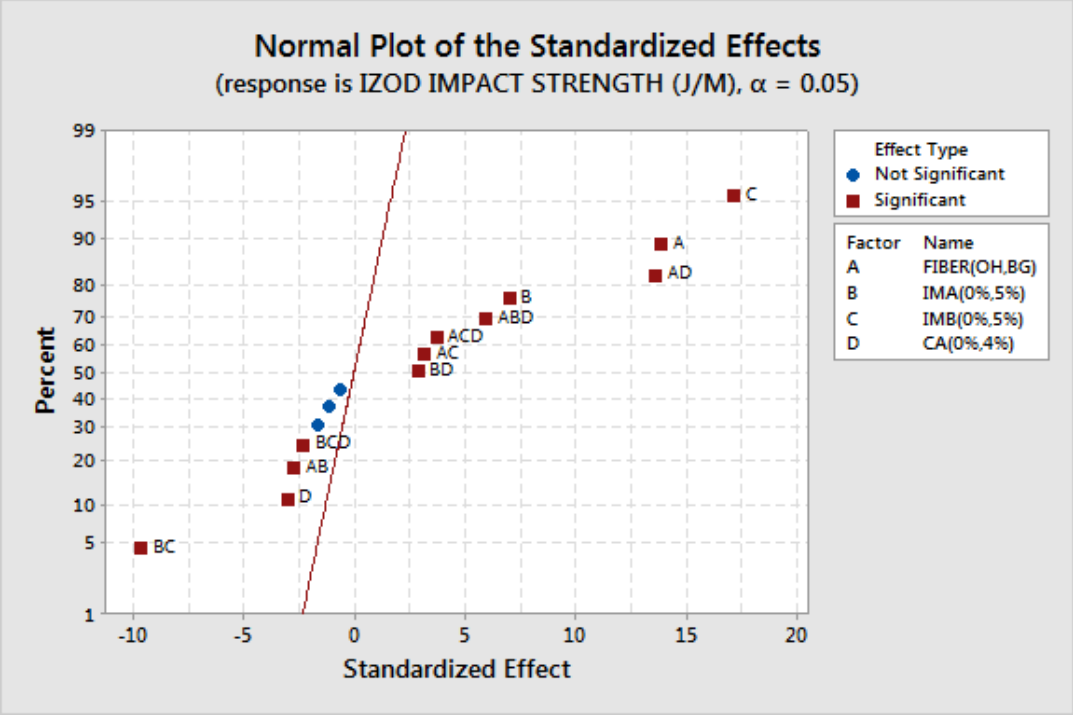

Figure 4-11: DOE (I) Izod Impact Normal Plot of standardized effects

To check that such assumptions were correct it is necessary to look at the residuals plot and see if the residuals are normally distributed or not. The points on this plot shown in Figure 4-12 are reasonably close to a straight line which supports the fact that the underlying assumptions of the analysis are satisfied.

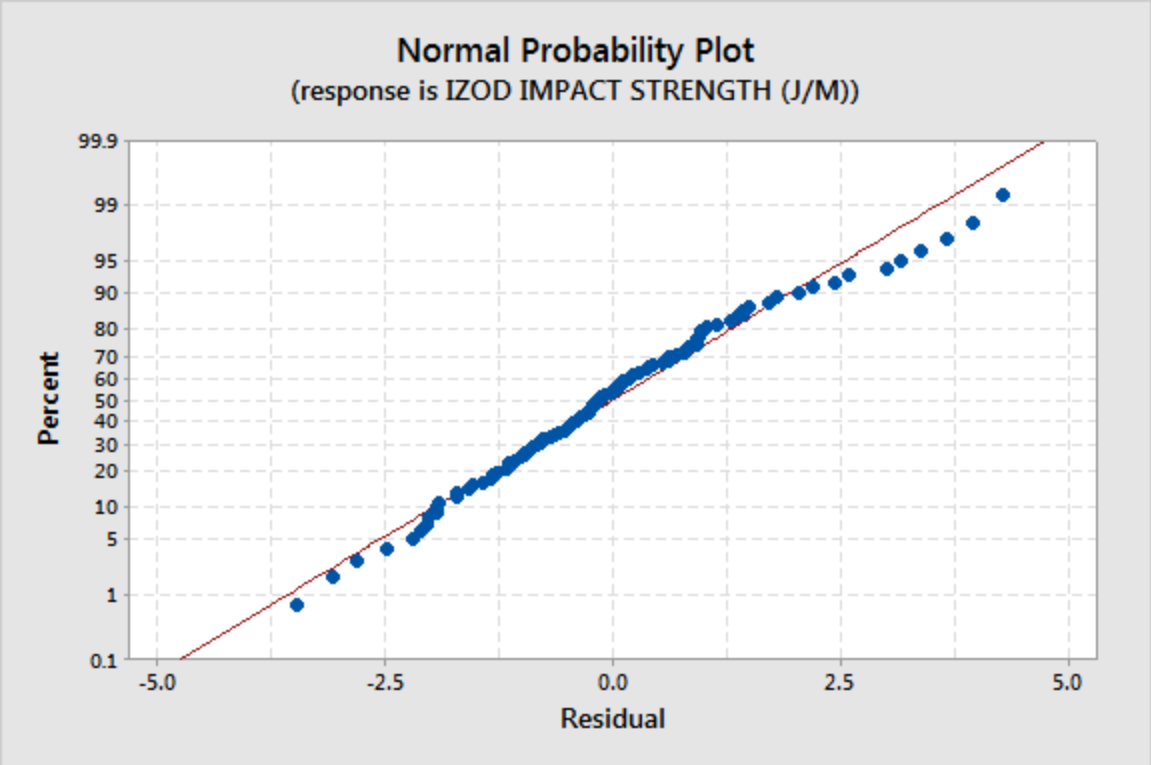

Figure 4-12: DOE (I) Izod Impact Normal probability plot

4.2.1.1.2 DOE (I): Statistical Method Analysis of Tensile Strength Response

Similar to the analysis of Izod Impact Strength data, a coded design matrix for tensile strength is created as illustrated in Table 7-3. We begin the analysis of tensile strength data by developing an Anova table to identify significance of each main factor or interaction combination factors. Based on an alpha value of 5%, it is concluded that factors or interactions with a lower than 5% P value are significant.

An Anova table (Table 7-4) is constructed based on the factorial design of experiment previously explained. Significant main factors or interactions are indicated with an asterisk beside the P-values.

The Regression Equation based on above Anova table is presented in Equation 4-2. Significant main factors and interactions are included in the regression equation and insignificant main factors and interactions are omitted from the equation.

Equation 4-2: DOE (I) Tensile Strength Regression equation

$$Tensile\ Strength\ (Mpa) = 34.420 + 3.010\,A - 0.620\,C + 6.111\,D + 0.628\,A \cdot B + 1.805\,A \cdot D + 0.491\,B \cdot C + 0.495\,C \cdot D + 0.557\,A \cdot B \cdot C - 0.410\,A \cdot B \cdot D + 0.371\,A \cdot B \cdot C \cdot D$$

$$Where: A = 1\ for\ BAGASSE\ as\ fiber, A = -1\ for\ OAT\ HULL\ as\ fiber$$

$$B = 1\ for\ IMA = 5\%, B = -1\ for\ IMA = 0\%$$

$$C = 1\ for\ IMB = 5\%, C = -1\ for\ IMB = 0\%$$

$$D = 1\ for\ Coupling\ Agent = 4\%, D = -1\ for\ Coupling\ Agent = 0\%$$

Based on the Anova table, a normal probability plot of effects is constructed as follows. The deviation of data points from the straight line shows that the data points shown in red are in fact significant. The following (Figure 4-13) confirms the significance of main effects and interactions that were analytically concluded.

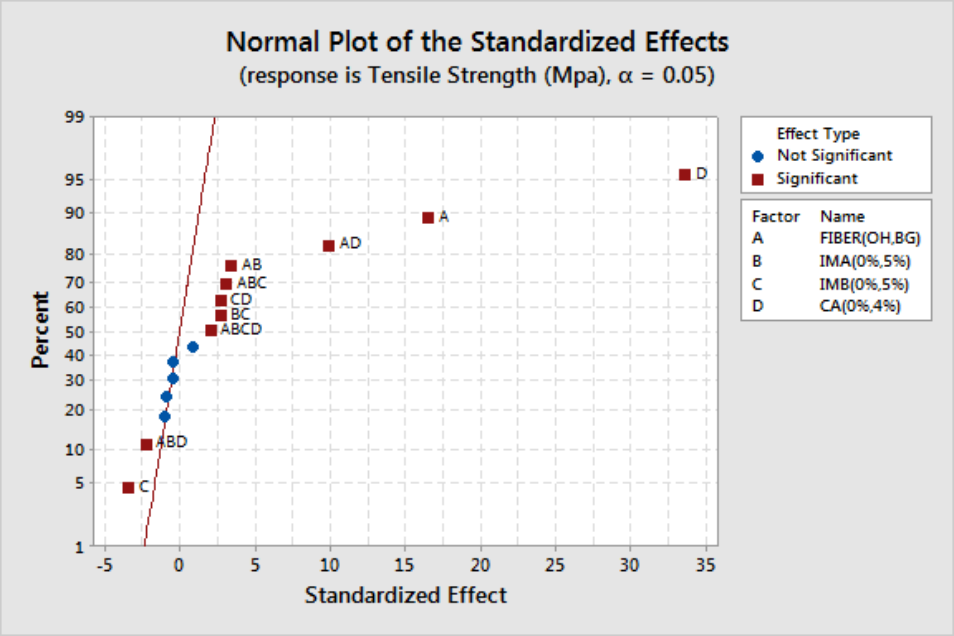

Figure 4-13: DOE (I) Normal Plot of Standardized Tensile Strength effects

To check that such assumptions were correct it is necessary to look at the residuals plot and see if the residuals are normally distributed or not. Compared to the same graph for Izod impact Strength, the points on the normal probability plot of tensile Strength response plot shown in Figure 4-14 are less close to a straight line. This supports the fact that underlying assumptions of the analysis are mildly satisfied comparatively.

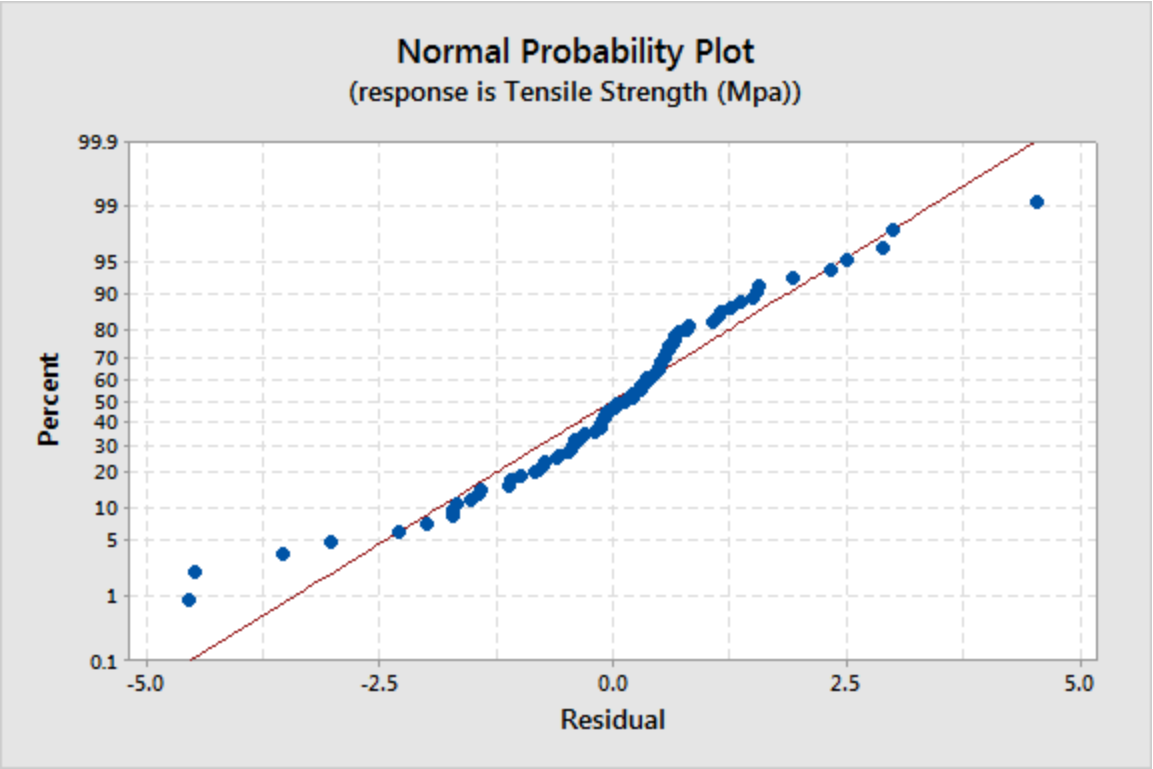

Figure 4-14: DOE (I) Tensile Strength Normal Probability Plot

4.2.1.1.3 DOE (I): Statistical Method Analysis of Flexural Modulus Response

For Flexural Modulus at 1% we similarly have Table 7-5. An Anova table (Table 7-6) is constructed based on the factorial design of experiment previously explained. Significant main factors or interactions are indicated with an asterisk beside the P-values.

The Regression Equation based on above Anova table is presented in Equation 4-3. Significant main factors and interactions are included in the regression equation and insignificant main factors and interactions are omitted from the equation.

Equation 4-3: DOE (I) Flexural Modulus Regression equation

$$FLEXURAL\ MODULUS\ (MPA)\ @1\% = 2196.3 + 339.0\,A - 55.5\,B - 43.1\,C + 57.5\,D + 30.5\,A*B + 45.4\,A*C + 77.2\,A*D + 48.3\,B*C - 37.5\,B*D + 35.9\,C*D - 56.9\,A*B*C + 68.2\,A*C*D$$

$$Where: A = 1\ for\ BAGAASSE\ as\ fiber, A = -1\ for\ OAT\ HULL\ as\ fiber$$

$$B = 1\ for\ IMA = 5\%, B = -1\ for\ IMA = 0\%$$

$$C = 1\ for\ IMB = 5\%, C = -1\ for\ IMB = 0\%$$

$$D = 1\ for\ Coupling\ Agent = 4\%, D = -1\ for\ Coupling\ Agent = 0\%$$

Based on the Anova table, a normal probability plot of effects (Figure 4-15) is constructed. The deviation of data points from the straight line shows that the data points shown in red are in fact significant. Following graph (Figure 4-15) confirms the significance of main effects and interactions that were analytically concluded using the Analysis of Variance (ANOVA).

Figure 4-15: DOE (I) Normal Plot of effects for Flexural Modulus @ 1%

To check if the assumptions for our two level replicated factorial design of experiment were correct it is necessary to look at the residuals plot and see if the residuals are normally distributed or not. The points on this plot shown in Figure 4-16 are reasonably close to a straight line which supports the fact that the underlying assumptions of the analysis are satisfied.

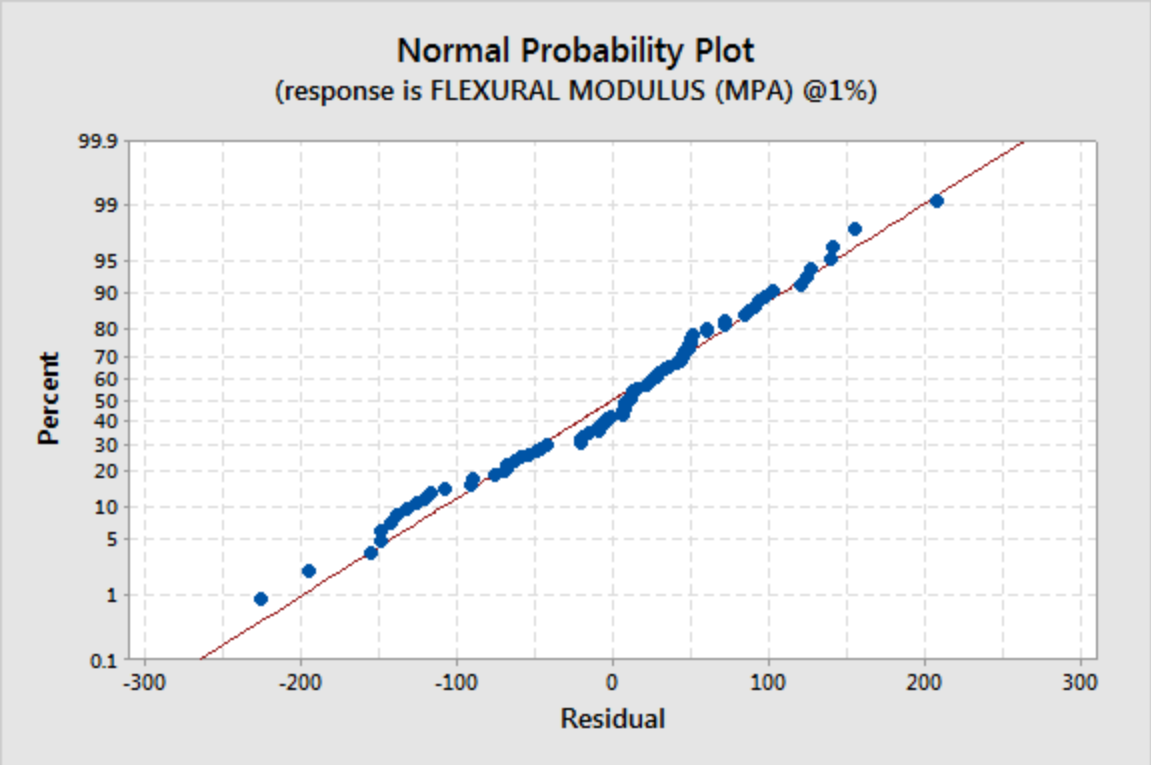

Figure 4-16: DOE (I) for Normal Probability Plot of Flexural Modulus @ 1%

4.2.1.1.4 DOE (I): Statistical Method Analysis of Mean Failure Energy Response

We begin the analysis of Table 7-7 by developing an Anova table (Table 7-8) to identify significance of each main factor or interaction combination factors based on an alpha value of 5%. As the experiment is not replicated, the error will have zero degrees of freedom and therefore there will be no F and P values to perform hypothesis testing.

To create one degree of freedom, we assume there is no 4-way interaction and therefore one degree of freedom will appear for error term of Anova table (Table 7-9):

The 3-way interaction term ACD appears not to be significant so this term can also be removed so that the degree of freedom of error term becomes 2 and the analysis becomes further reasonable. The new Anova table is presented in Table 7-10.

The 3-way interaction term ABC appears not to be significant too, so this term can also be removed so that the degree of freedom of error term becomes 3 and again the analysis becomes further reasonable. The new Anova table is presented in Table 7-11.

The 2-way interaction terms AB, BD and CD appear not to be significant too, so these terms can also be removed so that the degrees of freedom of error term becomes 6 and again the analysis becomes further reasonable. The new Anova table is presented in Table 7-12.

Table 7-12 appears to be the final Anova table as there are no more insignificant main effects or interaction terms. Terms denoted with an asterisk are significant.

The Regression Equation based on Table 7-12 is presented in Equation 4-4.

Equation 4-4: DOE (I) Mean Failure Energy Regression equation

$$\begin{aligned} &Mean\ Failure\ Energy\ (J) \\ &= 0.84412 + 0.06352\,A + 0.05590\,B + 0.09293\,C \\ &- 0.03998\,D + 0.03184\,A*C + 0.07731\,A*D \\ &- 0.07232\,B*C + 0.04610\,A*B*D + 0.02736\,B*C*D \qquad (\\ &Where: A = 1\ for\ BAGASSE\ as\ fiber, A = -1\ for\ OAT\ HULL\ as\ fiber \\ &B = 1\ for\ IMA = 5\%, B = -1\ for\ IMA = 0\% \\ &C = 1\ for\ IMB = 5\%, C = -1\ for\ IMB = 0\% \\ &D = 1\ for\ Coupling\ Agent = 4\%, D = -1\ for\ Coupling\ Agent = 0\% \end{aligned}$$

Based on this Anova table, a normal probability plot of effects is constructed as follows. The deviation of effects data points from the straight line shows that the data points are in fact significant.

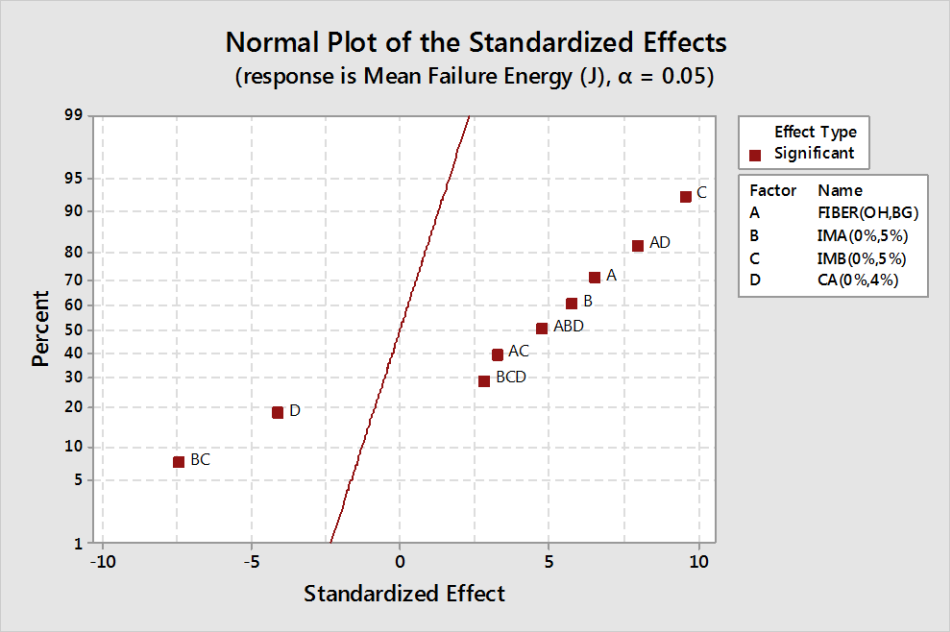

Figure 4-17: Normal Plot of standardized effects for Mean Failure Energy

To check that such assumptions were correct it is necessary to look at the residuals plot and see if the residuals are normally distributed or not. The points on this plot shown in Figure 4-18 are reasonably close to a straight line, although the distribution of the residual points are not well scattered below and above the mean line. This supports the hypothesis that underlying assumptions of the analysis are mildly satisfied.

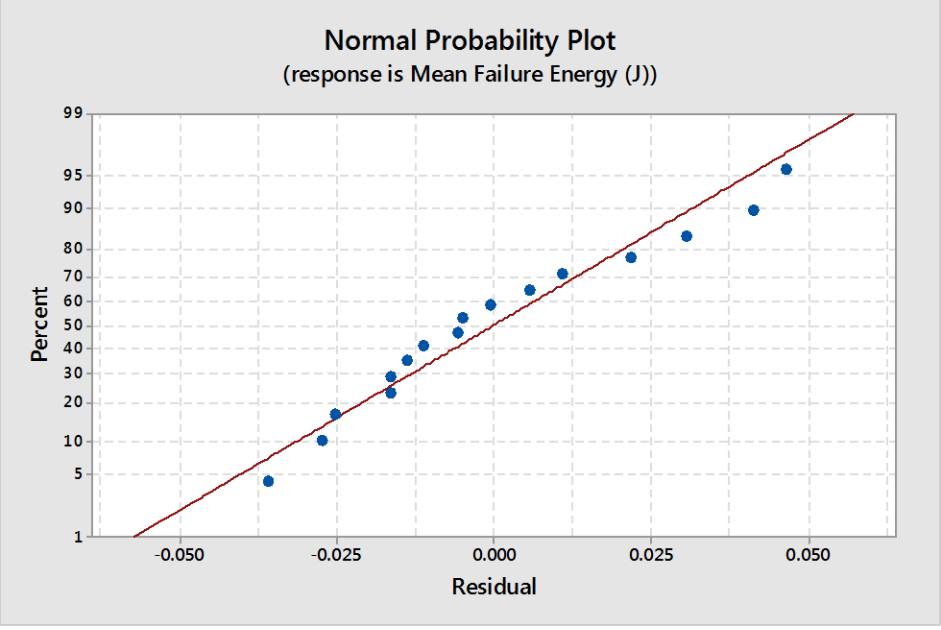

Figure 4-18: DOE (I) Normal Probability plot for mean failure energy

4.2.1.2 DOE (I) Main Effects and Interactions Analysis

A summary comparing main effects means in per cents of improvement or deterioration for DOE(I) is presented in Table 4-7. The table as well lists the significant interactions observed between the main effects.

Table 4-7: DOE(I) Summarized main effects and interactions for mechanical responses

DOE (I)			Mean Improvement (+%) , Mean Detorioration (-%), Interaction Exists (✓)			
			Izod Impact Strength	Tensile Strength	Flexural Modulus	Mean Failure Energy
Main Effects (from - to)	Oat Hull	Bagasse	16%	20%	36%	17%
	IMA 0%	IMA 5%	10%	-	-	17%
	IMB 0%	IMB 5%	20%	-	-	25%
	CA 0%	CA 4%	-	40%	-	8%
Interactions	CA % - Fiber type		✓	✓	-	✓
	IMA % - IMB %		✓	-	-	✓
	Fiber Type - IMB %		-	-	-	✓

4.2.1.2.1 DOE (I) Izod Impact Main Effects and Interactions Analysis

The main effects of Fiber type, impact modifiers (IMA, IMB) and Coupling agent are plotted in Figure 4-19. All main effects are positive except the coupling agent main effect which is almost neutral. As fiber type is changed from Oat hull to bagasse a significant increase of approximately 16% is observed in mean Izod impact strength. When impact modifier B (IMB) is introduced to the composite material, a significant increase of 20% is observed to the mean Izod impact strength of the composite material compared to impact modifier A (IMA) which when is introduced in to the composite material, increased the Izod impact strength by 10%. Based on main effects consideration only, the Coupling agent main effect does not significantly affect the Izod impact property when compared to other three factors.

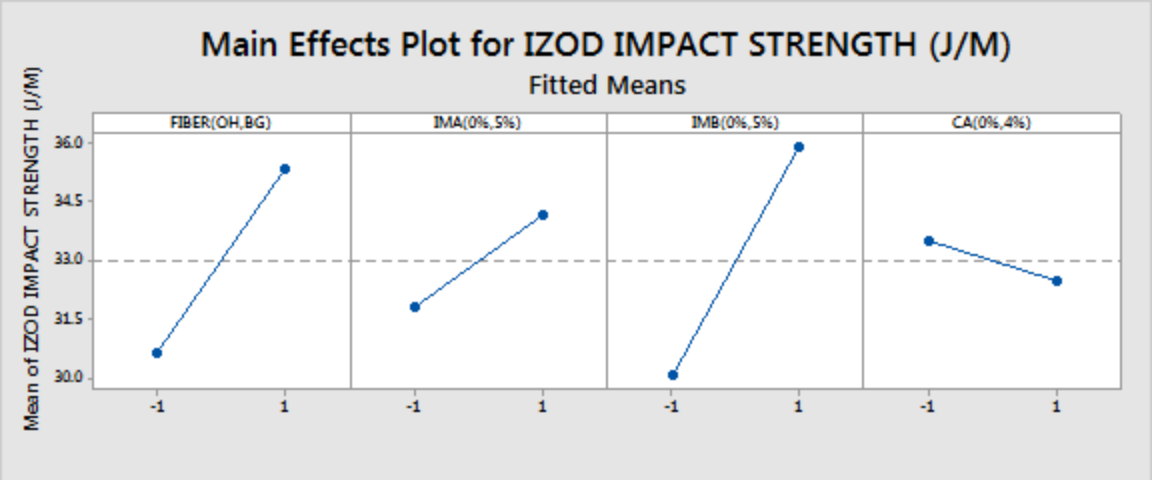

Figure 4-19: DOE (I) Izod Impact Main effects plot

If only these main effects are considered, maximum Izod impact strength would be obtained from running all factors at high level with coupling agent at high or low level. However, it is necessary to examine any interactions that are important. In fact, main effects do not have much meaning when they are involved in significant interactions.

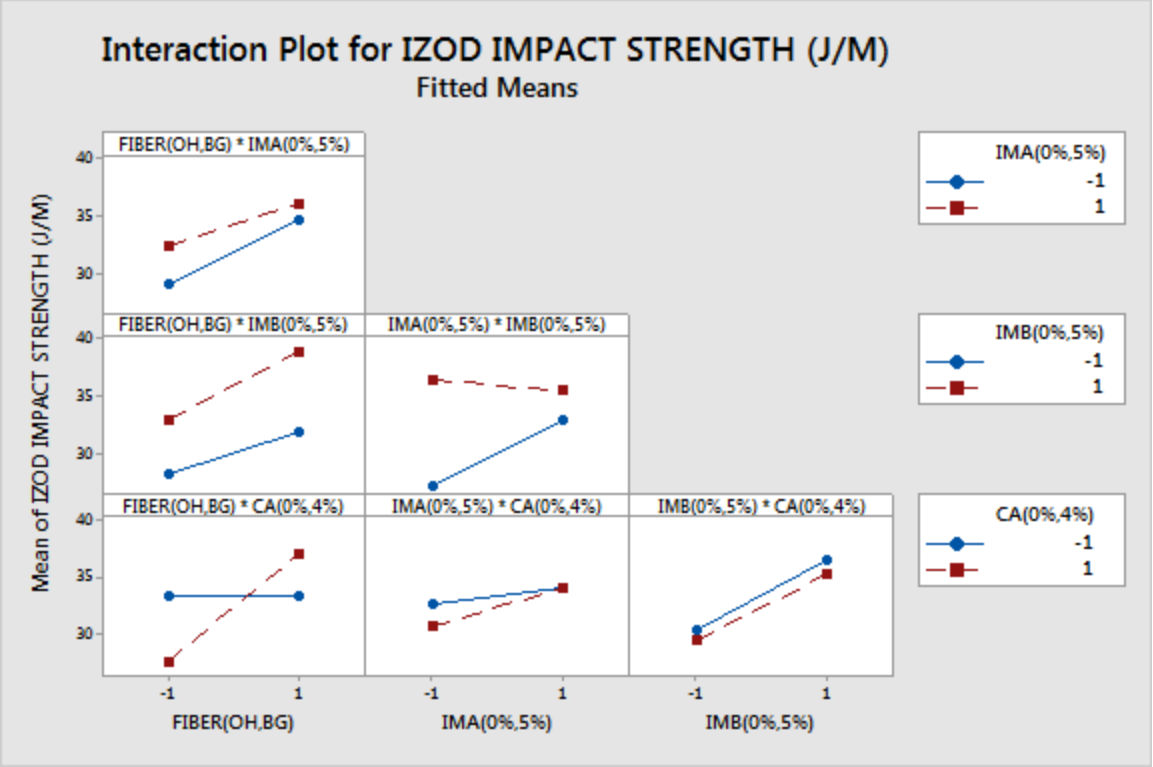

Figure 4-20: DOE (I) Izod Impact interaction plot

It can be concluded from interactions plot series shown in Figure 4-20 that there is significant interaction between Fiber type and coupling agent. When the coupling agent is at low level (0%), average Izod impact strength stays almost at the same level of about 35 (J/M), however, when the coupling agent is at high level (4%), fiber type effect appears to be significant; meaning, when we move from oat hull as the fiber to bagasse as the fiber of choice, there is an approximately 35% increase in the average Izod impact strength. It can be inferred that coupling agent is much more effective on Izod impact response of composites with bagasse fibers compared to composites with oat hull fibers. This can be further explained by availability of more hydroxyl groups on bagasse surface compared to oat hull, that maleic anhydride coupling agent reacts more and produces better adhesion of fibers to the polymer matrix compared to oat hull.

Another significant interaction is also notable in Figure 4-20. When IMB is at high level, which simply means it exists in the compound, it appears that changing the level of IMA is not effective on average Izod impact strength, however, when IMB is at low level and IMA is varied from 0% to 5%, there is a mild increase in average Izod impact strength of about 10%. This might illustrate that IMB and IMA cancel out each other's effect on Izod impact strength of the fiber polymer compound. The other interaction graphs indicate that their corresponding interacting factors are insignificant.

The graph in Figure 7-1 was generated based on an optimum solution considering both main effects and interactions to result in best possible Izod impact strength. Therefore, the best Izod impact strength would appear to be obtained when Fiber type is at high level (using bagasse fiber), IMA is at low level (0%), IMB is at high level (5%) and coupling agent is at high level (4%). This eliminates IMA from the formulation.

A response surface model was generated based on regression analysis of the data, the response surface contour plots generated from the model are shown in Figure 4-21. Notice that the contours are curved lines when an interaction exits while the contours are parallel straight lines when no interaction exists between main factors.

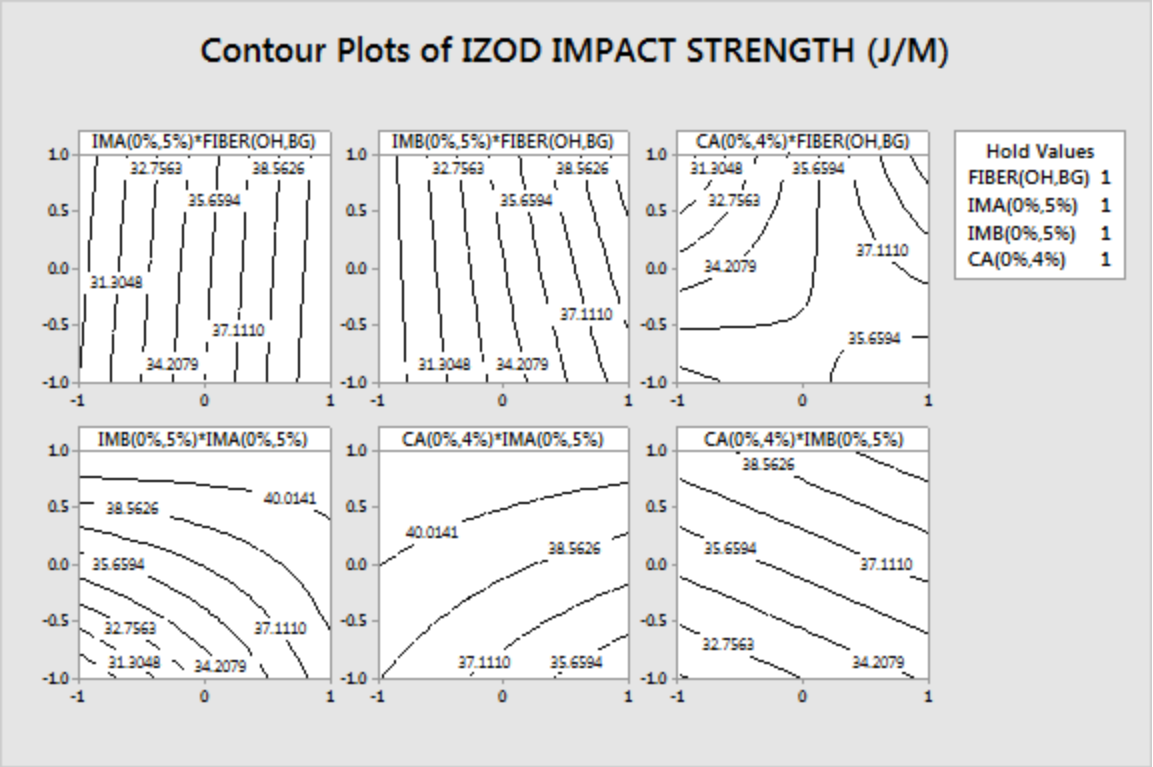

Figure 4-21: DOE (I) Izod Impact Contour Plots

We obtained similar conclusions from the interaction graphs.

4.2.1.2.2 DOE (I) Tensile Strength Main Effects and Interactions Analysis

The main effects of Fiber type, impact modifiers (IMA, IMB) and coupling agent are plotted in Figure 4-22. The impact modifiers main effect (IMA and IMB) appear to be neutral although the main effect of Fiber type and coupling agent are very significant. As fiber type is changed from oat hull to bagasse a significant increase of approximately 20% is observed in mean tensile strength. On other hand, as coupling agent is added to the composite blend, the mean tensile strength is increased by approximately 40% which is very significant.

Main effect of both impact modifiers A and B do not significantly affect the mean tensile strength property when compared to other two main factors of fiber type and coupling agent.

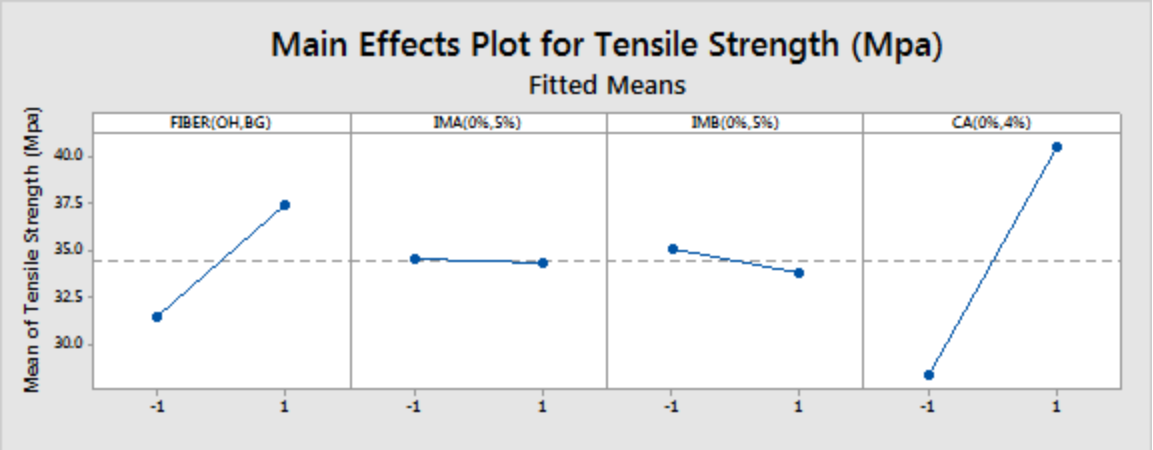

Figure 4-22: DOE (I) Tensile strength main effects plot

If only these main effects are considered, maximum tensile strength would be obtained from having fiber type and coupling agent at high level with impact modifiers at either level, however it is necessary to examine any interactions that are important. In fact, main effects do not have much meaning when they are involved in significant interactions.

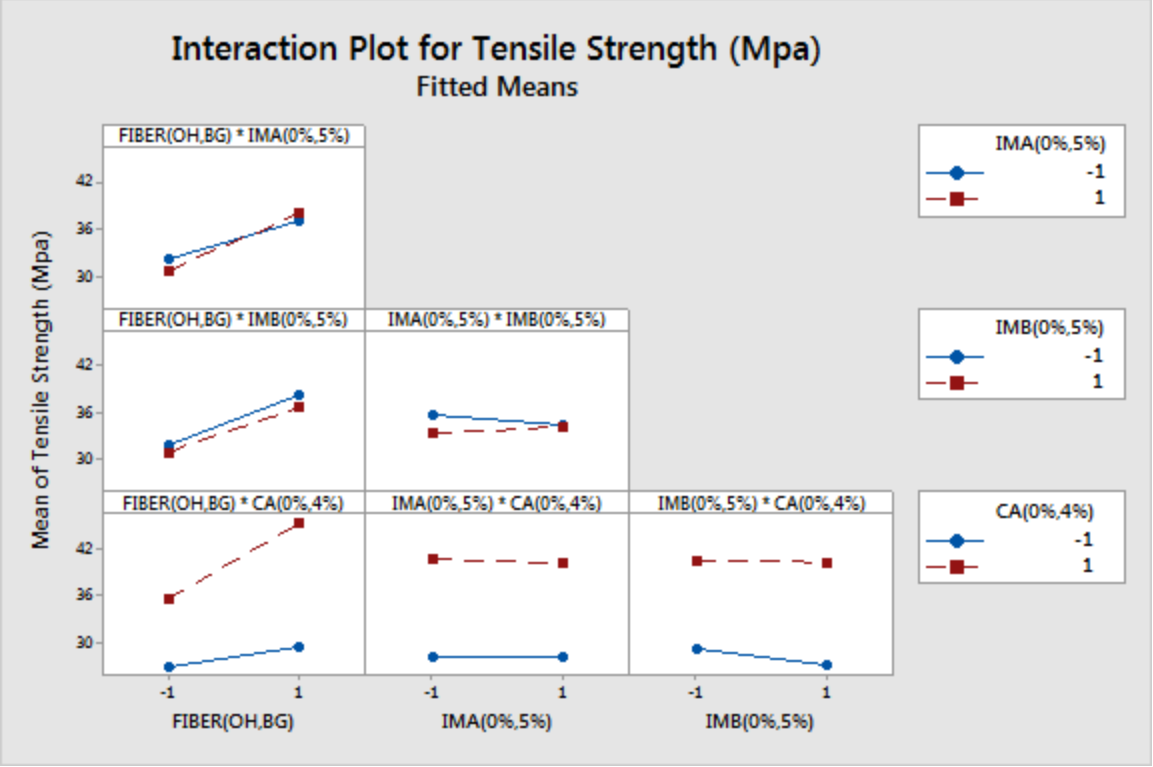

Figure 4-23: DOE (I) Tensile Strength interaction plot

It can be concluded from interactions plot series shown in Figure 4-23 that there is significant interaction between Fiber type and coupling agent. When the coupling agent is at low level (0%), average Tensile strength stays almost at the same level of about 30 (MPA), however, when the coupling agent is at high level (4%), fiber type effect appears to be significant; meaning, when we move from oat hull as the fiber to bagasse as the fiber of choice, there is an approximately 25% increase in the average tensile Strength. No other significant interaction plot is observed.

Figure 7-2 was generated based on an optimum solution considering both main effects and interactions to result in highest possible tensile strength. Therefore, the highest tensile strength would appear to be obtained when fiber type is at high level (using bagasse fiber), IMA is at low level (0%), IMB is at low level (0%) and coupling agent at high level (4%). This eliminates IMA and IMB from the formulation and reconfirms that bagasse and coupling agent are significant factors positively affecting the tensile strength of the composite.

A response surface model was generated based on regression analysis of the data. The response surface contour plots are generated from the model shown in Figure 4-24. Notice that the contours are curved lines when an interaction exits (i.e. for coupling agent-fiber type interaction) while the contours are parallel straight lines when no interaction exists between main factors (i.e. coupling agent – IMA interaction).

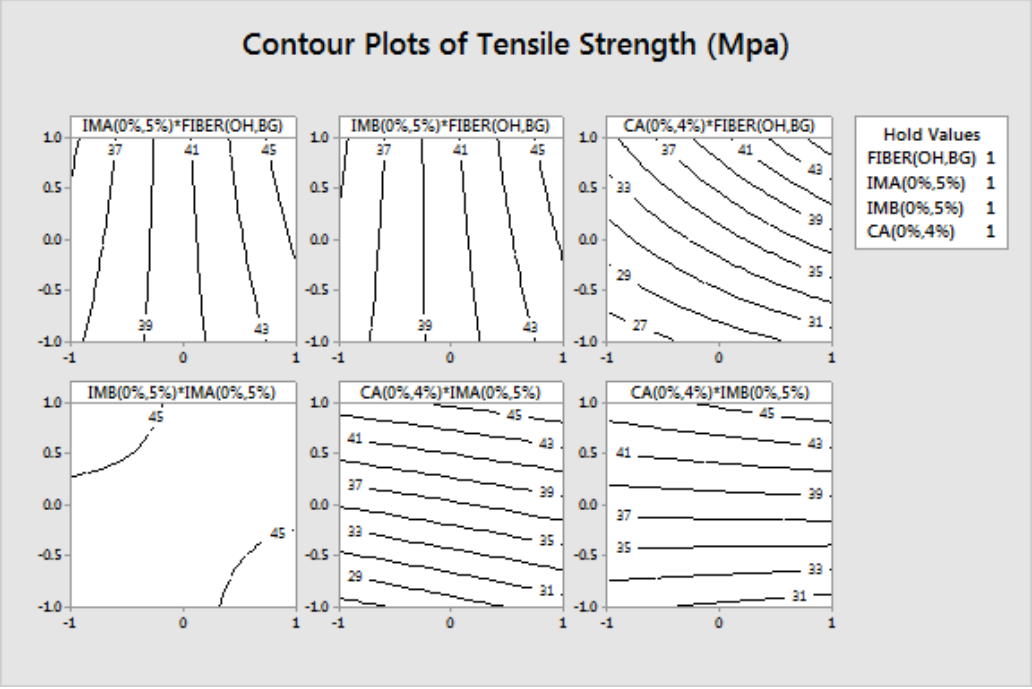

Figure 4-24: DOE (I) Tensile Strength Contour Plots

Similar results were obtained from the interactions graph.

4.2.1.2.3 DOE (I) Flexural Modulus Main Effects and Interactions Analysis

The main effects plot (Figure 4-25) shows positive effect for Fiber type and coupling agent when moving from low level to high level. A highly significant increase of approximately 36% in average Flexural Modulus @ 1% (MPA) is observed when we move from oat hull as fiber to bagasse as fiber. The main effects plot shows that both IMA and IMB have negative effect of approximately 5% on average flexural modulus, however, the effect of coupling agent on average Flexural modulus is a positive increase of approximately 5%. If only these main effects are considered, maximum flexural modulus would be obtained from having fiber type and coupling agent at high level with impact modifiers at low level (or 0%) however it is necessary to examine any interactions that are important. In fact, Main effects do not have much meaning when they are involved in significant interactions.

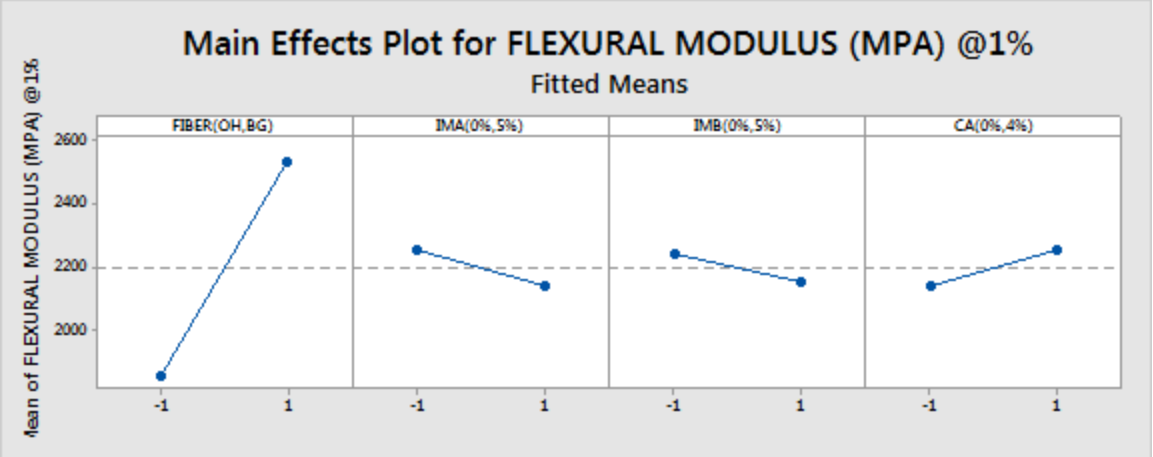

Figure 4-25: DOE (I) Main Effects plot for Flexural Modulus @ 1%

It can be concluded from the interactions plots (Figure 4-26) that there are no significant interactions between the main factors, affecting the average flexural modulus of the composite. Some mild interactions are detected: When coupling agent is at high level (4%), moving from oat hull as fiber to bagasse as fiber, the flexural modulus shows mildly more increase compared to same fiber alteration, when coupling is at low level (0%).

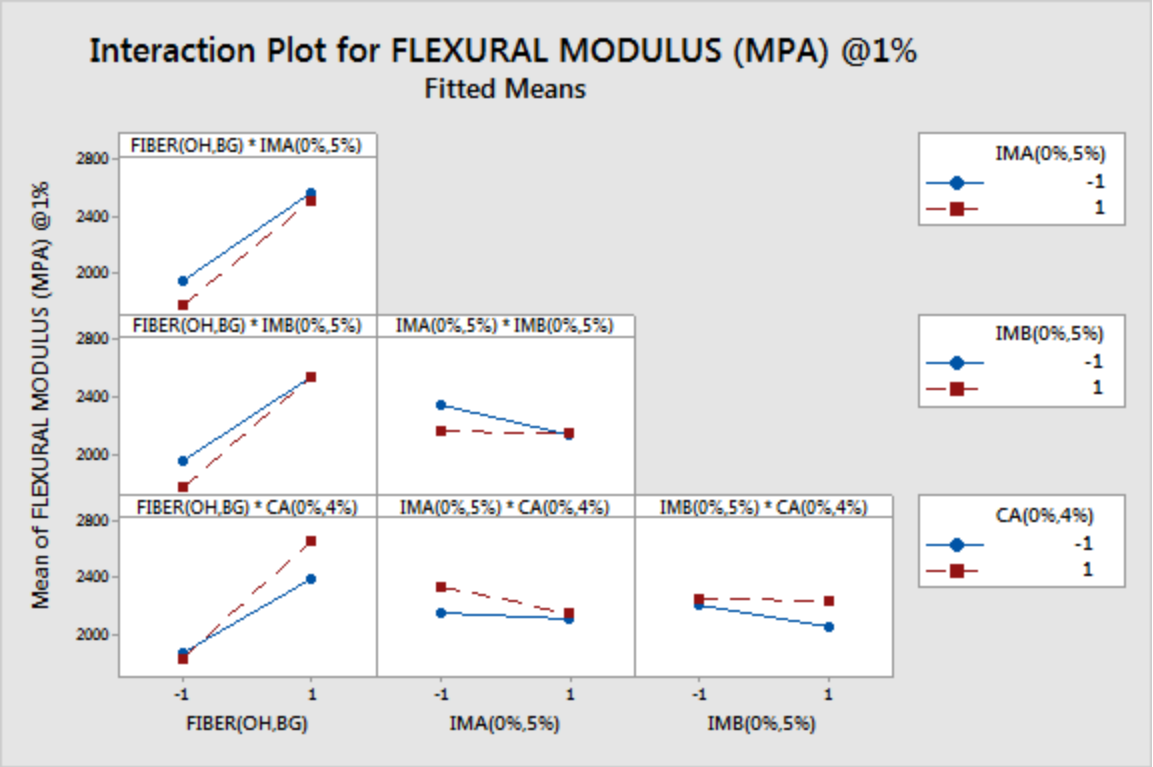

Figure 4-26: DOE (I) Interaction Plot for Flexural Modulus @ 1%

Figure 7-3 was generated based on an optimum solution considering both main effects and interactions to result in best possible flexural modulus. The highest flexural modulus would appear to be obtained when fiber type is at high level (using bagasse fiber), IMA is at low level (0%), IMB is at high level (5%) and coupling agent at high level (4%). This eliminates IMA from the formulation and reconfirms that bagasse and coupling agent are significant factors positively affecting the flexural modulus of the composite.

A response surface model was generated based on regression analysis of the data. The response surface contour plots generated from the model are shown in Figure 4-27. Notice that the contours are curved lines when an interaction exits (i.e. for coupling agent-fiber type interaction) while the contours are parallel straight lines when no interaction exists between main factors (i.e. fiber type – IMA or fiber type – IMB interaction).

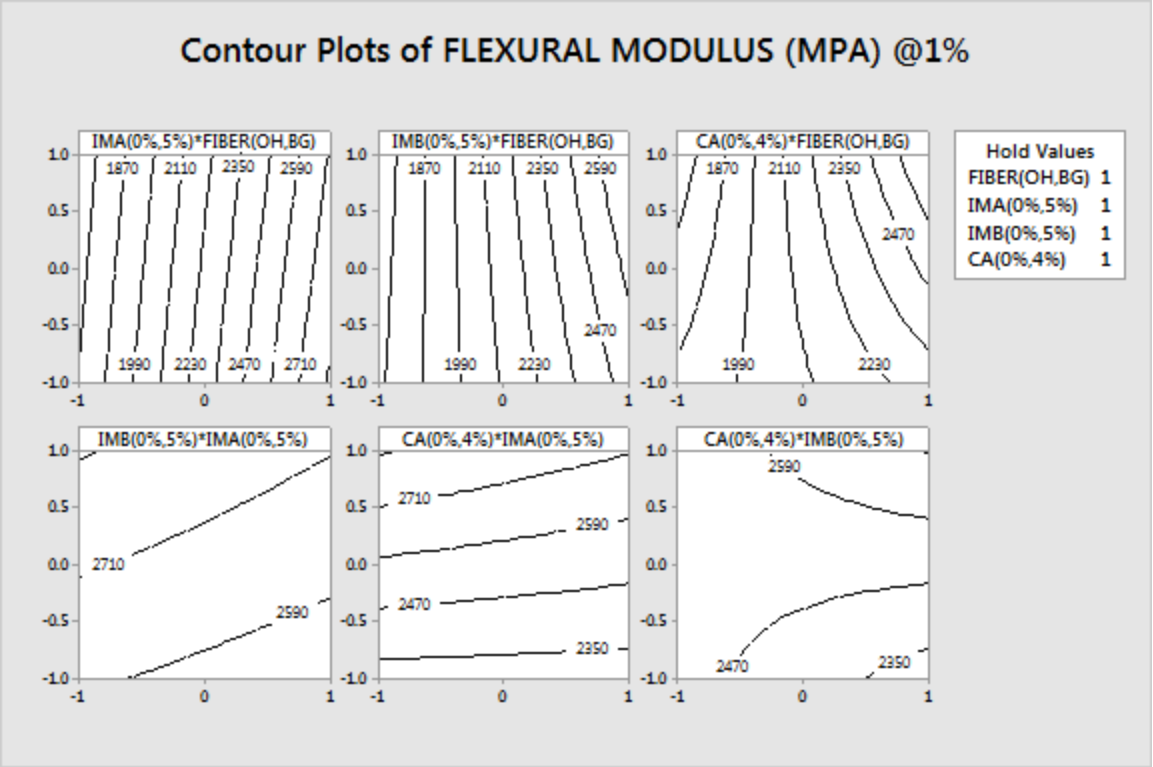

Figure 4-27: DOE (I) Contour Plots for Flexural Modulus @ 1%

Similar results were obtained from the interactions graph.

4.2.1.2.4 DOE (I) Mean Failure Energy Main Effects and Interactions Analysis

The main effects of fiber type, impact modifiers (IMA, IMB) and coupling agent are plotted below. All main effects are positive except the coupling agent main effect which is negative. As fiber type is changed from oat hull to bagasse an increase of approximately 15% is observed in mean failure energy (J). When impact modifier B (IMB) is introduced to the composite material, a significant increase of 25% is observed to the mean failure energy (J) of the composite material compared to impact modifier A (IMA) which when is introduced in to the composite material, increased the mean failure energy by 15%. Adding coupling agent to the formulation decreases the mean failure energy by approximately 8%.

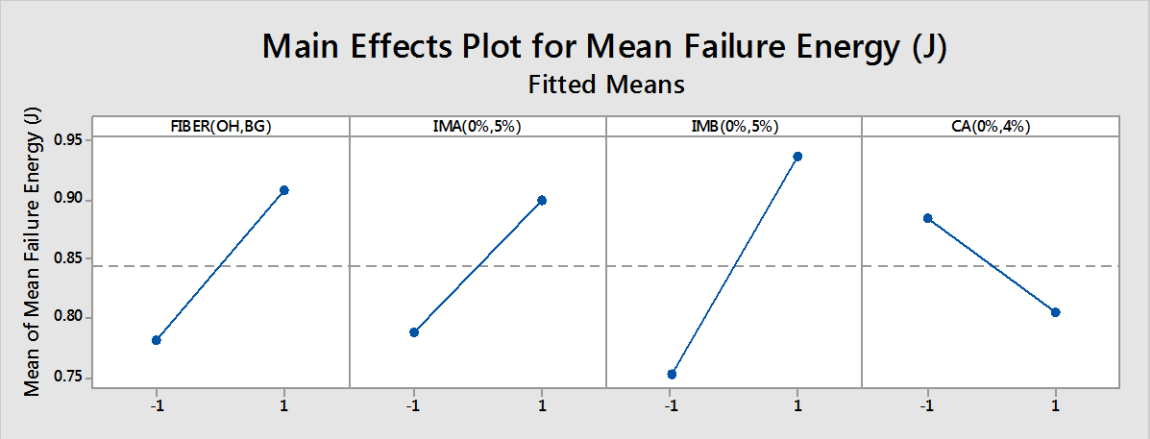

Figure 4-28: DOE (I) Main Effects plot for mean failure energy

If only these main effects are considered, maximum mean failure energy would be obtained from running all factors at high level with coupling agent at low level. However, it is necessary to examine any interactions that are important. In fact, main effects do not have much meaning when they are involved in significant interactions.

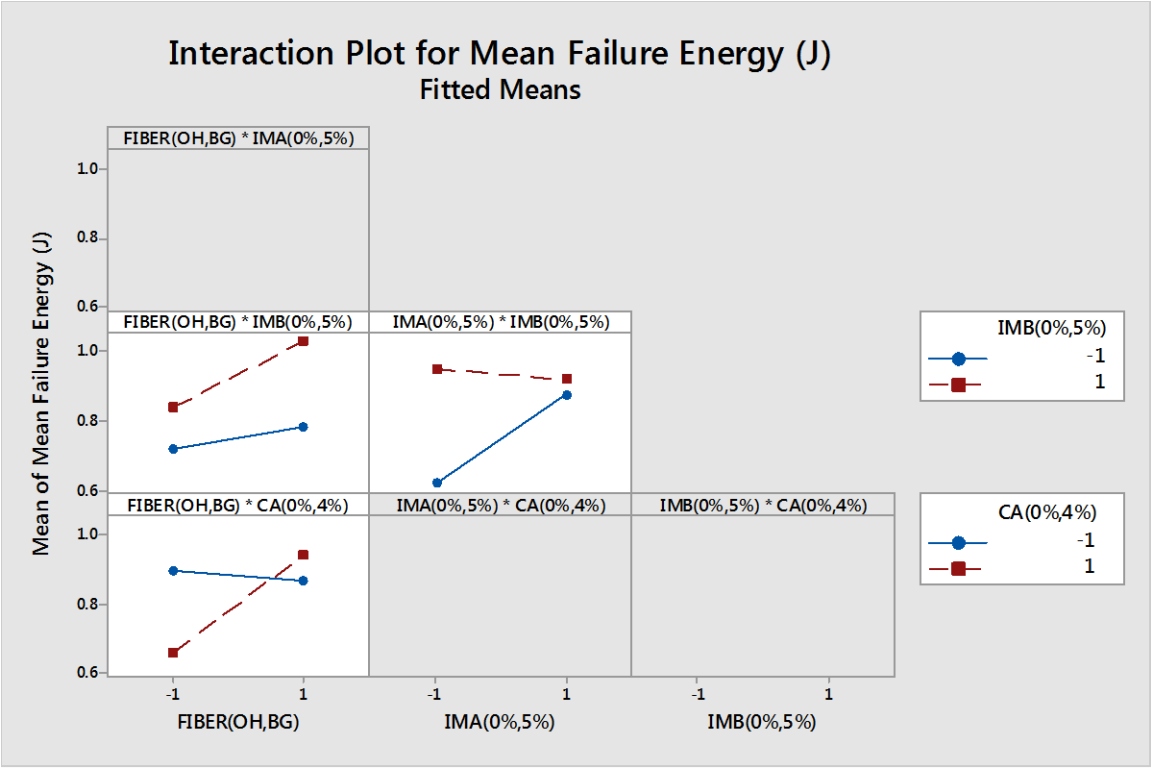

Figure 4-29: DOE (I) Interaction plot for mean failure energy

Interactions graphs are shown in Figure 4-29. Some of the interaction terms do not appear in the graph as some of interaction terms, due to insignificance, were considered as a replicate term of significant factors.

An outstanding interaction is observed between Fiber type effect and Coupling agent content effect. When no coupling agent is present in the formulation, changing the fiber type from oat hull to bagasse does not change the mean failure energy and stays at the 0.9 (J), however, when coupling agent is present in the formulation at high level (4%), changing the fiber type from oat hull to bagasse increases the mean failure energy by approximately 45% to 0.95 Joules.

Another notable interaction is between fiber type effect and impact modifier B effect. When IMB is at low level, changing the fiber type from oat hull to bagasse does not change the mean failure energy significantly and it stays at 0.75 (J), however, when IMB is present in the formulation, changing the fiber type from oat hull to bagasse increases the mean failure energy by 25% to 1.05 (J).

The graph in Figure 7-4 was generated based on an optimum solution considering both main effects and interactions to result in highest possible mean failure energy. Therefore, the best mean failure energy would appear to be obtained when fiber type is at high level (using bagasse fiber), IMA is at high level (5%), IMB is at high level (5%) and coupling agent is at high level (4%).

A response surface model was generated based on regression analysis of the data. The response surface contour plots generated from the model are shown in Figure 4-30. Notice that the contours are curved lines when an interaction exits while the contours are parallel straight lines when no interaction exists between main factors.

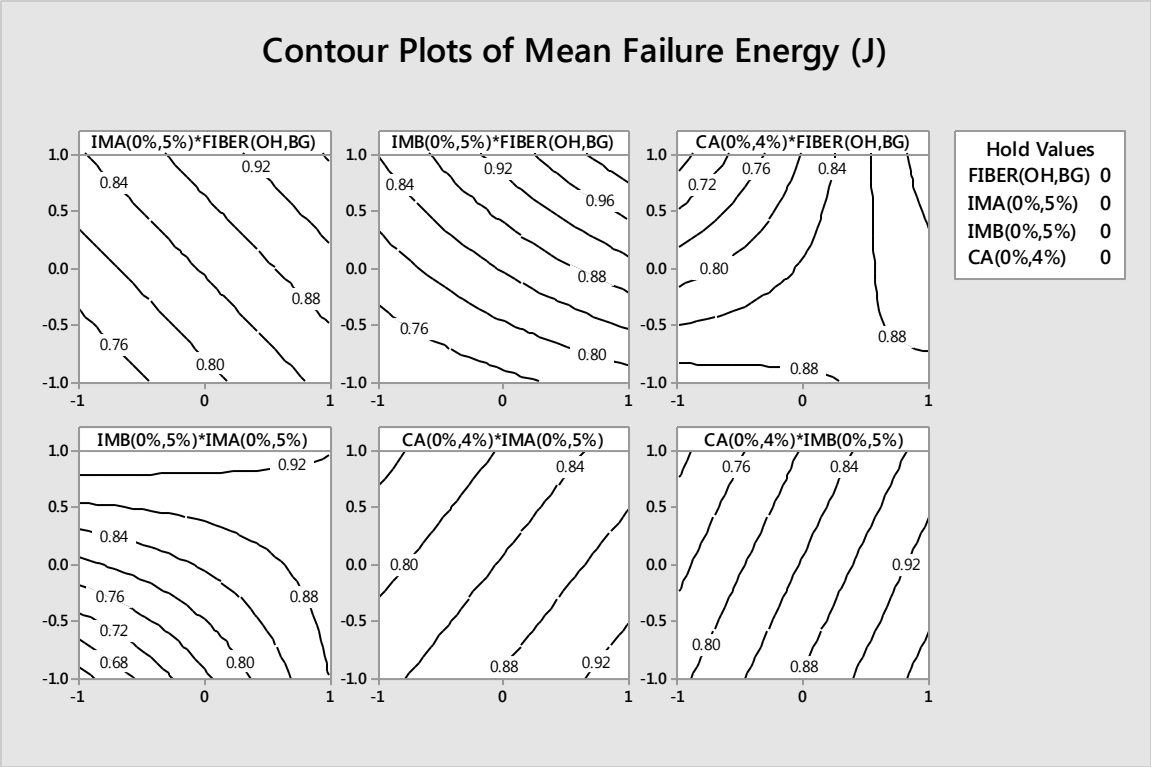

Figure 4-30: DOE (I) Mean Failure Energy Contour Plots

4.2.2 Design of Experiment II (DOE II)

For DOE (II) presented in Table 4-8, bagasse fiber is the only fiber type present in all experiments of this design, and the effect of polypropylene grade (Braskem or Polynar), impact modifier A (0% or 5%), impact modifier B (0% or 5%) and coupling agent (0% or 4%) on 1- Izod impact strength, 2-Tensile strength and 3- Flexural modulus and 4-Mean failure energy of compounded bagasse fiber-polypropylene composite is studied. According to each run number, Table 4-5 summarizes results of DOE (II).

Table 4-8: DOE(II)

Run #	Fiber Type	Fiber %	PP	PP	Impact Modifier		Antioxidant	C. Agent
			Braskem	Polynar	A	B		PP-MA
5	Bagasse	40	50.5	0	5	0	0.5	4
6	Bagasse	40	50.5	0	0	5	0.5	4
7	Bagasse	40	50.5	0	2.5	2.5	0.5	4
8	Bagasse	40	55.5	0	0	0	0.5	4
9	Bagasse	40	54.5	0	5	0	0.5	0
10	Bagasse	40	54.5	0	0	5	0.5	0
11	Bagasse	40	54.5	0	2.5	2.5	0.5	0
12	Bagasse	40	59.5	0	0	0	0.5	0
25	Bagasse	40	0	50.5	5	0	0.5	4
26	Bagasse	40	0	50.5	0	5	0.5	4
27	Bagasse	40	0	50.5	2.5	2.5	0.5	4
28	Bagasse	40	0	55.5	0	0	0.5	4
29	Bagasse	40	0	54.5	5	0	0.5	0
30	Bagasse	40	0	54.5	0	5	0.5	0
31	Bagasse	40	0	54.5	2.5	2.5	0.5	0
32	Bagasse	40	0	59.5	0	0	0.5	0

4.2.2.1 DOE (II) Statistical method Analysis

4.2.2.1.1 DOE (II) Statistical Method Analysis of IZOD IMPACT Response

Table 7-13 illustrates DOE (II) with Izod impact replicated responses. We begin the analysis of this data by developing an Anova table (Table 7-14) to identify significance of each main factor or interaction combination factors. Based on an alpha value of 5%, it is concluded that factors or interactions with a lower than 5% P value are significant.

The Regression Equation based on above table is as follows. Significant main factors and interactions are included in the regression equation and insignificant main factors and interactions are omitted from the equation.

Equation 4-5: DOE(II) Izod Impact Strength Regression Equation

$$IZOD\ IMPACT\ STRENGTH\ (J/M)$$
$$= 35.478 + 1.380\,B + 2.807\,C + 1.684\,D + 0.867\,A*B$$
$$- 0.588\,A*C - 1.583\,B*C + 0.906\,B*D + 0.729\,C*D$$
$$- 0.683\,A*B*D - 0.740\,B*C*D$$
$$Where: A = 1\ for\ Braskem\ PP\ , A = -1\ for\ Polynar\ PP$$
$$B = 1\ for\ IMA = 5\%, B = -1\ for\ IMA = 0\%$$
$$C = 1\ for\ IMB = 5\%, C = -1\ for\ IMB = 0\%$$
$$D = 1\ for\ Coupling\ Agent = 4\%, D = -1\ for\ Coupling\ Agent = 0\%$$

Based on this Anova table (Table 7-14), a normal probability plot of effects is created (Figure 4-31). The deviation of effects data points from the straight line shows that some of the data points are in fact significant.

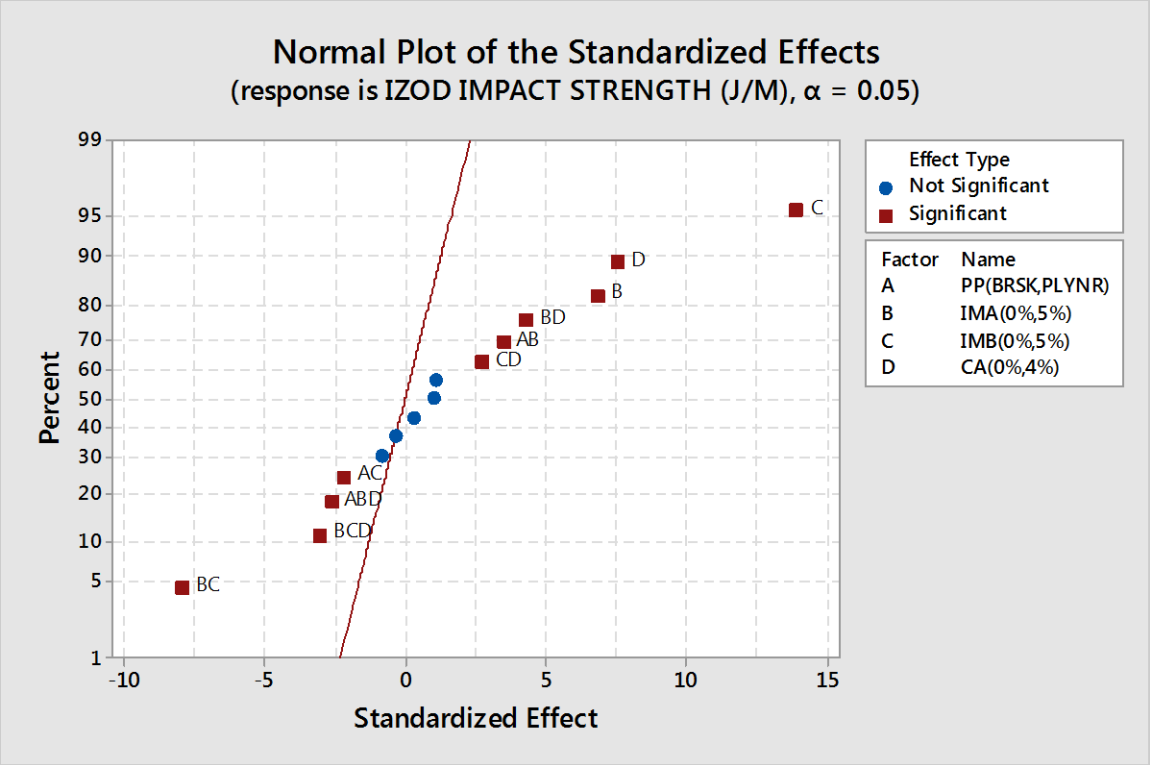

Figure 4-31: DOE (II) Normal Plot of standardized Effects of Izod Impact

To check that the normality assumptions were correct it is necessary to look at the residuals plot and see if the residuals are normally distributed or not. The points on this plot, shown in Figure 4-32, are reasonably close to a straight line which supports the fact that the underlying assumptions of the analysis are satisfied.

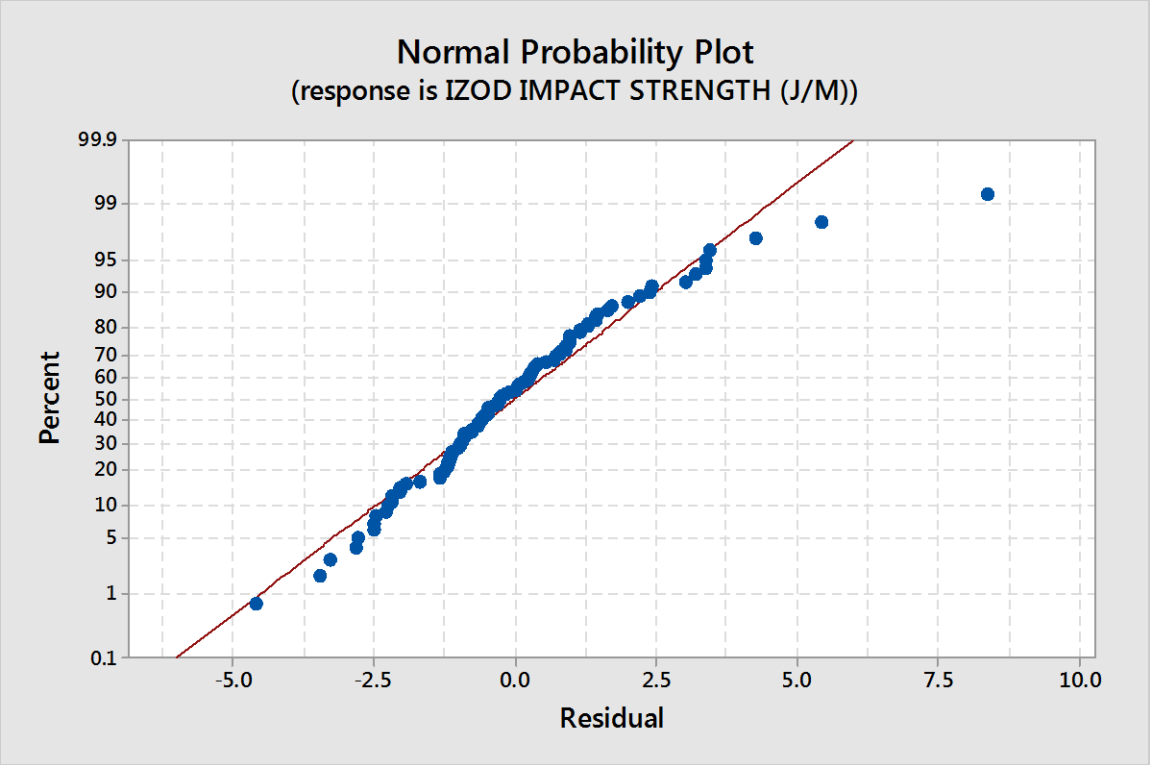

Figure 4-32: DOE (II) Normal Plorbability plot for Izod Impact Strength

4.2.2.1.2 DOE (II) Statistical Method Analysis of Tensile Strength Response

Table 7-15 shows the DOE (II) design matrix with Tensile Strength response.

Similar to the analysis of Izod Impact Strength data, we begin the analysis of tensile strength data by developing an Anova table to identify significance of each main factor or interaction combination factors. Based on an alpha value of 5%, it is concluded that factors or interactions with a lower than 5% P value are significant.

An Anova table (Table 7-16) is constructed based on the factorial design of experiment previously explained. Significant main factors or interactions are indicated with an asterisk beside the P-values.

The Regression Equation based on above Anova table (Table 7-16) is as follows. Significant main factors and interactions are included in the regression equation and insignificant main factors and interactions are omitted from the equation.

Equation 4-6: DOE(II) Tensile Strength Regression Equation

$$Tensile\ Strength\ (Mpa) = 31.497 - 5.933\,A + 1.211\,B - 1.197\,C + 6.410\,D - 1.505\,A*D + 1.013\,B*C$$

$$Where: A = 1\ for\ PP\ vendor\ Polynar\ as\ fiber, A = -1\ for\ PP\ vendor\ Braskem$$

$$B = 1\ for\ IMA = 5\%, B = -1\ for\ IMA = 0\%$$

$$C = 1\ for\ IMB = 5\%, C = -1\ for\ IMB = 0\%$$

$$D = 1\ for\ Coupling\ Agent = 4\%, D = -1\ for\ Coupling\ Agent = 0\%$$

Based on the Anova table (Table 7-16), a normal probability plot of effects is constructed and illustrated in Figure 4-33. The deviation of data points from the straight line shows that the data points shown in red are in fact significant. Following graph confirms the significance of main effects and interactions that were analytically concluded.

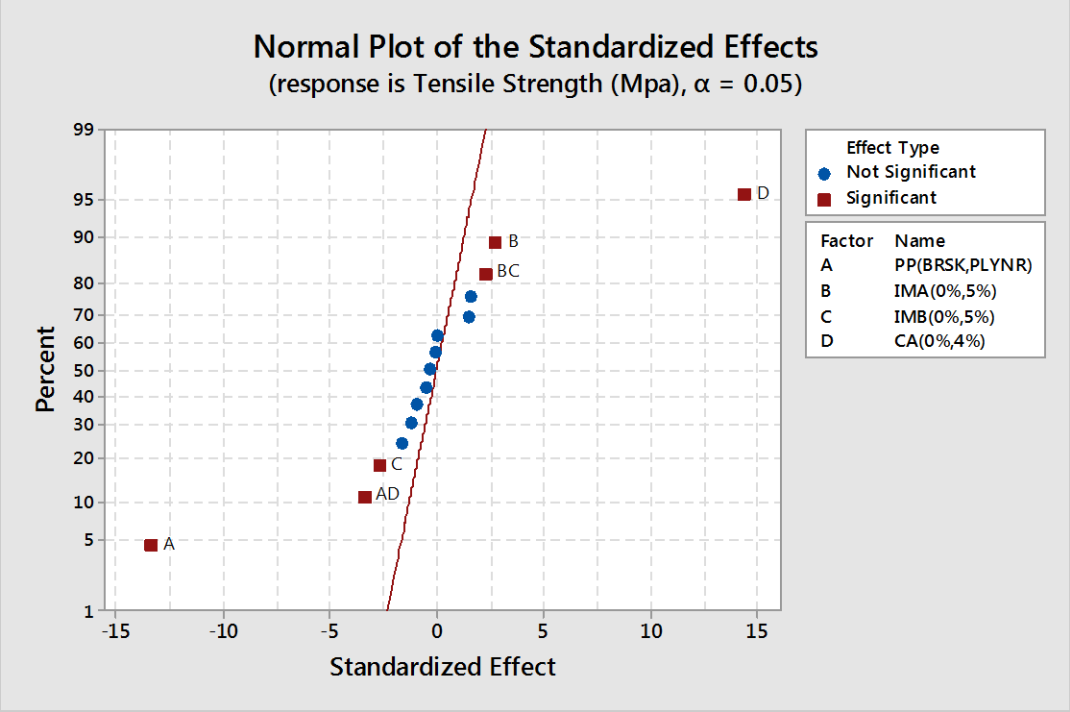

Figure 4-33: DOE (II) Normal Plot of Tensile Strength Standardized effects

To check that the underlying assumptions of this modelling were correct, it is necessary to look at the residuals plot and see if the residuals are normally distributed or not. Compared to the same graph for Izod impact strength, The points on the normal probability plot of tensile Strength response plot shown in Figure 4-34 are less close to a straight line and show somewhat of a curved graphic in parts. This supports the fact that underlying assumptions of the analysis are somewhat satisfied comparatively.

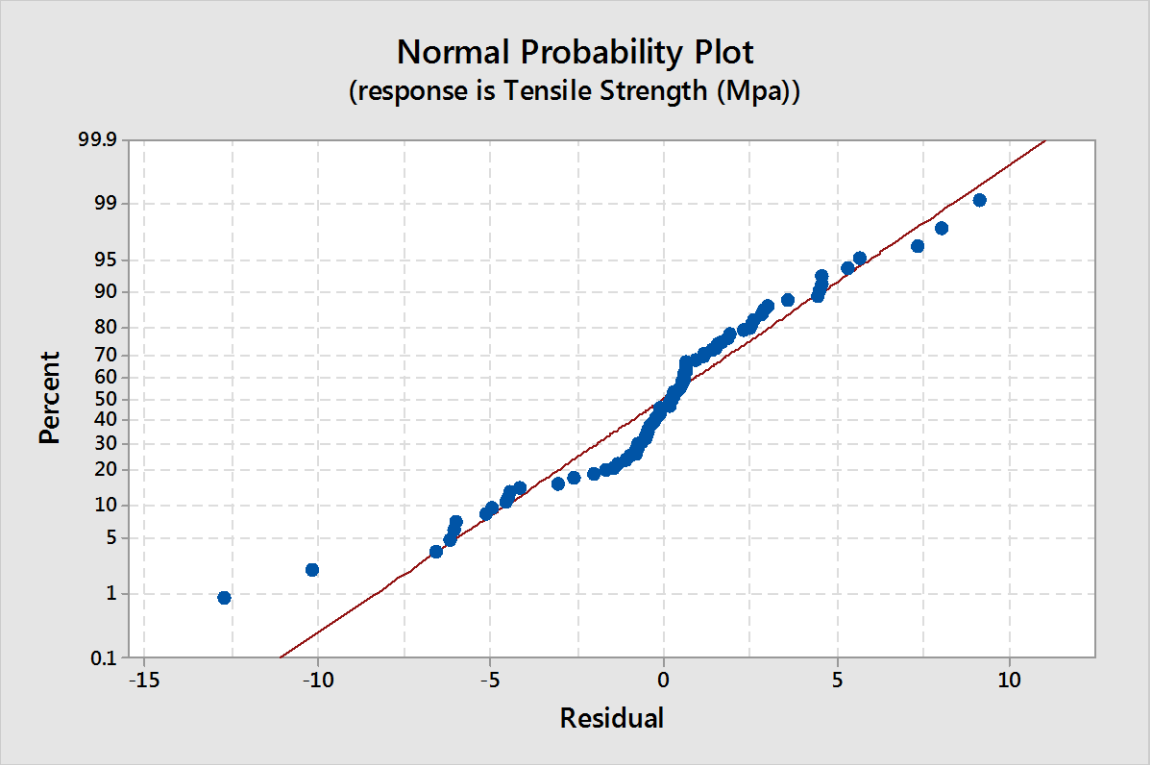

Figure 4-34: DOE (II) Normal Probability plot for Tensile Strength

4.2.2.1.3 DOE (II) Statistical Method Analysis of Flexural Modulus Response

Table 7-17 illustrates DOE (II) with replicated Flexural modulus at 1% responses.

An Anova table (Table 7-18) is constructed based on the factorial design of experiment previously explained. Significant main factors or interactions are indicated with an asterisk beside the P-values.

The Regression Equation based on above Anova table is below. Significant main factors and interactions are included in the regression equation and insignificant main factors and interactions are omitted from the equation.

Equation 4-7: DOE (II) Flexural Modulus Regression Equation

$$FLEXURAL\ MODULUS\ (MPA)\ @1\%$$
$$= 2511.1 - 24.2\,A - 31.8\,B + 123.5\,D - 23.7\,A*C$$
$$+ 38.8\,B*C + 44.0\,C*D$$
$$+ 47.4\,A*B*C + 25.1\,A*B*D - 60.1\,A*C*D$$
$$Where: A = 1\ for\ Polynar\ as\ PP\ vendor, A$$
$$= -1\ for\ Braskem\ as\ PP\ vendor$$
$$B = 1\ for\ IMA = 5\%, B = -1\ for\ IMA = 0\%$$
$$C = 1\ for\ IMB = 5\%, C = -1\ for\ IMB = 0\%$$
$$D = 1\ for\ Coupling\ Agent = 4\%, D = -1\ for\ Coupling\ Agent = 0\%$$

Based on the Anova table (Table 7-18), a normal probability plot of effects is constructed in Figure 4-35. The deviation of data points from the straight line shows that the data points shown in red are in fact significant. Following graph confirms the significance of main effects and interactions that were analytically concluded using the Analysis of Variance (ANOVA).

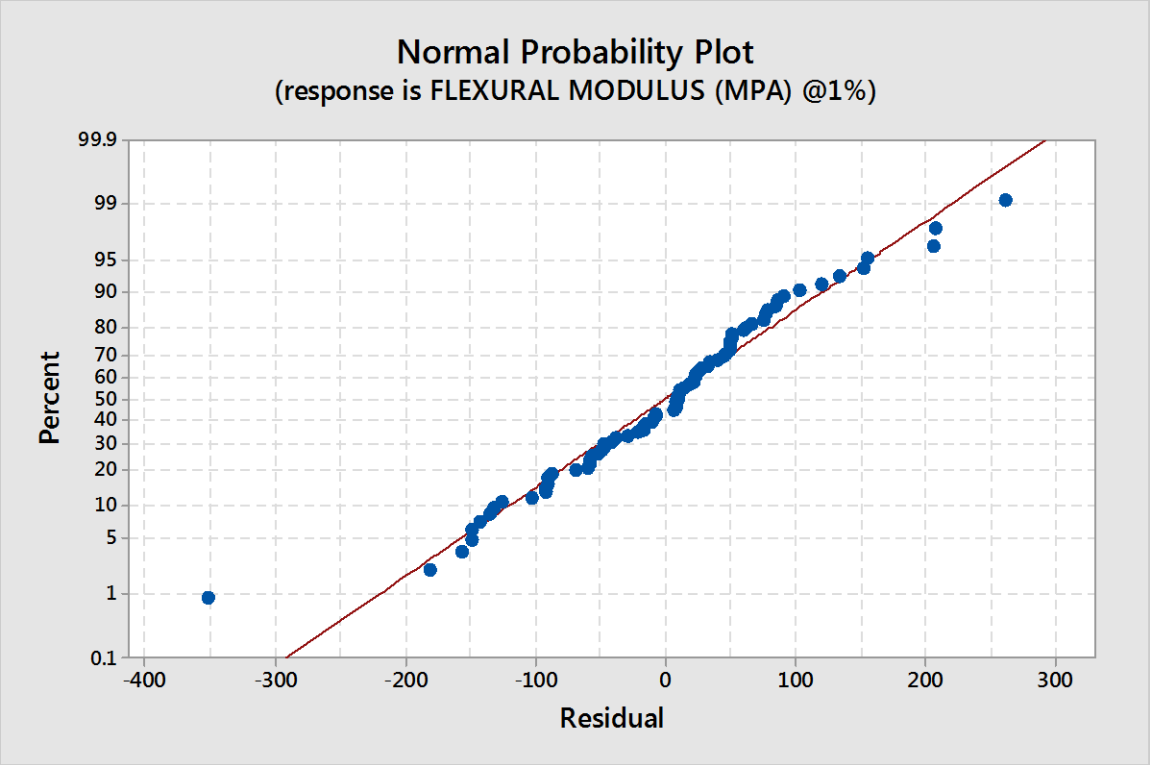

Figure 4-35: DOE (II) Normal Probability Plot of Flexural Modulus at 1%

To check if the assumptions for our two level replicated factorial design of experiment were correct it is necessary to look at the residuals plot and see if the residuals are normally distributed or not. The points in the plot shown in Figure 4-35 are reasonably close to a straight line which supports the fact that the underlying assumptions of the analysis are satisfied.

4.2.2.1.4 DOE (II) Statistical Method Analysis of Mean Failure Energy Response

Table 7-19 illustrates DOE (II) with Mean Failure Energy responses with no replication. We begin the analysis of this data by developing an Anova table (Table 7-20) to identify significance of each main factor or interaction combination factors based on an alpha value of 5%. As the experiment is not replicated, the error will have zero degrees of freedom and therefore there will be no F and P values to perform hypothesis testing. The Anova table is presented in Table 7-20.

To create one degree of freedom, we assume that there is no 4-way interaction and therefore one degree of freedom will appear for error term of Anova table as in Table 7-21.

All of the main factors and interactions appear to be insignificant. One way to seek some significance for main effects or two way interactions can be removing 3-way interaction terms and using them as replicates for main effects and 2-way interactions. The new Anova table will be as in Table 7-22.

Again, no significant main effects or interactions are observed. Now it may be reasonable to remove the two-way interactions and increase the alpha value to 15 to find out if there exists any significance in the main effects. The new Anova table will be as in Table 7-23.

Based on alpha value equal to 15, The main effects C (IMB) and D (Coupling agent) appear to be significant. The Anova Table 7-23 appears to be the final Anova table.

The Regression Equation based on Table 7-23 is as follows.

Equation 4-8: DOE (II) Mean Failure Energy Regression Equation

$$Mean\ Failure\ Energy\ (J) = 0.8352 - 0.0752\,C - 0.0658\,D$$

$$Where: C = 1\ for\ IMB = 5\%, C = -1\ for\ IMB = 0\%$$

$$D = 1\ for\ Coupling\ Agent = 4\%, D = -1\ for\ Coupling\ Agent = 0\%$$

Based on this Anova table, a normal probability plot of effects is constructed in Figure 4-36. The deviation of effects data points from straight line shows that the data points are in fact significant.

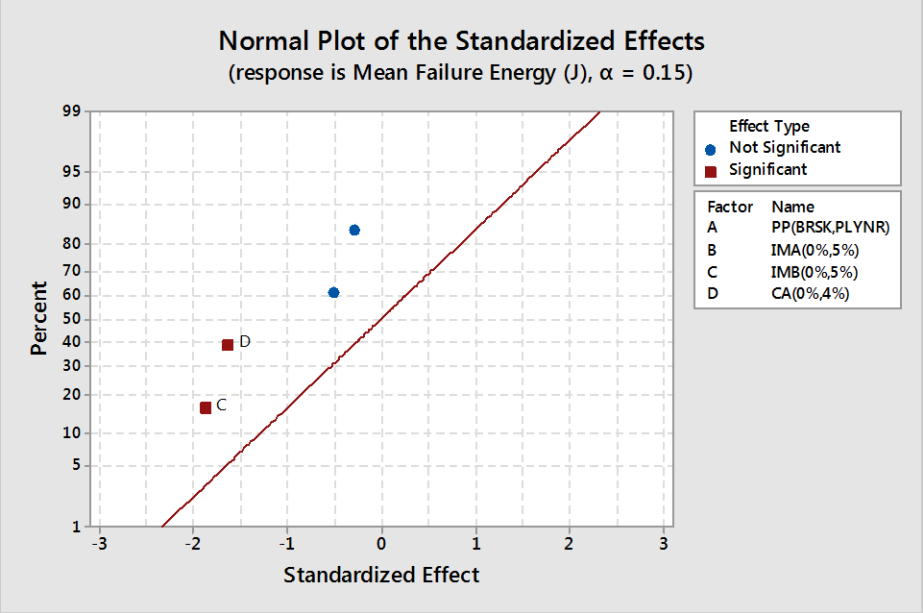

Figure 4-36: DOE (II) Normal plot of standardized effects of mean failure energy

To check that such assumptions were correct it is necessary to look at the residuals plot and see if the residuals are normally distributed or not. The points on this plot shown in Figure 4-37 are reasonably close to a straight line, this supports the hypotheses that were the basis of the analysis.

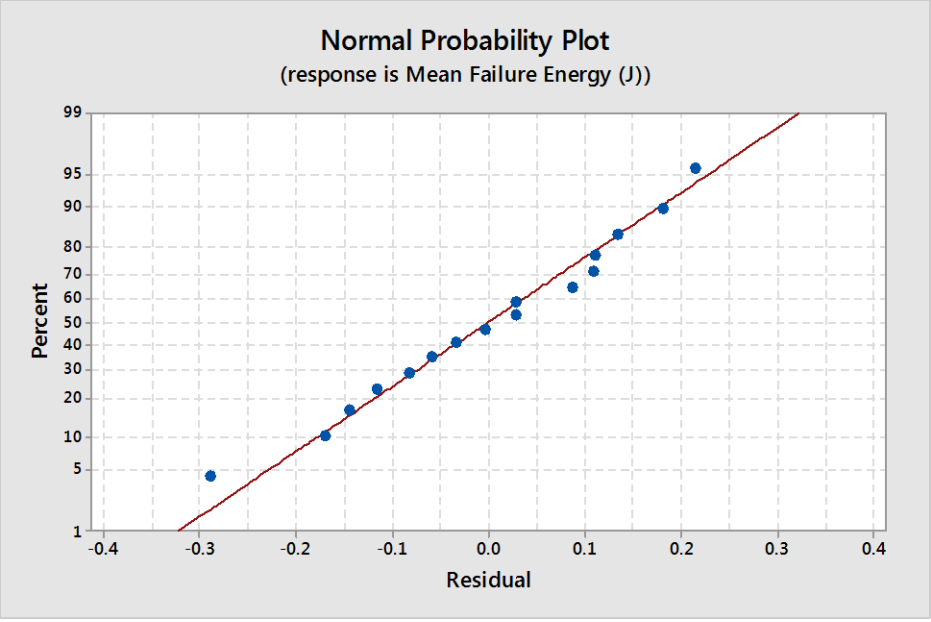

Figure 4-37: DOE (II) Normal probability plot for mean failure energy

4.2.2.2 DOE (II) Main Effects and Interactions Analysis

A summary comparing main effects means in per cents of improvement or deterioration for DOE(I) is presented in Table 4-9 . The table as well lists the significant interactions observed between the main effects.

Table 4-9: DOE (II) Summarized main effects and interactions for mechanical responses

DOE (II)			Mean Improvement (+%) , Mean Detorioration (-%), Interaction exists (✓)			
			Izod Impact Strength	Tensile Strength	Flexural Modulus	Mean Failure Energy
Main Effects (from - to)	Braskem	Polynar	-	-32%	-	-
	IMA 0%	IMA 5%	9%	-	-	-
	IMB 0%	IMB 5%	19%	-	-	-16%
	CA 0%	CA 4%	10%	51%	10%	-14%
Interactions	IMA % - CA %		✓	-	-	-
	IMA % - IMB %		✓	-	✓	✓
	PP grade - IMB %		-	-	✓	-
	IMB % - CA %		-	-	✓	✓

4.2.2.2.1 DOE (II) Izod Impact Main Effects and Interactions Analysis

The main effects of pp grades, impact modifiers (IMA, IMB) and coupling agent are plotted in Figure 4-38. All main effects are positive except the pp grade main effect which is almost neutral. Highest main effect increase is observed when impact modifier B is introduced to the formulation which increases the izod impact strength by approximately 19%. Coupling agent and impact modifier A have almost same effect of approximately 9% increase in the izod impact strength.

If only these main effects are considered, maximum izod impact strength would be obtained from running all factors at high level with PP from Braskem or Polynar. However, it is necessary to examine any interactions that are important. In fact, main effects do not have much meaning when they are involved in significant interactions.

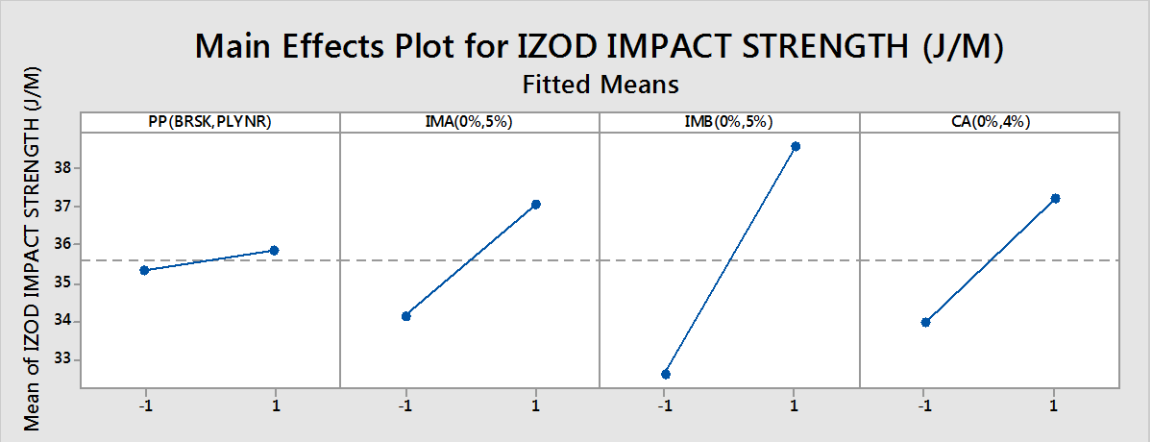

Figure 4-38: DOE (II) Main Effects Plot for Izod Impact

Based on interactions figure (Figure 4-39), a few interactions are observed between main effects. When IMB is at high level (5%), introducing IMA to the formulation does not affect the izod impact strength, however, when IMB is at low level (0%), introducing IMA to the formulation increases izod impact strength by approximately 22%. It also appears to be an interaction between IMA and coupling agent. When coupling agent is at low level, adding IMA does not affect the izod impact strength, however, when CA is at high level (4%), adding IMA to the blend, increases the izod impact strength by approximately 15%.

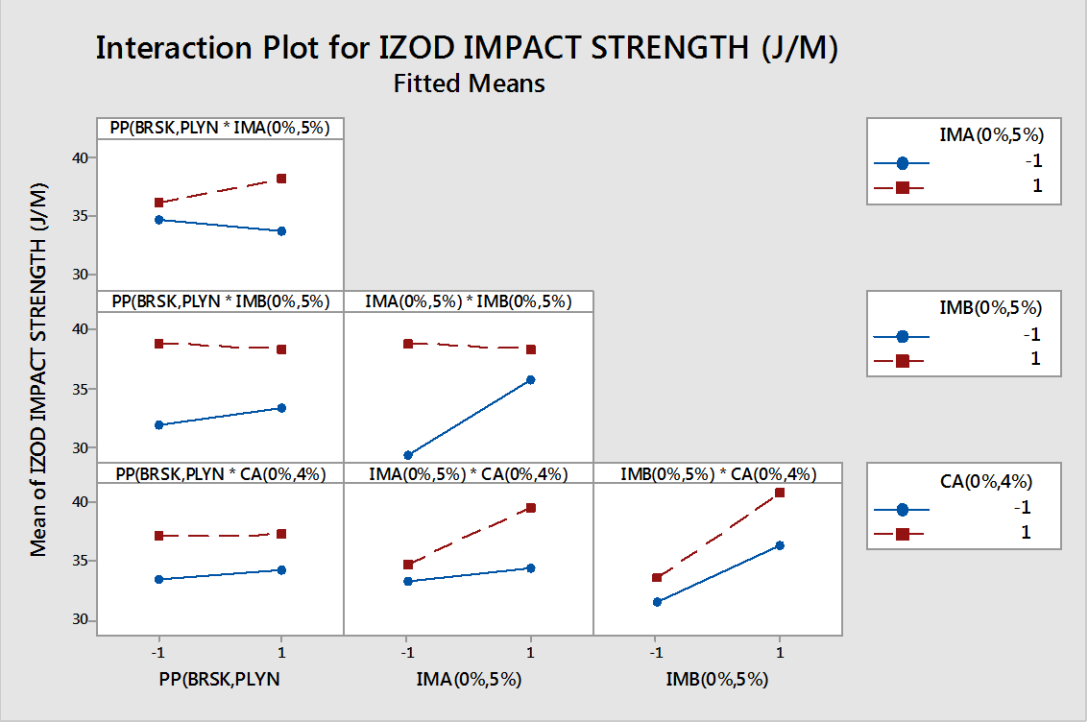

Figure 4-39: DOE (II) Interaction Plot for Izod Impact

The graph in Figure 7-5 was generated based on an optimum solution considering both main effects and interactions to result in best possible Izod impact strength. The best Izod impact strength would appear to be obtained when PP grade is at low level (using Braskem PP), IMA is at low level (0%), IMB is at high level (5%) and coupling agent is at high level (4%). This eliminates IMA from the formulation.

A response surface model was generated based on regression analysis of the data. The response surface contour plots generated from the model are shown in Figure 4-40. Notice that the contours are curved lines when an interaction exists while the contours are parallel straight lines when no interaction exists between main factors.

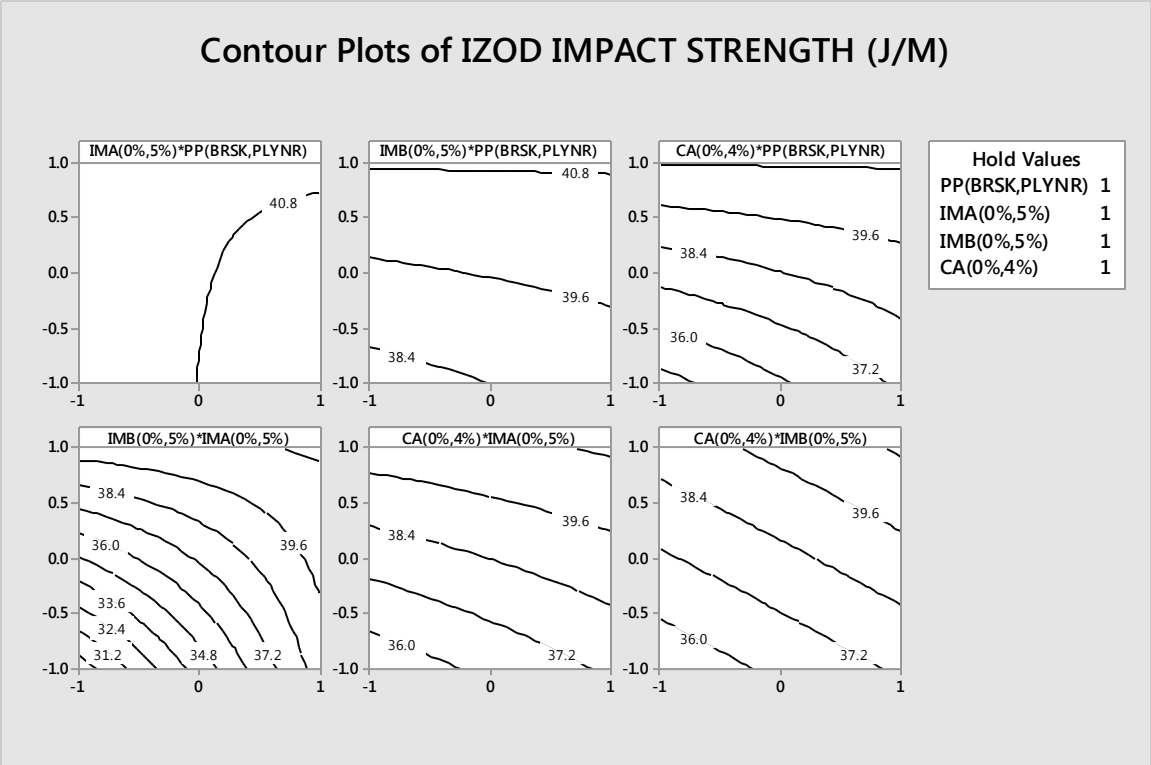

Figure 4-40: DOE (II) Contour Plots for Izod Impact

We obtained similar conclusions from the interaction graphs.

4.2.2.2.2 DOE (II) Tensile Strength Main Effects and Interactions Analysis

The main effects of PP grade, impact modifiers (IMA, IMB) and coupling agent are plotted below. The impact modifiers main effect (IMA and IMB) appear to be neutral however, the main effect of fiber type and coupling agent are very significant. As PP grade is changed from Braskem to Polynar

a significant decrease of approximately 32% is observed in mean tensile strength. On the other hand, as coupling agent is added to the composite blend, the mean tensile strength is increased by approximately 40% which is very significant.

If only these main effects are considered, maximum tensile strength would be obtained from having Braskem as PP grade and coupling agent at high level with impact modifiers at either level, however, it is necessary to examine any interactions that are important. In fact, main effects do not have much meaning when they are involved in significant interactions.

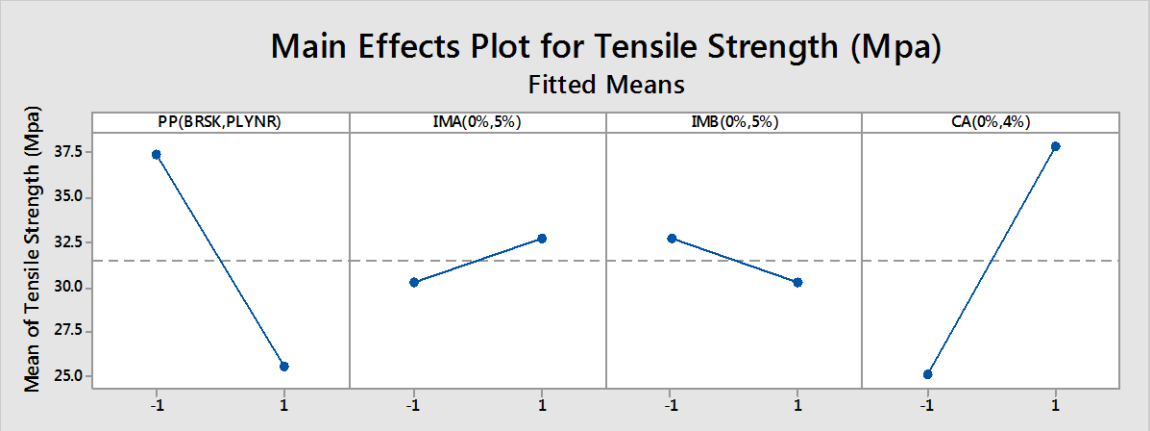

Figure 4-41: DOE (II) Main Effects plot for Tensile Strength

It can be concluded from interactions plot series shown in Figure 4-42 that there is no major interaction between all factors as interaction graphs appear to be approximately parallel. A mild interaction is observed between PP grade effect and coupling agent effect. With coupling agent being at lower level (0%), changing PP grade from Braskem to Polynar decreases tensile strength by approximately 30%, however, with coupling agent being at higher level (4%), changing PP grade from Braskem to Polynar, decreases tensile strength by approximately 35% which is very mildly significant.

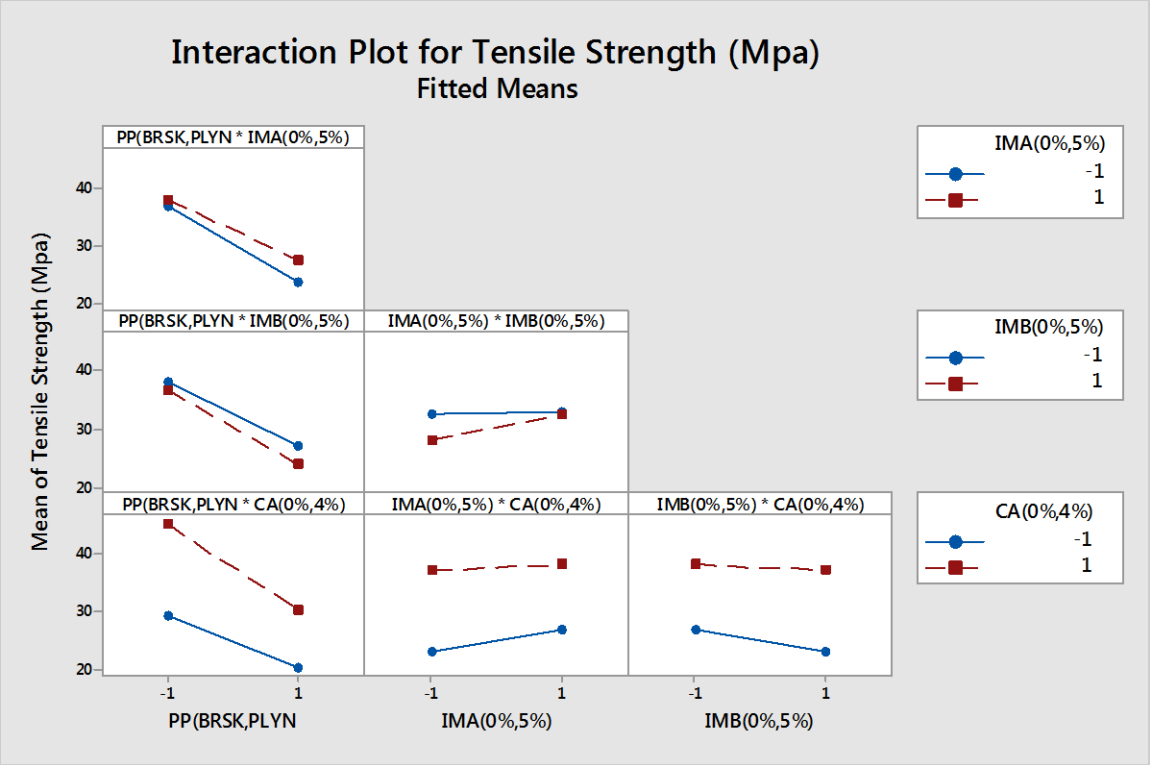

Figure 4-42: DOE (II) Interaction plot for Tensile Strength

The graph in Figure 7-6 was generated based on an optimum solution considering both main effects and interactions to result in best possible Tensile strength. Therefore, the highest Tensile strength would appear to be obtained when PP grade is at high level (Braskem PP), IMA is at low level (0%), IMB is at low level (0%) and coupling agent at high level (4%). This eliminates IMA and IMB from the formulation and reconfirms that Braskem PP and Coupling agent at 4% level are significant factors positively affecting the tensile strength of the composite.

A response surface model was generated based on regression analysis of the data. The response surface contour plots generated from the model are shown in Figure 4-43. Notice that the contours are curved lines when an interaction exits (i.e. for coupling agent-PP grade interaction) while the contours are parallel straight lines when no interaction exists between main factors (i.e. PP grade – IMA interaction).

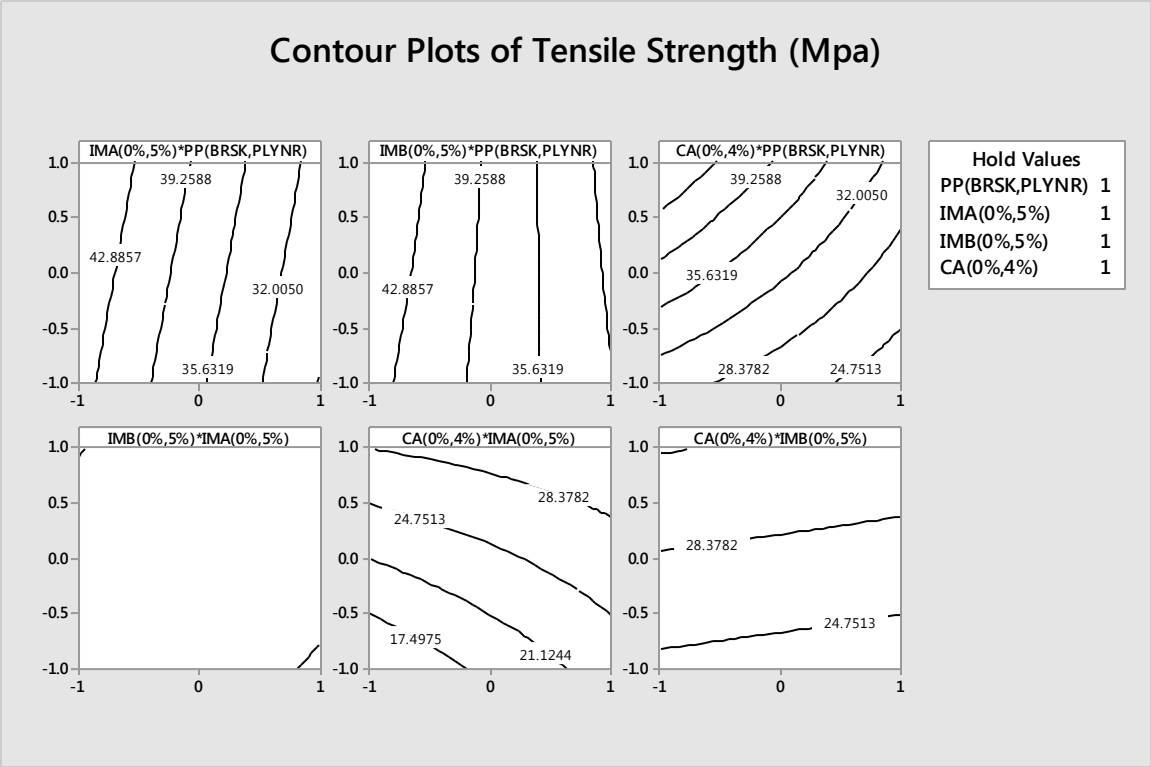

Figure 4-43: DOE (II) Contour plots for Tensile Strength

We obtained similar results from the interactions graph.

4.2.2.2.3 DOE (II) Flexural Modulus Main Effects and Interactions Analysis

The main effects plot shows a comparative neutral effect for main effects of PP type, IMA and IMB, however, for main effect of coupling agent, an approximately 10% increase in flexural modulus at 1% is observed when coupling agent is added to the bagasse-PP composite formulation.

If only these main effects are considered, maximum flexural modulus would be obtained from having PP grade, IMA and IMB at either high or low level and having coupling agent at high level (4%), however, it is necessary to examine any interactions that are important. In fact, Main effects do not have much meaning when they are involved in significant interactions.

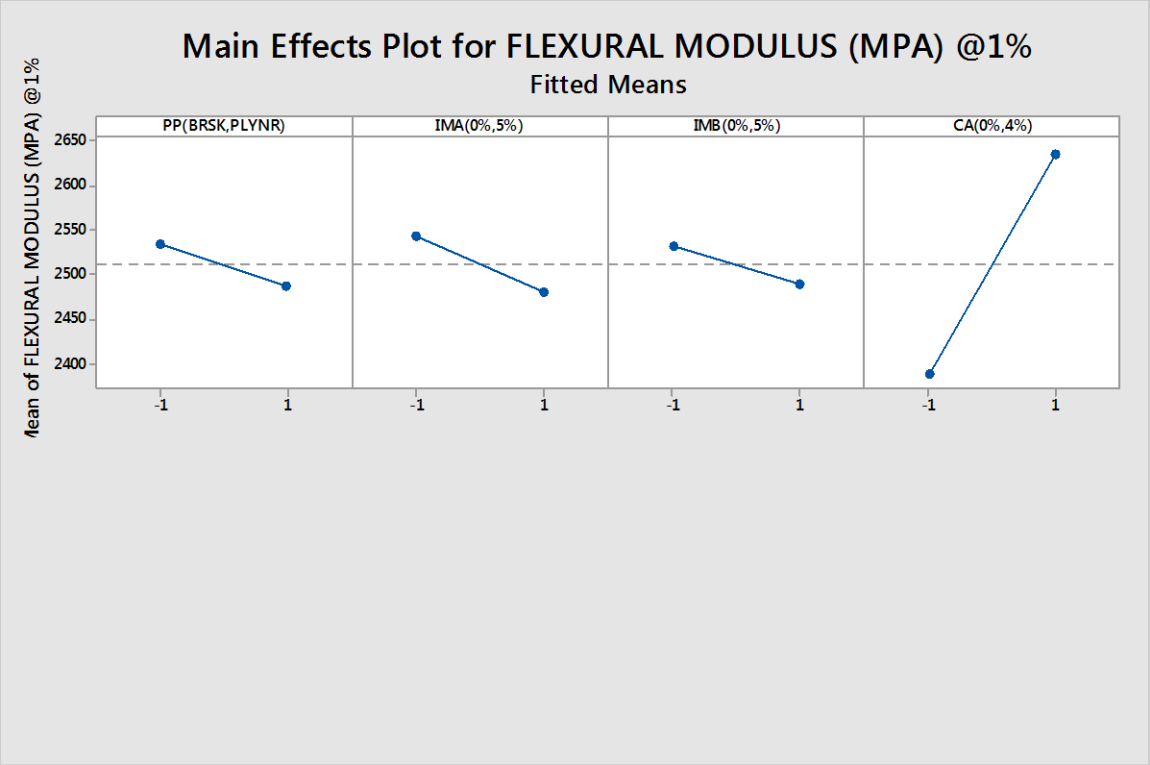

Figure 4-44: DOE (II) Main effects plot for flexural modulus at 1%

Some mild interactions are observed from the interactions plots in Figure 4-45. When IMB is at high level (5%), adding IMA does not affect the flexural modulus at 1%, however, when IMB is at low level (0%), adding IMA decreases the flexural modulus by approximately 5%. It is also observed that when coupling agent is at low level (0%), adding IMB to the formulation decreases the flexural modulus by approximately 5%, however, when coupling agent is at high level (4%), adding IMB to the formulation increases the flexural modulus by approximately 2%. This means that IMB has a negative impact on the flexural modulus of the composite and coupling agent has positive impact on the contrary.

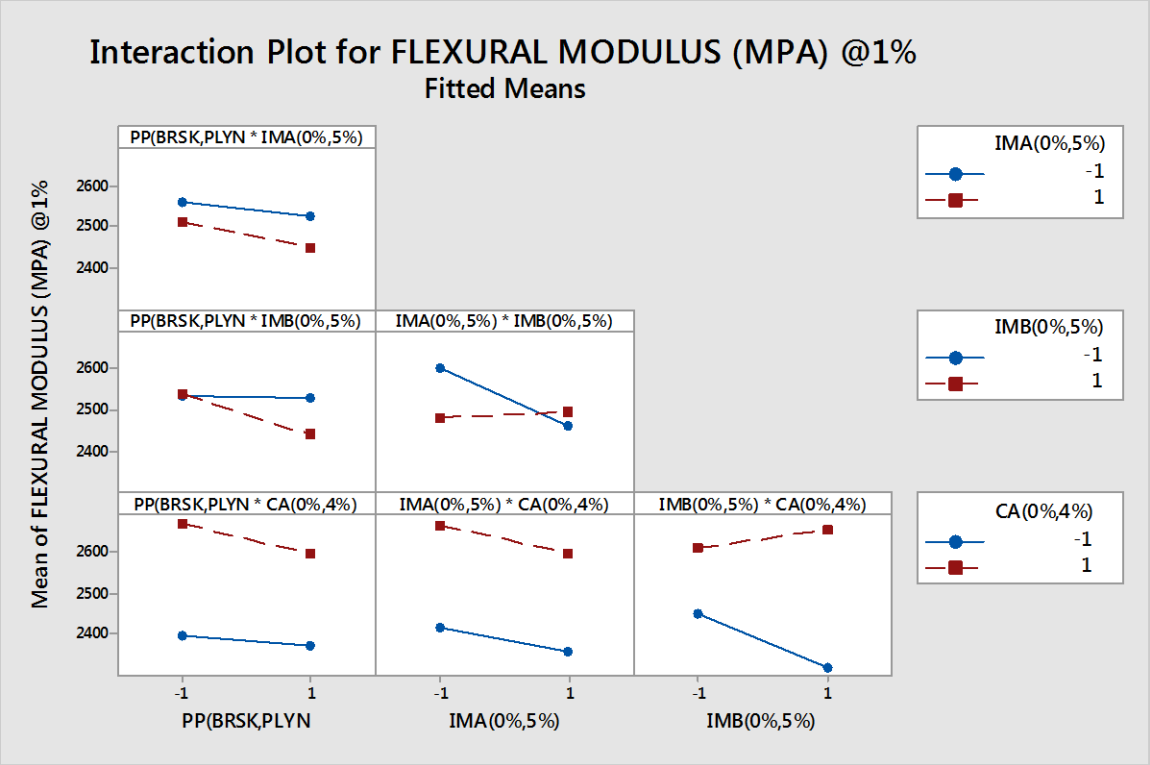

Figure 4-45: DOE (II) Interactions plot for flexural modulus at 1%

The graph in Figure 7-7 was generated based on an optimum solution considering both main effects and interactions to result in best possible flexural modulus. The highest flexural modulus would appear to be obtained when PP grade is Braskem, IMA is at low level (0%), IMB is at high level (5%) and coupling agent at high level (4%). This eliminates IMA from the formulation and confirms Braskem PP to be superior compared to Polynar PP for flexural modulus response.

A response surface model was generated based on regression analysis of the data. The response surface contour plots generated from the model are shown in Figure 4-46. Notice that the contours are curved lines when an interaction exits (i.e. for IMB – PP grade interaction) while the contours are parallel straight lines when no interaction exists between main factors (i.e. Coupling agent – PP grade interaction).

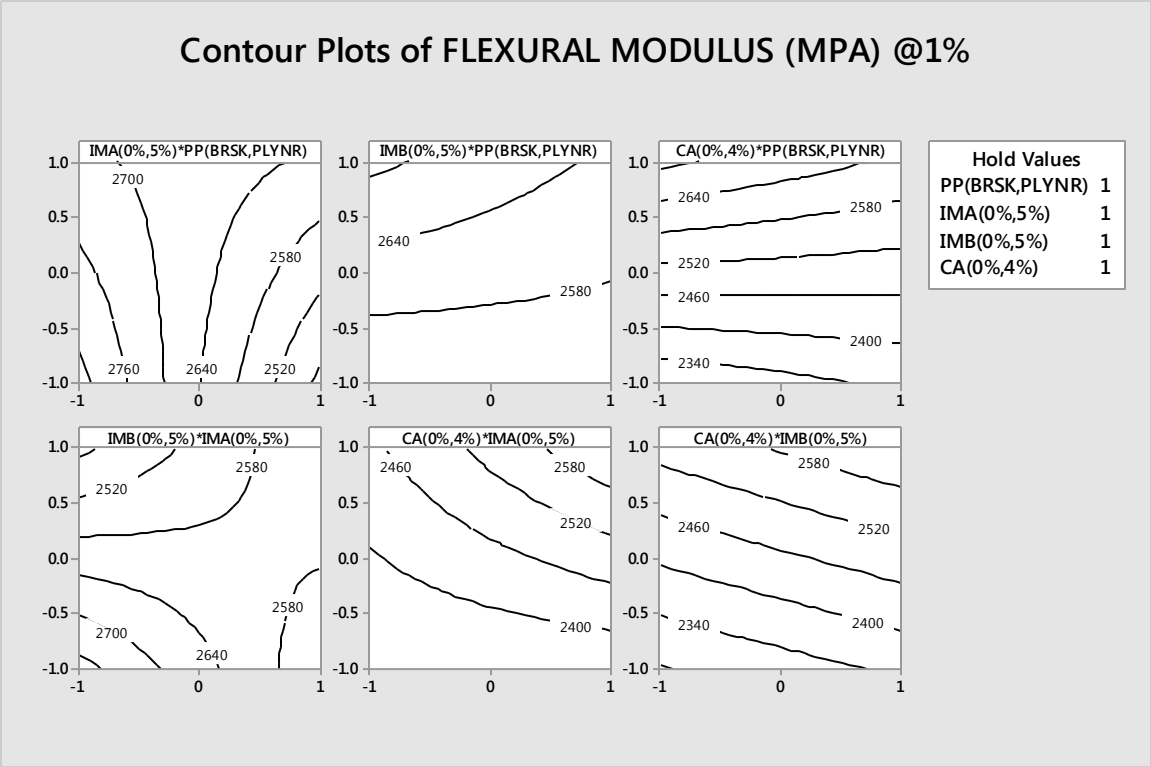

Figure 4-46: DOE (II) Contour plots of flexural modulus at 1%

Similar results were obtained from the interactions graphs.

4.2.2.2.4 DOE (II) Mean Failure Energy Main Effects and Interactions Analysis

The main effects of PP grade, impact modifiers (IMA, IMB) and coupling agent are plotted below. PP grade effect and IMA content effect appear to be neutral, however, IMB effect and Coupling agent effect appear to be negative. As impact modifier content is increased from 0% to 5%, mean of failure energy is decreased by approximately 20%. As coupling agent content is increased from 0% to 4%, mean of failure energy is decreased by approximately 15%.

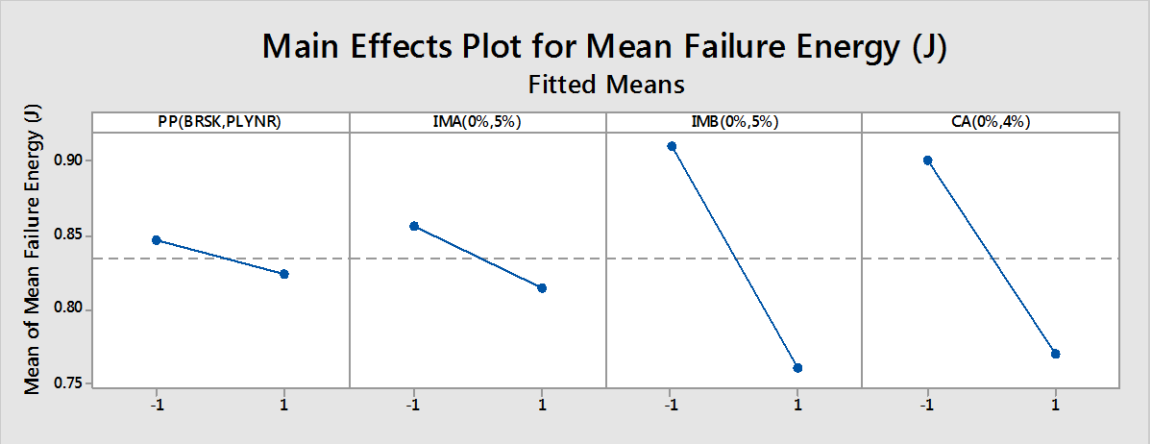

Figure 4-47: DOE (II) Mean Failure Energy Main Effects

If only these main effects are considered, maximum Mean Failure Energy would be obtained from having all DOE (II) factors at low level, however, it is necessary to examine any interactions that are important. In fact, Main effects do not have much meaning when they are involved in significant interactions.

Figure 4-48 indicates that high interaction is detected between IMB and Coupling Agent. While coupling agent is at high level (4%), adding IMB to the compound does not affect the mean failure energy response, however, while coupling agent is absent, adding IMB to compound significantly decreases the mean failure energy by about 27%. Mild interactions between IMA % - IMB %, PP grade - IMB %, PP grade - coupling agent and IMA % - Coupling Agent % are observed that may be considered not significant.

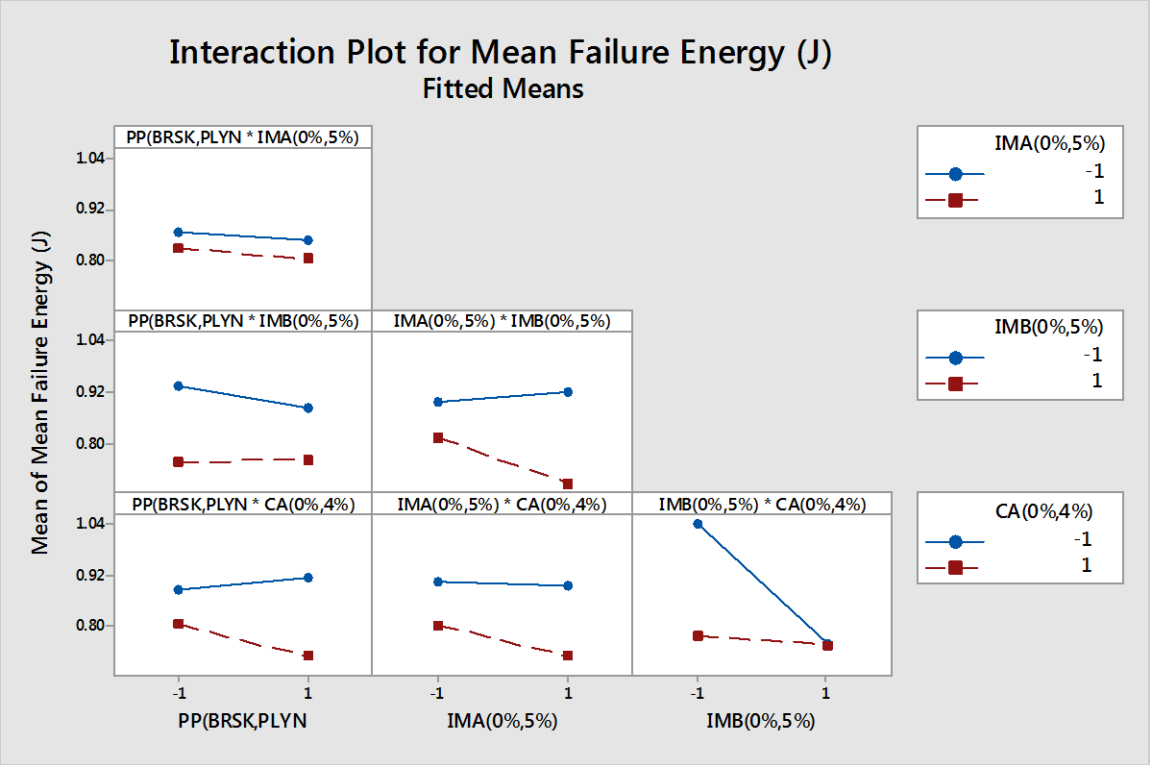

Figure 4-48: Interactions graph for DOE (II) Mean Failure Energy

The graph in Figure 7-8 was generated based on an optimum solution considering both main effects and interactions to result in highest possible mean failure energy. The highest mean failure energy would appear to be obtained when PP grade is Braskem, IMA is at low level (0%), IMB is at high level (0%) and coupling agent is at low level (0%).

A response surface model was generated based on regression analysis of the data. The response surface contour plots generated from the model are shown in Figure 4-49. Notice that the contours are curved lines when an interaction exits while the contours are parallel straight lines when no interaction exists between main factors.

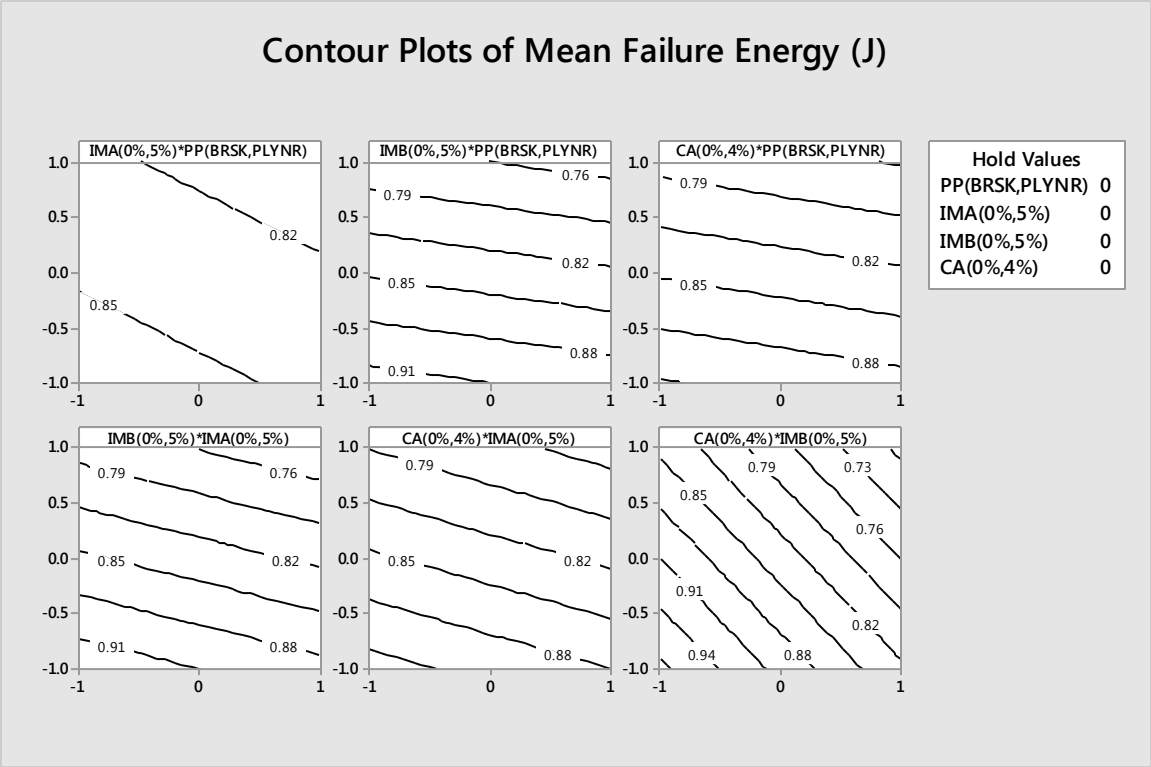

Figure 4-49: DOE(II) Contour plots for mean failure energy

We obtained similar conclusions from the interaction graphs.

4.2.3 Design of Experiment III (DOE III)

For DOE (III) the goal is to identify effective factors and interactions in maximizing the Izod impact strength, flexural modulus and tensile strength of compounds. To achieve this goal, a two level factorial experiment with 4 factors and 5 replications per run is carried out. Number of runs are 16 runs and each run is repeated 5 times, therefore total number of runs is 80 experiments.

Table 4-10: DOE (III)

Run #	Fiber Type	Fiber %	PP	PP	Impact Modifier		Antioxidant	C. Agent
			Braskem	Polynar	A	B		PP-MA
1	none	0	99.5	0	0	0	0.5	0
2	none	0	94.5	0	5	0	0.5	0
3	none	0	94.5	0	0	5	0.5	0
4	none	0	94.5	0	2.5	2.5	0.5	0
9	Bagasse	40	54.5	0	5	0	0.5	0
10	Bagasse	40	54.5	0	0	5	0.5	0
11	Bagasse	40	54.5	0	2.5	2.5	0.5	0
12	Bagasse	40	59.5	0	0	0	0.5	0
21	none	0	0	99.5	0	0	0.5	0
22	none	0	0	94.5	5	0	0.5	0
23	none	0	0	94.5	0	5	0.5	0
24	none	0	0	94.5	2.5	2.5	0.5	0
29	Bagasse	40	0	54.5	5	0	0.5	0
30	Bagasse	40	0	54.5	0	5	0.5	0
31	Bagasse	40	0	54.5	2.5	2.5	0.5	0
32	Bagasse	40	0	59.5	0	0	0.5	0

4.2.3.1 DOE (III) Statistical method Analysis

4.2.3.1.1 DOE (III) Statistical Method Analysis of IZOD IMPACT Response

Table 7-24 illustrates DOE (III) with Izod Impact replicated responses.

We begin the analysis of this data by developing an Anova Table 7-25 to identify significance of each main factor or interaction combination factors. Based on an alpha value of 5%, it is concluded that factors or interactions with a lower than 5% P value are significant.

The Regression Equation based Table 7-25 is below. Significant main factors and interactions are included in the regression equation and insignificant main factors and interactions are omitted from the equation.

Equation 4-9: DOE(III) Izod Impact Strength Regression Equation

$$IZOD\ IMPACT\ STRENGTH\ (J/M) = 30.887 + 3.075\,A + 3.244\,B + 3.609\,D - 2.823\,A*B - 1.195\,A*D + 1.511\,B*D - 0.841\,C*D + 0.949\,A*B*C - 2.043\,A*B*D + 0.592\,A*B*C*D$$

$$Where: A = 1\ for\ Bagasse\ at\ 40\%, A = -1\ for\ Bagasse\ at\ 0\%$$

$$B = 1\ for\ Polynar\ PP, B = -1\ for\ Braskem\ PP$$

$$C = 1\ for\ IMA = 5\%, C = -1\ for\ IMA = 0\%$$

$$D = 1\ for\ IMB = 5\%, D = -1\ for\ IMB = 0\%$$

Based on the Anova table (Table 7-25), a normal probability plot of effects is constructed in Figure 4-50. The deviation of effects data points from the straight line shows that the data points are in fact significant.

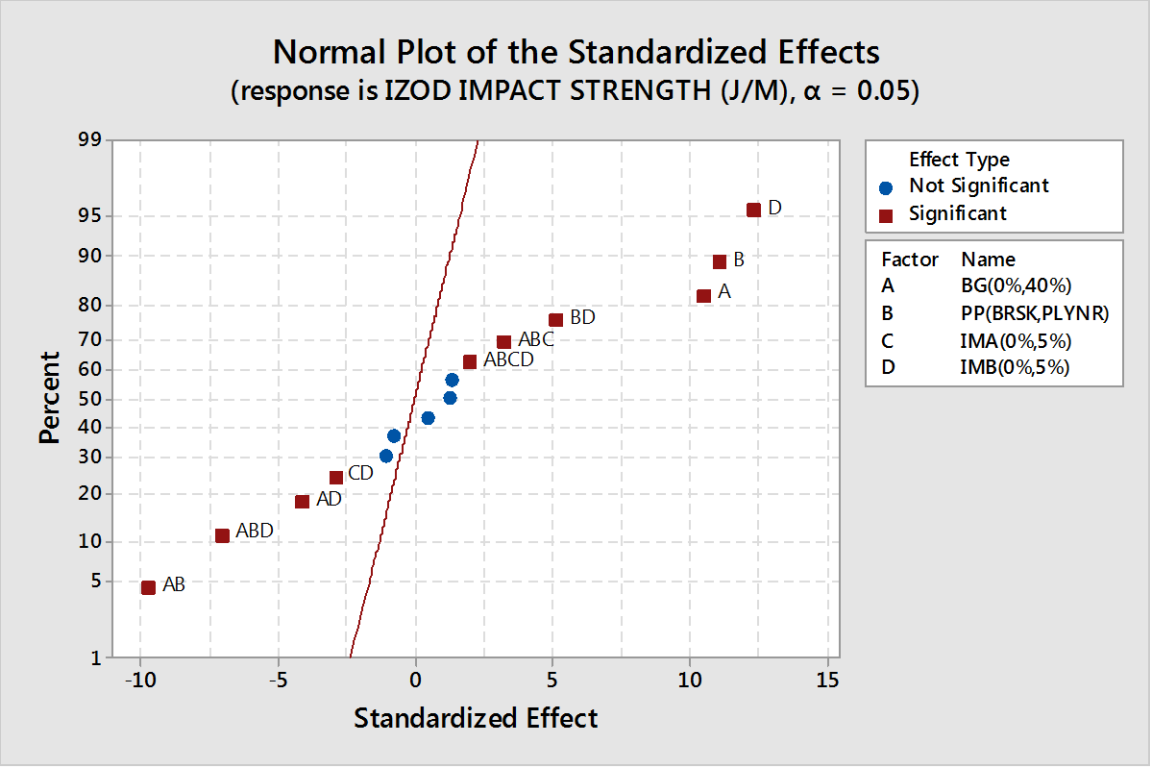

Figure 4-50: DOE (III) Izod Impact Strength Normal Plot of standardized effects

To check that the normality assumptions were correct it is necessary to look at the residuals plot and see if the residuals are normally distributed or not. The points on this plot shown in Figure 4-51 are mildly close to a straight line which mildly supports that the underlying assumptions of the analysis are satisfied.

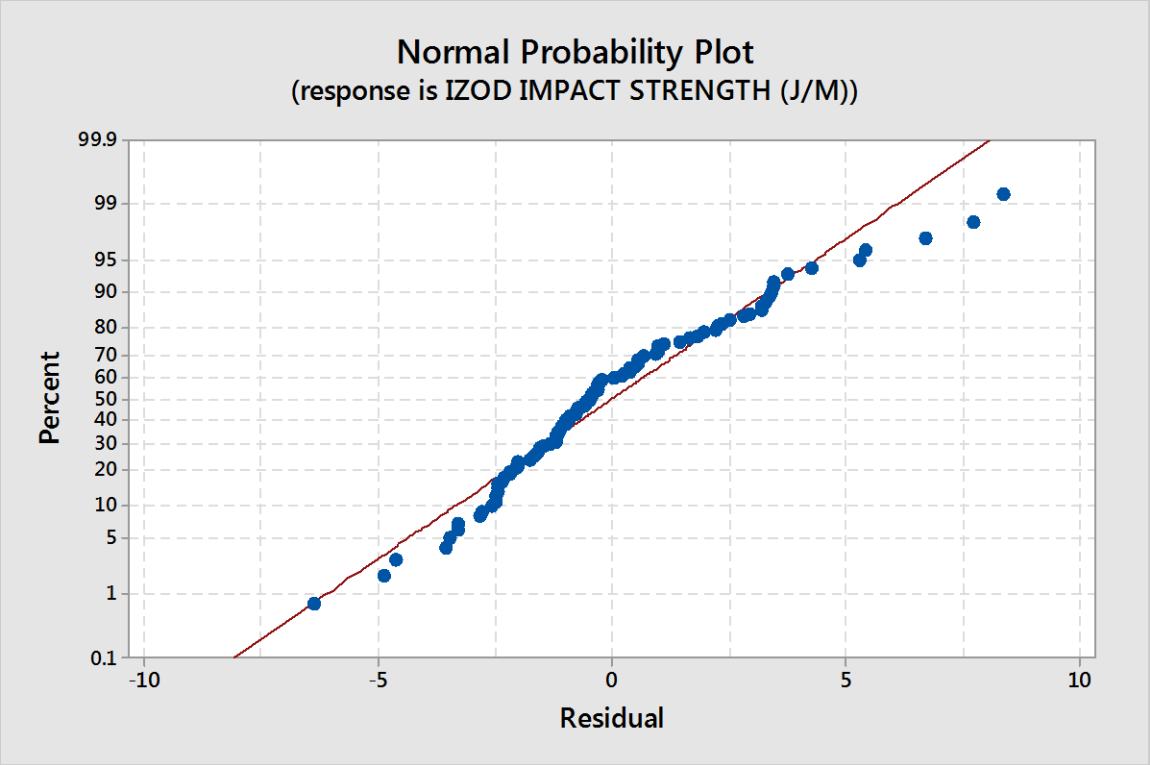

Figure 4-51: DOE (III) Izod Impact Strength Normal Probability Plot

4.2.3.1.2 DOE (III) Statistical Method Analysis of Tensile Strength Response

Table 7-26 illustrates DOE (III) replicated design matrix.

Similar to the analysis of Izod Impact Strength data, we begin the analysis of tensile strength data by developing an Anova table (Table 7-27) to identify significance of each main factor or interaction combination factors. Based on an alpha value of 5%, it is concluded that factors or interactions with a lower than 5% P value are significant.

The Anova table is constructed based on the factorial design of experiment previously explained. Significant main factors or interactions are indicated with an asterisk beside the P-values.

The Regression Equation based on the Anova table (Table 7-27) is below. Significant main factors and interactions are included in the regression equation and insignificant main factors and interactions are omitted from the equation.

Equation 4-10: DOE (III) Tensile Strength Regression Equation

$$Tensile\ Strength\ (Mpa) = 29.958 - 4.872\,A - 2.602\,B - 1.807\,D - 1.826\,A*B + 1.766\,A*C + 1.324\,C*D$$

$$Where: A = 1\ for\ Bagasse\ as\ fiber, A = -1\ No\ Bagasse\ fiber$$

$$B = 1\ for\ Polynar\ as\ PP\ vendor, B = -1\ for\ Braskem\ as\ PP\ vendor$$

$$C = 1\ for\ IMA = 5\%, B = -1\ for\ IMA = 0\%$$

$$D = 1\ for\ IMB = 5\%, C = -1\ for\ IMB = 0\%$$

Based on Anova table (Table 7-27), a normal probability plot of effects is constructed in Figure 4-52. The deviation of data points from the straight line shows that the data points shown in red are in fact significant. Figure 4-52 confirms the significance of main effects and interactions that were analytically concluded.

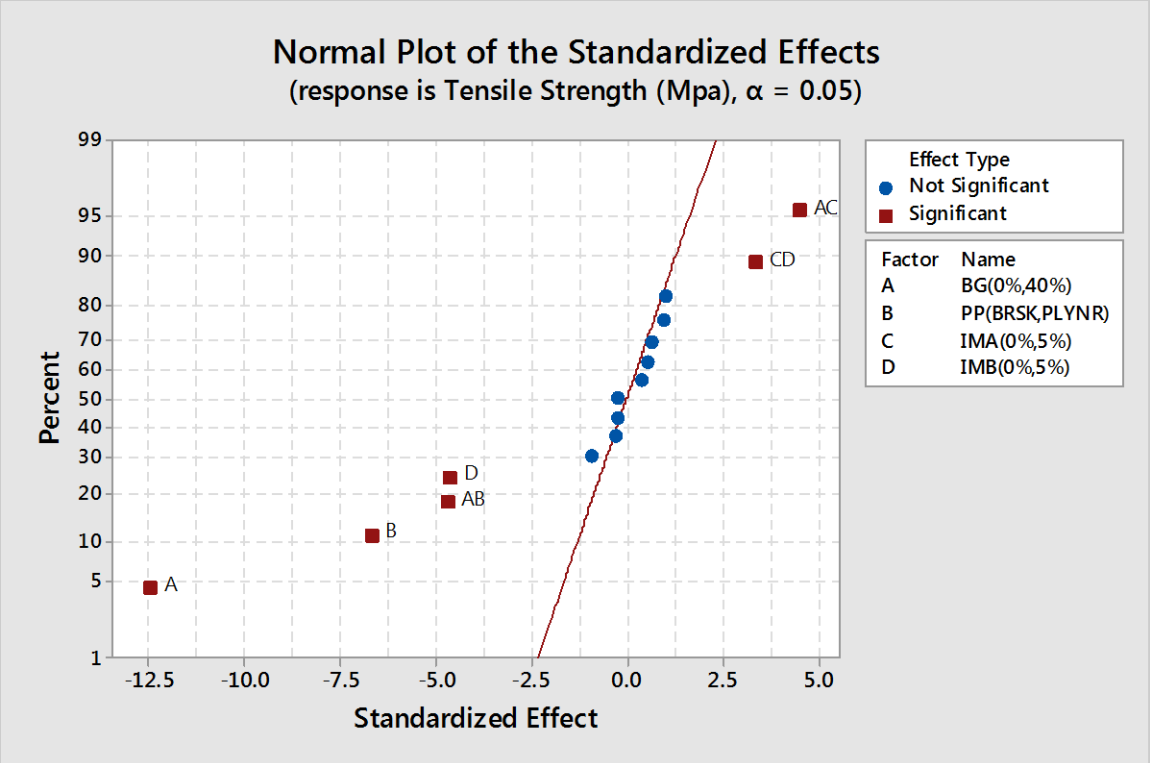

Figure 4-52: DOE (III) Normal Plot for Tensile Strength

To check that the normality assumptions made were correct it is necessary to look at the residuals plot and see if the residuals are normally distributed or not. Compared to the same graph for Izod impact Strength, The points on the normal probability plot of tensile strength response plot shown in Figure 4-53 are much less close to a straight line and show somewhat of a curved graphic in parts in its entirety . This supports the fact that underlying assumptions of the analysis are not satisfied comparatively and the normality assumptions made before start of the analysis are not satisfied.

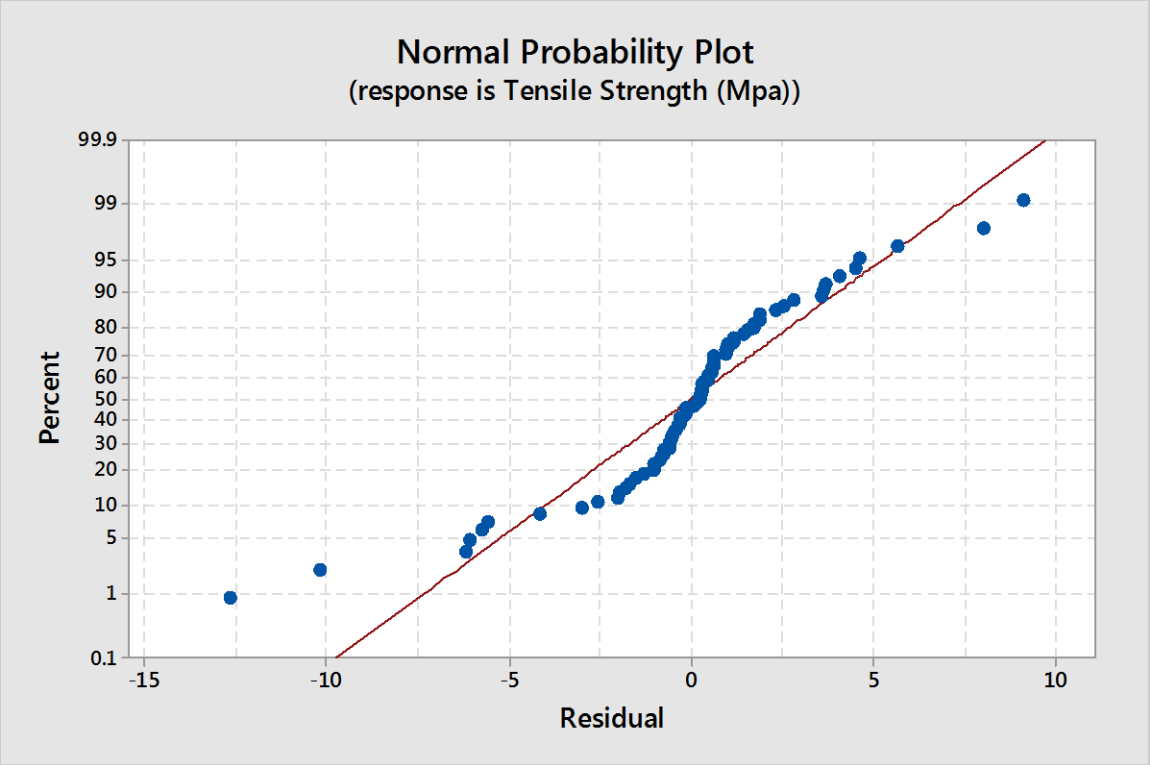

Figure 4-53: DOE (III) Tensile Strength Normal probability plot

4.2.3.1.3 DOE (III) Statistical Method Analysis of Flexural Modulus Response

Table 7-28 illustrates DOE (III) replicated design matrix with flexural modulus at 1%. An Anova table is constructed in Table 7-29 based on the factorial design of experiment previously explained. Significant main factors or interactions are indicated with an asterisk beside the P-values.

The Regression Equation based on the Anova table (Table 7-29) is as follows. Significant main factors and interactions are included in the regression equation and insignificant main factors and interactions are omitted from the equation.

Equation 4-11: DOE (III) Flexural Modulus Regression Equation

$$FLEXURAL\ MODULUS\ (MPA)\ @1\% = 1763.55 + 624.14\,A + 48.67\,B - 24.31\,D - 61.57\,A * B - 22.67\,A * C - 41.21\,A * D + 34.35\,B * D + 43.85\,C * D - 25.70\,A * B * C + 29.83\,B * C * D$$

$$Where:$$

$$A = 1\ for\ Bagasse\ content\ at\ 40\%, A = -1\ for\ Bagasse\ content\ at\ 0\%$$

$$B = 1\ for\ Polynar\ as\ PP\ vendor, B = -1\ for\ Braskem\ as\ PP\ vendor$$

$$C = 1\ for\ IMA = 5\%, B = -1\ for\ IMA = 0\%$$

$$D = 1\ for\ IMB = 5\%, C = -1\ for\ IMB = 0\%$$

Based on Anova table (Table 7-29), a normal probability plot of effects is constructed in Figure 4-54. The deviation of data points from the straight line shows that the data points shown in red are in fact significant. Following graph confirms the significance of main effects and interactions that were analytically concluded using the Analysis of Variance (ANOVA) table (Table 7-29).

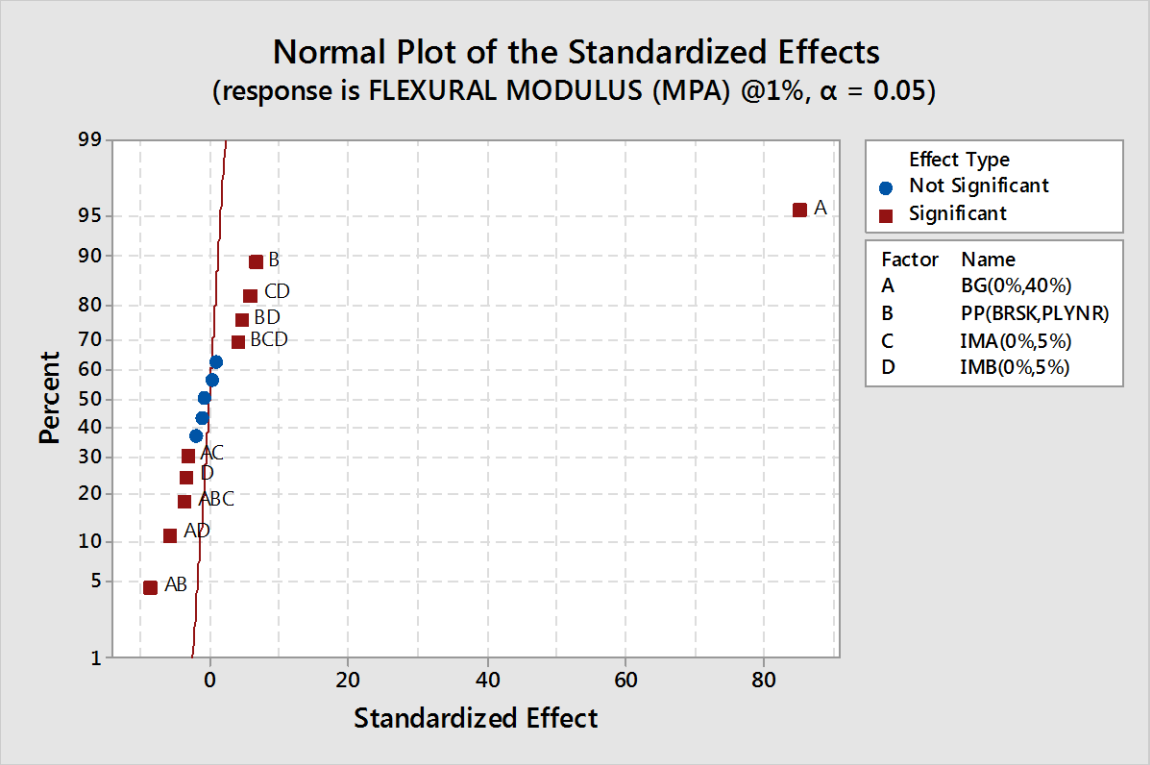

Figure 4-54: DOE (III) Normal Plot of standardized effects of flexural modulus at 1%

To check if the assumptions for our two level replicated factorial design of experiment were correct it is necessary to look at the residuals plot and see if the residuals are normally distributed or not. The points on this plot shown in Figure 4-55 are reasonably close to a straight line which supports the fact that the underlying assumptions of the analysis are satisfied.

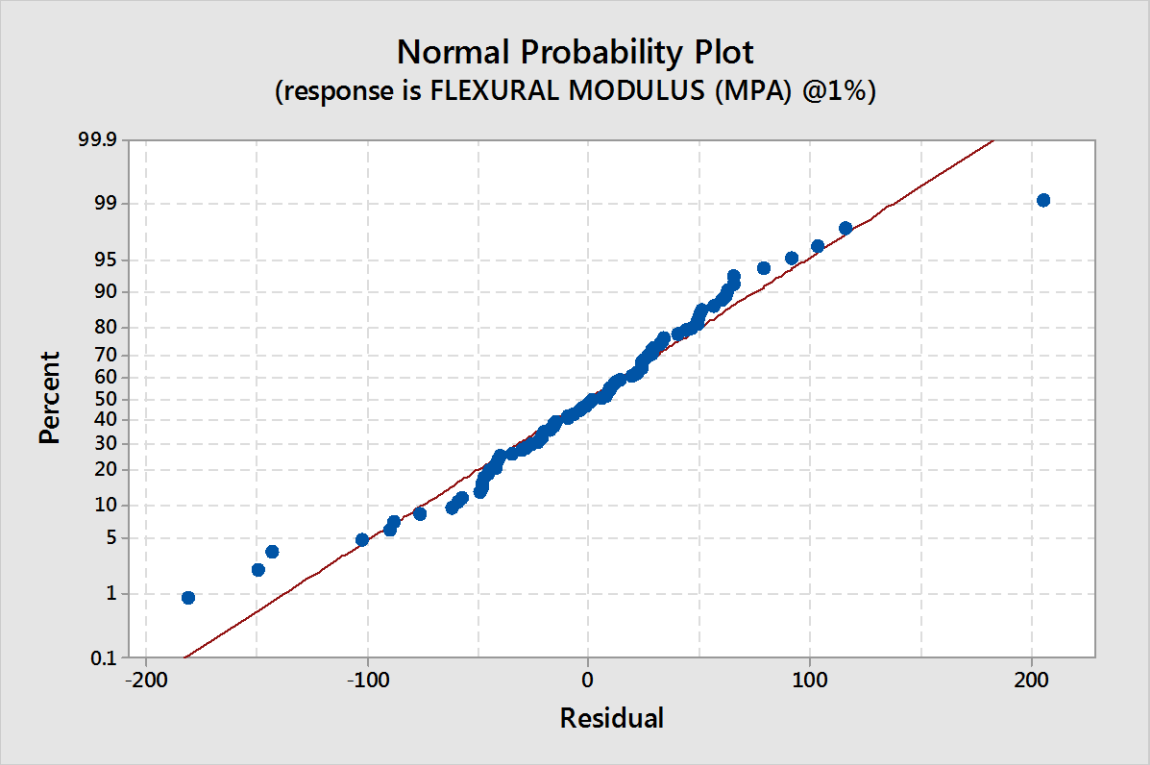

Figure 4-55: DOE (III) Normal probability plot for flexural modulus at 1%

4.2.3.1.4 DOE (III) Statistical Method Analysis of Mean Failure Energy Response

Table 7-30 illustrates non-replicated design matrix for DOE (III). We begin the analysis of this data by developing an Anova table (Table 7-31) to identify significance of each main factor or interaction combination factors based on an alpha value of 5%. As the experiment is not replicated, the error will have zero degrees of freedom and therefore there will be no F and P values to perform hypothesis testing. To create one degree of freedom for error term, we assume there is no 4-way interaction and therefore one degree of freedom will appear for error term of Anova table (Table 7-32)

The new Anova table (Table 7-32) has some important information. It shows that linear terms are significant (P value is 3.7%). It also shows that 2-way interactions P value is 6.2% and 3-way interactions P value is 7.8%. This shows that linear terms are significant, 2-way and 3-way interactions are next significant terms in the hierarchy of significance. To create further degrees of freedom for error term and hence more reliability for the model, 3-way interaction terms are removed and the model will become as in Table 7-33.

It is observed from Table 7-33 that the main effect of A (bagasse content) is significant and the rest of terms are not significant.

It is needed to choose from the above two Anova tables, the table that appears to be more reliable. The first table with one degree of freedom for error term suggests 6 main effects terms and interaction terms to be significant, however, the second table with 5 degrees of freedom for the error term suggests that only one term is significant (The main effect A or Bagasse content.)

Due to the low number of performed tests (only one test for every formulation), the Anova table with 5 degrees of freedom for error term appears to be more reliable compared to Anova table with only 1 degree of freedom for error term. Therefore, although more significant main effects and interaction terms are observed in the first Anova table, it appears to be more reasonable to choose the second Anova table as the basis to find significant terms.

The Regression Equation based on second Anova table is as follows.

Equation 4-12: DOE (III) Mean Failure Energy Regression Equation

$$Mean\ Failure\ Energy\ (J)\ =\ 0.9317\ -\ 0.1322\ BG(0\%, 40\%)$$

$$Where: A = 1\ for\ BAGASSE\ Content\ 40\%, A = -1\ for\ BAGASSE\ Content\ 0\%$$

Based on this Anova table, a normal probability plot of effects is constructed Figure 4-56. The deviation of effects data points from the straight line shows that the data points are in fact significant.

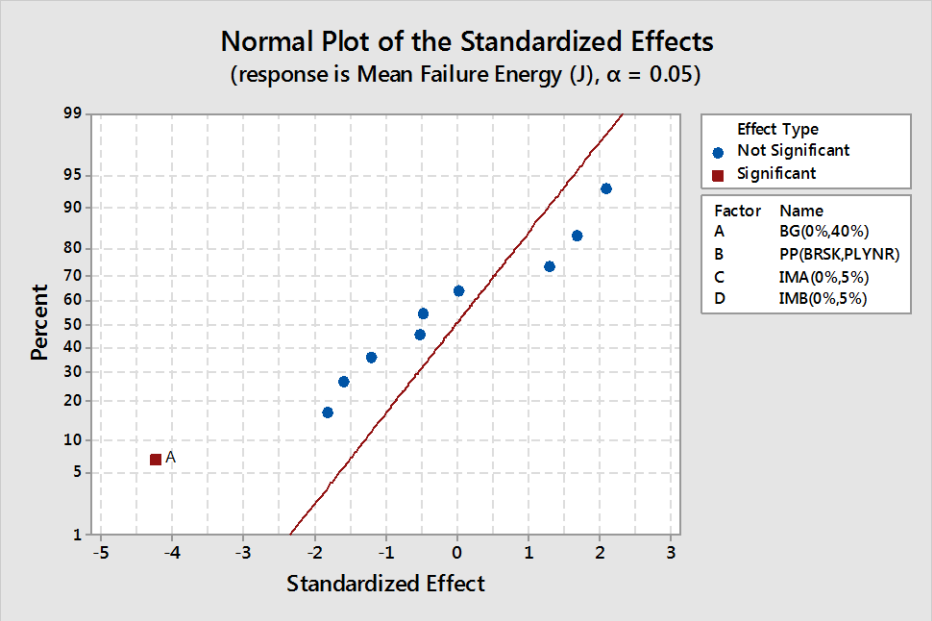

Figure 4-56: DOE (III) Normal plot for mean failure energy

To check that such assumptions were correct it is necessary to look at the residuals plot and see if the residuals are normally distributed or not. The points on this plot shown in Figure 4-57 are reasonably close to a straight line, although the distribution of the residual points are not well scattered below and above the mean line. This supports the hypothesis that underlying assumptions of the analysis are mildly satisfied.

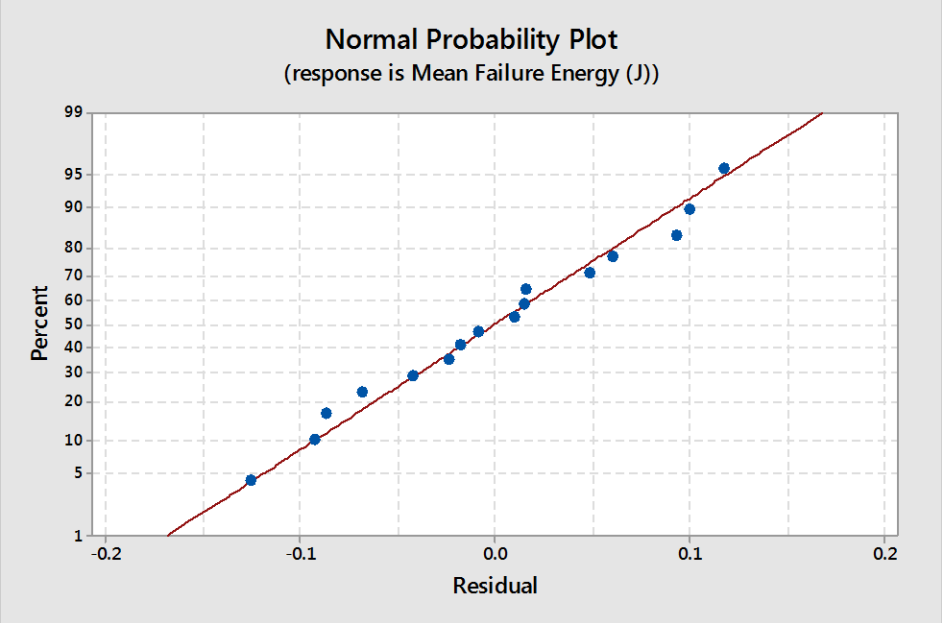

Figure 4-57: DOE (III) Normal probability plot for mean failure energy

4.2.3.2 DOE (III) Main Effects and Interactions Analysis

A summary comparing main effects means in per cents of improvement, or deterioration, for DOE(I), is presented in Table 4-11. The table as well lists the significant interactions observed between the main effects.

Table 4-11: DOE (III) Summarized main effects and interactions for mechanical responses

DOE (III)			Mean Improvement (+%) , Mean Deterioration (-%), Interaction exists (✓)			
			Izod Impact Strength	Tensile Strength	Flexural Modulus	Mean Failure Energy
Main Effects (from - to)	BG 0%	BG 40%	22%	-28%	110%	-24%
	PP Braskem	PP Polynar	23%	-16%	-	-
	IMA 0%	IMA 5%	-	-	-	-8%
	IMB 0%	IMB 5%	27%	-11%	-	11%
Interactions	BG % - PP grade		✓	✓	-	-
	PP grade - IMB %		✓	-	-	-
	BG% - PP grade		-	-	-	✓
	BG % - IMA %		-	✓	-	✓
	BG% - IMB %		-	-	-	✓
	PP grade - IMB %		-	-	-	✓
	IMA % - IMB %		-	✓	-	-

4.2.3.2.1 DOE (III) Izod Impact Main Effects and Interactions Analysis

The main effects of bagasse fiber, PP grade, IMA and IMB are plotted below. All main effects are positive except the IMA main effect which is almost neutral. Highest main effect increase is observed when Impact Modifier B is introduced to the formulation which increases the Izod impact strength by approximately 30%.

If only these main effects are considered, maximum Izod impact strength would be obtained from running all factors at high level with IMA at either level. It is necessary to examine any interactions that are important. In fact, Main effects do not have much meaning when they are involved in significant interactions.

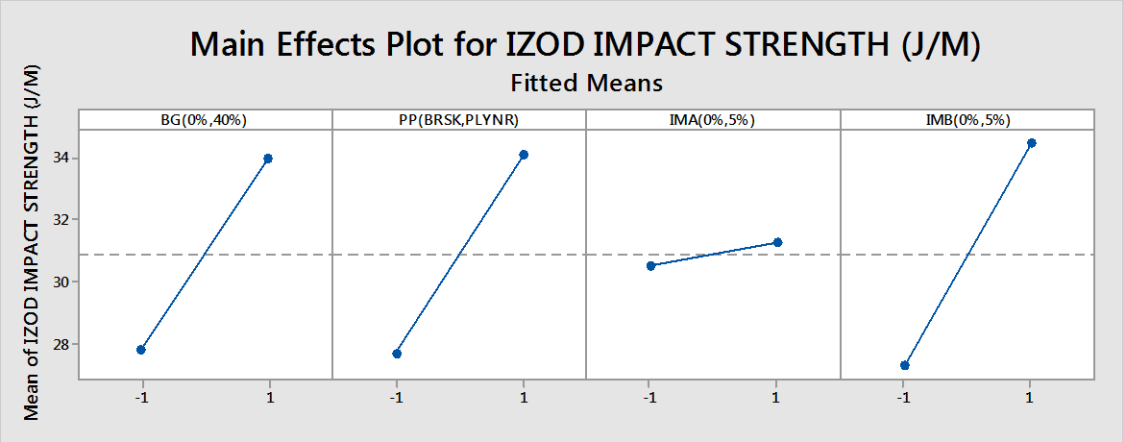

Figure 4-58: DOE (III) Main Effects of Izod Impact Strength

Based on interactions Figure 4-59, a few interactions are observed between main effects. With Polynar as PP grade, introducing bagasse into formulation does not change the mean Izod impact strength, staying constant at approximately 35 (J/M) for Polynar PP – Bagasse Composite, however, with Braskem as PP grade, introducing bagasse into formulation, increases mean Izod impact strength by 60% for Braskem PP – bagasse composite to increase Izod impact strength from approximately 27 (J/M) to approximately 35 (J/M).

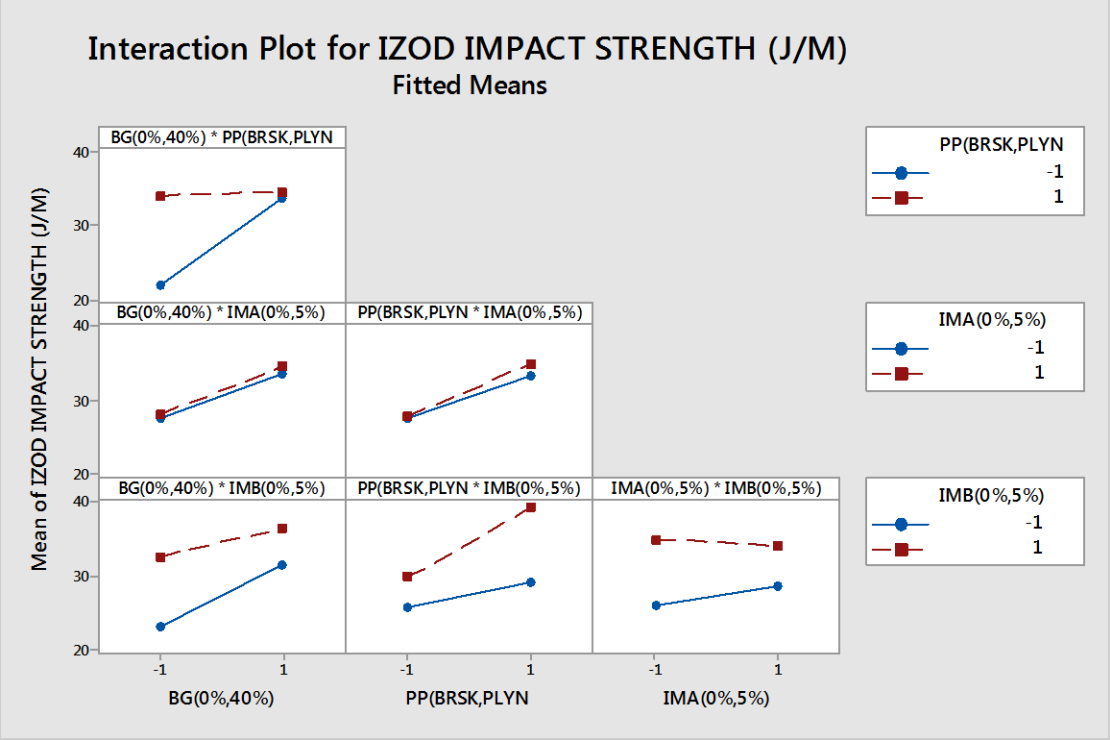

Figure 4-59: DOE (III) Interactions plot for Izod impact Strength

The graph in Figure 7-9 was generated based on an optimum solution considering both main effects and interactions to result in best possible Izod impact strength. Therefore, the best Izod impact strength would appear to be obtained when there is no bagasse present in the formulation, Braskem is the PP grade, no IMA present and IMB is at high level (5%). Using this recipe, maximum Izod impact strength obtained is approximately 44 (J/M). This, however, does not help us as the goal of this study is to use Bagasse as a filler.

Keeping Bagasse at high level (40%) in Figure 7-10 it can be concluded that best Izod impact strength with bagasse present in the formulation is obtained when Braskem is the PP grade, no IMA is present in the formulation and IMB is at high level (5%). Using this recipe, maximum Izod impact of 38.6 (J/M) is obtained which is 12% lower than the maximum Izod impact strength without bagasse as filler.

A response surface model was generated based on regression analysis of the data. The response surface contour plots generated from the model are shown in Figure 4-60. Notice that the contours are curved lines when an interaction exists while the contours are parallel straight lines when no interaction exists between main factors.

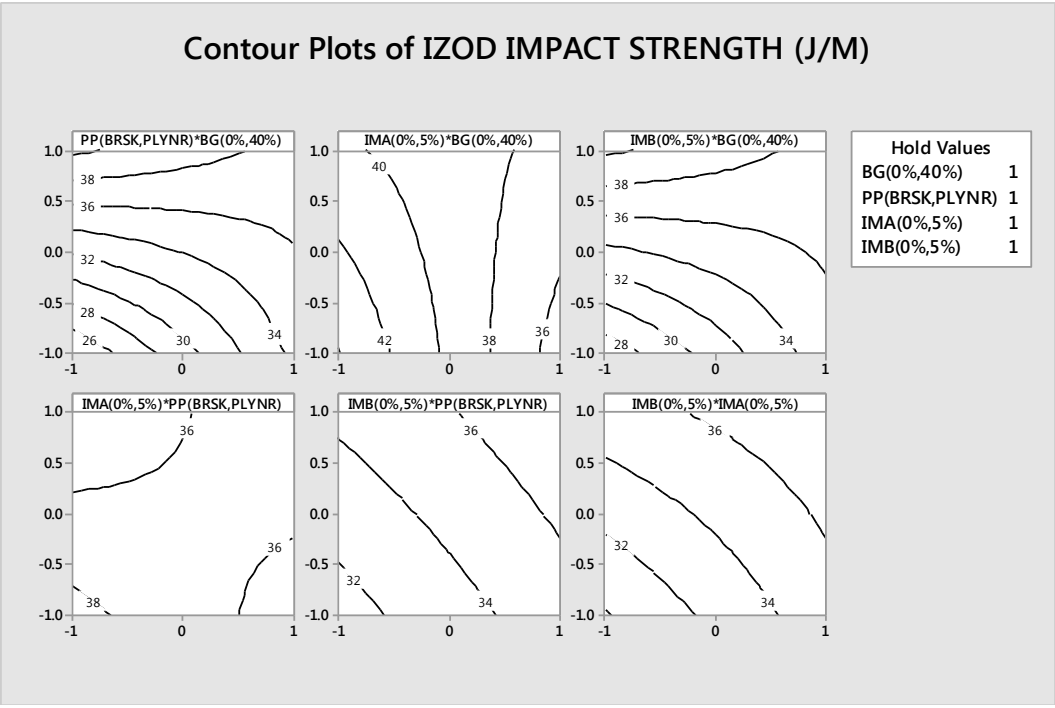

Figure 4-60: DOE (III) Contour plots of Izod Impact Strength

4.2.3.2.2 DOE (III) Tensile Strength Main Effects and Interactions Analysis

The main effects of Bagasse content (0% or 40%), PP grade (Braskem or Polynar) and impact modifiers A and B content (0% or 5%) are plotted below. All main effects show a negative impact on mean tensile strength when moving from low level to high level except for main effect of IMA which a neutral behaviour is observed. Highest negative impact is observed when bagasse is added to the formulation. Bagasse decreases the mean tensile strength by approximately 29%.

If only these main effects are considered, tensile strength would be obtained from running all factors at low level with IMA at high or low level. However, it is necessary to examine any interactions that are important. In fact, main effects do not have much meaning when they are involved in significant interactions.

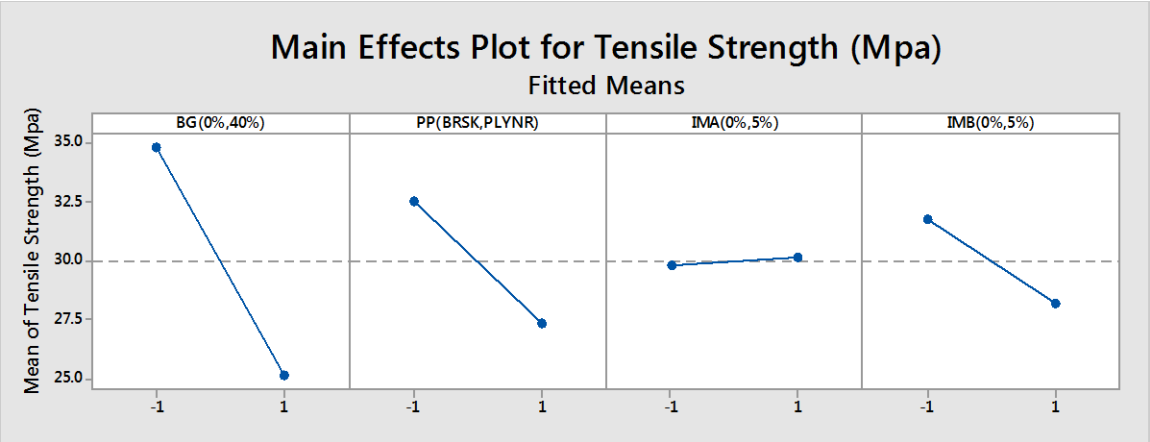

Figure 4-61: DOE (III) Main effects plot for tensile strength

It can be concluded from interactions plot series shown in Figure 4-62 that there are some mild interactions between main effects. When Polynar PP is used, adding bagasse to the formulation decreases the mean tensile strength by approximately 37%, however, when Braskem PP is used, adding bagasse to the formulation decreases the mean tensile strength approximately 11%. This implies better bonding of bagasse with Braskem PP compared to Polynar PP.

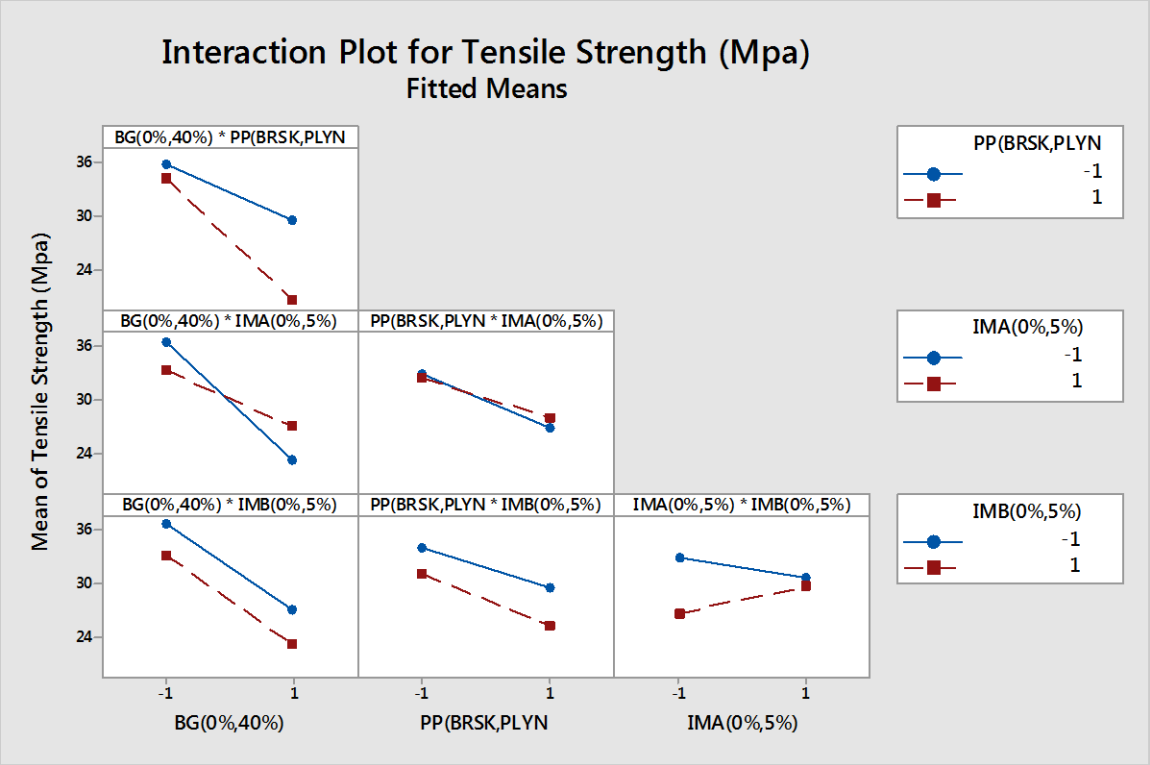

Figure 4-62: DOE (III) Interaction plot for tensile strength

The graph in Figure 7-11 was generated based on an optimum solution considering both main effects and interactions to result in best possible tensile strength. Therefore, the highest tensile strength of 40.10 (MPA) would appear to be obtained when bagasse is at low level (0%), PP grade is at low level (Braskem) IMA is at low level (0%), IMB is at low level (0%). This eliminates bagasse, IMA and IMB from the formulation which obviously contradicts with the purpose of this study.

Another optimization is done when bagasse content is at high level (40%) as in Figure 7-12. Highest tensile strength with bagasse at high level (40%) is obtained when Polynar is used as PP grade, IMA at high level (5%) and IMB at low level (0%). At this optimized point, a tensile strength of 31.31 (MPA) is obtained which is approximately 22% lower than mean tensile strength value obtained when pure Braskem PP is used.

A response surface model was generated based on regression analysis of the data. The response surface contour plots generated from the model are shown in Figure 4-63. Notice that the contours are curved lines when an interaction exits.

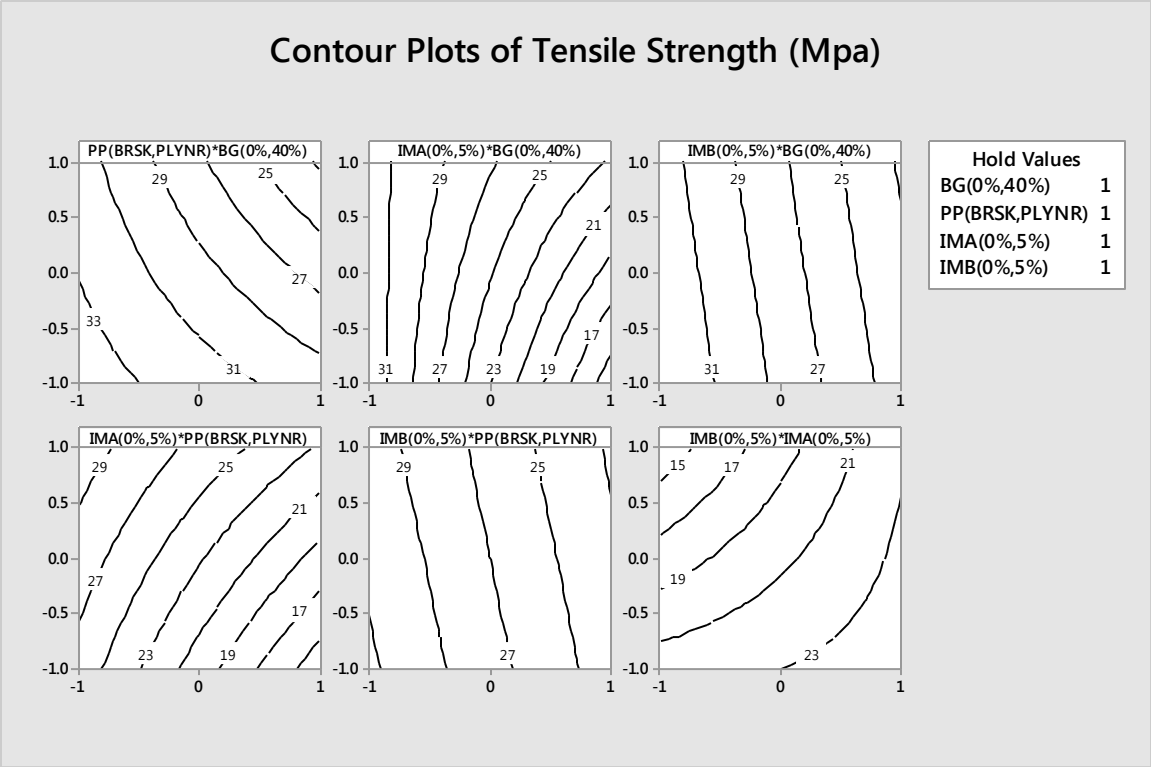

Figure 4-63: DOE (III) Contour plot for Tensile Strength

We obtained similar results from the interactions graph.

4.2.3.2.3 DOE (III) Flexural Modulus Main Effects and Interactions Analysis

The main effects plot in Figure 4-64 shows a comparative neutral effect for main effects of PP grade, IMA and IMB, however, for main effect of bagasse content, an approximately 115% (one hundred fifteen percent) increase in flexural modulus at 1% is observed when Bagasse is used as fiber, compared to no bagasse content (pp only).

If only these main effects are considered, maximum flexural modulus at 1% would be obtained from having PP grade, IMA and IMB at either high or low level and having bagasse content at high level (40%), however, it is necessary to examine any interactions that are important. In fact, main effects do not have much meaning when they are involved in significant interactions.

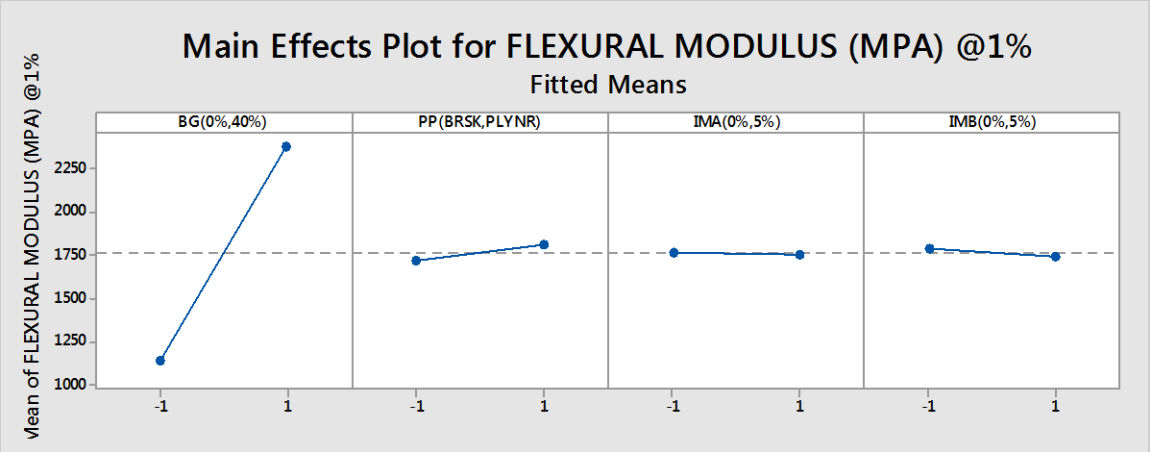

Figure 4-64: DOE (III) Main effects of Flexural modulus at 1%

Referring to interaction plot in Figure 4-65, it can be concluded that no interactions exist between main effects terms. Therefore, previous conclusion about effect of Bagasse content on mean flexural modulus at 1% appears to be a well-supported conclusion.

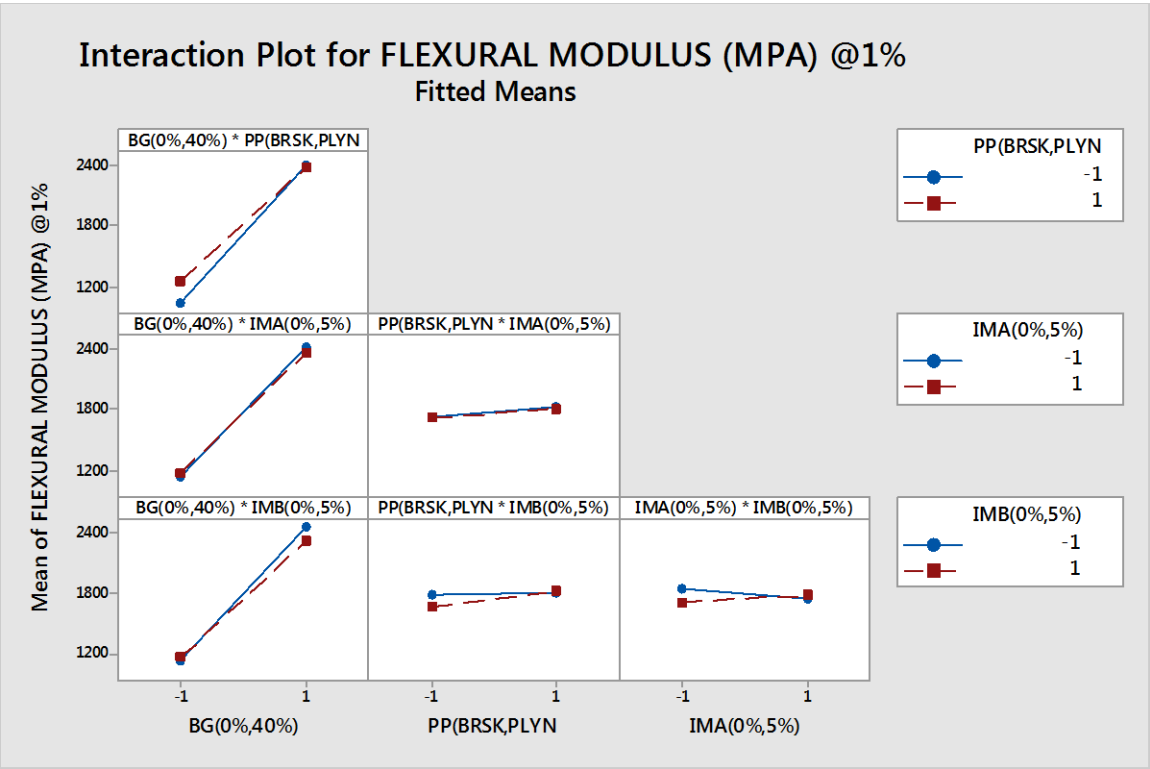

Figure 4-65: DOE (III) Interaction plot for flexural modulus at 1%

The graph in Figure 7-13 was generated based on an optimum solution considering both main effects and interactions to result in best possible flexural modulus. The highest flexural modulus at

1% would appear to be obtained when PP grade is Braskem, IMA is at low level (0%), IMB is at low level (5%) and bagasse content at high level (40%). This eliminates IMA and IMB from the formulation and confirms Braskem PP to be superior compared to Polynar PP for flexural modulus at 1% response.

A response surface model was generated based on regression analysis of the data. The response surface contour plots generated from the model are shown in Figure 4-66. Notice that for scalar quantities, the contours are curved lines when an interaction exits and the contours are parallel straight lines when no interaction exists between the main effects.

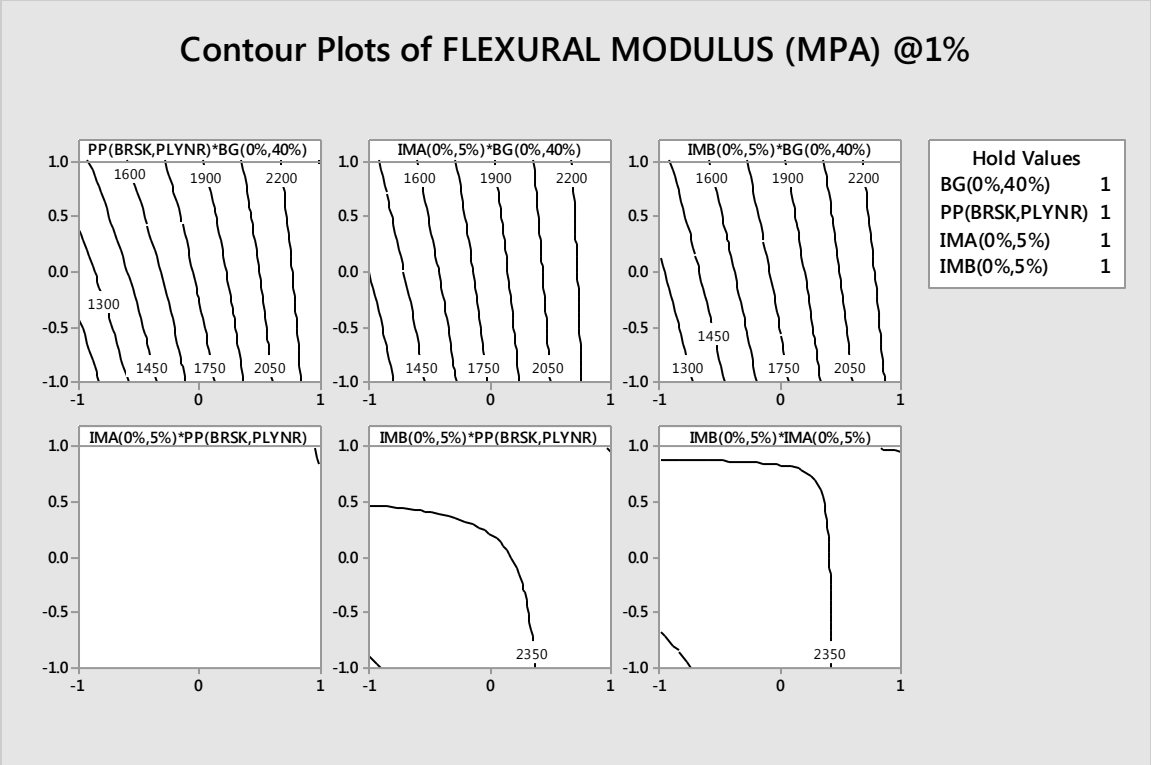

Figure 4-66: DOE (III) Contour plots for flexural modulus at 1%

Similar results were obtained from the interactions graphs.

4.2.3.2.4 DOE (III) Mean Failure Energy Main Effects and Interactions Analysis

The main effects impacting the mean of mean failure Energy (J) are illustrated in Figure 4-67. Based on previous Anova tables, main effect A (bagasse content) is a significant effect. Therefore, as Bagasse content is changed from 0% to 40%, the mean of mean failure energy is reduced by

approximately 25%. There are no reliable significant interactions observed based on previous Anova table.

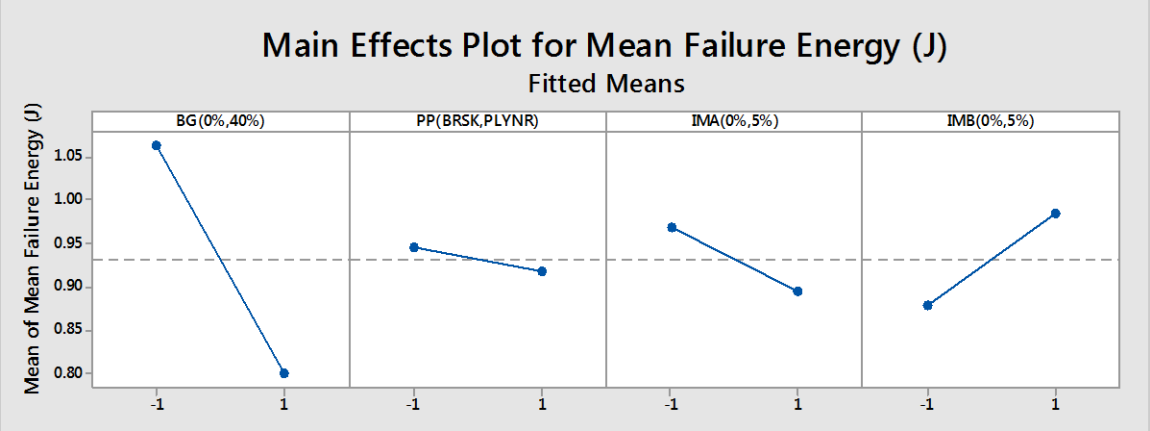

Figure 4-67: DOE (III) Main effects plot for mean failure energy

If only these main effects are considered, maximum Mean Failure Energy would be obtained from having all DOE (III) factors at low level except for IMB, however, it is necessary to examine any interactions that are important. In fact, main effects do not have much meaning when they are involved in significant interactions.

Figure 4-68, illustrates interaction between main factors for DOE(III) mean failure energy response. Rather mild interactions are detected between various main factors as indicated in Table 4-11. One interaction exists between bagasse - IMA which appears to be rather significant. While IMA is present in the compound, adding bagasse doesn't reduce the mean failure energy much, however, when IMA is not present in the compound, adding bagasse significantly reduces the mean failure energy by approximately 35% which proves the effectiveness of IMA in the bagasse polypropylene compound resistance against impact.

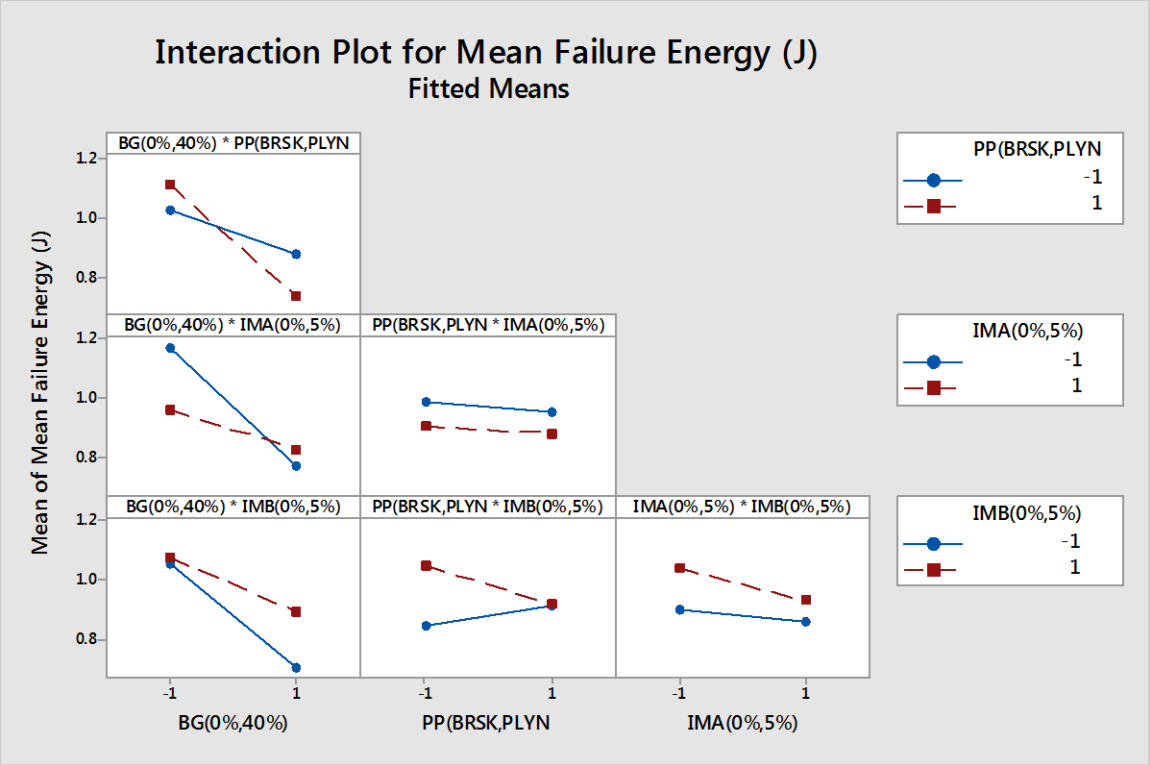

Figure 4-68: DOE(III) Interactions plot for mean failure energy

The graph in Figure 7-14 was generated based on an optimum solution considering both main effects and interactions to result in highest possible mean failure energy. Therefore, the best mean failure energy would appear to be obtained when Bagasse content is at low level (0%), PP type is Braskem, IMA is at low level (0%), IMB is at low level (0%).

A response surface model was generated based on regression analysis of the data. The response surface contour plots generated from the model are shown in Figure 4-69. Notice that the contours are curved lines when an interaction exits while the contours are parallel straight lines when no interaction exists between main factors. This graph is not reliable as based on Anova table there are no reliably significant interactions.

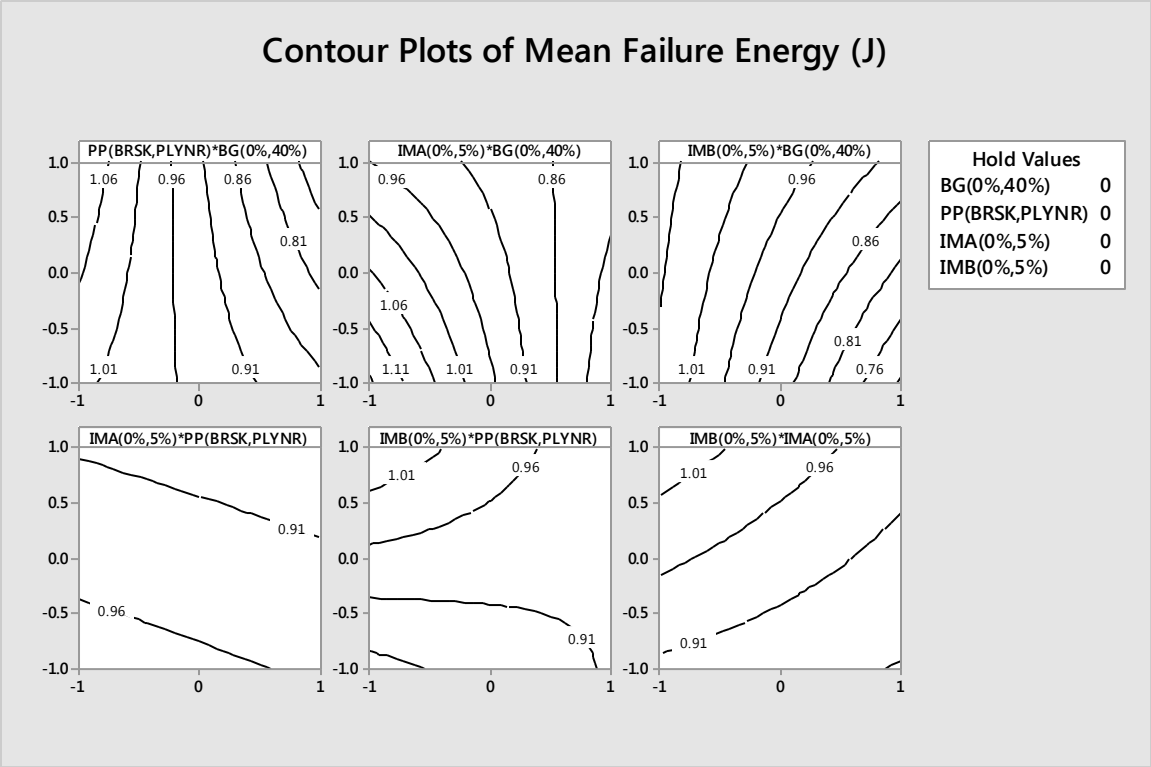

Figure 4-69: DOE (III) Contour plots for mean failure energy

4.3 Scanning Electron Microscopy (SEM) Image Analysis

SEM of Izod impacted surface of various formulation combinations of bagasse or oat hull Composites have been studied using SEM (Scanning Electron Microscopy)

Comparing Figure 4-71 and Figure 4-75 where fibers, polypropylene and PPMA are present in the formulation, it appears that the interface of bagasse fiber with the matrix is almost not recognizable (Figure 4-71)and no fibers have been pulled out of the matrix, however, the fiber matrix interface for oat hull fibers appears to comparatively be well recognizable (Figure 4-75) and oat hull fibers have been pulled out of polypropylene matrix, which confirms better interfacial adhesion of bagasse due to chemical linkage between hydroxyl groups of fiber surface with MA of PPMA compared to interfacial adhesion of oat hull to PPMA.

Comparing BG-PP combination (Figure 4-70) to OH-PP combination (Figure 4-74), where both composites do not contain any impact modifier or coupling agent, it can be inferred that although the number of fiber pull outs from the matrix appear to be the same for both BG-PP and OH-PP, but the size of OH-PP fiber pull out holes appear to be way larger compared to the size of BG-PP fiber pull out holes. As well, the mixture of PP-BG appears to be more homogeneous compared to PP-OH mixture. (Figure 4-70 and Figure 4-74)

Air pockets appear to be formed with PP-BG-IMA,B-PPMA (Figure 4-73) as well as in the OH-PP-PPMA (Figure 4-75). These air pockets may have been formed during injection molding of test samples or due to chemical reaction between impact modifiers and coupling agent.

Comparing Figure 4-76 and Figure 4-77 where the latter contains OH, PP, IM and PPMA while the former contains OH, PP and IM shows similar low fiber-matrix adhesion at presence of impact modifier only or impact modifier accompanied by coupling agent. Figure 4-72 however, as many fibers are pulled out, shows even worse fiber-matrix adhesion for composites consisted of BG, PP and Impact modifiers in absence of PPMA.

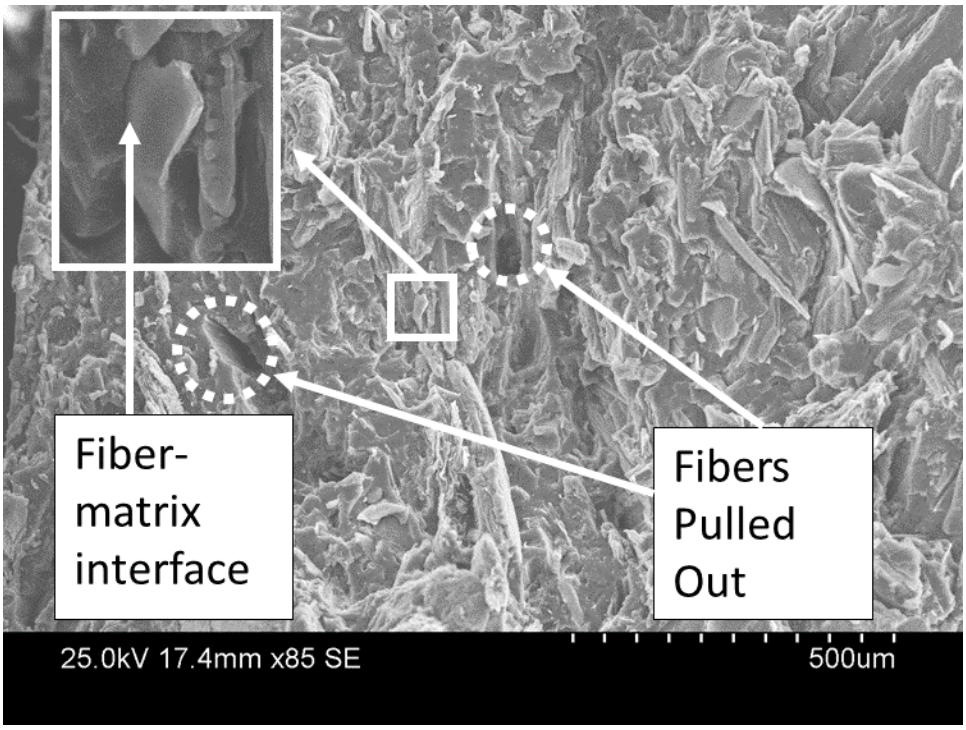

Figure 4-70: Bagasse (40%), Polypropylene (59.5%), A.O. (0.5%)

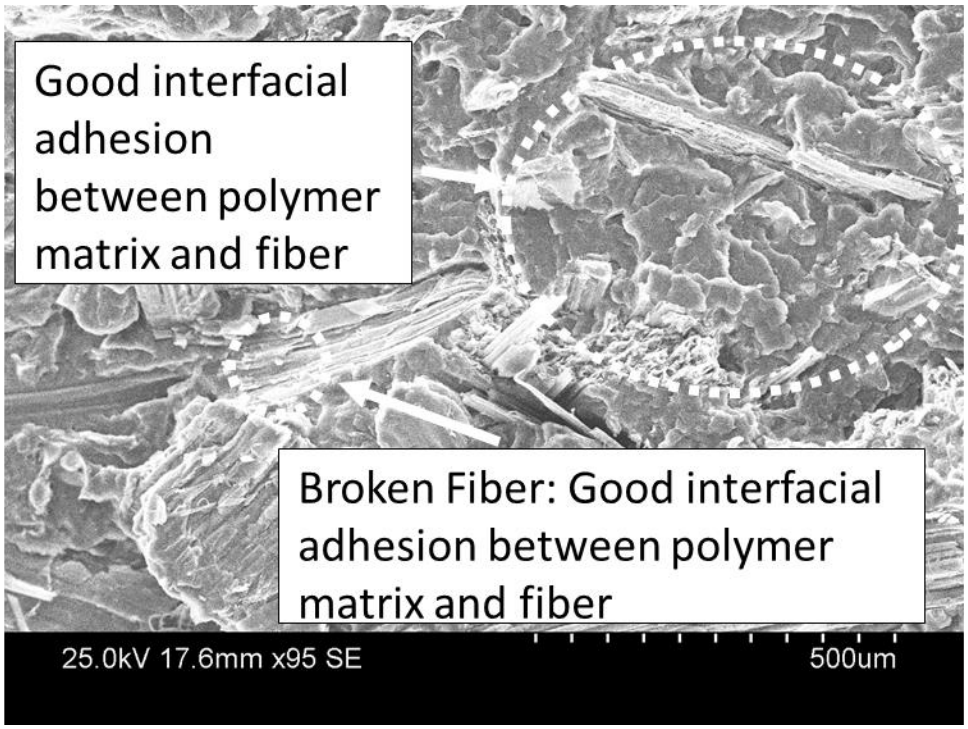

Figure 4-71: Bagasse (40%), Polypropylene (55.5%), PPMA (4%), A.O. (0.5%)

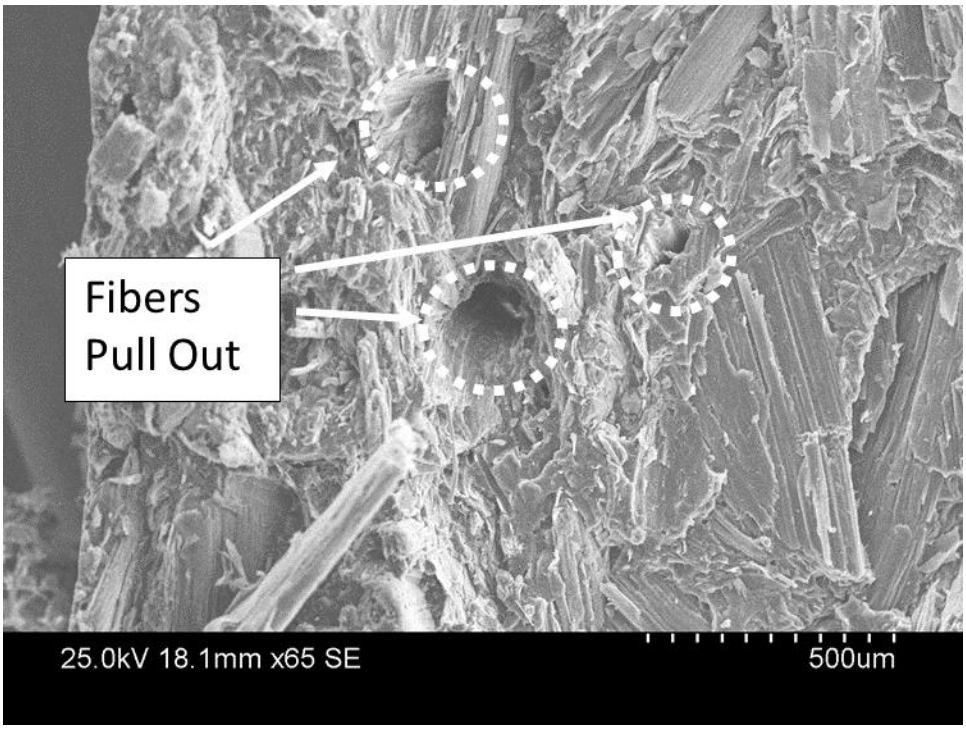

Figure 4-72: Bagasse (40%), Polypropylene (54.5%), Impact modifier(5%), A.O. (0.5%)

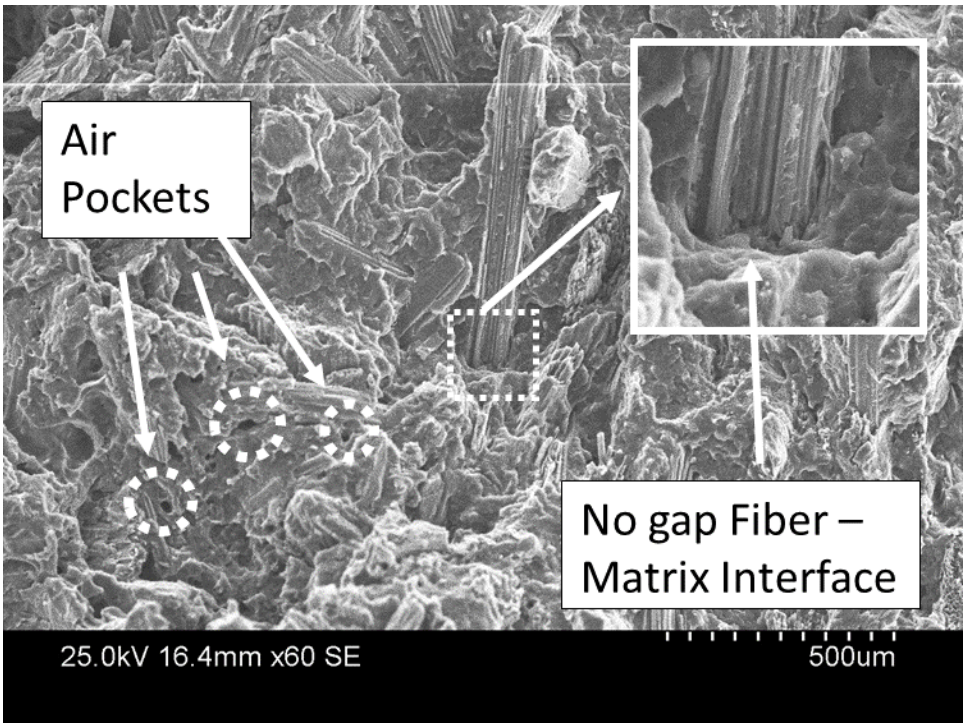

Figure 4-73: Bagasse (40%), Polypropylene (50.5%), Impact modifier (5%), PPMA (4%), A.O. (0.5%)

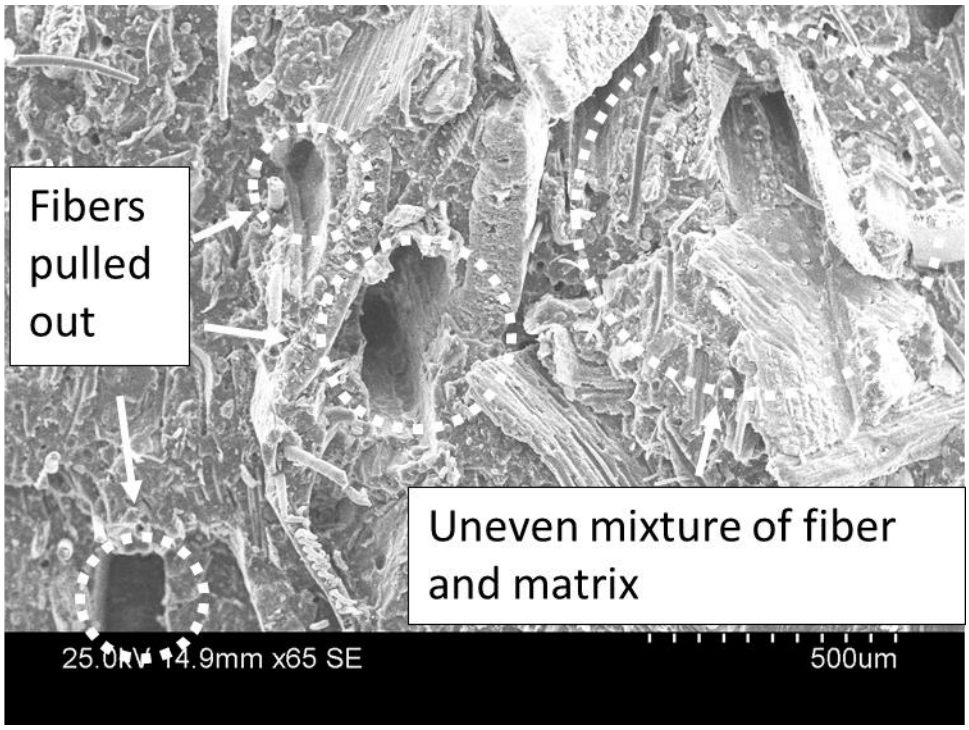

Figure 4-74: Oat Hull (40%), Polypropylene (59.5%), A.O. (0.5%)

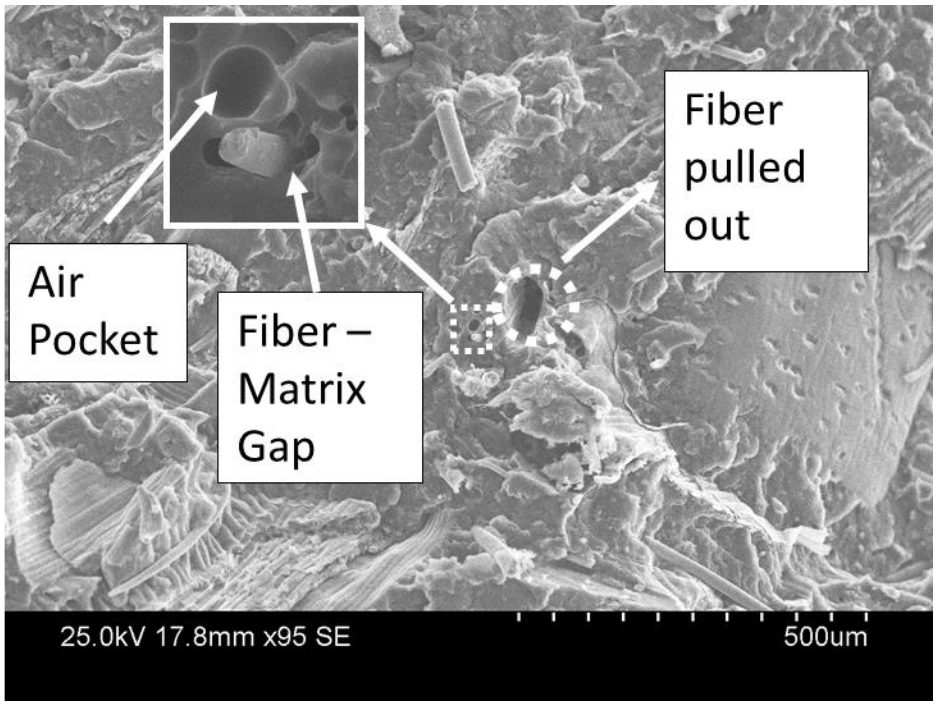

Figure 4-75: Oat Hull (40%), Polypropylene (55.5%), PPMA (4%), A.O. (0.5%)

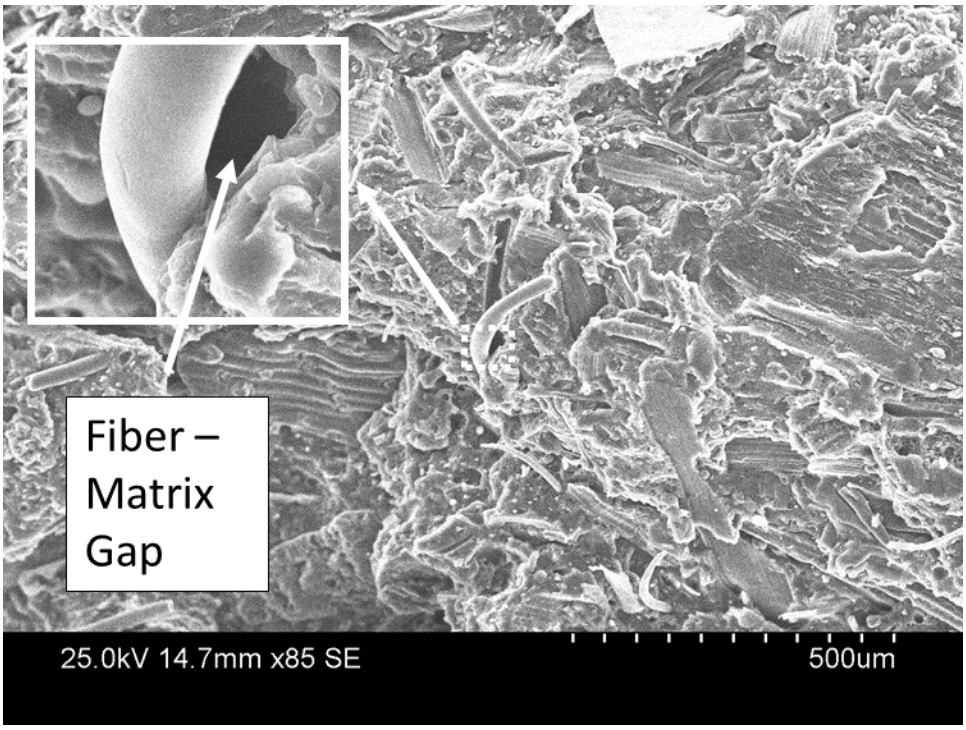

Figure 4-76: Oat Hull (40%), Polypropylene (54.5%), Impact modifier (5%), A.O. (0.5%)

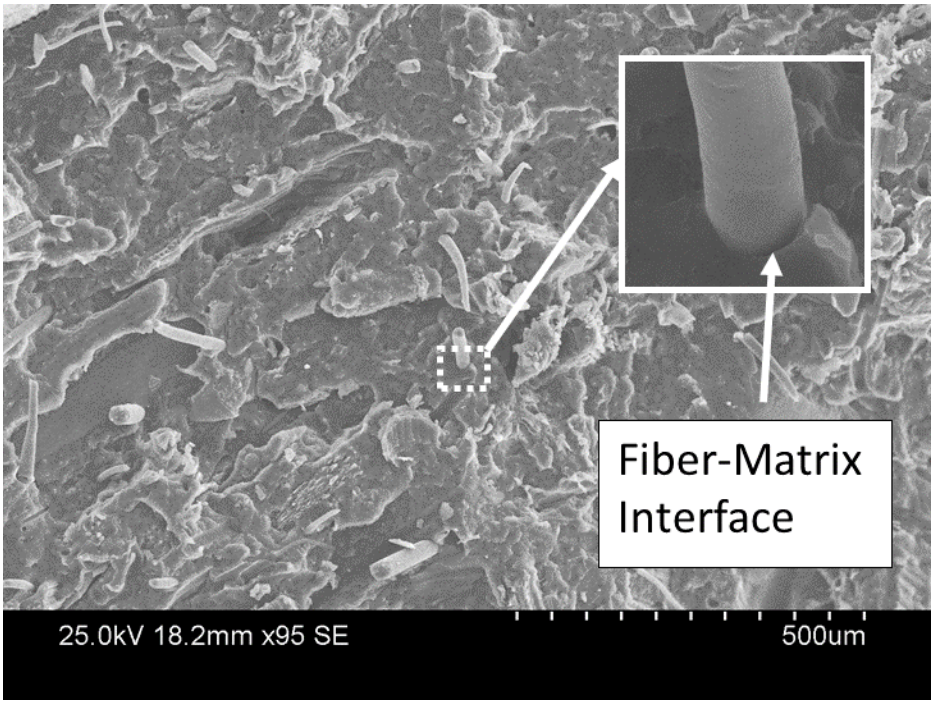

Figure 4-77: Oat Hull (40%), Polypropylene (50.5%), Impact modifier (5%), PPMA (4%), A.O. (0.5%)

DOE (IV) for UV weathering & impact location effects on Multi-axial impact properties of NFPC roofing shakes

Table 4-12 illustrates the DOE (IV) results for testing four impact responses on commercialized final product using 2 level factorial design of experiment as described in section 3.2.6.7. The statistical method of 2 level factorial design is analyzed in section 4.3.1 and the results including main effects and interactions are analyzed separately in section 4.3.2.

Table 4-12: DOE (IV) results for Multi-Axial Impact responses

			Maximum load (kN)		Deflection at max load (mm)		Energy to max load (J)		Total energy (J)	
UV Exposure	Location of impact	Back Reinforc-ement	AVG	St.Dev	AVG	St.Dev	AVG	St.Dev	AVG	St.Dev
0 h	Middle	No	1.83	0.31	3.29	1.51	3.93	1.79	14.65	4.94
0 h	Middle	Yes	1.99	0.35	3.64	0.74	5.29	1.19	11.95	2.44
0 h	Side	No	1.66	0.41	3.06	0.69	3.49	0.81	11.29	4.19
0 h	Side	Yes	1.94	0.48	2.28	0.94	2.93	1.87	15.84	3.59
1000 h	Middle	No	1.94	0.43	3.32	1.37	4.24	1.85	12.18	0.98
1000 h	Middle	Yes	1.31	0.30	3.01	0.58	2.80	1.23	8.08	2.57
1000 h	Side	No	1.60	0.39	2.89	0.87	3.29	1.64	10.89	6.52
1000 h	Side	Yes	2.08	0.68	2.68	0.98	3.48	1.56	13.65	6.02

4.3.1 Statistical Method Analysis of DOE (IV) for UV weathering & impact location effects on multi-axial impact properties of NFPC roofing shakes

We begin the analysis of data in Table 7-34 by developing four Anova tables to identify significance of each main factor or interaction combination factors. Based on an alpha value of 5%, it is concluded that factors or interactions with a lower than 15% P value are significant. Table 7-35, Table 7-36, Table 7-37 and

Table 7-38 illustrate Anova table for maximum load, deflection at maximum load, energy to maximum load and total energy responses, respectively. The regression equations of each response are as following:

Equation 4-13: Regression Equation for (a) Maximum Load (b) Deflection at max load (c) Energy to max load (d) Total Energy

$$(a)\ Maximum\ load\ (kN)$$
$$= 1.7933 - 0.0612\,A + 0.0261\,B + 0.0371\,C + 0.0812\,A * B - 0.0732\,A * C + 0.1556\,B * C + 0.1258\,A * B * C$$

$$(b)\ Deflection\ at \max load\ (mm)$$
$$= 3.022 - 0.046\,A - 0.294\,B - 0.119\,C + 0.104\,A * B - 0.015\,A * C - 0.129\,B * C + 0.153\,A * B * C$$

$$(c)\ Energy\ to\ max\ load\ (J)$$
$$= 3.682 - 0.228\,A - 0.384\,B - 0.055\,C + 0.316\,A * B - 0.257\,A * C - 0.037\,B * C + 0.441\,A * B * C$$

$$(d)\ Total\ energy\ (J)$$
$$= 12.314 - 1.116\,A + 0.603\,B + 0.064\,C + 0.469\,A * B - 0.400\,A * C + 1.764\,B * C - 0.050\,A * B * C$$

$Where$:

$A = UV\ Hours, A = -1\ for\ 0h\ and\ A = 1\ for\ 1000h;$

$B = Location\ of\ impact, B = -1\ for\ middle\ and\ B = 1\ for\ side;$

$C = Back\ Reinforcement, C = -1\ for\ without\ back\ reinforcement\ and\ C = 1\ for\ with\ back\ reinforcement$

Based on Anova tables, normal probability plots of effects are constructed for each measured responses. The deviation of data points from the straight line shows that the data points shown in red are significant. Graphs in Figure 4-78 (a), (b), (c) and (d) confirm the significance of main effects and interactions that were analytically concluded using the Analysis of Variance (ANOVA).

To check that normality assumptions were correct it is necessary to look at the residuals plot and see if the residuals are normally distributed or not. The points on these plots shown in Figure 4-79 (a),

(b), (c) and (d) are reasonably close to a straight line, although the distribution of the residual points are not well scattered below and above the mean line for Figure 4-79 (b) and (d) which belongs to deflection to maximum load and total energy. Generally, it can be stated that normal residual plots mildly support the underlying hypothesis assumptions of the analysis.

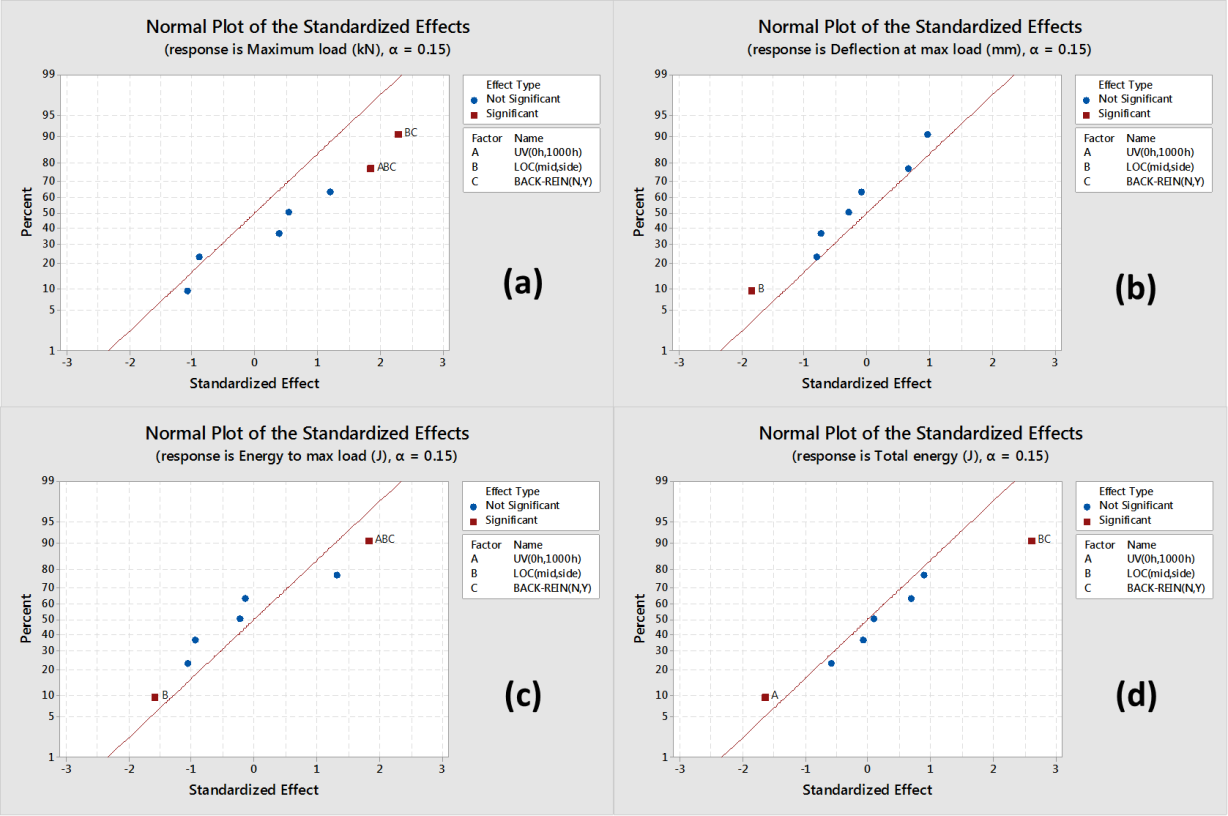

Figure 4-78: (a) Commercial Final Product Normal plot for maximum load response, (b) Commercial Final Product Normal plot for deflection at maximum load response, (c) Commercial Final Product Normal plot for energy to maximum load response, (d) Commercial Final Product Normal plot for total energy response

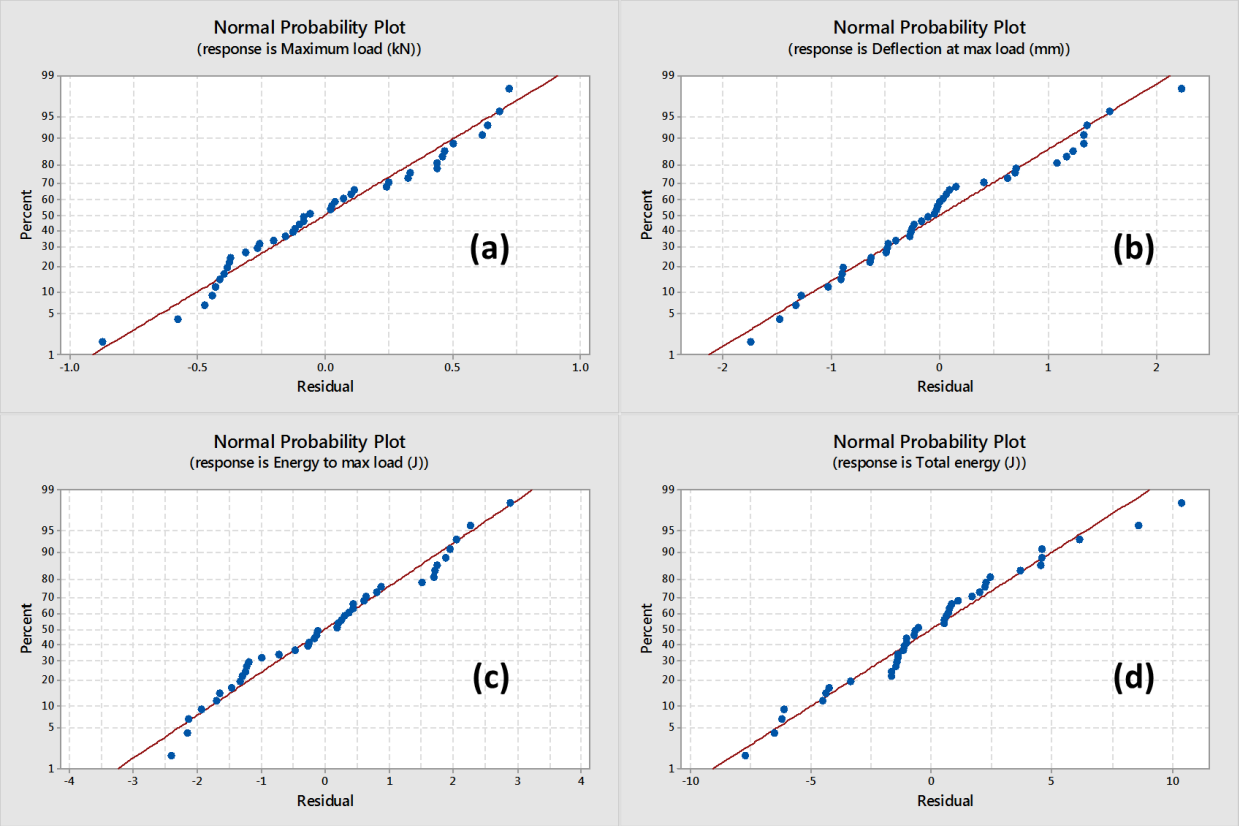

Figure 4-79: (a) Commercial Final Product Normal Residual plot for maximum load response, (b) Commercial Final Product Normal Residual plot for deflection at maximum load response, (c) Commercial Final Product Normal Residual plot for energy to maximum load response, (d) Commercial Final Product Normal Residual plot for total energy response

4.3.2 Main Effects & Interactions Analysis of DOE (IV) for UV weathering & impact location effects on multi-axial impact properties of NFPC roofing shakes

A summary comparing main effects means in per cents of improvement or deterioration for DOE (IV) is presented in Table 4-13. The table as well lists the significant interactions observed between the main effects.

Table 4-13: UV Weathering and impact location main effects and interactions on multi-axial Impact Responses on NFPC Commercial Roofing Product

UV Weathering and impact location main effects and interactions on multi-axial Impact Responses on NFPC Commercial Roofing Product			Improvement (+%), Deterioration (-%), interaction exist (✓)			
			Total Energy	Energy to Max. Load	Deflection at Max. Load	Maximum Load
Main Effects (from - to)	UV 0h	UV 1000h	-17%	-12%	-	-6%
	Impact location middle	Impact Location Side	10%	-20%	-18%	-
	Impact location without back reinforcement	Impact Location with back reinforcement	-	-	-6%	-
Interactions	UV hours-Impact Location		✓	✓	✓	✓
	UVhours-Back Reinforcement		✓	✓	-	✓
	Impact Location-Back Reinforcement		✓	-	✓	✓

4.3.2.1 Main Effects and Interactions of Total Energy Response

Figure 4-80 shows main effects plot for total energy. It indicates that as we expose the composite shakes to UV radiation for 1000 hours, the total energy is decreased by about 17%. Another observation is that as we move from middle of surface of composite shake to side, total energy is increased by about 10%. It is noticeable also that having any reinforcement at the back of the shake is not noticeably effective on the total energy.

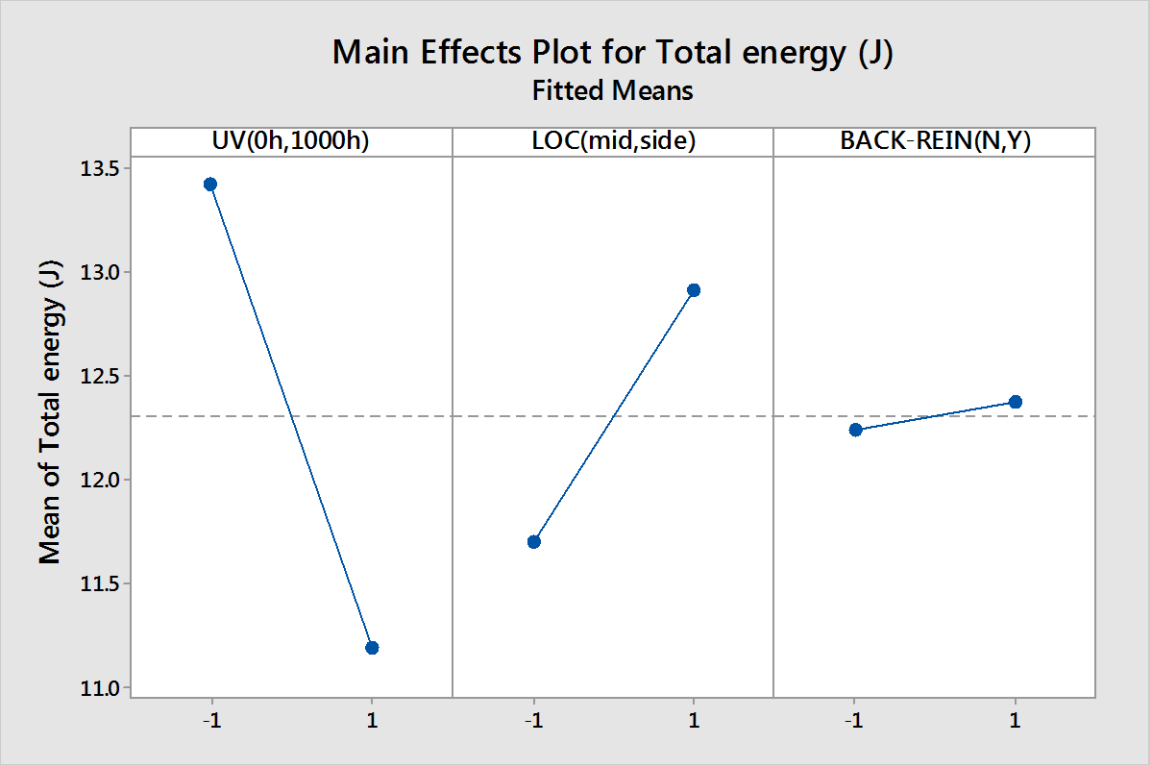

Figure 4-80: Commercial Final product total energy main effects

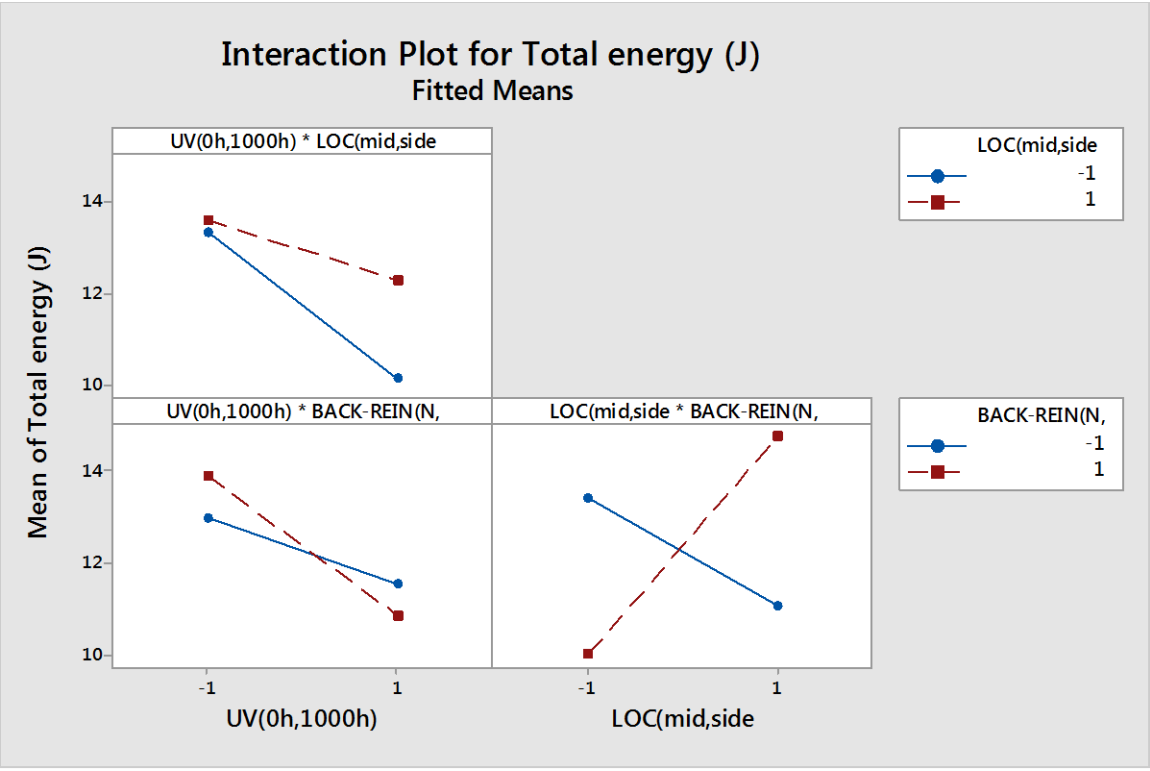

Figure 4-81: Commercial Final product total energy interaction plot

Figure 4-81 shows interaction plot for total energy. It indicates that as we move from side to middle of surface of the composite shake, the UV radiation causes approximately twice more decrease to total energy which indicates that UV radiation causes more damage to middle surface of the composite shake compared to the side of the composite shake. Also it can be concluded that with back reinforcement, the total energy increases as we go from mid to side of the surface of the composite shake, however, without back reinforcement, the total energy decreases as we go from mid to side of the surface of the composite shake which indicates the substantial effect of back reinforcement on total energy.

It also can be concluded that with back reinforcement, total energy decreases by approximately 20% when exposed to UV exposure for 1000 hours, however, without back reinforcement total energy decreases by about 8% when exposed to 1000 hours of UV exposure. This indicates that UV exposure causes more damage to surfaces with back reinforcement.

A response surface model was generated based on regression analysis of the data. The response surface contour plots generated from the model are shown in Figure 7-19. Notice that the contours are curved lines when an interaction exits while the contours are parallel straight lines when no interaction exists between main factors.

4.3.2.2 Main Effects and Interactions of Energy to Maximum Load Response

Based on Figure 4-82, moving the impact head from middle of composite shake to side of the shake decreases the mean energy to max load by approximately 20%. The UV exposure decreases the mean of energy to max load by approximately 12%. The back reinforcement appears not to be effective on mean energy to max load.

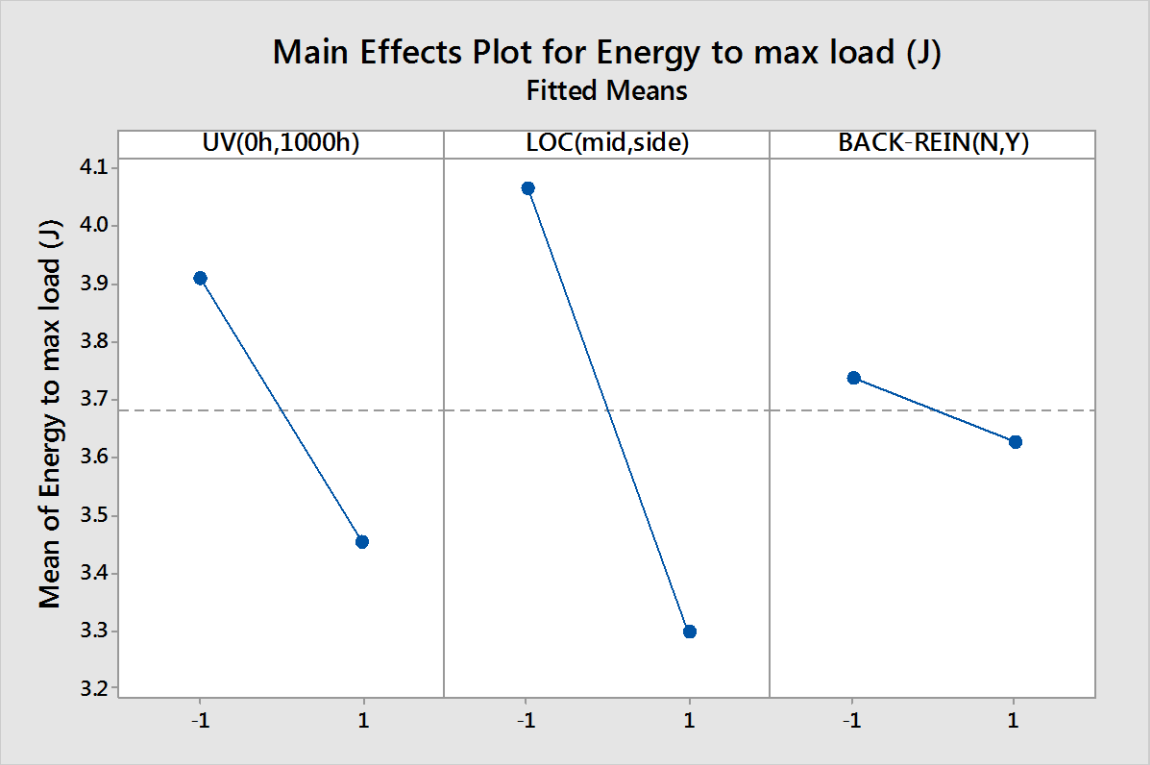

Figure 4-82: Commercial Final product energy to max load main effects

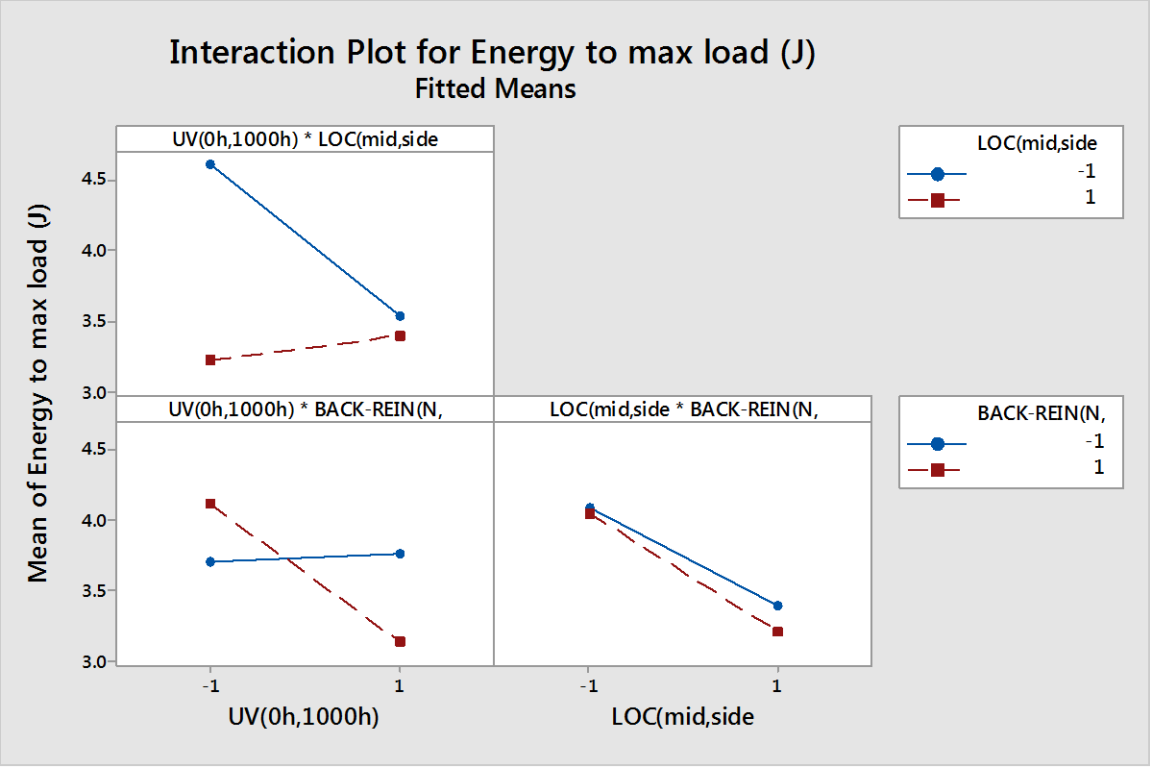

Figure 4-83: Commercial Final product energy to max load interactions

Based on interactions graphs in Figure 4-83 for energy to max load (J), mean of energy to max load stays almost constant when shake side of the composite shake is exposed to UV radiation, however, when the middle of surface of composite shake is exposed to UV radiation for 1000 hours, mean of energy to max load of composite shake is decreased by approximately 24%. It also appears that when there is no back reinforcement for the surface of the composite shake, UV exposure does not affect mean of energy to max load, however, when back reinforcement exists for the surface of the composite shake, UV exposure for 1000 hours decreases mean of energy to max load of the composite shake by approximately 25%.

A response surface model was generated based on regression analysis of the data. The response surface contour plots generated from the model are shown in Figure 7-20. Notice that the contours are curved lines when an interaction exits while the contours are parallel straight lines when no interaction exists between main factors.

4.3.2.3 Main Effects and Interactions of Deflection at Max Load Response

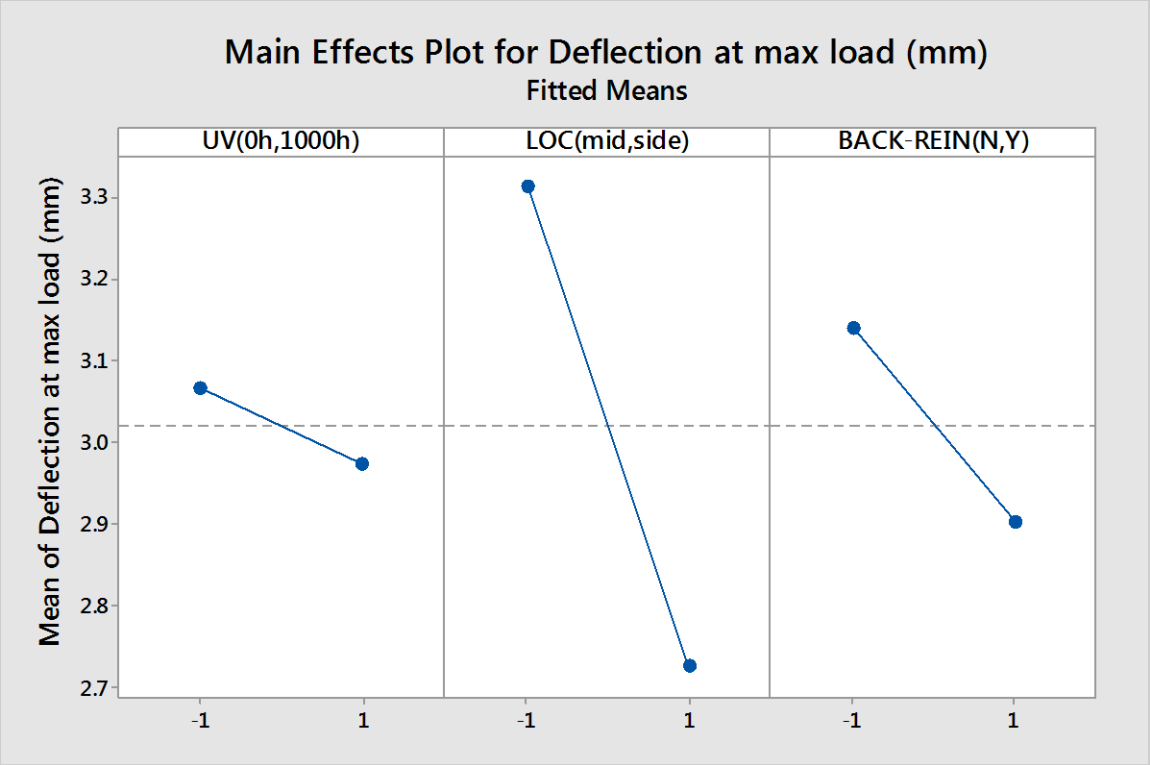

Figure 4-84: Commercial Final product deflection at max load main effects

Based on graph in Figure 4-84, the exposure of composite shakes to UV radiation appears not to be effective on deflection at max load, however, as we move from middle to side of the surface of the

composite shake there appears to be an approximately 18% decrease in average mean of deflection at max load. Back reinforcement appears not to be very effective in mean of deflection at max load.

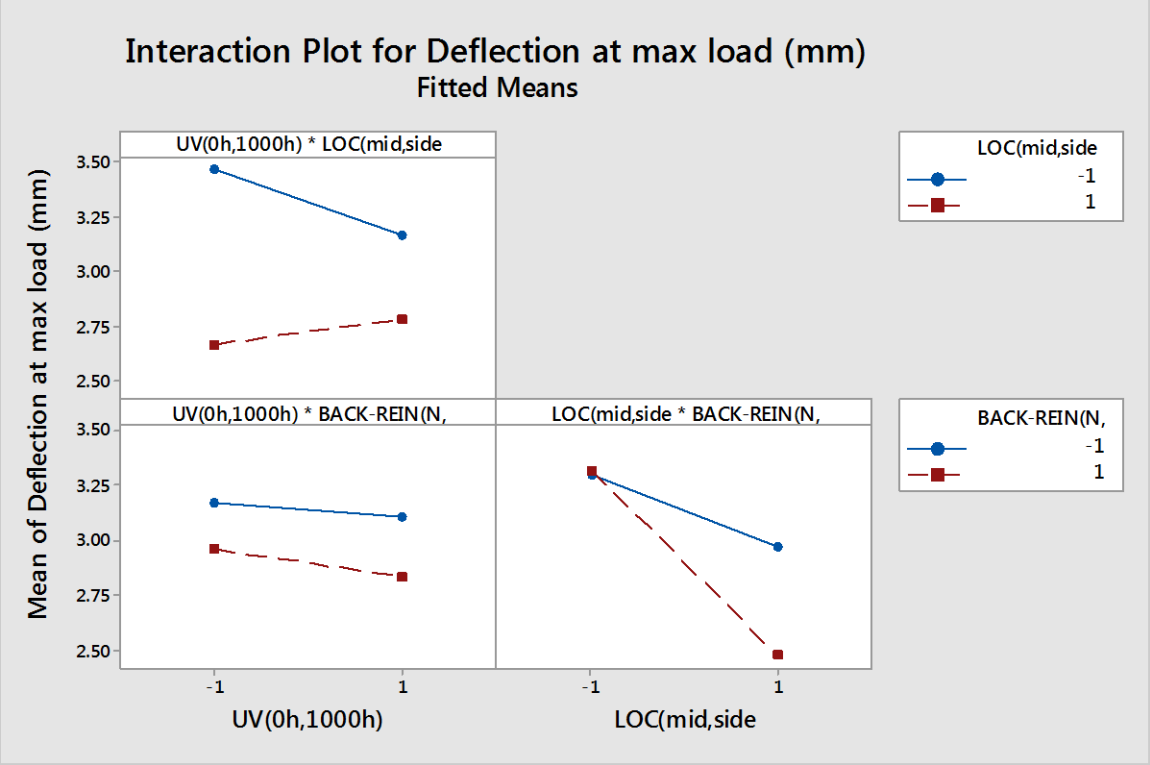

Figure 4-85: Commercial Final product deflection at max load main effects

Commenting on graph in Figure 4-85, a significant interaction is observed between location of impact (side or mid) and back reinforcement (No or Yes). As we move from middle to side of the surface of composite shake, part of the surface of the composite shake without back reinforcement show higher mean of deflection at max load compared to part of the surface of the composite shake with back reinforcement.

A response surface model was generated based on regression analysis of the data. The response surface contour plots generated from the model are shown in Figure 7-21. Notice that the contours are curved lines when an interaction exits while the contours are parallel straight lines when no interaction exists between main factors.

4.3.2.4 Main Effects and Interactions of Maximum Load Response

Based on graph in Figure 4-86, mean of maximum load decreases by approximately 6% due to exposure to UV for 1000 hours, however, factors such as location of impact (mid or side) or back reinforcement (no or yes) appear not to be significantly effective on the mean of maximum load.

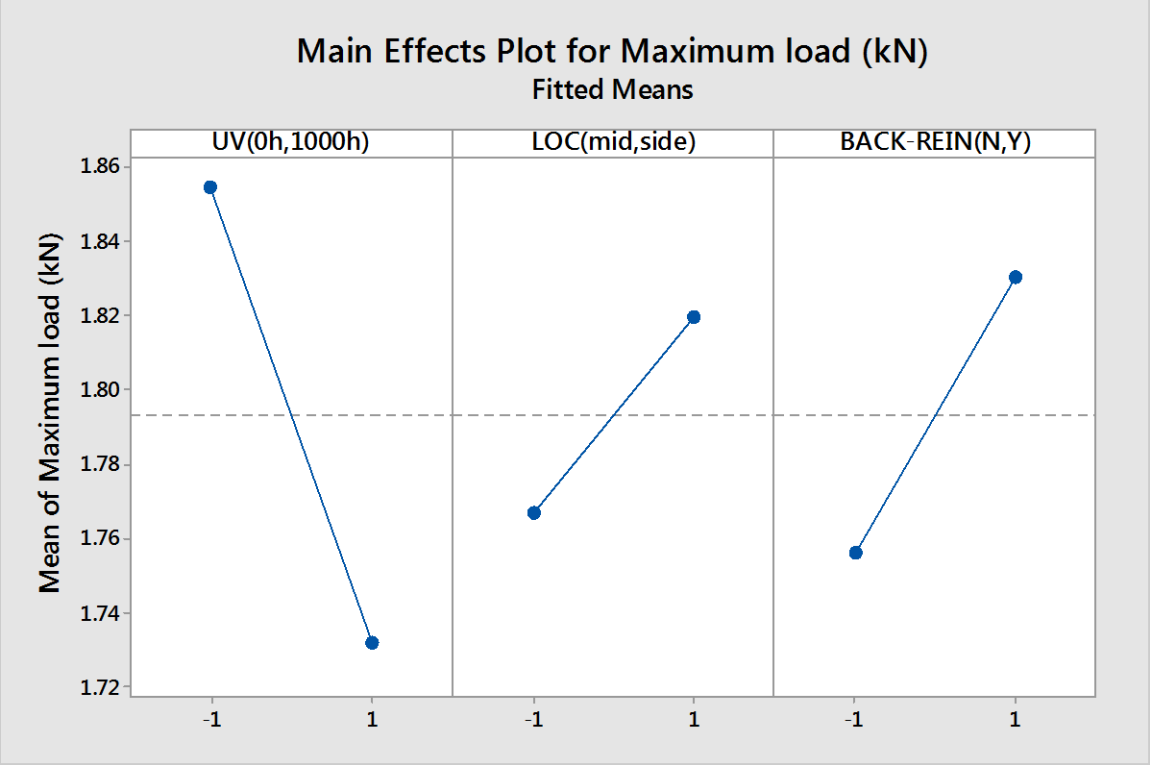

Figure 4-86: Commercial Final product maximum load main effects

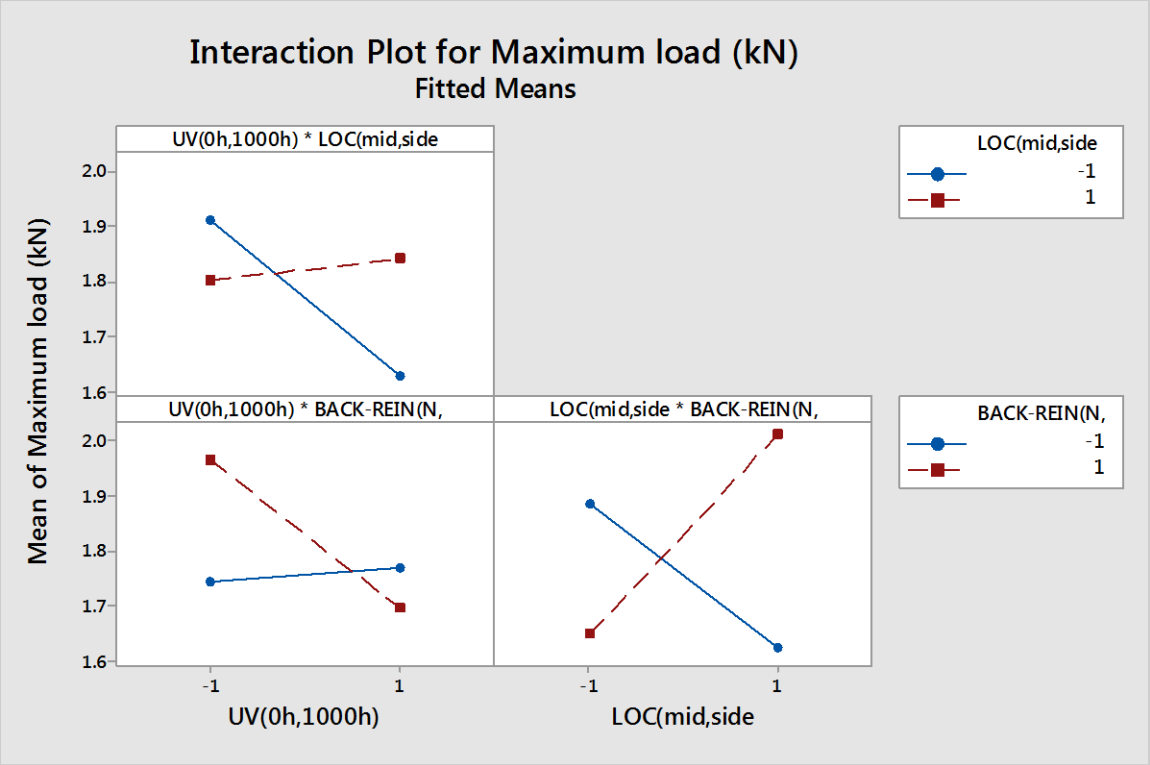

Figure 4-87: Commercial Final product maximum load interactions

It can be inferred from interactions graphs in Figure 4-87 that at the side of the composite shake, UV exposure is not effective, however, in the middle of surface of the composite shake, UV exposure is substantially effective and decreased the mean of maximum load by approximately 14%. It also can be concluded that when there is no reinforcement at the back of the composite shake, UV exposure is not effective, however, when there is back reinforcement at the back of the composite shake, mean of maximum load is decreased substantially by approximately 13%.

Figure 7-15, Figure 7-16,Figure 7-17 and Figure 7-18 show the optimum solution to maximize each of the responses studied above in the commercial final product.

As per Figure 7-16 and Figure 7-17 deflection to max load and energy to max load appear to be obtained when product was not exposed to UV and location of Dynatup impact is in the middle of surface of the shake with back reinforcement. As per Figure 7-15, maximum total energy is obtained when the shakes are not exposed to UV and location of Dynatup impact is at the side of the surface of the shake with back reinforcement. As per Figure 7-18, maximum load appears to be obtained when shakes are exposed to UV for 1000 hrs and location of Dynatup impact is at the side of the shake with back reinforcement.

A response surface model was generated based on regression analysis of the data. The response surface contour plots generated from the model are shown in Figure 7-22. Notice that the contours are curved lines when an interaction exits while the contours are parallel straight lines when no interaction exists between main factors.

To check if the assumptions for our two level replicated factorial design of experiment were correct it is necessary to look at the residuals plot and see if the residuals are normally distributed or not. The points on this plot shown in Figure 7-23, Figure 7-24 and Figure 7-25 are reasonably close to a straight line which supports the fact that the underlying assumptions for maximum load, deflection to maximum load and energy to maximum load of the analysis are satisfied, however Figure 7-26 appears not to be a good fit to straight line and therefore, underlying assumptions for total energy appear not to well satisfied.

5 Conclusions and Recommendations

Oat hull and bagasse fibers were milled, sieved and analyzed for length of fibers and aspect ratios. It was found that bagasse fibers lengths were between 0.1mm to 8mm, and oat hull fibers lengths between 0.03mm to 9mm. Majority of oat hull fibers were smaller than 0.5 mm and had an aspect ratio between 1 and 3 while majority of bagasse fibers were larger than 0.5 mm and had an aspect ratio between 3 to 9.

For DOE (I), which was mainly designed to compare effect of oat hull and bagasse fibers on properties of natural fiber - PP compound, it was concluded based on main effects and interactions that bagasse interacts much better compared to oat hull with coupling agent (36% highest flexural modulus and 40% higher tensile modulus). As well IMB appeared to be more effective in increasing impact properties especially, increasing mean of mean failure energy by 20% and mean of Izod impact energy by 16%. For effect of Impact modifiers on impact properties, IMB and IMA showed strong interaction and appeared to cancel out one another effect suggesting to be used separately. Statistical methods generally validated the results. Best normal residual plot fit was for Izod impact results which was almost linear, and the worst fit belonged to mean failure energy results.

For DOE (II), which dealt with comparing effect of PP from two grades and additives at two levels in bagasse - polypropylene composites, it was concluded that Polynar polypropylene has negative impact on tensile properties decreasing it by about 32%, although acted same as Braskem PP for other mechanical tests. Coupling agent appeared to be very effective again, increasing tensile strength by about 51% at 4% level although having a mild deteriorating effect on mean failure energy. Two main interacting factors were IMA and IMB again. No interaction between main factors was detected for tensile response. Statistical methods analysis generally validated the results except for tensile strength results in which the normal residual plot was curved and not a good fit to a straight line.

For DOE(III), which mainly dealt with comparing bagasse-PP compounds with pure PP from two grades with or without impact modifiers, it was found that bagasse was very effective on flexural modulus (110% higher flexural modulus than pure PP) and on Izod impact (22% higher Izod impact energy than pure PP), however, bagasse decreased the tensile and mean failure energy by about 25%. Polynar PP was found to produce higher Izod impact energy (23% higher) however, decreased the

tensile properties. Flexural modulus results showed no interaction between main factors, however, a significant interaction was detected between Bagasse-PP for Izod impact and tensile tests.

SEM Images of impacted portion of Izod impact samples generally supported the underlying assumptions of the coupling agent effect. The images confirmed adhesion effect of MAPP on both oat hull and bagasse, although for bagasse, a better adhesion is clearly observed in the SEM images.

For DOE (IV), effect of UV weathering and impact location was studied on multi-axial impact responses of NFPC commercial roofing product. 1000 hours of UV radiation deteriorated total energy, energy to maximum load and maximum load of roofing product by 6%-17%, however, did not affect the max load deflection. The location of impact either in middle or side or with/without back reinforcement, was comparatively not found to be effective on multi-axial impact properties except for energy to maximum load and deflection at maximum load which both deteriorated by about 20% when impact was changed from middle of roofing product to edge of it. The statistical method used (2 level factorial DOE) was validated using normal residual plots, however, it was found that assumptions of normality were only slightly valid for deflection to maximum load and total energy responses.

It is recommended to prepare and perform the UV weathering tests on actual laboratory prepared samples and analyze the SEM images of UV weathered samples before and after multi-axial impact, Izod impact and other mechanical tests.

It is further recommended to design a 3 level replicated factorial experiment with main effects such as fiber percentages, fiber types, matrix type, coupling agent percentages, impact modifier percentage and UV exposure hours all in three levels with mechanical tests as responses and possibly use fractional factorial design to reduce number of runs to have a more controlled and detailed study of the use of natural fibers plastics composites in construction applications.

It is also recommended to look at the effect of natural fiber plastic composite processing methods such as injection molding, compression molding, extrusion and other processes on final properties of the NFPC.

It is recommended also to perform TGA analysis on natural fiber composites to analyze degradation profile of bagasse fibers compared to oat hull or other fibers. Also it would be helpful to study effect

of compounding variables and fibers on glass transition temperature of the polymer matrix using Differential Scanning Calorimetry.

Finally, it is recommended to analyze the effect of water absorption on impact and other mechanical properties of NFPC due to hydrophilic nature of natural fibers.

6 Bibliography

Abu-Sharkh, B., & Hamid, H. (2004). Degradation study of date palm fibre/polypropylene composites in natural and artificial weathering: Mechanical and thermal analysis. *Polymer Degradation and Stability, 85*(3), 967-973.

Amelinckx, S., van Dyck, D., van Landuyt, J., & van Tendeloo, G. (2008). *Handbook of microscopy, handbook of microscopy: Applications in materials science, solid-state physics, and chemistry. methods II* John Wiley & Sons.

ASTM D1708-13. (2013). ASTM D1708-13, standard test method for tensile properties of plastics by use of microtensile specimens, ASTM international, west conshohocken, PA, 2013, www.astm.org.

ASTM D256-10. (2010). ASTM D256-10, standard test methods for determining the izod pendulum impact resistance of plastics, ASTM international, west conshohocken, PA, 2010, www.astm.org.

ASTM D3763-15. (2015). ASTM D3763-15, standard test method for high speed puncture properties of plastics using load and displacement sensors, ASTM international, west conshohocken, PA, 2015, www.astm.org.

ASTM D5420-10. (2010). ASTM D5420-10, standard test method for impact resistance of flat, rigid plastic specimen by means of a striker impacted by a falling weight (gardner impact), ASTM international, west conshohocken, PA, 2010, www.astm.org.

ASTM D7031-11. (2011). ASTM D7031-11, standard guide for evaluating mechanical and physical properties of wood-plastic composite products, ASTM international, west conshohocken, PA, 2011, www.astm.org.

ASTM D790-10. (2010). ASTM D790-10, standard test methods for flexural properties of unreinforced and reinforced plastics and electrical insulating materials, ASTM international, west conshohocken, PA, 2010, www.astm.org.

ASTM G154-12a. (2012). ASTM G154-12a, standard practice for operating fluorescent ultraviolet (UV) lamp apparatus for exposure of nonmetallic materials, ASTM international, west conshohocken, PA, 2012, www.astm.org.

Biron, M. (2012). *Thermoplastics and thermoplastic composites* William Andrew.

Bledzki, A. K., & Faruk, O. (2004). Wood fiber reinforced polypropylene composites: Compression and injection molding process. *Polymer-Plastics Technology and Engineering, 43*(3), 871-888.

Bledzki, A. K., & Gassan, J. (1999). Composites reinforced with cellulose based fibres. *Progress in Polymer Science, 24*(2), 221-274. doi:http://dx.doi.org/10.1016/S0079-6700(98)00018-5

Bledzki, A., & Faruk, O. (2003). Wood fibre reinforced polypropylene composites: Effect of fibre geometry and coupling agent on physico- mechanical properties. *Applied Composite Materials, 10*(6), 365-379. doi:10.1023/A:1025741100628

Bogoeva- Gaceva, G., Avella, M., Malinconico, M., Buzarovska, A., Grozdanov, A., Gentile, G., & Errico, M. E. (2007). Natural fiber eco- composites. *Polymer Composites, 28*(1), 98-107.

Bryce, D. M. (1999). *Plastic injection molding: Manufacturing startup and management* Society of Manufacturing Engineers.

Clemons, C. M. (2000). Woodfiber-plastic composites in the united States–History and current and future markets. *The Proceedings of the 3rd International Wood and Natural Fibre Composites Symposium; Kassel, Germany,* 1-7.

Clemons, C. (2002). Wood- plastic composites in the united states: The interfacing of two industries. *Forest Products Journal, 52*(6), 10-18.

Faruk, O., Bledzki, A. K., Fink, H., & Sain, M. (2012). Biocomposites reinforced with natural fibers: 2000–2010. *Progress in Polymer Science, 37*(11), 1552-1596.

Giles Jr, H. F., Mount III, E. M., & Wagner Jr, J. R. (2004). *Extrusion: The definitive processing guide and handbook* William Andrew.

Global wood plastic composite (polyethylene, polyvinylchloride, propylene, and others) market - trends & forecasts (2014 - 2019) (2014).

Gras notice 000342: Oat hull fiber. (2010). Retrieved from http://www.fda.gov/ucm/groups/fdagov-public/@fdagov-foods-gen/documents/document/ucm269543.pdf

Hagen, H., Boersma, J., & van Koten, G. (2002). Homogeneous vanadium-based catalysts for the Ziegler–Natta polymerization of α-olefins. *Chemical Society Reviews, 31*(6), 357-364.

Haider, A., & Eder, A. (2010). Markets, applications, and processes for wood polymer composites (WPC) in europe. *Proceedings: 1st International Conference on Processing Technologies for the Forest and Bio-Based Products Industries, Salzburg/Kuchl, Austria,* 146-151.

Herrera-Franco, P., & Valadez-Gonzalez, A. (2005). A study of the mechanical properties of short natural-fiber reinforced composites. *Composites Part B: Engineering, 36*(8), 597-608.

Jacob, A. (2006). WPC industry focuses on performance and cost. *Reinforced Plastics, 50*(5), 32-33.

Joseph, P., Rabello, M. S., Mattoso, L., Joseph, K., & Thomas, S. (2002). Environmental effects on the degradation behaviour of sisal fibre reinforced polypropylene composites. *Composites Science and Technology, 62*(10), 1357-1372.

Jústiz-Smith, N. G., Virgo, G. J., & Buchanan, V. E. (2008). Potential of jamaican banana, coconut coir and bagasse fibres as composite materials. *Materials Characterization, 59*(9), 1273-1278. doi:http://dx.doi.org/10.1016/j.matchar.2007.10.011

Karian, H. (2003). *Handbook of polypropylene and polypropylene composites, revised and expanded* CRC press.

Karnani, R., Krishnan, M., & Narayan, R. (1997). Biofiber- reinforced polypropylene composites. *Polymer Engineering & Science, 37*(2), 476-483.

Klyosov, A. A. (. (2007). *Wood-plastic composites*. Hoboken, N.J.: Wiley-Interscience.

López- Bañuelos, R., Moscoso, F., Ortega- Gudiño, P., Mendizabal, E., Rodrigue, D., & González- Núñez, R. (2012). Rotational molding of polyethylene composites based on agave fibers. *Polymer Engineering & Science, 52*(12), 2489-2497.

Luz, S., Gonçalves, A., & Del'Arco, A. (2007). Mechanical behavior and microstructural analysis of sugarcane bagasse fibers reinforced polypropylene composites. *Composites Part A: Applied Science and Manufacturing, 38*(6), 1455-1461.

Margoto, O. H., Moris, Vírginia A da S., & Paiva, Jane M F de. (2015). MECHANICAL PROPERTIES OF POLYPROPYLENE MATRIX COMPOSITES WITH JUTE FIBER FABRIC. *10th International Conference on Composite Science and Technology ICCST/10,*

Market study: Polypropylene (3rd edition). Retrieved from http://www.ceresana.com/en/market-studies/plastics/polypropylene/

Matsuda, Y., Hara, M., Mano, T., Okamoto, K., & Ishikawa, M. (2005). The effect of the volume fraction of dispersed phase on toughness of injection molded polypropylene blended with SEBS, SEPS, and SEP. *Polymer Engineering and Science, 45*(12), 1630.

Mohanty, A. K., Misra, M., & Drzal, L. T. (2005). *Natural fibers, biopolymers, and biocomposites* CRC Press.

MONTGOMERY, D. (2001). Desing and analysis of experiments.

Moore, E. P. (1996). *Polypropylene handbook* Hanser/Gardner Publications.

Muasher, M., & Sain, M. (2006). The efficacy of photostabilizers on the color change of wood filled plastic composites. *Polymer Degradation and Stability, 91*(5), 1156-1165.

Oats. Encyclopædia britannica. Retrieved from http://www.britannica.com/topic/oats

Park, S. (2013). Renewable thermoplastic composites for environmentally friendly and sustainable applications.

Pereira, P. H. F., Rosa, M. d. F., Cioffi, M. O. H., Benini, Kelly Cristina Coelho de Carvalho, Milanese, A. C., Voorwald, H. J. C., & Mulinari, D. R. (2015). Vegetal fibers in polymeric composites: A review. *Polímeros, 25*(1), 9-22.

Pickering, K. (2008). *Properties and performance of natural-fibre composites* Elsevier.

Pritchard, G. (2004). Two technologies merge: Wood plastic composites. *Reinforced Plastics, 48*(6), 26-29. doi:10.1016/S0034-3617(04)00339-X

Qiu, W., Endo, T., & Hirotsu, T. (2006). Interfacial interaction, morphology, and tensile properties of a composite of highly crystalline cellulose and maleated polypropylene. *Journal of Applied Polymer Science, 102*(4), 3830-3841.

Ramaraj, B. (2007). Mechanical and thermal properties of polypropylene/sugarcane bagasse composites. *Journal of Applied Polymer Science, 103*(6), 3827-3832.

Razi, P., & Raman, A. (2000). Studies on impact fracture properties of wood-polymer composites. *Journal of Composite Materials, 34*(12), 980-997.

Rowell, R. M., Sanadi, A. R., Caulfield, D. F., & Jacobson, R. E. (1997). Utilization of natural fibers in plastic composites: Problems and opportunities. *Lignocellulosic-Plastic Composites,* , 23-51.

Samariha, A., Bastani, A., Nemati, M., Kiaei, M., Nosrati, H., & Farsi, M. (2013). Investigation of the mechanical properties of bagasse flour/polypropylene composites. *Mechanics of Composite Materials, 49*(4), 447-454. doi:10.1007/s11029-013-9361-3

Sasaki, M., Adschiri, T., & Arai, K. (2003). Fractionation of sugarcane bagasse by hydrothermal treatment. *Bioresource Technology, 86*(3), 301-304.

Sharma, R., & Maiti, S. (2015). Effects of crystallinity of polypropylene (PP) on the mechanical properties of PP/styrene-ethylene-butylene-styrene-g-maleic anhydride (SEBS-g-MA)/teak wood flour (TWF) composites. *Polymer Bulletin, 72*(3), 627-643.

Shibata, S., Cao, Y., & Fukumoto, I. (2006). Study of the flexural modulus of natural fiber/polypropylene composites by injection molding. *Journal of Applied Polymer Science, 100*(2), 911-917. doi:10.1002/app.22609

Shimizu, K., & Saito, H. (2009). Orientation of cylindrical microdomains of triblock copolymers by in situ stress–strain- birefringence measurements. *Journal of Polymer Science Part B: Polymer Physics, 47*(7), 715-723.

Stewart, R. (2010). Building on the advantages of composites in construction. *Reinforced Plastics, 54*(5), 20-27.

Sun, J., Sun, X., Zhao, H., & Sun, R. (2004). Isolation and characterization of cellulose from sugarcane bagasse. *Polymer Degradation and Stability, 84*(2), 331-339.

Tjong, S. C., Xu, S., Li, R. K., & Mai, Y. (2002). Mechanical behavior and fracture toughness evaluation of maleic anhydride compatibilized short glass fiber/SEBS/polypropylene hybrid composites. *Composites Science and Technology, 62*(6), 831-840.

Tolinski, M. (2015). *Additives for polyolefins: Getting the most out of polypropylene, polyethylene and TPO* William Andrew.

Trex Company, Inc. (2012). Trex 2012 installation guide. Retrieved from https://www.trex.com/trex/groups/content/@techsvc/documents/document/trex_002278.pdf

Vachon, D. (2002). *Continuous Phase Silicone Blends,*

Verma, D., Gope, P., Maheshwari, M., & Sharma, R. (2012). Bagasse fiber composites-A review. *J.Mater.Environ.Sci, 3*(6), 1079-1092.

Voigt, W., & Todesco, R. (2002). New approaches to the melt stabilization of polyolefins. *Polymer Degradation and Stability, 77*(3), 397-402.

Wambua, P., Ivens, J., & Verpoest, I. (2003). Natural fibres: Can they replace glass in fibre reinforced plastics? *Composites Science and Technology, 63*(9), 1259-1264.

7 Appendix

Table 7-1: DOE (I) Coded Design Matrix with responses

	FIBER	IMA	IMB	C. Agent	IZOD IMPACT STRENGTH (J/M)					
high	BG	5%	5%	4%						
symbol	1	1	1	1						
low	OH	0%	0%	0%						
symbol	-1	-1	-1	-1						
RUN #	A	B	C	D	Rep 1	Rep 2	Rep 3	Rep 4	Rep 5	Rep 6
1	1	1	-1	1	36.6	38.8	37.0	37.0	38.7	39.3
2	1	-1	1	1	39.0	41.5	41.0	43.9	40.8	42.6
3	1	1	1	1	38.1	39.0	41.0	43.9	40.8	42.6
4	1	-1	-1	1	29.7	28.8	28.7	28.3	27.2	27.8
5	1	1	-1	-1	29.1	30.7	31.6	30.3	30.8	34.6
6	1	-1	1	-1	36.6	42.9	37.8	37.3	37.5	39.6
7	1	1	1	-1	35.4	33.8	33.4	34.9	34.2	34.6
8	1	-1	-1	-1	28.9	32.2	30.1	31.0	31.5	26.6
9	-1	1	-1	1	26.6	32.0	29.5	29.8	27.3	27.8
10	-1	-1	1	1	30.3	29.5	31.9	27.9	29.6	29.9
11	-1	1	1	1	27.1	30.5	27.6	29.8	30.8	28.2
12	-1	-1	-1	1	24.8	23.4	23.3	21.8	23.2	24.0
13	-1	1	-1	-1	33.4	32.3	36.3	31.6	34.6	33.8
14	-1	-1	1	-1	39.2	35.4	33.9	36.4	33.9	34.7
15	-1	1	1	-1	37.2	37.2	34.5	37.7	37.5	41.6
16	-1	-1	-1	-1	26.4	27.2	26.0	28.0	27.6	26.8

Table 7-2: DOE (I) Izod Impact Analysis of Variance

Source	Code	DF	Adj SS	Adj MS	F-Value	P-Value
Linear						
FIBER(OH,BG)	A	1	538.22	538.218	192.33	0.00%*
IMA(0%,5%)	B	1	137.55	137.554	49.15	0.00%*
IMB(0%,5%)	C	1	827.33	827.33	295.64	0.00%*
CA(0%,4%)	D	1	25.46	25.46	9.1	0.30%*
2-Way Interactions						
FIBER(OH,BG)*IMA(0%,5%)	AB	1	20.82	20.819	7.44	0.80%*
FIBER(OH,BG)*IMB(0%,5%)	AC	1	28.34	28.342	10.13	0.20%*
FIBER(OH,BG)*CA(0%,4%)	AD	1	520.16	520.159	185.87	0.00%*
IMA(0%,5%)*IMB(0%,5%)	BC	1	259.98	259.976	92.9	0.00%*
IMA(0%,5%)*CA(0%,4%)	BD	1	23.17	23.167	8.28	0.50%*
IMB(0%,5%)*CA(0%,4%)	CD	1	1.02	1.019	0.36	54.80%
3-Way Interactions						
FIBER(OH,BG)*IMA(0%,5%)*IMB(0%,5%)	ABC	1	7.75	7.752	2.77	10.00%
FIBER(OH,BG)*IMA(0%,5%)*CA(0%,4%)	ABD	1	98.13	98.132	35.07	0.00%*
FIBER(OH,BG)*IMB(0%,5%)*CA(0%,4%)	ACD	1	38.87	38.872	13.89	0.00%*
IMA(0%,5%)*IMB(0%,5%)*CA(0%,4%)	BCD	1	15.19	15.189	5.43	2.20%*
4-Way Interactions						
FIBER(OH,BG)*IMA(0%,5%)* IMB(0%,5%)*CA(0%,4%)	ABCD	1	3.54	3.544	1.27	26.40%
Error		80	223.88	2.798		
Total		95	2769.41			

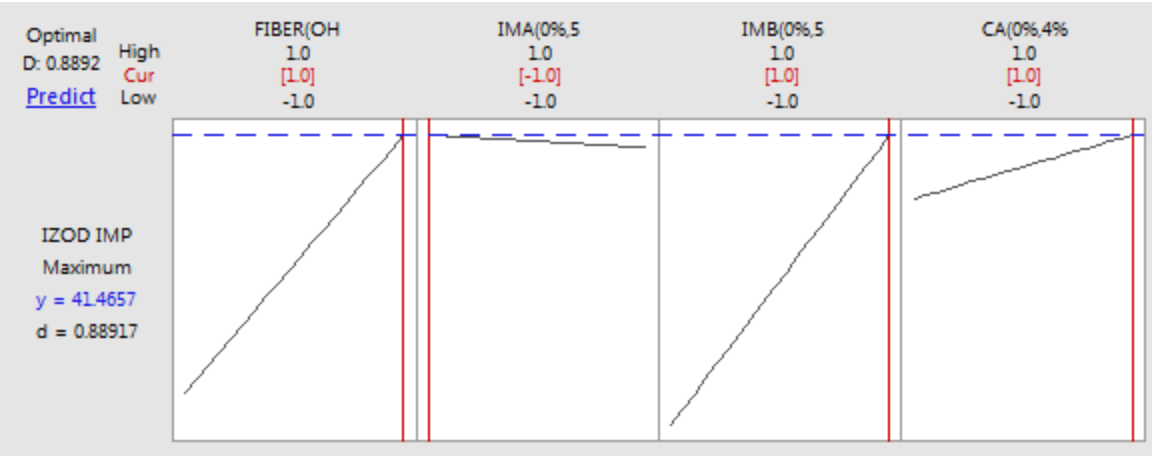

Figure 7-1: DOE (I) Izod Impact optimal point

Table 7-3: DOE (I) Coded Design Matrix with Tensile Strength response

	FIBER	IMA	IMB	CA	TENSILE STRENGTH (MPA)				
high	BG	5%	5%	4%					
symbol	1	1	1	1					
low	OH	0%	0%	0%					
symbol	-1	-1	-1	-1					
RUN	A	B	C	D	Rep 1	Rep 2	Rep 3	Rep 4	Rep 5
1	1	1	-1	1	43.9	39.5	45.6	46.6	44.7
2	1	-1	1	1	46.8	39.5	43.0	44.6	45.9
3	1	1	1	1	46.7	47.9	45.4	46.4	46.2
4	1	-1	-1	1	48.0	46.4	46.4	46.0	47.4
5	1	1	-1	-1	29.7	31.6	31.0	32.5	31.9
6	1	-1	1	-1	28.5	26.1	23.2	26.8	26.4
7	1	1	1	-1	29.6	30.3	29.2	30.4	30.4
8	1	-1	-1	-1	29.8	28.6	31.1	32.1	31.2
9	-1	1	-1	1	37.0	34.5	34.2	37.4	36.4
10	-1	-1	1	1	36.0	37.4	35.9	36.5	37.2
11	-1	1	1	1	34.5	34.5	33.4	34.6	35.8
12	-1	-1	-1	1	33.5	34.1	32.3	40.4	38.8
13	-1	1	-1	-1	26.4	27.3	25.1	26.6	27.4
14	-1	-1	1	-1	27.1	26.4	27.4	27.1	26.3
15	-1	1	1	-1	25.6	25.7	25.4	25.9	26.3
16	-1	-1	-1	-1	29.6	29.7	29.5	27.7	29.6

Table 7-4: DOE (I) Anova for Tensile Strength response

Source	Code	DF	Adj SS	Adj MS	F-Value	P-Value
Linear						
FIBER(OH,BG)	A	1	724.63	724.63	274.33	0.00%*
IMA(0%,5%)	B	1	0.6	0.6	0.23	63.50%
IMB(0%,5%)	C	1	30.8	30.8	11.66	0.10%*
CA(0%,4%)	D	1	2987.28	2987.28	1130.94	0.00%*
2-Way Interactions						
FIBER(OH,BG)*IM	AB	1	31.52	31.52	11.93	0.10%*
FIBER(OH,BG)*IMB	AC	1	1.99	1.99	0.75	38.90%
FIBER(OH,BG)*CA(	AD	1	260.63	260.63	98.67	0.00%*
IMA(0%,5%)*IMB(0	BC	1	19.26	19.26	7.29	0.90%*
IMA(0%,5%)*CA(0%	BD	1	2.86	2.86	1.08	30.20%
IMB(0%,5%)*CA(0%,	CD	1	19.59	19.59	7.42	0.80%*
3-Way Interactions						
FIBER(OH,BG)*IM	ABC	1	24.79	24.79	9.38	0.30%*
FIBER(OH,BG)*IM	ABD	1	13.44	13.44	5.09	2.80%*
FIBER(OH,BG)*IMB	ACD	1	2.29	2.29	0.87	35.50%
IMA(0%,5%)*IMB(0	BCD	1	0.51	0.51	0.19	66.20%
4-Way Interactions						
FIBER(OH,BG)*IM	ABCD	1	11.03	11.03	4.17	4.50%*
Error		64	169.05	2.64		
Total		79	4300.25			

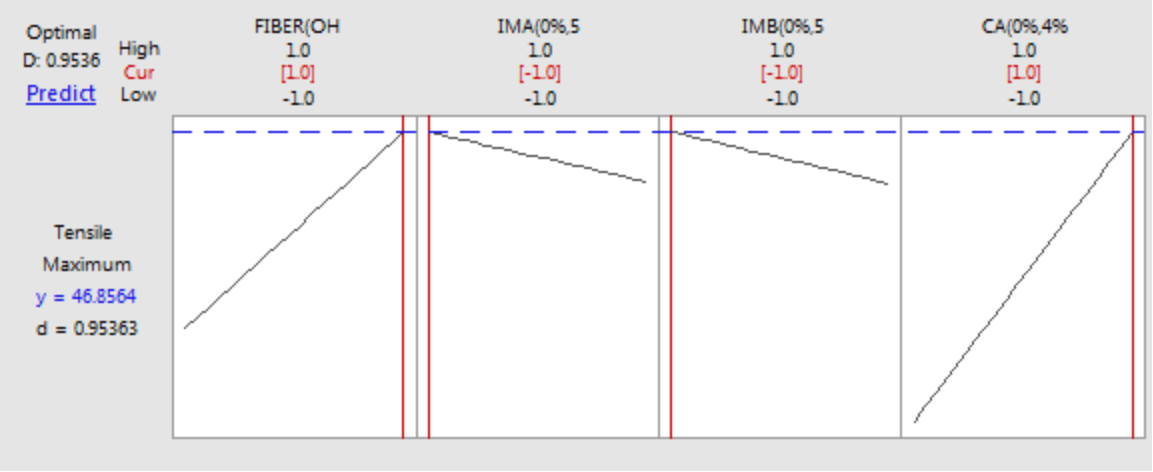

Figure 7-2: DOE (I) Tensile Stregnth Optimal solution plot

Table 7-5: Coded Design Matrix with Flexural Modulus @ 1% responses

	FIBER	IMA	IMB	C.	FLEXURAL MODULUS @1% (MPA)				
high	BG	5%	5%	4%					
symbol	1	1	1	1					
low	OH	0%	0%	0%					
symbol	-1	-1	-1	-1					
RUN	A	B	C	D	Rep 1	Rep 2	Rep 3	Rep 4	Rep 5
1	1	1	-1	1	2571.6	2570.5	2462.9	2474.8	2527.8
2	1	-1	1	1	3046.7	2923.4	2690.5	2850.6	2683.0
3	1	1	1	1	2834.7	2800.9	2645.8	2582.2	2706.0
4	1	-1	-1	1	2655.0	2480.4	2617.6	2514.4	2761.1
5	1	1	-1	-1	2502.2	2469.9	2519.7	2545.5	2521.7
6	1	-1	1	-1	2328.4	2363.6	2287.6	2254.7	2282.9
7	1	1	1	-1	2396.8	2385.4	2338.0	2144.7	2204.4
8	1	-1	-1	-1	2514.6	2539.9	2516.9	2544.3	2350.5
9	-1	1	-1	1	1775.2	1608.9	1726.3	1737.7	1802.6
10	-1	-1	1	1	1784.1	1754.8	1680.0	1769.3	1791.6
11	-1	1	1	1	1705.3	1770.9	1684.4	1569.2	1657.8
12	-1	-1	-1	1	2069.8	2193.8	2166.6	2177.1	2326.0
13	-1	1	-1	-1	1710.9	1640.3	1829.1	1794.1	1920.7
14	-1	-1	1	-1	1737.7	1870.1	1548.4	1756.5	1803.9
15	-1	1	1	-1	1944.2	1845.0	1835.7	1939.7	1928.8
16	-1	-1	-1	-1	2185.8	2212.1	2160.0	1862.3	2017.8

Table 7-6: DOE (I) Anova for Flexural Modulus @ 1%

Source	Co	DF	Adj SS	Adj MS	F-	P-
Linear						
FIBER(OH,BG)	A	1	919187	919187	1018.44	0.00%*
IMA(0%,5%)	B	1	246615	246615	27.32	0.00%*
IMB(0%,5%)	C	1	148872	148872	16.49	0.00%*
CA(0%,4%)	D	1	264086	264086	29.26	0.00%*
2-Way Interactions						
FIBER(OH,BG)*IMA(0%,5%)	AB	1	74444	74444	8.25	0.60%*
FIBER(OH,BG)*IMB(0%,5%)	AC	1	164604	164604	18.24	0.00%*
FIBER(OH,BG)*CA(0%,4%)	AD	1	477362	477362	52.89	0.00%*
IMA(0%,5%)*IMB(0%,5%)	BC	1	186800	186800	20.7	0.00%*
IMA(0%,5%)*CA(0%,4%)	BD	1	112437	112437	12.46	0.10%*
IMB(0%,5%)*CA(0%,4%)	CD	1	103184	103184	11.43	0.10%*
3-Way Interactions						
FIBER(OH,BG)*IMA(0%,5%)*IMB(0%,5%)	ABC	1	259294	259294	28.73	0.00%*
FIBER(OH,BG)*IMA(0%,5%)*CA(0%,4%)	ABD	1	8369	8369	0.93	33.90%
FIBER(OH,BG)*IMB(0%,5%)*CA(0%,4%)	ACD	1	372599	372599	41.28	0.00%*
IMA(0%,5%)*IMB(0%,5%)*CA(0%,4%)	BCD	1	3031	3031	0.34	56.40%
4-Way Interactions						
FIBER(OH,BG)*IMA(0%,5%)*IMB(0%,5%)*CA(0%,4%)	ABCD	1	1677	1677	0.19	66.80%
Error		64	577626	9025		
Total		79	121928			

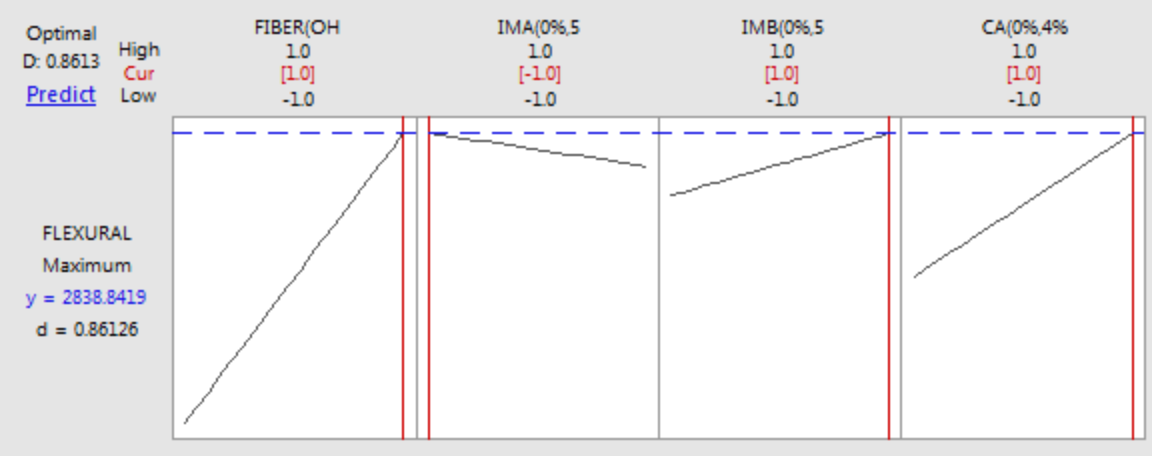

Figure 7-3: DOE (I) Optimal solution for Flexural Modulus @ 1%

Table 7-7: DOE (I) Coded Design Matrix with Mean Failure Energy responses

	FIBER	IMA	IMB	C. Agent	Mean Failure Energy (J)
high	BAGASSE	5%	5%	4%	
symbol	1	1	1	1	
low	OATHULL	0%	0%	0%	
symbol	-1	-1	-1	-1	
RUN #	A	B	C	D	
1	1	1	-1	1	0.97
2	1	-1	1	1	0.99
3	1	1	1	1	1.15
4	1	-1	-1	1	0.67
5	1	1	-1	-1	0.82
6	1	-1	1	-1	1.10
7	1	1	1	-1	0.90
8	1	-1	-1	-1	0.67
9	-1	1	-1	1	0.70
10	-1	-1	1	1	0.73
11	-1	1	1	1	0.68
12	-1	-1	-1	1	0.53
13	-1	1	-1	-1	1.02
14	-1	-1	1	-1	1.00
15	-1	1	1	-1	0.95
16	-1	-1	-1	-1	0.62

Table 7-8: DOE (I) Anova with zero degrees of freedom for Mean Failure Energy responses

Source	DF	Adj SS	Adj MS	F-	P-
Model	15	0.5288	0.0352	*	*
Linear	4	0.2783	0.0695	*	*
A - FIBER(OH,BG)	1	0.0645	0.0645	*	*
B - IMA(0%,5%)	1	0.0500	0.0500	*	*
C - IMB(0%,5%)	1	0.1381	0.1381	*	*
D - CA(0%,4%)	1	0.0255	0.0255	*	*
2-Way Interactions	6	0.2017	0.0336	*	*
A x B - FIBER(OH,BG)*IMA(0%,5%)	1	0.0001	0.0001	*	*
A x C - FIBER(OH,BG)*IMB(0%,5%)	1	0.0162	0.0162	*	*
A x D - FIBER(OH,BG)*CA(0%,4%)	1	0.0956	0.0956	*	*
B x C - IMA(0%,5%)*IMB(0%,5%)	1	0.0836	0.0836	*	*
B x D - IMA(0%,5%)*CA(0%,4%)	1	0.0047	0.0047	*	*
C x D - IMB(0%,5%)*CA(0%,4%)	1	0.0012	0.0012	*	*
3-Way Interactions	4	0.0487	0.0121	*	*
A x B x C -	1	0.0021	0.0021	*	*
A x B x D -	1	0.0339	0.0339	*	*
A x C x D -	1	0.0006	0.0006	*	*
B x C x D -	1	0.0119	0.0119	*	*
4-Way Interactions	1	0.0000	0.0000	*	*
A x B x C x D -	1	0.0000	0.0000	*	*
Error	0	*	*		
Total	15	0.5288			

Table 7-9: DOE (I) Anova with one degree of freedom for error term of Mean Failure Energy responses

Source	D	Adj SS	Adj MS	F-Value	P-value
Linear					
A - FIBER(OH,BG)	1	0.06455	0.06455	5468.77	0.9%*
B - IMA(0%,5%)	1	0.05000	0.05000	4235.72	1%*
C - IMB(0%,5%)	1	0.13817	0.13817	11704.8	0.6%*
D - CA(0%,4%)	1	0.02557	0.02557	2166.69	1.4%*
2-Way Interactions					
A x B - FIBER(OH,BG)*IMA(0%,5%)	1	0.00019	0.00019	16.33	15.40%
A x C - FIBER(OH,BG)*IMB(0%,5%)	1	0.01622	0.01622	1374.39	1.7%*
A x D - FIBER(OH,BG)*CA(0%,4%)	1	0.09563	0.09563	8100.75	0.7%*
B x C - IMA(0%,5%)*IMB(0%,5%)	1	0.08369	0.08369	7089.58	0.8%*
B x D - IMA(0%,5%)*CA(0%,4%)	1	0.00479	0.00479	406.04	3.2%*
C x D - IMB(0%,5%)*CA(0%,4%)	1	0.00126	0.00126	106.79	6.10%
3-Way Interactions					
A x B x C -	1	0.00214	0.00214	181.96	4.7%*
A x B x D -	1	0.03399	0.03399	2880	1.2%*
A x C x D -	1	0.00061	0.00061	52.38	8.70%
B x C x D -	1	0.01197	0.01197	1014.48	2%*
Error	1	0.00001	0.00001		
Total	15	0.52886			

Table 7-10: DOE (I) Anova with 2 degrees of freedom for error term of Mean Failure Energy responses

Source	DF	Adj SS	Adj MS	F-Value	P-Value
Linear					
A - FIBER(OH,BG)	1	0.064559	0.064559	204.89	0.5%*
B - IMA(0%,5%)	1	0.050003	0.050003	158.69	0.6%*
C - IMB(0%,5%)	1	0.138176	0.138176	438.52	0.2%*
D - CA(0%,4%)	1	0.025578	0.025578	81.18	1.2%*
2-Way Interactions					
A x B - FIBER(OH,BG)*IMA(0%,5%)	1	0.000193	0.000193	0.61	51.60%
A x C - FIBER(OH,BG)*IMB(0%,5%)	1	0.016225	0.016225	51.49	1.9%*
A x D - FIBER(OH,BG)*CA(0%,4%)	1	0.09563	0.09563	303.49	0.3%*
B x C - IMA(0%,5%)*IMB(0%,5%)	1	0.083693	0.083693	265.61	0.4%*
B x D - IMA(0%,5%)*CA(0%,4%)	1	0.004793	0.004793	15.21	6%*
C x D - IMB(0%,5%)*CA(0%,4%)	1	0.001261	0.001261	4	18.30%
3-Way Interactions					
A x B x C -	1	0.002148	0.002148	6.82	12.10%
A x B x D -	1	0.033999	0.033999	107.9	0.9%*
B x C x D -	1	0.011976	0.011976	38.01	2.5%*
Error	2	0.00063	0.000315		
Total	15	0.528865			

Table 7-11: DOE (I) Anova with 3 degrees of freedom for error term of Mean Failure Energy responses

Source	DF	Adj SS	Adj MS	F-Value	P-Value
Linear					
A - FIBER(OH,BG)	1	0.06455	0.06455	69.71	0.4%*
B - IMA(0%,5%)	1	0.05000	0.05000	53.99	0.5%*
C - IMB(0%,5%)	1	0.13817	0.13817	149.2	0.1%*
D - CA(0%,4%)	1	0.02557	0.02557	27.62	1.3%*
2-Way Interactions					
A x B - FIBER(OH,BG)*IMA(0%,5%)	1	0.00019	0.00019	0.21	67.90%
A x C - FIBER(OH,BG)*IMB(0%,5%)	1	0.01622	0.01622	17.52	2.5%*
A x D - FIBER(OH,BG)*CA(0%,4%)	1	0.09563	0.09563	103.26	0.2%*
B x C - IMA(0%,5%)*IMB(0%,5%)	1	0.08369	0.08369	90.37	0.2%*
B x D - IMA(0%,5%)*CA(0%,4%)	1	0.00479	0.00479	5.18	10.70%
C x D - IMB(0%,5%)*CA(0%,4%)	1	0.00126	0.00126	1.36	32.80%
3-Way Interactions					
A x B x D -	1	0.03399	0.03399	36.71	0.9%*
B x C x D -	1	0.01197	0.01197	12.93	3.7%*
Error	3	0.00277	0.00092		
Total	15	0.52886			

Table 7-12: DOE (I) Anova with 6 degrees of freedom for error term of Mean Failure Energy responses

Source	D	Adj SS	Adj MS	F-Value	P-Value
Linear					
A - FIBER(OH,BG)	1	0.06455	0.06455	42.92	0.1%*
B - IMA(0%,5%)	1	0.05000	0.05000	33.24	0.1%*
C - IMB(0%,5%)	1	0.13817	0.13817	91.86	0%*
D - CA(0%,4%)	1	0.02557	0.02557	17	0.6%*
2-Way Interactions					
A x C - FIBER(OH,BG)*IMB(0%,5%)	1	0.01622	0.01622	10.79	1.7%*
A x D - FIBER(OH,BG)*CA(0%,4%)	1	0.09563	0.09563	63.58	0%*
B x C - IMA(0%,5%)*IMB(0%,5%)	1	0.08369	0.08369	55.64	0%*
3-Way Interactions					
A x B x D -	1	0.03399	0.03399	22.6	0.3%*
B x C x D -	1	0.01197	0.01197	7.96	3%*
Error	6	0.00902	0.00150		
Total	15	0.52886			

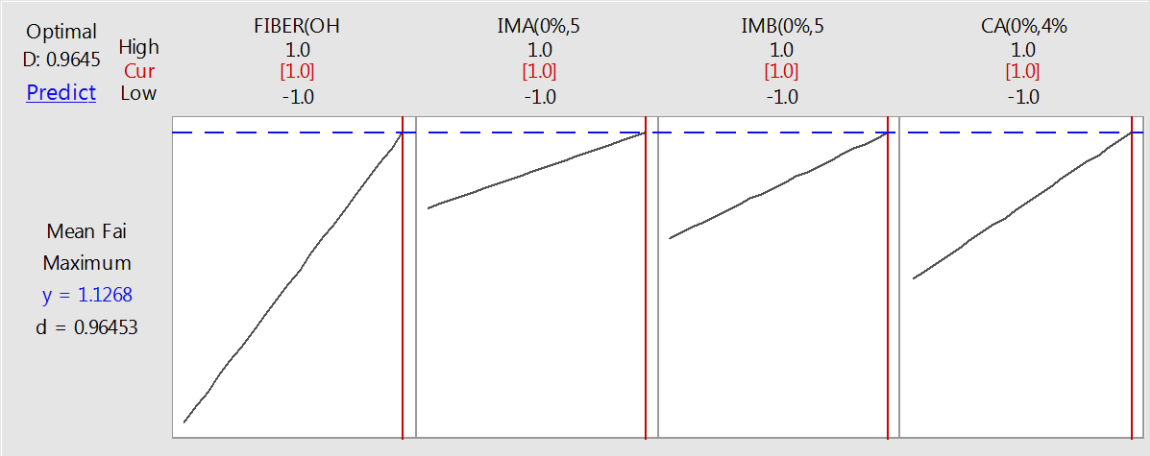

Figure 7-4: DOE (I) Optimum solution for mean failure energy

Table 7-13: DOE (II) Coded Design Matrix with Izod Impact responses

	PP grade	IMA	IMB	C. Agent	IZOD IMPACT STRENGTH (J/M)					
high	Polynar	5%	5%	4%						
symb	1	1	1	1						
low	Braskem	0%	0%	0%						
symb	-1	-1	-1	-1						
RUN	A	B	C	D	Rep 1	Rep 2	Rep 3	Rep 4	Rep 5	Rep 6
1	-1	1	-1	1	36.6	38.8	37.0	37.0	38.7	39.3
2	-1	-1	1	1	39.0	41.5	41.0	43.9	40.8	42.6
3	-1	1	1	1	38.1	39.0	41.0	43.9	40.8	42.6
4	-1	-1	-1	1	29.7	28.8	28.7	28.3	27.2	27.8
5	-1	1	-1	-1	29.1	30.7	31.6	30.3	30.8	34.5
6	-1	-1	1	-1	36.6	42.9	37.8	37.3	37.5	39.6
7	-1	1	1	-1	35.4	33.8	33.4	34.9	34.1	34.6
8	-1	-1	-1	-1	28.9	32.2	30.1	30.9	31.5	26.6
9	1	1	-1	1	39.8	39.7	38.0	40.1	36.7	39.2
10	1	-1	1	1	38.8	39.8	41.4	40.3	40.8	39.5
11	1	1	1	1	42.9	41.1	40.3	38.4	41.2	41.6
12	1	-1	-1	1	31.7	30.7	28.5	27.0	29.6	28.2
13	1	1	-1	-1	36.8	36.1	32.7	38.4	34.0	33.0
14	1	-1	1	-1	34.7	34.0	34.2	33.0	34.6	40.6
15	1	1	1	-1	37.1	37.1	35.7	40.8	32.8	40.8
16	1	-1	-1	-1	26.6	28.9	29.6	27.1	38.2	28.7

Table 7-14: DOE (II) Anova for Izod Impact Strength

Source	DF	Adj SS	Adj MS	F-Value	P-Value
Linear					
PP(BRSK,PLYNR)	1	4.71	4.713	1.16	29%
IMA(0%,5%)	1	152.29	152.29	37.51	0% *
IMB(0%,5%)	1	630.53	630.52	155.3	0% *
CA(0%,4%)	1	226.87	226.87	55.88	0% *
2-Way Interactions					
PP(BRSK,PLYNR)*IMA(0%,5%)	1	60.07	60.074	14.8	0% *
PP(BRSK,PLYNR)*IMB(0%,5%)	1	27.67	27.67	6.82	1.1% *
PP(BRSK,PLYNR)*CA(0%,4%)	1	0.34	0.343	0.08	77%
IMA(0%,5%)*IMB(0%,5%)	1	200.54	200.54	49.39	0% *
IMA(0%,5%)*CA(0%,4%)	1	65.7	65.698	16.18	0% *
IMB(0%,5%)*CA(0%,4%)	1	42.55	42.555	10.48	0.2% *
3-Way Interactions					
PP(BRSK,PLYNR)*IMA(0%,5%)*IMB(0%,5%)	1	1.14	1.143	0.28	60%
PP(BRSK,PLYNR)*IMA(0%,5%)*CA(0%,4%)	1	37.32	37.315	9.19	0.4% *
PP(BRSK,PLYNR)*IMB(0%,5%)*CA(0%,4%)	1	3.73	3.726	0.92	34%
IMA(0%,5%)*IMB(0%,5%)*CA(0%,4%)	1	43.82	43.815	10.79	0.2% *
4-Way Interactions					
PP(BRSK,PLYNR)*IMA(0%,5%)*IMB(0%,5%)*CA(0%,4%)	1	0	0.001	0	99%
Error	64	259.84	4.06		
Total	79	1757.1			

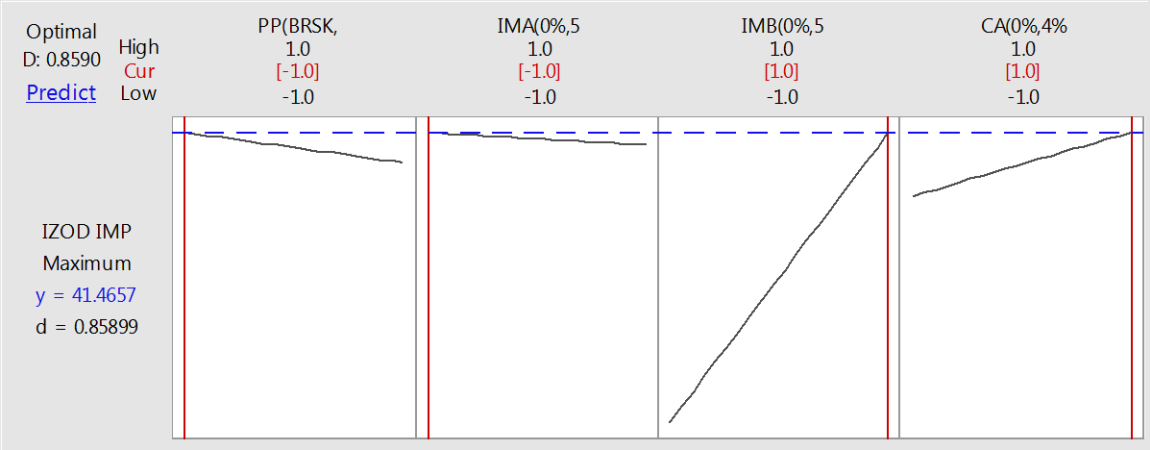

Figure 7-5: DOE (II) Optimum solution for Izod Impact Stregth

Table 7-15: DOE (II) Coded Design Matrix of Tensile Strength response

	PP grade	IMA	IMB	C. Agent	TENSILE STRENGTH (MPA)				
high	Polynar	5%	5%	4%					
symbol	1	1	1	1					
low	Braskem	0%	0%	0%					
symbol	-1	-1	-1	-1					
RUN #	A	B	C	D	Rep 1	Rep	Rep	Rep	Rep
1	1	1	-1	1	43.9	39.5	45.6	46.6	44.7
2	1	-1	1	1	46.8	39.5	43.0	44.6	45.9
3	1	1	1	1	46.7	47.9	45.4	46.4	46.2
4	1	-1	-1	1	48.0	46.4	46.4	46.0	47.4
5	1	1	-1	-1	29.7	31.6	31.0	32.5	31.9
6	1	-1	1	-1	28.5	26.1	23.2	26.8	26.4
7	1	1	1	-1	29.6	30.3	29.2	30.4	30.4
8	1	-1	-1	-1	29.8	28.6	31.1	32.1	31.2
9	-1	1	-1	1	27.2	35.0	36.6	29.6	32.3
10	-1	-1	1	1	29.0	21.7	35.7	31.3	23.9
11	-1	1	1	1	30.2	29.5	33.4	35.4	25.7
12	-1	-1	-1	1	30.0	33.2	35.9	24.5	29.1
13	-1	1	-1	-1	25.9	17.9	23.5	24.2	28.6
14	-1	-1	1	-1	1.2	21.9	19.5	23.0	3.7
15	-1	1	1	-1	18.6	26.4	23.7	22.6	22.5
16	-1	-1	-1	-1	16.0	26.5	21.3	22.6	23.7

Table 7-16: DOE (II) Anova for Izod Impact Strength

Source	DF	Adj SS	Adj MS	F-Value	P-Value
Linear					
A - PP(BRSK,PLYNR)	1	2816.4	2816.4	177.99	0% *
B - IMA(0%,5%)	1	117.23	117.23	7.41	0.8%
C - IMB(0%,5%)	1	114.67	114.67	7.25	0.9%
D - CA(0%,4%)	1	3287.4	3287.4	207.76	0% *
2-Way Interactions					
A x B - PP(BRSK,PLYNR)*IMA(0%,5%)	1	35.86	35.86	2.27	13.70
A x C - PP(BRSK,PLYNR)*IMB(0%,5%)	1	14.05	14.05	0.89	35.00
A x D - PP(BRSK,PLYNR)*CA(0%,4%)	1	181.28	181.28	11.46	0.1%
B X C - IMA(0%,5%)*IMB(0%,5%)	1	82.06	82.06	5.19	2.6%
B x D - IMA(0%,5%)*CA(0%,4%)	1	41.5	41.5	2.62	11.00
C x D - IMB(0%,5%)*CA(0%,4%)	1	39.17	39.17	2.48	12.10
3-Way Interactions					
A x B x C -	1	0.1	0.1	0.01	93.80
A x B x D -	1	1.18	1.18	0.07	78.60
A x C x D -	1	0.1	0.1	0.01	93.60
B x C x D -	1	3.95	3.95	0.25	61.90
4-Way Interactions					
A x B x C x D -	1	21.11	21.11	1.33	25.20
Error	64	1012.7	15.82		
Total	79	7768.8			

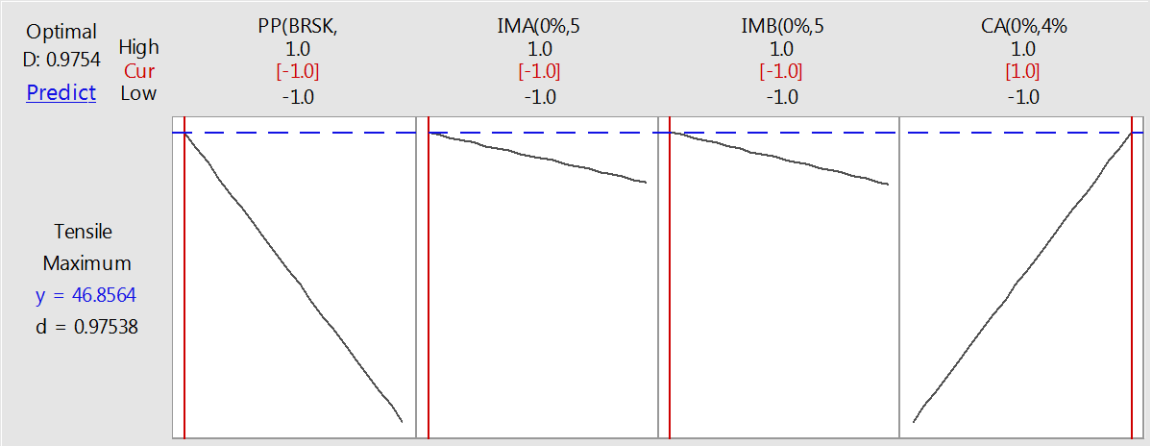

Figure 7-6: DOE (II) Optimum solution for Tensile Strength

Table 7-17: DOE (II) Coded Design Matrix with Flexural Modulus at 1% responses

	PP grade	IMA	IMB	C. Agent	FLEXURAL MODULUS @1% (MPA)				
high	Polynar	5%	5%	4%					
symbol	1	1	1	1					
low	Braskem	0%	0%	0%					
symbol	-1	-1	-1	-1					
RUN	A	B	C	D	Rep 1	Rep 2	Rep 3	Rep 4	Rep 5
1	1	1	-1	1	2571.6	2570.5	2462.9	2474.8	2527.8
2	1	-1	1	1	3046.7	2923.4	2690.5	2850.6	2683.0
3	1	1	1	1	2834.7	2800.9	2645.8	2582.2	2706.0
4	1	-1	-1	1	2655.0	2480.4	2617.6	2514.4	2761.1
5	1	1	-1	-1	2502.2	2469.9	2519.7	2545.5	2521.7
6	1	-1	1	-1	2328.4	2363.6	2287.6	2254.7	2282.9
7	1	1	1	-1	2396.8	2385.4	2338.0	2144.7	2204.4
8	1	-1	-1	-1	2514.6	2539.9	2516.9	2544.3	2350.5
9	-1	1	-1	1	2690.8	2546.6	2447.2	2478.8	2531.3
10	-1	-1	1	1	2388.9	2582.1	2514.2	2395.8	2356.7
11	-1	1	1	1	2689.3	2493.1	2635.9	2703.1	2619.2
12	-1	-1	-1	1	2744.0	2430.8	2859.4	2833.2	3043.4
13	-1	1	-1	-1	2295.5	2285.3	2299.6	2325.9	2173.8
14	-1	-1	1	-1	2381.1	2349.5	2362.5	2325.8	2283.8
15	-1	1	1	-1	2365.2	2379.4	2384.0	2303.0	2322.5
16	-1	-1	-1	-1	2610.8	2737.3	2443.8	2351.0	2516.0

Table 7-18: DOE (II) Analysis of Variance for Flexural Modulus at 1%

Source	DF	Adj SS	Adj MS	F-Value	P-Value
Linear					
A - PP(BRSK,PLYNR)	1	46668	46668	4.23	4.4% *
B - IMA(0%,5%)	1	80730	80730	7.32	0.9% *
C - IMB(0%,5%)	1	37005	37005	3.36	7.2%
CA(0%,4%)	1	121920	121920	110.57	0% *
2-Way Interactions					
A x B - PP(BRSK,PLYNR)*IMA(0%,5%)	1	3645	3645	0.33	56.7%
A x C - PP(BRSK,PLYNR)*IMB(0%,5%)	1	45046	45046	4.09	4.7% *
A x D - PP(BRSK,PLYNR)*CA(0%,4%)	1	10127	10127	0.92	34.1%
B x C - IMA(0%,5%)*IMB(0%,5%)	1	120503	120503	10.93	0.2% *
B x D - IMA(0%,5%)*CA(0%,4%)	1	389	389	0.04	85.2%
C x D - IMB(0%,5%)*CA(0%,4%)	1	154975	154975	14.06	0% *
3-Way Interactions					
A x B x C -	1	179896	179896	16.32	0% *
A x B x D -	1	50224	50224	4.56	3.7% *
A x C x D -	1	289405	289405	26.25	0% *
B x C x D -	1	6584	6584	0.6	44.3%
4-Way Interactions					
A x B x C x D -	1	9074	9074	0.82	36.8%
Error	64	705666	11026		
Total	79	295913			

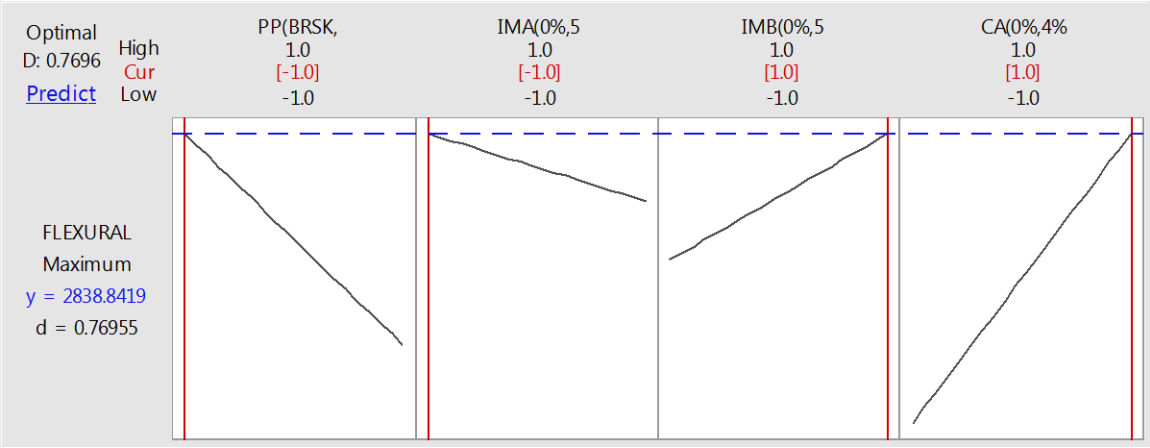

Figure 7-7: DOE (II) Optimum solution for flexural modulus at 1%

Table 7-19: DOE (II) Coded Design Matrix of Mean failure energy

	PP grade	IMA	IMB	C. Agent	Mean Failure Energy (J)
high	Polynar	5%	5%	4%	
symbol	1	1	1	1	
low	Braskem	0%	0%	0%	
symbol	-1	-1	-1	-1	
RUN #	A	B	C	D	
1	1	1	-1	1	0.97
2	1	-1	1	1	0.99
3	1	1	1	1	1.15
4	1	-1	-1	1	0.67
5	1	1	-1	-1	0.82
6	1	-1	1	-1	1.10
7	1	1	1	-1	0.90
8	1	-1	-1	-1	0.67
9	-1	1	-1	1	0.75
10	-1	-1	1	1	0.95
11	-1	1	1	1	0.92
12	-1	-1	-1	1	0.56
13	-1	1	-1	-1	0.79
14	-1	-1	1	-1	0.78
15	-1	1	1	-1	0.80
16	-1	-1	-1	-1	0.55

Table 7-20: DOE (II) Anova with zero degree of freedom for error term for Mean failure energy

Source	DF	Adj SS	Adj MS	F-Value	P-Value
Linear					
A - PP(BRSK,PLYNR)	1	0.0020	0.0020	*	*
B - IMA(0%,5%)	1	0.0067	0.0067	*	*
C - IMB(0%,5%)	1	0.0905	0.0905	*	*
D - CA(0%,4%)	1	0.0693	0.0693	*	*
2-Way Interactions					
A X B - PP(BRSK,PLYNR)*IMA(0%,5%)	1	0.0000	0.0000	*	*
A X C - PP(BRSK,PLYNR)*IMB(0%,5%)	1	0.0039	0.0039	*	*
A X D - PP(BRSK,PLYNR)*CA(0%,4%)	1	0.0106	0.0106	*	*
B X C - IMA(0%,5%)*IMB(0%,5%)	1	0.0165	0.0165	*	*
B X D - IMA(0%,5%)*CA(0%,4%)	1	0.0040	0.0040	*	*
C X D - IMB(0%,5%)*CA(0%,4%)	1	0.0685	0.0685	*	*
3-Way Interactions					
A X B X C -	1	0.0285	0.0285	*	*
A X B X D -	1	0.0125	0.0125	*	*
A X C X D -	1	0.0005	0.0005	*	*
B X C X D -	1	0.0011	0.0011	*	*
4-Way Interactions					
A X B X C X D -	1	0.1413	0.1413	*	*
Error	0	*	*		
Total	15	0.4565			

Table 7-21: DOE (II) Anova with one degree of freedom for error term for Mean failure energy

Source	DF	Adj SS	Adj MS	F-Value	P-Value
Linear					
A - PP(BRSK,PLYNR)	1	0.00206	0.00206	0.01	92%
B - IMA(0%,5%)	1	0.00678	0.00678	0.05	86%
C - IMB(0%,5%)	1	0.09054	0.09054	0.64	57%
D - CA(0%,4%)	1	0.06933	0.06933	0.49	61%
2-Way Interactions					
A X B - PP(BRSK,PLYNR)*IMA(0%,5%)	1	0.00001	0.00001	0	99%
A X C - PP(BRSK,PLYNR)*IMB(0%,5%)	1	0.00394	0.00394	0.03	90%
A X D - PP(BRSK,PLYNR)*CA(0%,4%)	1	0.01069	0.01069	0.08	83%
B X C - IMA(0%,5%)*IMB(0%,5%)	1	0.01651	0.01651	0.12	79%
B X D - IMA(0%,5%)*CA(0%,4%)	1	0.00404	0.00404	0.03	89%
C X D - IMB(0%,5%)*CA(0%,4%)	1	0.06850	0.06850	0.48	61%
3-Way Interactions					
A X B X C -	1	0.02852	0.02852	0.2	73%
A X B X D -	1	0.01257	0.01257	0.09	82%
A X B X D -	1	0.00057	0.00057	0	96%
B X C X D -	1	0.00110	0.00110	0.01	94%
Error	1	0.14130	0.14130		
Total	15	0.45652			

Table 7-22: DOE (II) Anova with 5 degrees of freedom for error term for Mean failure energy

Source	DF	Adj SS	Adj MS	F-Value	P-Value
Linear					
PP(BRSK,PLYNR)	1	0.002063	0.002063	0.06	82%
IMA(0%,5%)	1	0.006782	0.006782	0.18	69%
IMB(0%,5%)	1	0.090548	0.090548	2.46	18%
CA(0%,4%)	1	0.069334	0.069334	1.88	23%
2-Way Interactions					
PP(BRSK,PLYNR)*IMA(0%,5%)	1	0.000012	0.000012	0	99%
PP(BRSK,PLYNR)*IMB(0%,5%)	1	0.003948	0.003948	0.11	76%
PP(BRSK,PLYNR)*CA(0%,4%)	1	0.01069	0.01069	0.29	61%
IMA(0%,5%)*IMB(0%,5%)	1	0.016515	0.016515	0.45	53%
IMA(0%,5%)*CA(0%,4%)	1	0.004049	0.004049	0.11	75%
IMB(0%,5%)*CA(0%,4%)	1	0.068502	0.068502	1.86	23%
Error	5	0.184085	0.036817		
Total	15	0.456529			

Table 7-23: DOE (II) Anova with 11 degrees of freedom for error term for Mean failure energy

Source	DF	Adj SS	Adj MS	F-Value	P-Value
Model	4	0.168726	0.042182	1.61	24%
Linear	4	0.168726	0.042182	1.61	24%
A - PP(BRSK,PLYNR)	1	0.002063	0.002063	0.08	78%
B - IMA(0%,5%)	1	0.006782	0.006782	0.26	62%
C - IMB(0%,5%)	1	0.090548	0.090548	3.46	9% *
D - CA(0%,4%)	1	0.069334	0.069334	2.65	13.2% *
Error	11	0.287802	0.026164		
Total	15	0.456529			

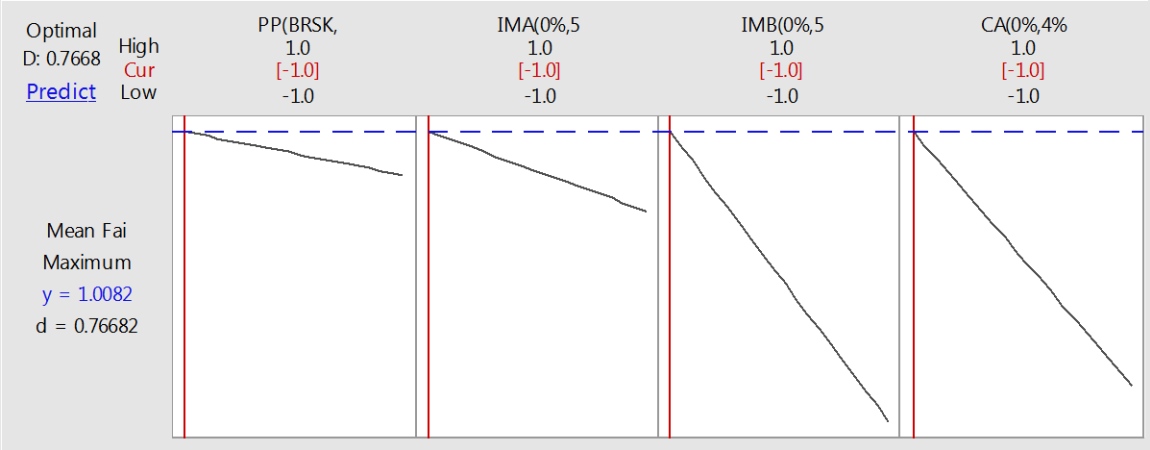

Figure 7-8: DOE (II) Optimum solution for Mean failure energy

Table 7-24: DOE (III) Coded Design Matrix with izod impact responses

	Bagasse	PP grade	IMA	IMB	IZOD IMPACT STRENGTH (J/M)					
high	40%	Polynar	5%	5%						
symbo	1	1	1	1						
low	0%	Braskem	0%	0%						
symbo	-1	-1	-1	-1						
Form.	A	B	C	D	Rep 1	Rep 2	Rep 3	Rep 4	Rep 5	Rep 6
1	-1	-1	-1	-1	19.5	18.5	21.8	20.5	17.5	21.9
2	-1	-1	1	-1	21.6	23.6	18.6	24.5	18.6	19.4
3	-1	-1	-1	1	21.6	19.1	24.7	20.9	22.5	22.6
4	-1	-1	1	1	30.8	23.0	21.6	22.5	22.9	23.7
5	1	-1	1	-1	29.1	30.7	31.6	30.3	30.8	34.5
6	1	-1	-1	1	36.6	42.9	37.8	37.3	37.5	39.6
7	1	-1	1	1	35.4	33.8	33.4	34.9	34.1	34.6
8	1	-1	-1	-1	28.9	32.2	30.1	30.9	31.5	26.6
9	-1	1	-1	-1	27.5	23.8	24.7	22.8	23.6	23.6
10	-1	1	1	-1	24.4	20.4	27.8	29.6	29.0	29.1
11	-1	1	-1	1	47.9	51.8	39.2	41.5	41.8	42.3
12	-1	1	1	1	38.4	37.1	43.6	45.7	40.6	36.8
13	1	1	1	-1	36.8	36.1	32.7	38.4	34.0	33.0
14	1	1	-1	1	34.7	34.0	34.2	33.0	34.6	40.6
15	1	1	1	1	37.1	37.1	35.7	40.8	32.8	40.8
16	1	1	-1	-1	26.6	28.9	29.6	27.1	38.2	28.7

Table 7-25: DOE (III) Anova izod impact

Source	DF	Adj SS	Adj MS	F-Value	P-Value
Linear					
A - BG(0%,40%)	1	907.8	907.8	111.61	0% *
B - PP(BRSK,PLYNR)	1	1010.3	1010.3	124.23	0% *
C - IMA(0%,5%)	1	15.18	15.18	1.87	17.6%
D - IMB(0%,5%)	1	1250.5	1250.5	153.75	0% *
2-Way Interactions					
A x B - BG(0%,40%)*PP(BRSK,PLYNR)	1	765.32	765.32	94.1	0% *
A x C - BG(0%,40%)*IMA(0%,5%)	1	2.25	2.25	0.28	60.0%
A x D - BG(0%,40%)*IMB(0%,5%)	1	137.18	137.18	16.87	0% *
B x C - PP(BRSK,PLYNR)*IMA(0%,5%)	1	13.32	13.32	1.64	20.4%
B x D - PP(BRSK,PLYNR)*IMB(0%,5%)	1	219.09	219.09	26.94	0% *
C x D - IMA(0%,5%)*IMB(0%,5%)	1	67.94	67.94	8.35	0.5%
3-Way Interactions					
A x B x C -	1	86.49	86.49	10.63	0.2%
A x B x D -	1	400.53	400.53	49.25	0% *
A x C x D -	1	4.43	4.43	0.54	46.3%
B x C x D -	1	9.1	9.1	1.12	29.3%
4-Way Interactions					
A x B x C x D -	1	33.6	33.6	4.13	4.5%
Error	80	650.67	8.13		
Total	95	5573.7			

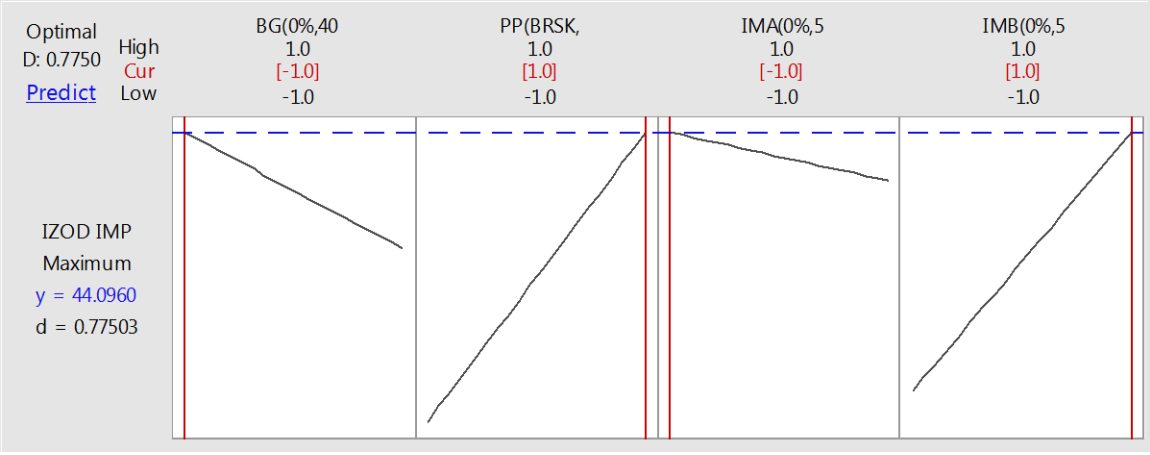

Figure 7-9: DOE (III) Optimum solution for Izod impact Strength

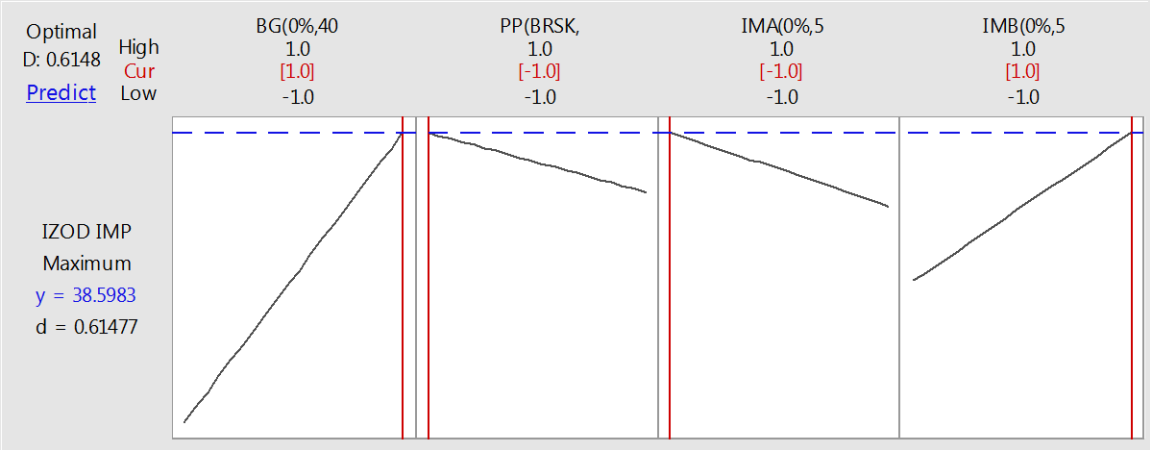

Figure 7-10: DOE (III) Optimum solution for Izod Impact Strength

Table 7-26: DOE (III) Coded Design Matrix with Tensile responses

	Bagasse	PP grade	IMA	IMB	TENSILE STRENGTH (MPA)				
high	40%	Polynar	5%	5%					
symbol	1	1	1	1					
low	0%	Braskem	0%	0%					
symbol	-1	-1	-1	-1					
RUN	A	B	C	D	Rep 1	Rep	Rep	Rep	Rep
1	1	1	-1	1	39.1	38.8	39.8	41.8	41.1
2	1	-1	1	1	34.2	33.0	32.1	34.3	36.6
3	1	1	1	1	37.8	38.0	38.3	28.7	28.5
4	1	-1	-1	1	34.4	35.4	33.0	35.0	32.2
5	1	1	-1	-1	29.7	31.6	31.0	32.5	31.9
6	1	-1	1	-1	28.5	26.1	23.2	26.8	26.4
7	1	1	1	-1	29.6	30.3	29.2	30.4	30.4
8	1	-1	-1	-1	29.8	28.6	31.1	32.1	31.2
9	-1	1	-1	1	39.6	41.8	38.7	38.5	36.5
10	-1	-1	1	1	32.4	34.0	32.4	32.6	33.6
11	-1	1	1	1	32.2	30.8	31.9	32.7	34.2
12	-1	-1	-1	1	33.0	31.9	31.0	31.2	32.1
13	-1	1	-1	-1	25.9	17.9	23.5	24.2	28.6
14	-1	-1	1	-1	1.2	21.9	19.5	23.0	3.7
15	-1	1	1	-1	18.6	26.4	23.7	22.6	22.5
16	-1	-1	-1	-1	16.0	26.5	21.3	22.6	23.7

Table 7-27: DOE (III) Anova for Tensile Strength

Source	DF	Adj SS	Adj MS	F-Value	P-Value
Linear					
A - BG(0%,40%)	1	1898.8	1898.8	154.63	0% *
B - PP(BRSK,PLYNR)	1	541.79	541.79	44.12	0% *
C -IMA(0%,5%)	1	2.16	2.16	0.18	68%
D - IMB(0%,5%)	1	261.17	261.17	21.27	0% *
2-Way Interactions					
A x B - BG(0%,40%)*PP(BRSK,PLYNR)	1	266.64	266.64	21.71	0% *
A x C - BG(0%,40%)*IMA(0%,5%)	1	249.6	249.6	20.33	0% *
A x D - BG(0%,40%)*IMB(0%,5%)	1	0.65	0.65	0.05	82%
B x C - PP(BRSK,PLYNR)*IMA(0%,5%)	1	11.57	11.57	0.94	34%
B x D - PP(BRSK,PLYNR)*IMB(0%,5%)	1	9.58	9.58	0.78	38%
C x D - IMA(0%,5%)*IMB(0%,5%)	1	140.15	140.15	11.41	0.1% *
3-Way Interactions					
A x B x C -	1	13.49	13.49	1.1	30%
A x B x D -	1	0.94	0.94	0.08	78%
A x C x D -	1	0.63	0.63	0.05	82%
B x C x D -	1	3.89	3.89	0.32	58%
4-Way Interactions					
A x B x C x D -	1	5.35	5.35	0.44	51%
Error	64	785.95	12.28		
Total	79	4192.4			

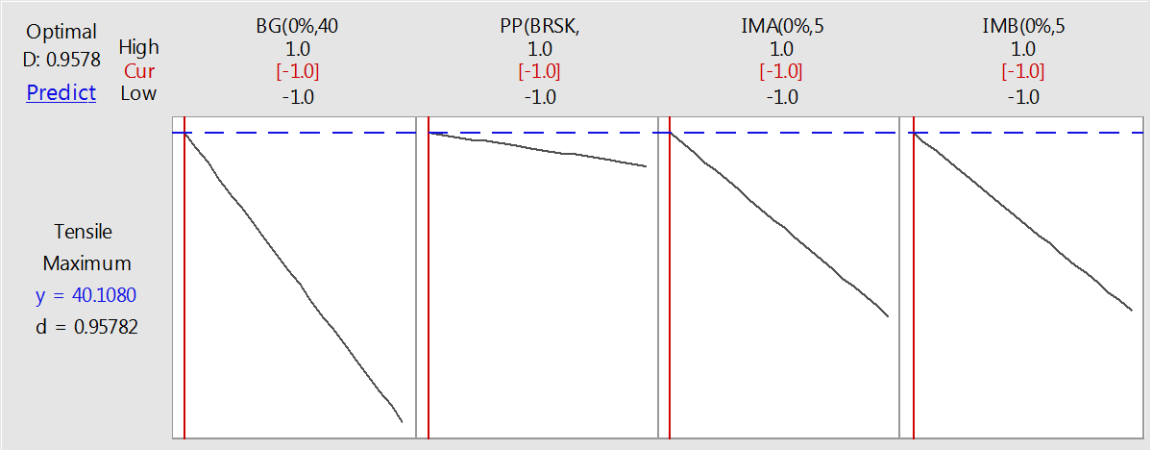

Figure 7-11: DOE (III) Optimal solution for tensile strength, (unacceptable)

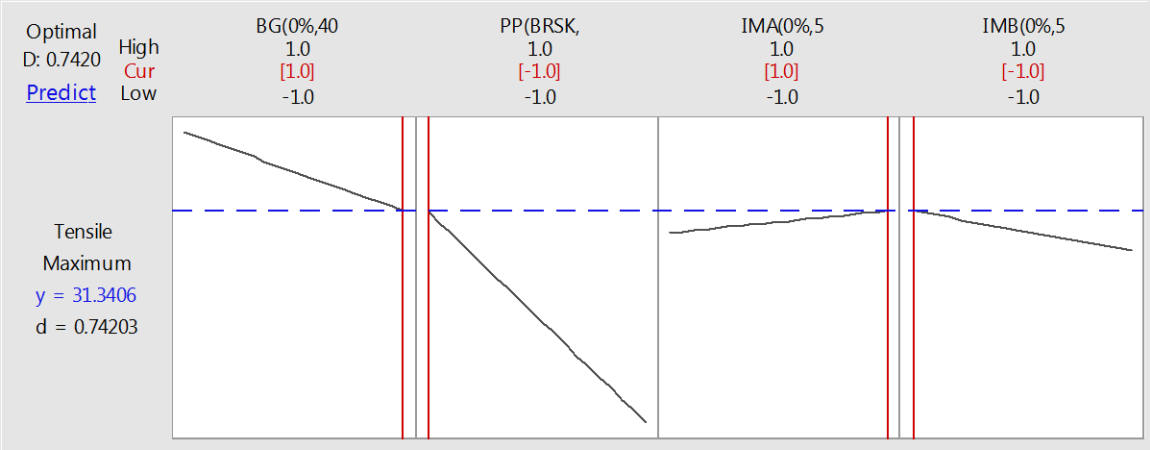

Figure 7-12: DOE (III) Optimal solution for tensile strength (acceptable)

Table 7-28: DOE (III) Coded design matrix with Flexural Modulus at 1% response

	Bagasse Content	PP grade	IMA	IMB	FLEXURAL MODULUS @1% (MPA)				
high	40%	Polynar	5%	5%					
symbol	1	1	1	1					
low	0%	Braskem	0%	0%					
symbol	-1	-1	-1	-1					
RUN	A	B	C	D	Rep 1	Rep 2	Rep 3	Rep 4	Rep 5
1	-1	-1	-1	-1	1115.4	1049.3	1133.0	1095.3	1024.2
2	-1	-1	1	-1	1067.7	1012.1	958.4	982.8	1007.4
3	-1	-1	-1	1	975.9	1048.5	952.3	941.9	994.1
4	-1	-1	1	1	1041.4	1003.2	1000.5	1160.7	1019.6
5	1	-1	1	-1	2502.2	2469.9	2519.7	2545.5	2521.7
6	1	-1	-1	1	2328.4	2363.6	2287.6	2254.7	2282.9
7	1	-1	1	1	2396.8	2385.4	2338.0	2144.7	2204.4
8	1	-1	-1	-1	2514.6	2539.9	2516.9	2544.3	2350.5
9	-1	1	-1	-1	1170.1	1200.8	1245.0	1302.0	1311.8
10	-1	1	1	-1	1152.0	1181.9	1106.9	1178.9	1155.3
11	-1	1	-1	1	1142.5	1161.6	1211.2	1165.5	1232.2
12	-1	1	1	1	1353.8	1444.7	1405.4	1477.5	1394.0
13	1	1	1	-1	2295.5	2285.3	2299.6	2325.9	2173.8
14	1	1	-1	1	2381.1	2349.5	2362.5	2325.8	2283.8
15	1	1	1	1	2365.2	2379.4	2384.0	2303.0	2322.5
16	1	1	-1	-1	2610.8	2737.3	2443.8	2351.0	2516.0

Table 7-29: DOE (III) Anova for flexural modulus at 1%

Source	DF	Adj SS	Adj MS	F-Value	P-Value
Linear					
A - BG(0%,40%)	1	311638	311638	7248.	0% *
B - PP(BRSK,PLYNR)	1	189496	189496	44.07	0% *
C - IMA(0%,5%)	1	3796	3796	0.88	35.1%
D - IMB(0%,5%)	1	47285	47285	11	0.2% *
2-Way Interactions					
A x B - BG(0%,40%)*PP(BRSK,PLYNR)	1	303277	303277	70.54	0% *
A x C - BG(0%,40%)*IMA(0%,5%)	1	41124	41124	9.56	0.3% *
A x D - BG(0%,40%)*IMB(0%,5%)	1	135855	135855	31.6	0% *
B x C - PP(BRSK,PLYNR)*IMA(0%,5%)	1	2981	2981	0.69	40.8%
B x D - PP(BRSK,PLYNR)*IMB(0%,5%)	1	94379	94379	21.95	0% *
C x D - IMA(0%,5%)*IMB(0%,5%)	1	153859	153859	35.78	0% *
3-Way Interactions					
A x B x C -	1	52846	52846	12.29	0.1% *
A x B x D -	1	343	343	0.08	77.9%
A x C x D -	1	15941	15941	3.71	5.9%
B x C x D -	1	71169	71169	16.55	0% *
4-Way Interactions					
A x B x C x D -	1	3858	3858	0.9	34.7%
Error	64	275171	4300		
Total	79	325551			

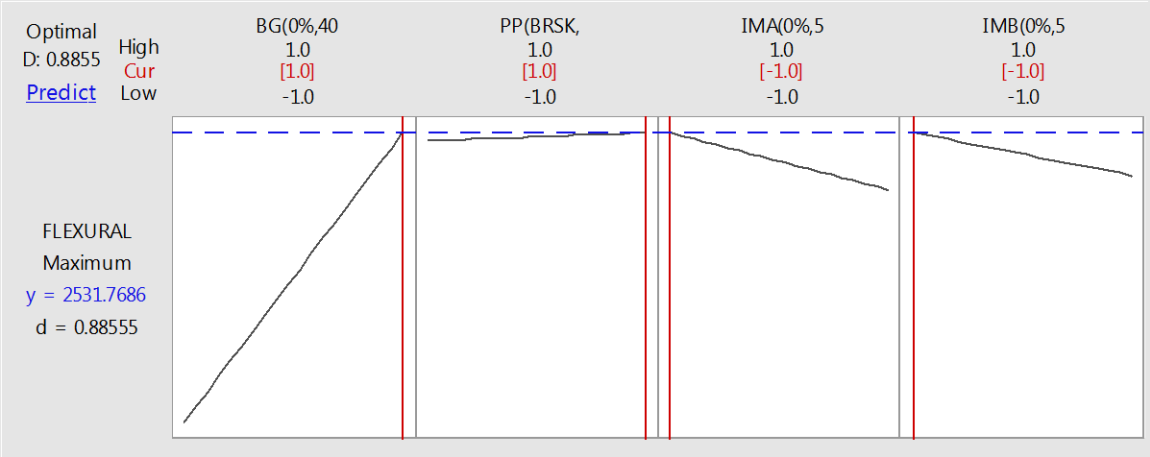

Figure 7-13: DOE (III) Optimum soution for flexural strength at 1%

Table 7-30: DOE (III) Coded Design Matrix with mean failure energy responses

	BAGASSE	PP grade	IMA	IMB	Mean Failure Energy (J)
high	40%	POLYNAR	5%	5%	
symbol	1	1	1	1	
low	0%	BRASKEM	0%	0%	
symbol	-1	-1	-1	-1	
RUN #	A	B	C	D	
1	1	1	-1	1	1.04
2	1	-1	1	1	0.85
3	1	1	1	1	1.14
4	1	-1	-1	1	1.06
5	1	1	-1	-1	0.82
6	1	-1	1	-1	1.10
7	1	1	1	-1	0.90
8	1	-1	-1	-1	0.67
9	-1	1	-1	1	1.35
10	-1	-1	1	1	0.97
11	-1	1	1	1	1.15
12	-1	-1	-1	1	0.96
13	-1	1	-1	-1	0.79
14	-1	-1	1	-1	0.78
15	-1	1	1	-1	0.80
16	-1	-1	-1	-1	0.55

Table 7-31: DOE (III) Anova for mean failure energy (0 degree of freedom for error term)

Source	DF	Adj SS	Adj MS	F-Value	P-Value
Linear					
A - BG(0%,40%)	1	0.2795	0.2795	*	*
B - PP(BRSK,PLYNR)	1	0.0032	0.0032	*	*
C - IMA(0%,5%)	1	0.0226	0.0226	*	*
D - IMB(0%,5%)	1	0.0448	0.0448	*	*
2-Way Interaction					
A x B - BG(0%,40%)*PP(BRSK,PLYNR)	1	0.0510	0.0510	*	*
A x C - BG(0%,40%)*IMA(0%,5%)	1	0.0698	0.0698	*	*
A x D - BG(0%,40%)*IMB(0%,5%)	1	0.0266	0.0266	*	*
B x C - PP(BRSK,PLYNR)*IMA(0%,5%)	1	0.0000	0.0000	*	*
B x D - PP(BRSK,PLYNR)*IMB(0%,5%)	1	0.0391	0.0391	*	*
C x D - IMA(0%,5%)*IMB(0%,5%)	1	0.0040	0.0040	*	*
3-Way Interaction					
A x B x C -	1	0.0232	0.0232	*	*
A x B x D -	1	0.0040	0.0040	*	*
A x C x D -	1	0.0482	0.0482	*	*
B x C x D -	1	0.0025	0.0025	*	*
4-Way Interaction					
A x B x C x D -	1	0.0002	0.0002	*	*
Error	0	*	*		
Total	15	0.6195			

Table 7-32: DOE (III) Anova for mean failure energy (1 degree of freedom for error term)

Source	DF	Adj SS	Adj MS	F-Value	P-Value
Model	14	0.61933	0.04423	208.58	5.4%
Linear	4	0.35033	0.08758	412.95	3.7%*
A - BG(0%,40%)	1	0.27951	0.27951	1317.8	1.8%*
B - PP(BRSK,PLYNR)	1	0.00328	0.00328	15.48	15.8%
C - IMA(0%,5%)	1	0.02266	0.02266	106.84	6.1%
D - IMB(0%,5%)	1	0.04487	0.04487	211.6	4.4%*
2-Way Interactions	6	0.19089	0.03181	150	6.2%
A x B - BG(0%,40%)*PP(BRSK,PLYNR)	1	0.05107	0.05107	240.79	4.1%*
A x C - BG(0%,40%)*IMA(0%,5%)	1	0.06987	0.06987	329.46	3.5%*
A x D - BG(0%,40%)*IMB(0%,5%)	1	0.02668	0.02668	125.83	5.7%
B x C - PP(BRSK,PLYNR)*IMA(0%,5%)	1	0.00002	0.00002	0.13	77.8%
B x D - PP(BRSK,PLYNR)*IMB(0%,5%)	1	0.03915	0.03915	184.62	4.7%*
C x D - IMA(0%,5%)*IMB(0%,5%)	1	0.00407	0.00407	19.19	14.3%
3-Way Interactions	4	0.07810	0.01952	92.07	7.8%
A x B x C -	1	0.02322	0.02322	109.52	6.1%
A x B x D -	1	0.00401	0.00401	18.93	14.4%
A x C x D -	1	0.04827	0.04827	227.62	4.2%*
B x C x D -	1	0.00258	0.00258	12.2	17.8%
Error	1	0.00021	0.00021		
Total	15	0.61954			

Table 7-33: DOE (III) Anova for mean failure energy (5 degree of freedom for error term)

Source	DF	Adj SS	Adj MS	F-Value	P-Value
Model	10	0.541225	0.054122	3.46	9.2%
Linear	4	0.350335	0.087584	5.59	4.3%*
A - BG(0%,40%)	1	0.279513	0.279513	17.84	0.8%*
B - PP(BRSK,PLYNR)	1	0.003283	0.003283	0.21	66.6%
C - IMA(0%,5%)	1	0.02266	0.02266	1.45	28.3%
D - IMB(0%,5%)	1	0.044879	0.044879	2.87	15.1%
2-Way Interactions	6	0.19089	0.031815	2.03	22.7%
A x B -	1	0.05107	0.05107	3.26	13.1%
A x C - BG(0%,40%)*IMA(0%,5%)	1	0.069876	0.069876	4.46	8.8%
A x D - BG(0%,40%)*IMB(0%,5%)	1	0.026689	0.026689	1.7	24.9%
B x C -	1	0.000028	0.000028	0	96.8%
B x D -	1	0.039157	0.039157	2.5	17.5%
C x D - IMA(0%,5%)*IMB(0%,5%)	1	0.004071	0.004071	0.26	63.2%
Error	5	0.078319	0.015664		
Total	15	0.619544			

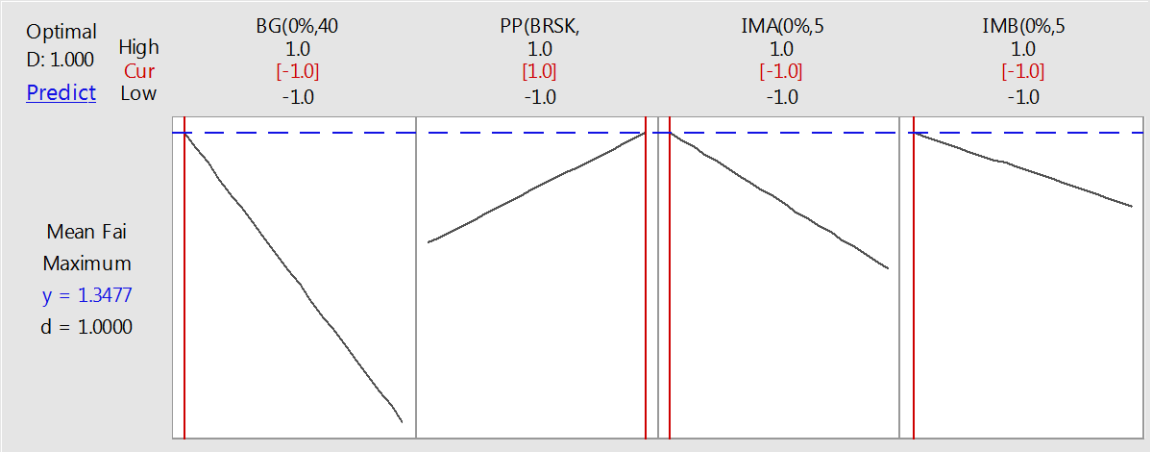

Figure 7-14: DOE (III) Optimum solution for mean failure energy

Table 7-34: Commercial final product 2 level factorial design matrix and responses

UV(-1: 0 h,1:1000 h)	Location of impact (-1: mid,1: side)	Back Reint (-1: No,1: Yes)	Run #	Max load (kN)	Defl. at max load (mm)	E to max load	Tot energy (J)
-1	-1	-1	Run 1	1.67	3.18	3.80	18.36
			Run 2	1.46	5.52	5.99	10.28
			Run 3	1.86	3.91	5.45	19.23
			Run 4	2.29	2.02	2.64	16.93
			Run 5	1.87	1.81	1.78	8.43
-1	-1	1	Run 6	1.58	3.16	3.83	7.70
			Run 7	1.79	4.88	7.04	12.57
			Run 8	2.24	3.70	5.73	12.46
			Run 9	2.46	3.00	5.04	13.07
			Run 10	1.89	3.48	4.81	13.93
-1	1	-1	Run 11	1.99	3.04	4.30	12.12
			Run 12	1.22	2.80	2.49	4.80
			Run 13	1.26	4.23	3.79	10.11
			Run 14	1.73	2.43	2.77	13.52
			Run 15	2.10	2.78	4.09	15.89
-1	1	1	Run 16	1.36	2.05	1.73	12.49
			Run 17	2.56	2.32	3.81	14.81
			Run 18	2.18	1.39	1.61	15.11
			Run 19	2.04	3.85	5.83	21.99
			Run 20	1.56	1.81	1.68	14.82
1	-1	-1	Run 21	1.51	2.42	2.60	12.94
			Run 22	1.82	4.68	5.93	12.73
			Run 23	1.86	3.27	4.44	11.64
			Run 24	1.86	4.66	6.12	10.70
			Run 25	2.66	1.58	2.11	12.87
1	-1	1	Run 26	0.93	2.09	1.10	6.96
			Run 27	1.74	3.71	4.51	12.64
			Run 28	1.42	3.15	3.23	6.69
			Run 29	1.25	2.98	2.54	7.40
			Run 30	1.19	3.10	2.63	6.70
1	1	-1	Run 31	1.93	2.63	3.54	21.26
			Run 32	1.28	2.40	2.07	9.44
			Run 33	2.10	3.59	5.56	12.58
			Run 34	1.34	3.98	3.93	6.40
			Run 35	1.33	1.87	1.37	4.78
1	1	1	Run 36	2.11	2.68	3.86	11.99
			Run 37	2.77	3.09	5.43	16.09
			Run 38	1.61	1.35	1.08	12.01
			Run 39	2.72	2.27	3.67	22.24
			Run 40	1.21	4.00	3.36	5.91

Table 7-35: Commercial final product Analysis of variance for maximum load response

Source		DF	SS	MS	F-Value	P-Value
	UV(0h,1000h)	1	0.15	0.15	0.8	37.70
	LOC(mid,side)	1	0.0272	0.0272	0.15	70.60
	BACK-REIN(N,Y)	1	0.0549	0.0549	0.29	59.20
2-Way	Interactions					
	UV(0h,1000h)*LOC(mid,side)	1	0.2636	0.2636	1.41	24.40
	UV(0h,1000h)*BACK-REIN(N,Y)	1	0.2144	0.2144	1.15	29.30
	LOC(mid,side)*BACK-REIN(N,Y)	1	0.969	0.969	5.18	3.00%
3-Way	Interactions					
	UV(0h,1000h)*LOC(mid,side)*BACK-	1	0.633	0.633	3.38	7.50%
Error		32	5.9914	0.1872		
Total		39	8.3035			

Table 7-36: Commercial final product Anova for Deflection at max load

Source		DF	SS	MS	F-Value	P-Value
	UV(0h,1000h)	1	0.0846	0.0846	0.08	77.50
	LOC(mid,side)	1	3.4619	3.4619	3.41	7.40%
	BACK-REIN(N,Y)	1	0.5649	0.5649	0.56	46.10
2-Way	Interactions					
	UV(0h,1000h)*LOC(mid,side)	1	0.4322	0.4322	0.43	51.90
	UV(0h,1000h)*BACK-REIN(N,Y)	1	0.0086	0.0086	0.01	92.70
	LOC(mid,side)*BACK-REIN(N,Y)	1	0.6616	0.6616	0.65	42.60
3-Way	Interactions					
	UV(0h,1000h)*LOC(mid,side)*BACK-	1	0.9387	0.9387	0.92	34.40
Error		32	32.529	1.0165		
Total		39	38.681			

Table 7-37: Commercial final product Anova for Energy to max load

Source		DF	SS	MS	F-	P-Value
	UV(0h,1000h)	1	2.0705	2.0705	0.88	35.50%
	LOC(mid,side)	1	5.8846	5.8846	2.5	12.30%
	BACK-REIN(N,Y)	1	0.1229	0.1229	0.05	82.10%
2-Way	Interactions					
	UV(0h,1000h)*LOC(mid,side)	1	4.005	4.005	1.7	20.10%
	UV(0h,1000h)*BACK-REIN(N,Y)	1	2.6352	2.6352	1.12	29.80%
	LOC(mid,side)*BACK-REIN(N,Y)	1	0.0536	0.0536	0.02	88.10%
3-Way	Interactions					
	UV(0h,1000h)*LOC(mid,side)*BACK	1	7.7962	7.7962	3.32	7.80%*
Error		32	75.186	2.3496		
Total		39	97.754			

Table 7-38: Commercial Final Product Anova for Total Energy (J)

Source		DF	SS	MS	F-Value	P-Value
	UV(0h,1000h)	1	49.816	49.816	2.71	11.00%
	LOC(mid,side)	1	14.556	14.556	0.79	38.00%
	BACK-REIN(N,Y)	1	0.166	0.166	0.01	92.50%
2-Way	Interactions					
	UV(0h,1000h)*LOC(mid,side)	1	8.784	8.784	0.48	49.50%
	UV(0h,1000h)*BACK-REIN(N,Y)	1	6.4	6.4	0.35	55.90%
	LOC(mid,side)*BACK-REIN(N,Y)	1	124.47	124.47	6.77	1.40% *
3-Way	Interactions					
	UV(0h,1000h)*LOC(mid,side)*BACK-	1	0.1	0.1	0.01	94.20%
Error		32	588.77	18.399		
Total		39	793.07			

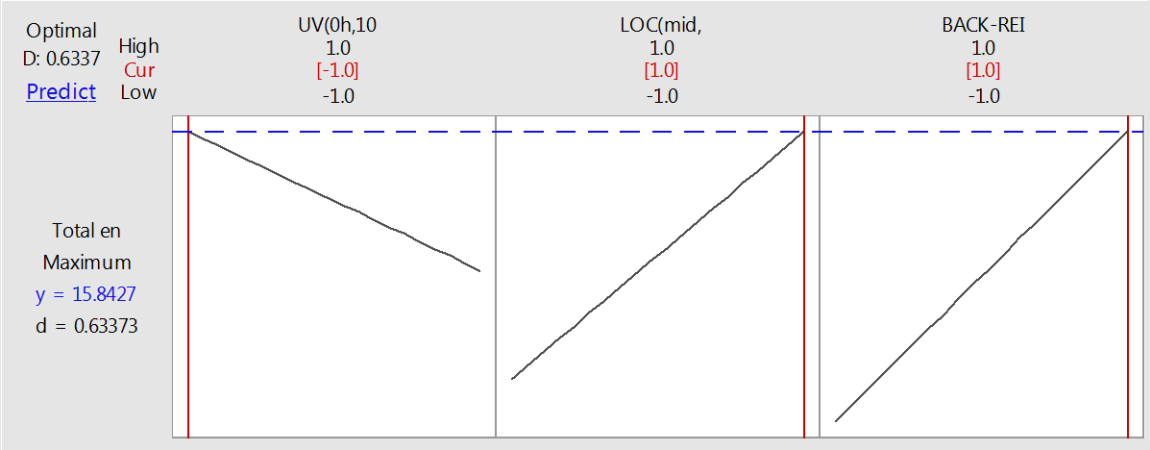

Figure 7-15: Commercial final product optimum solution for maximum energy

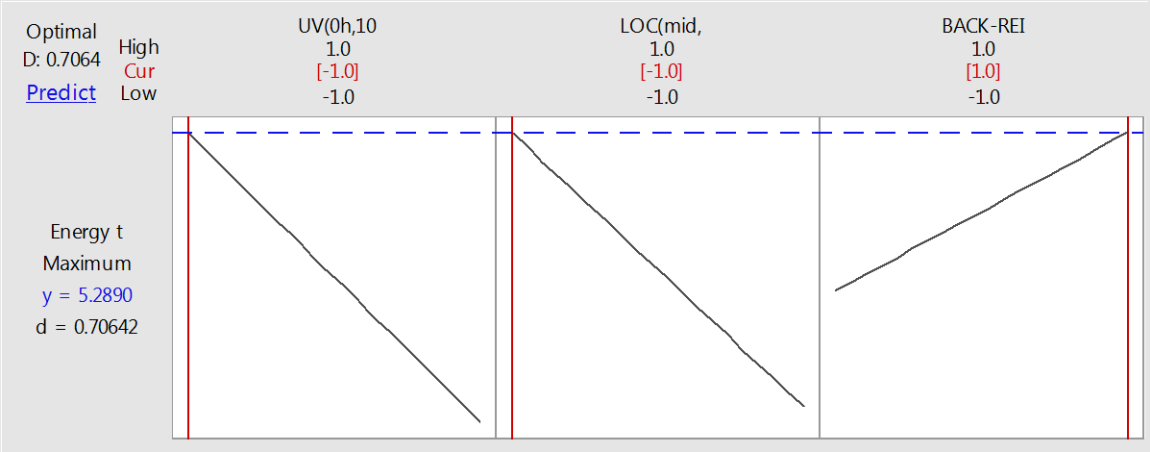

Figure 7-16: Commercial final product optimum solution for energy to maximum load

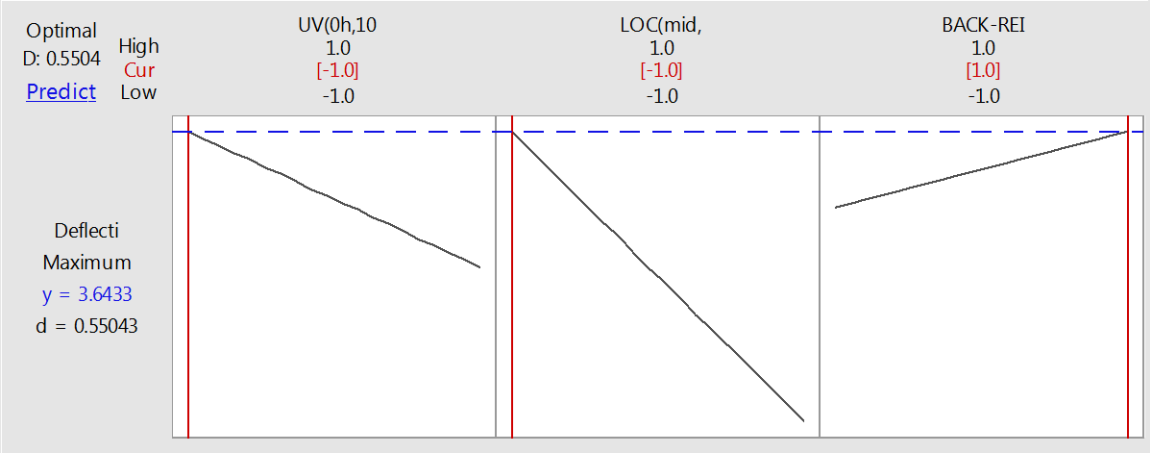

Figure 7-17: Commercial final product optimum solution for deflection to maximum load

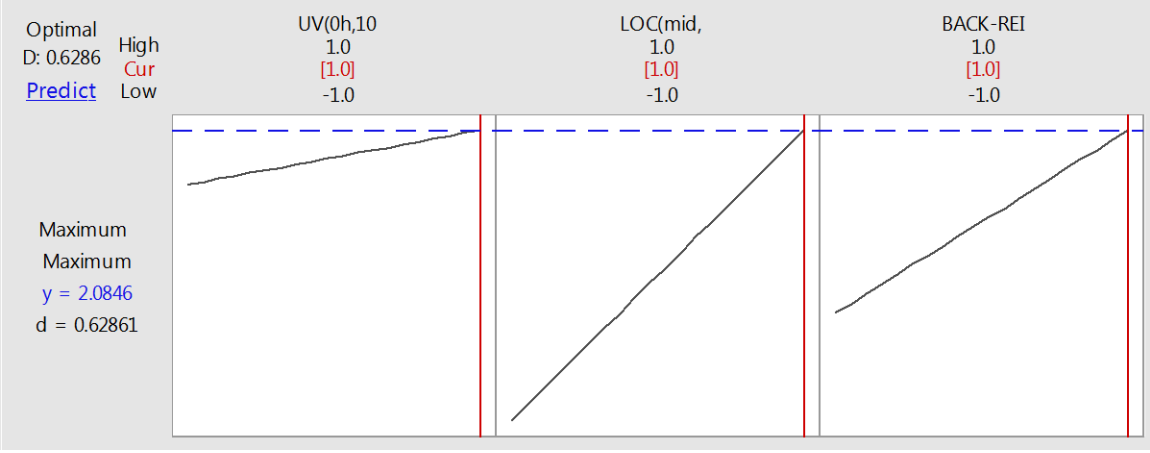

Figure 7-18: Commercial final product optimum solution for maximum load

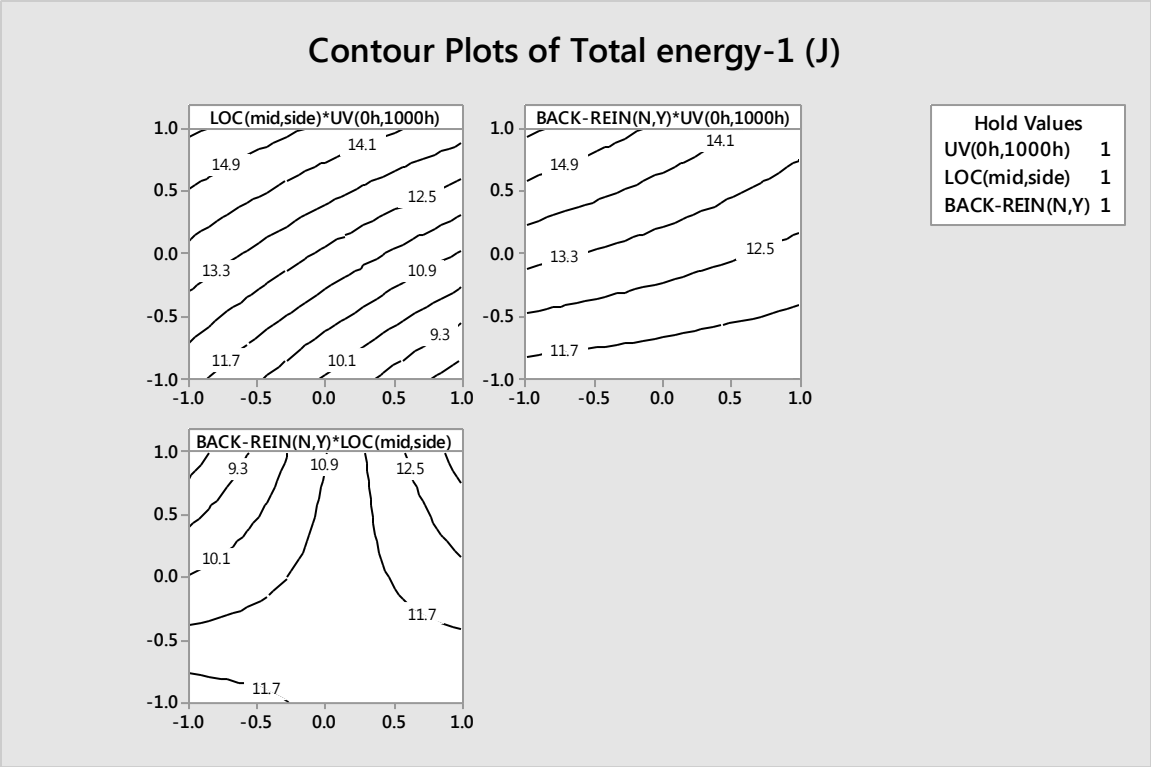

Figure 7-19: Commercial final product contour plots for total energy

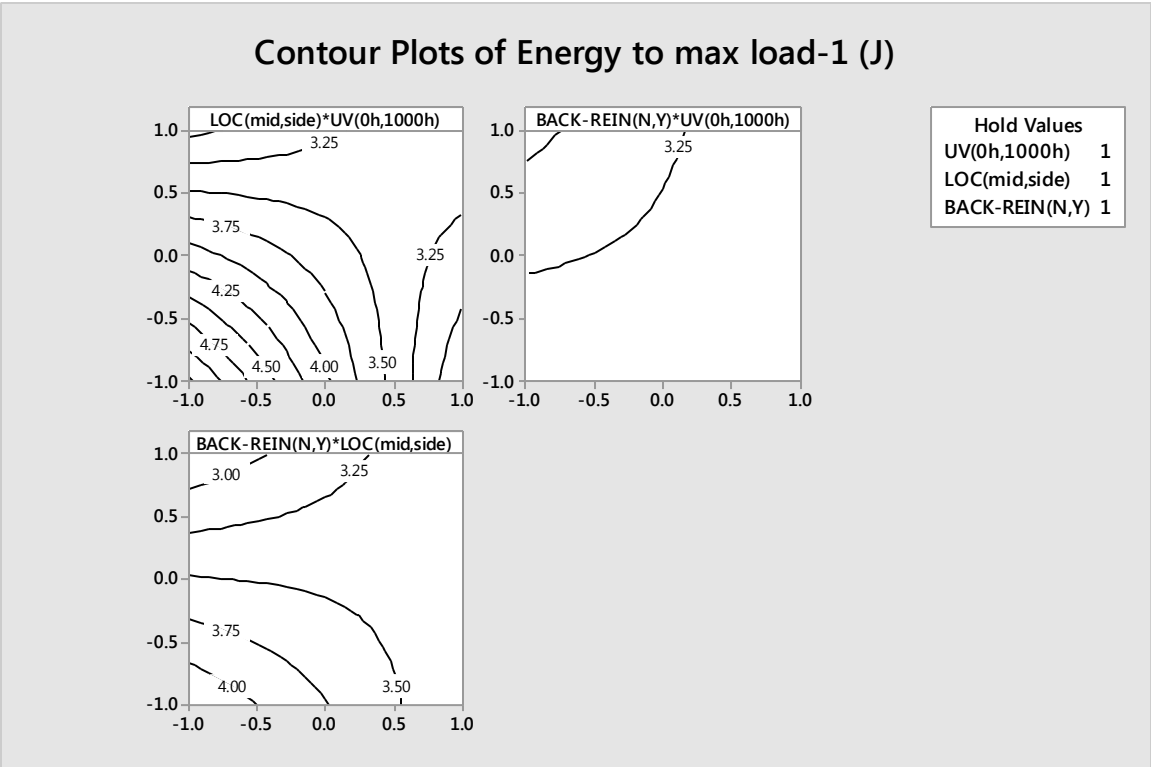

Figure 7-20: Commercial final product contour plots for energy to max load

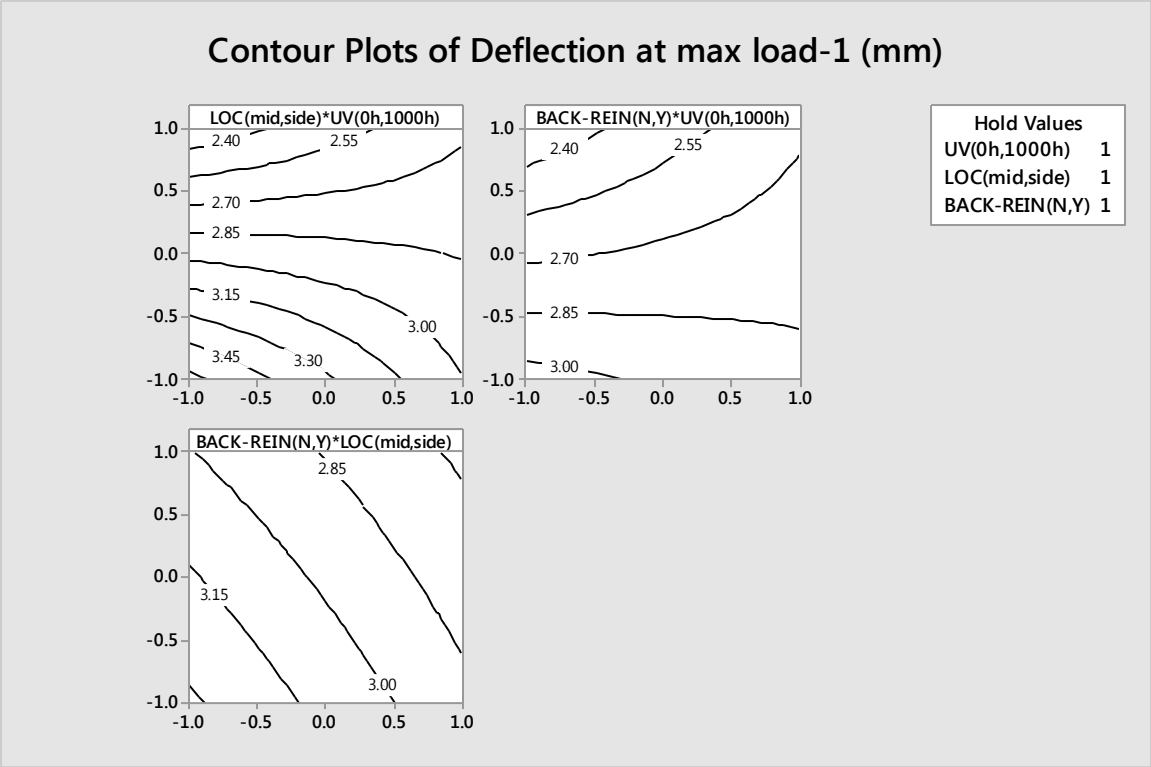

Figure 7-21: Commercial final product contour plots for deflection at max load

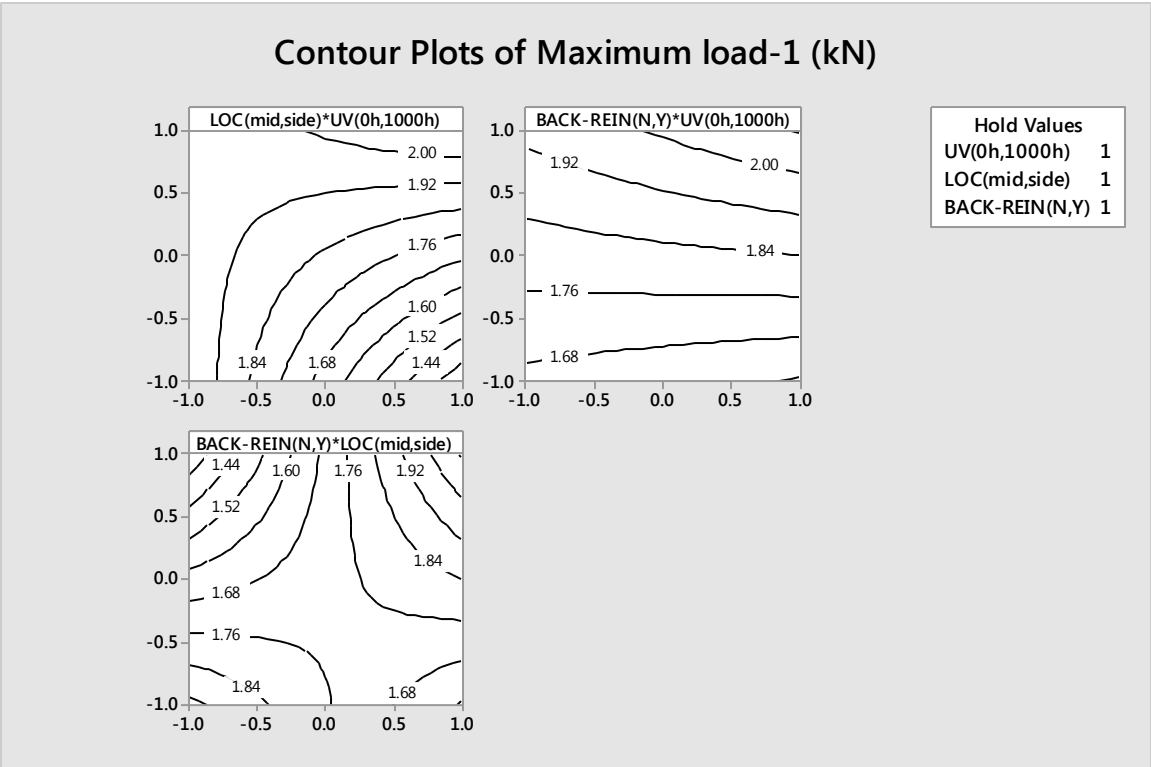

Figure 7-22: Commercial final product contour plots for maximum load

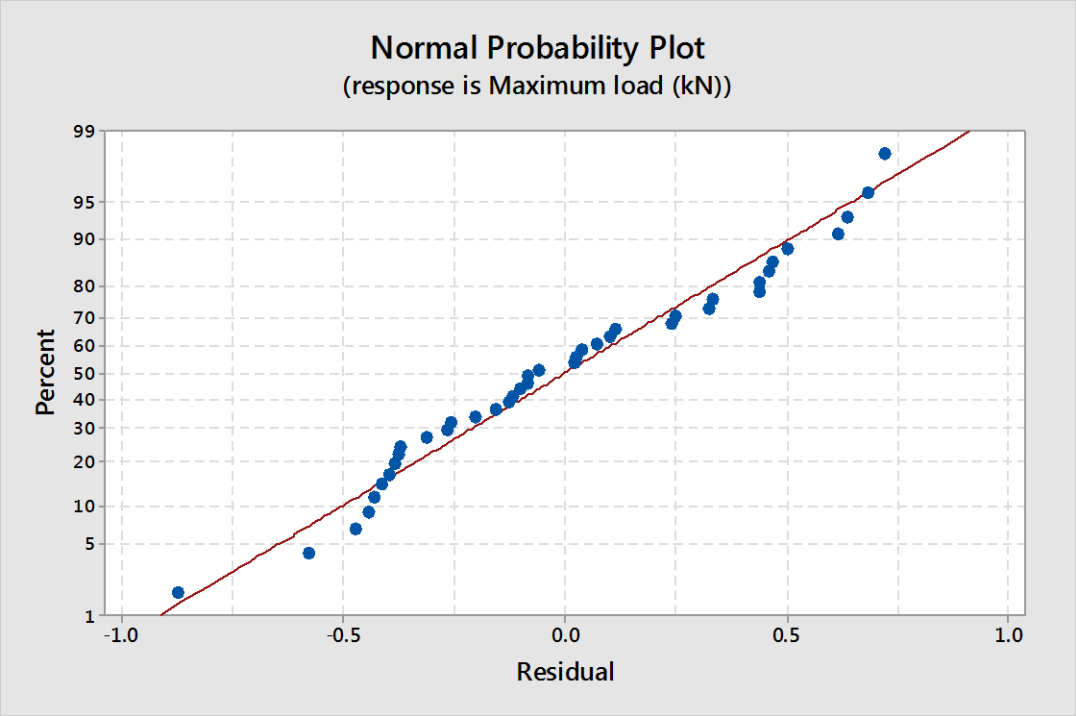

Figure 7-23: DOE (IV) Normal Residuals Plot for Maximum Load

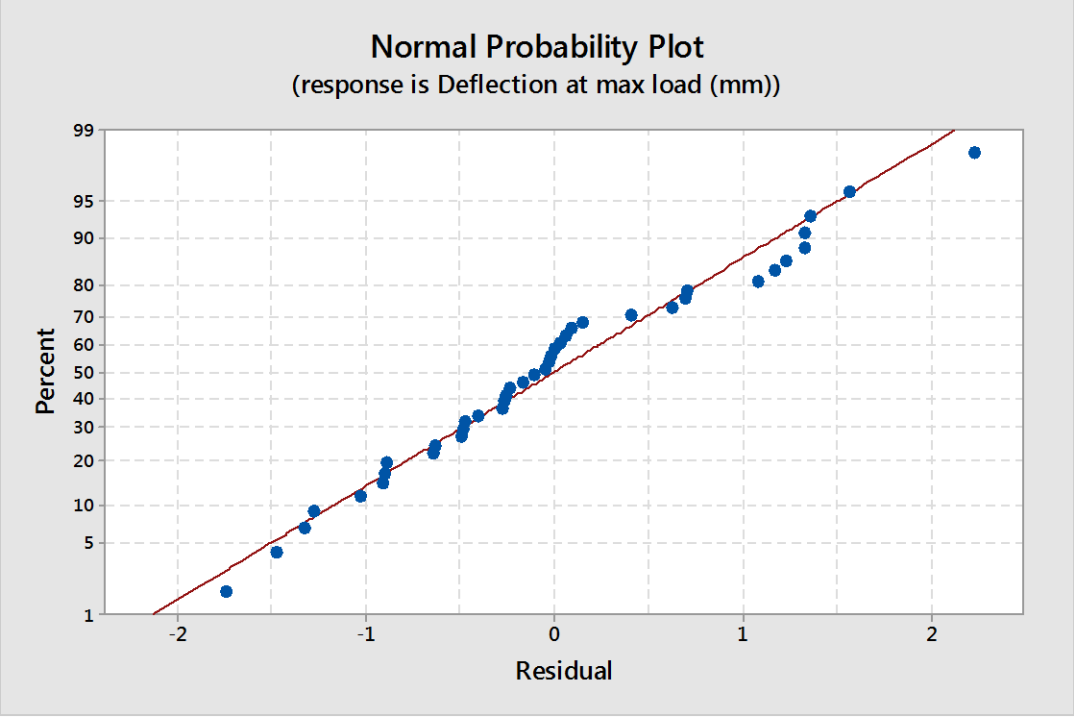

Figure 7-24: DOE (IV) Normal Residuals Plot for Deflection at Maximum Load

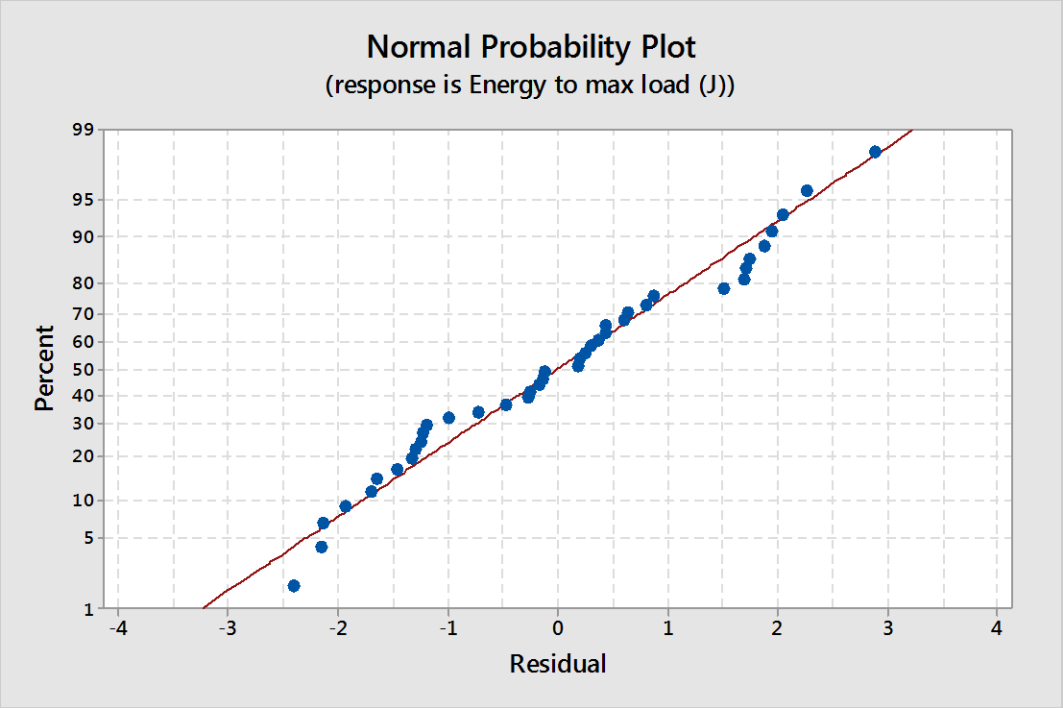

Figure 7-25: DOE (IV) Normal Residuals Plot for Energy to Maximum Load

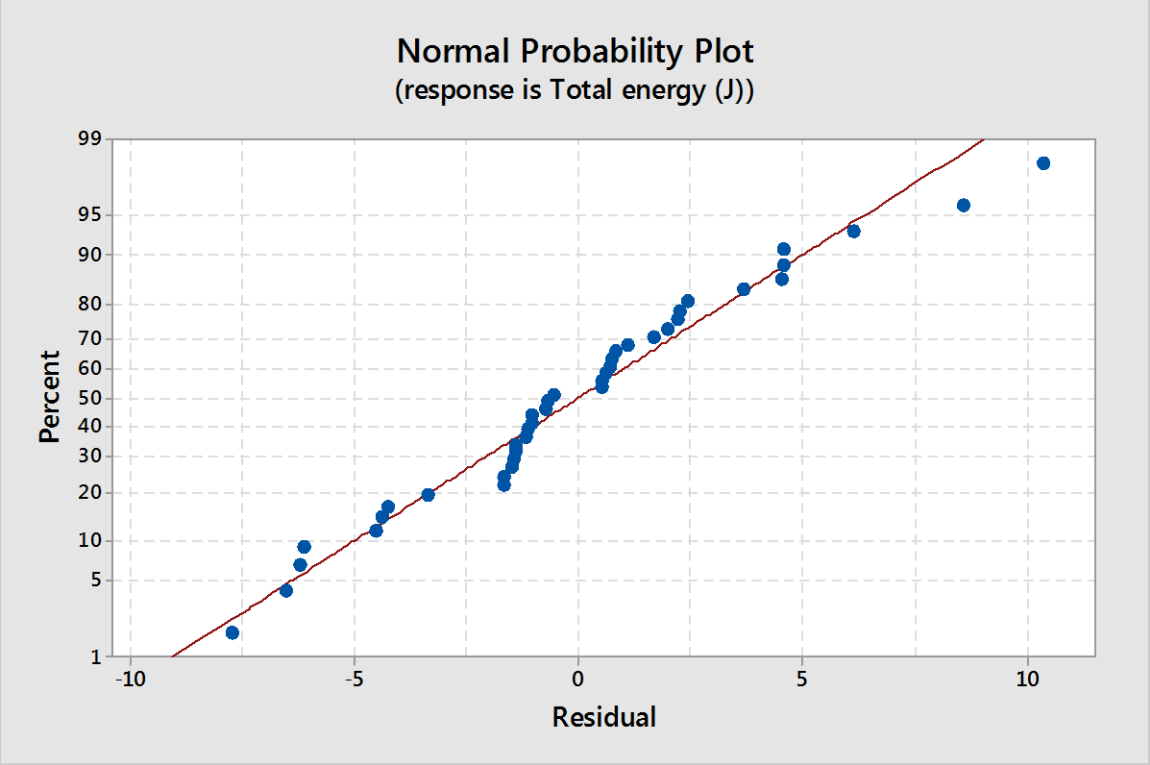

Figure 7-26: DOE (IV) Normal Residuals Plot for Total Energy

PHYSICAL AND MECHANICAL PROPERTIES FOR TREX ACCENTS®

	TEST METHOD	VALUES	
Abrasion Resistance	ASTM D2394	.01 wear/1000 revs.	
Hardness	ASTM D143	562 kg (5 kn)	
Self-Ignition Temperature	ASTM D1929	743°F (395°C)	
Flash-Ignition Temperature	ASTM D1929	698°F (370°C)	
Flame Spread (a) [Fire Defense]™	ASTM E84	80 [40]	
Water Absorption (sanded surface) 24 hr. immersion	ASTM D1037	4.3%	
Water Absorption (unsanded surface) 24 hr. immersion	ASTM D1037	1.7%	
	Typical Trex® Values for Coefficient of Thermal Expansion/Contraction (36" (91.4 cm) long samples)		
Thermal	Width	35.2 x 10-6 to 42.7 x 10-6 (inch/inch/°F) 644 x 10-6 to 776 x 10-6 (length/length/°C)	
	Length	16.1 x 10-6 to 19.2 x 10-6 (inch/inch/°F) 297 x 10-6 to 356 x 10-6 (length/length/°C)	
Moisture	Typical Trex Values for Long-Term Water Immersion (36"/91.4 cm long samples) Width ~3%	Typical Trex Values for Constant High Humidity (6"/15.2 cm long samples) ~1%	
Nail Withdrawal (c)	ASTM D1761	163 lbs/in (1.12 Mpa)	
Screw Withdrawal (c)	ASTM D1761	558 lbs/in (3.85 Mpa)	
Static Coefficient of Friction - Dry (d)	ASTM D2047	0.53/0.55	
Static Coefficient of Friction - Dry (d)	ASTM F1679	0.59/0.70	
Static Coefficient of Friction - Wet (d)	ASTM F1679	0.70/0.75	
Fungus Resistance (White & Brown Rot)	ASTM D1413	Rating = No Decay	
Termite Resistance (e)	AWPA E1-72	Rating = 9.6	
Specific Gravity (typical)	ASTM D2395	0.91 to 0.95	
		ULTIMATE (TYPICAL) VALUES	DESIGN VALUES
Compression Parallel (f)(g)	ASTM D198	1806 psi (12.45 Mpa)	550 psi (3.79 Mpa)
Compression Perpendicular (f)(h)	ASTM D143	1944 psi (13.40 Mpa)	625 psi (4.31 Mpa)
Tensile Strength (f)	ASTM D198	854 psi (5.89 Mpa)	250 psi (1.72 Mpa)
Shear Strength (f)	ASTM D143	561 psi (3.87 Mpa)	200 psi (1.38 Mpa)
Modulus of Rupture (f)	ASTM D4761	1423 psi (9.81 Mpa)	250 psi (1.72 Mpa)
Modulus of Elasticity (f)	ASTM D4761	175,000 psi (1206 Mpa)	100,000 psi (689.48 Mpa)
Thermal Conductivity	ASTM C177	1.57 BTU-in/hr-ft @85°F (.0023 W/cm/°C)	
Leachate (i)	TCLP-EPA 1311	Pass	

NOTES:
(a) Corresponding Smoke Developed Index is 285.
(b) Values shown are for reference only. These values should not be used to calculate gapping for Trex. Follow Trex installation literature for proper width-to-width and end-to-end gapping information.
(c) 8d common wire nail. No. 10 wood screw.
(d) ASTM D2047 test conducted on sanded/unsanded unweathered samples with leather surface.
ASTM F1679 test conducted on sanded/unsanded weathered samples with neolite surface.
(e) Material weight loss was 0%.
(f) Ultimate strength values are not meant for design analysis. Testing performed on a 1" x 5.5" (2.5 cm x 14 cm) cross section. Design values are for temperatures up to 130°F (54°C).
(g) Compressive strength parallel to the length.
(h) Compressive strength perpendicular to length.
(i) Leaching was below levels established by EPA for all constituent categories.

Figure 7-27: Trex Accents decking physical and mechanical datasheet((Trex Company, 2012)

Polynar Co

Manufacturer of Polypropylene

POLYPROPYLENE

ISO 9001

OHSAS 18001

ISO 14001

P-FI-160 Homopolymer

Description:

"Polynar P-FI-160" is polypropylene homopolymer with good flow properties and medium molecular weight distribution intended for fiber extrusion applications.

"Polynar P-FI-160" has a high fluidity and best suits for the production of staple fibers, bulk continuous filament (BCF). And continuous filament(CF)

"Polynar P-FI-160" is suitable for food contact.

Processing Method: Fiber extrusion

Features:

homopolymer
good flow properties
consistent processability
medium molecular weight distribution

Typical Applications:

BCF andCF yarn
Staple fibers
Carpet , diapers, medical disposables, wipes and other applications include filters and fabrics for the automotive , clothing and furniture industry.

TYPICAL PROPERTIES	VALUE	UNIT	METHOD
Physical			
Melt Flow Rate (230 °C, 2.16kg)	16.0	g/10min	ASTM D1238
Density	0.90	g/cm^3	ASTM D1505
Mechanical			
Flexural Modulus	1550	MPa	ASTM D790
Tensile Strength at Yield	33	MPa	ASTM D638
Tensile Elongation at Yield	12	%	ASTM D638
Izod Impact Strength (notched) at 23 °C	30	J/m	ASTM D256
Thermal			
Vicat softening point (10N)	154	°C	ASTM D1525
H.D.T. (0.46 Mpa)	95	°C	ASTM D648

Head Office: NO:10 ,Danially Alley ,Andarzgoo Boulevard, TEHRAN-IRAN
TEL:(+9821)22212087 FAX:(+9821)22201946
Factory: West of TABRIZ Petrochemical Complex – TABRIZ-IRAN
TEL:(+98411)4201000 FAX:(+98411)4201001
www.polynar.com **Email:info@polynar.ir**

Figure 7-28: Polypropylene grade P-FI-160 datasheet

Braskem

Polypropylene **D180M**

Sub-group
Homopolymer

Description
Low gas fade

Applications
Suggested uses include BCF multi-filiments, high tenacity continuous filament yarn, fine denier staple fibers

Control Properties:	ASTM Method	Units	Values
Nominal Melt Flow Rate (230°C/2.16kg)	D-1238	g/10 min	18

Typical Properties:	ASTM Method	Units	Values
Tensile Strength at Yield (2 in/min, 50 mm/min)	D-638	psi(MPa)	5,100(35)
Elongation at Yield (2 in/min, 50 mm/min)	D-638	%	9
Flexural Modulus (0.05 in/min, 1.3 mm/min, 1% secant)	D-790A	psi(MPa)	190,000(1,310)
Notched Izod Impact Strength at 23°C	D-256A	ft-lbs/in(J/m)	0.5(27)
Rockwell Hardness	D-785	R	104
Tenacity of Fibers (3.3 draw ratio, 1,250 m/min roll speed, 225Â°C spin temperature, D1000/68)	D-2256	g/denier	2.9
Elongation of Fibers (3.3 draw ratio, 1,250 m/min roll speed, 225Â°C spin temperature, D1000/68)	D-2256	%	93
Suggested Takeup Roll Speed	Braskem	ft/min(m/min)	6,561(2,000)

Final Remarks
1. This resin meets the requirements for olefin polymers as defined in 21 CFR, section 177.1520 issued by the Food and Drug Administration. The additives present meet the applicable regulations.
2. This information reflects typical values obtained in our laboratories, but should not be considered as absolute or as warranted values. Only the properties and values mentioned on the Certificate of Quality are considered as guarantee of the product.
3. In some applications, Braskem has developed tailor-made resins to reach specific requirements.
4. In case of doubt regarding utilization, or for other applications, please contact Technical Service.
5. The values in this report can be modified without prior communication from Braskem.
6. Braskem polyolefin products do not have additives with heavy metals or organotin-based materials.

Revision Date:
6/20/2013
www.braskem.com

Figure 7-29: Polypropylene grade D180M datasheet

DuPont Fusabond® MD353D Random Copolymer Polypropylene (discontinued **)

Categories: Other Engineering Material; Additive/Filler for Polymer; Polymer; Thermoplastic; Polypropylene (PP)

Material Notes: **Typical Use:**

- Coupling agent
- Long glass filled polypropylene
- Coupling agent for nonhalogen, flame retarded wire and cable compounds containing magnesium hydroxide
- Adhesion promoter
- Natural fiber wood-plastic compounds

Availability: North America

Information provided by DuPont.

Vendors: No vendors are listed for this material. Please click here if you are a supplier and would like information on how to add your listing to this material.

Physical Properties	Metric	English	Comments
Melt Flow	450 g/10 min @Load 2.16 kg, Temperature 190 °C	450 g/10 min @Load 4.76 lb, Temperature 374 °F	

Thermal Properties	Metric	English	Comments
Melting Point	136 °C	277 °F	

Descriptive Properties			
MAH Graft Level, wt%		Very High	FTIR (DuPont)

**

Materials flagged as discontinued (D) are no longer part of the manufacturer's standard product line according to our latest information. These materials may be available by special order, in distribution inventory, or reinstated as an active product. Data sheets from materials that are no longer available remain in MatWeb to assist users in finding replacement materials.

Users of our Advanced Search (registration required) may exclude discontinued materials from search results.

Some of the values displayed above may have been converted from their original units and/or rounded in order to display the information in a consistent format. Users requiring more precise data for scientific or engineering calculations can click on the property value to see the original value as well as raw conversions to equivalent units. We advise that you only use the original value or one of its raw conversions in your calculations to minimize rounding error. We also ask that you refer to MatWeb's terms of use regarding this information. Click here to view all the property values for this datasheet as they were originally entered into MatWeb.

Figure 7-30: Coupling agent grade MD353D datasheet

K0038 Europe/Africa September 2007	Kraton® G1650 E	Data Document

Description

Kraton® G-1650 polymer is a clear linear triblock copolymer based on styrene and ethylene/butylene, S-E/B-S, with bound styrene of 29.2% mass. It is supplied from Europe in two physical forms, indicated as follows in the grade nomenclature:

- G-1650E supplied as undusted 'fluffy' crumb
- G-1650ES supplied as 'fluffy' crumb dusted with amorphous silica

Kraton G-1650 polymer is used for formulating adhesives and coatings, as base material for compound formulations, as a modifier of thermoplastics and as a modifier of bitumen. The inherent stability of the mid block suggests the use of G-1650 in applications that must withstand weathering and high processing temperatures.

Sales Specifications

Property	Test Method	Units	Sales Specification Range
Bound styrene [a]	BMS0407	%mass	27.7 - 30.7
Volatile matter	KM04	%mass	0.5 max.
Ash	ISO 247A	%m/m	0.4 - 0.6 (ES)
Total extractables	KM05	%mass	1.0 max.
Solution viscosity [b]	BMS0380	Pa.s	1.0 - 1.9
Antioxidant content [c]	KM08	%mass	0.03 min.

[a] Measured on the polymer after the hydrogenation

[b] Measured on 20% mass solution in toluene at 25°C using a Brookfield viscometer, LTF or LTV model

[c] Primary phenolic antioxidant

Typical Properties (These are typical values and may not routinely be measured on finished product)

Property	Test Method	Units	Typical Value
Specific gravity	ISO 2781		0.91
Tensile strength [d]	ISO 37	MPa	35
Elongation at break [d]	ISO 37	%	500
300% modulus [d]	ISO 37	MPa	5.6

[d] Measured on films cast from a solution in toluene

Packaging

Kraton Polymers are available in a number of different pack types. For information specific to this grade please contact your local Kraton Polymers representative.

Figure 7-31: Impact midfier A (Kraton grade G1650) datasheet

K0180 North America 8/4/2009	Kraton® G1701 M Polymer	Data Document

Identifier : K180DDe09U

Description

Kraton G1701 M is a clear, linear diblock copolymer based on styrene and ethylene/propylene with a polystyrene content of 37%. It is supplied from North America in the physical form identified below.

- Kraton G1701 MU - supplied as a powder.

Kraton G1701 M is used as a modifier of bitumen and polymers. It is also suitable as an ingredient in formulating compounds for footwear applications and may be used in formulating adhesives, sealants, and coatings.

Sales Specifications

Property	Test Method	Units	Sales Specification Range	Notes
Polystyrene Content	KM 03	%m	34.7 TO 38.5	b
Volatile Matter	KM 04	%m	<= 1.0	
Total Extractables	KM 05	%m	<= 3.0	
Antioxidant	KM 08	%w	0.03 TO 0.20	a
Visc,Kin,1.70%w (ENJ404@100C)	BAM 1201	cSt	15.0 TO 19.0	

a Non-staining phenolic antioxidant.
b Measured on the polymer before hydrogenation.

Typical Properties (These are typical values and may not routinely be measured on finished product)

Property	Test Method	Units	Typical Value	Notes
Melt Index 230°C, 5 kg	ASTM D 1238	gms/10 min.	1	
Diblock Content	n/a		100%	
Tensile Strength	ASTM D 412	psi	300	
Specific Gravity	ASTM D 792	g/cc	.92	
Styrene / Rubber ratio	n/a		37/63	
Hardness, Shore A	ASTM D 2240	Shore A (10 sec)	64	
Elongation at Break	ASTM D 412	%	100%	

Packaging

Kraton Polymers are available in a number of different package types. For information specific to this grade, please contact your local Kraton Polymers representative.

Figure 7-32: Impact midfier B (Kraton grade G1701) datasheet

Ciba Inc

Ciba

Ciba® IRGAFOS® 168

Hydrolytically Stable Phosphite Processing Stabilizer

Characterization	IRGAFOS 168 is a hydrolytically stable phosphite processing stabilizer. As a secondary antioxidant, IRGAFOS 168 reacts during processing with hydroperoxides formed by autoxidation of polymers preventing process induced degradation and extending the performance of primary antioxidants.
Chemical name	Tris(2,4-ditert-butylphenyl)phosphite
CAS number	31570-04-4
Structure	IRGAFOS 168 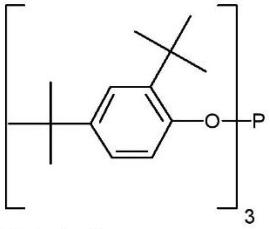
Molecular weight	646.9 g/mol
Applications	The application range of IRGAFOS 168 -synergistically combined with other Ciba anti-oxidants - comprises polyolefins and olefin-copolymers such as polyethylene (e.g. HDPE, LLDPE), polypropylene, polybutene and ethylene-vinylacetate copolymers as well as polycarbonates and polyamides. The blends can also be used in polyesters, styrene homo- and copolymers, adhesives and natural and synthetic tackifier resins, elastomers such as BR, SEBS, SBS, and other organic substrates. IRGAFOS 168 blends can be used in combination with light stabilizers of the TINUVIN and CHIMASSORB range.
Features/benefits	IRGAFOS 168 is an organophosphite of low volatility and is particularly resistant to hydrolysis. It protects polymers which are prone to oxidation, during the processing steps (compounding/ pelletizing, fabrication and recycling) from molecular weight change (e.g. chain scission/crosslinking) and prevents discoloration. IRGAFOS 168 performs best when combined with other Ciba antioxidants. Blends of IRGAFOS 168 with antioxidants of the IRGANOX range (IRGANOX B-blends) and with Hydroxylamine FS042 are particularly effective. The IRGANOX range antioxidants additionally provide storage stability and give the polymer long term protection against thermo-oxidative degradation. IRGAFOS 168 comprised in phenol free systems with other appropriate Ciba stabilizers addresses specific stabilization requirements.

Product forms	*Code:*	IRGAFOS 168
	Appearance:	Powder: white, free-flowing powder FF(C): white free-flowing granules

Figure 7-33: Antioxdant Irgafos grade 168 datasheet

Technical Information | **Plastic Additives**

TI/EVK 1001 e
September 2010 Page 1 of 2

Supersedes edition dated Juni 2010

BASF
The Chemical Company

® = registered Trademark of BASF SE

Irganox® 1010

Phenolic primary antioxidant for processing and long-term thermal stabilization

Characterization

Irganox 1010 – a sterically hindered phenolic antioxidant – is a highly effective, non discoloring stabilizer for organic substrates such as plastics, synthetic fibers, elastomers, adhesives, waxes, oils and fats. It protects these substrates against thermo-oxidative degradation.

Chemical name

Pentaerythritol tetrakis(3-(3,5-di-tert-butyl-4-hydroxyphenyl)propionate)

CAS number

6683-19-8

Structure

Irganox 1010

Chemical formula

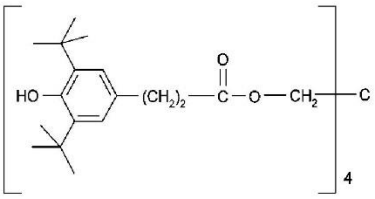

Molecular weight

1178 g/mol

Applications

Irganox 1010 can be applied in polyolefins, such as polyethylene, polypropylene, polybutene and olefin copolymers such as ethylene-vinylacetate copolymers. Also, its use is recommended for the processing of polymers such as polyacetals, polyamides and polyurethanes, polyesters, PVC, styrene homo- and copolymers, ABS, elastomers such as butyl rubber (IIR), SBS, SEBS, EPM and EPDM as well as other synthetic rubbers, adhesives, natural and synthetic tackifier resins, and other organic substrates.

Features/benefits

Irganox 1010 has good compatibility, high resistance to extraction and low volatility. It is odorless and tasteless. The product can be used in combination with other additives such as costabilizers (e. g. thioethers, phosphites, phosphonites), light stabilizers and other functional stabilizers. The effectiveness of the blends of Irganox 1010 with Irgafos 168 (Irganox B-blends) or with Irgafos 168 and Irgafos FS042 is particularly noteworthy.

Product forms

Irganox 1010	white, free-flowing powder
Irganox 1010 FF	white, free-flowing granules
Irganox 1010 DD	white to slightly green pellets

Figure 7-34: Antioxidant Irganox grade 1010 datasheet